Thermodynamic Modelling and Experimental Investigation of Two Bed Solar Vapour Adsorption Cooling System

DOCTOR OF PHILOSOPHY

ASIF SHA A.

Register No. D-TKM18JAN006

Department of Mechanical Engineering

TKM College of Engineering, Kollam

APJ ABDUL KALAM TECHNOLOGICAL UNIVERSITY

Thiruvananthapuram

2023

Thermodynamic Modelling and Experimental Investigation of Two Bed Solar Vapour Adsorption Cooling System

Submitted in partial fulfilment of the requirements of the degree of

DOCTOR OF PHILOSOPHY

ASIF SHA A.

Register No. D-TKM18JAN006

Supervisor:

Dr. BAIJU V.

Department of Mechanical Engineering

TKM College of Engineering, Kollam

APJ ABDUL KALAM TECHNOLOGICAL UNIVERSITY

Thiruvananthapuram

2023

DECLARATION

I declare that this written submission represents my ideas in my own words and where others' ideas or words have been included, I have adequately cited and referenced the original sources. I also declare that I have adhered to all principles of academic honesty and integrity and have not misrepresented or fabricated or falsified any idea/data/fact/source in my submission. I understand that any violation of the above will be cause for disciplinary action by the University and can also evoke penal action from the sources which have thus not been properly cited or from whom proper permissions have not been taken when needed.

ASIF SHA A.

Register No. D-TKM18JAN006

Date:18-03-2023

CERTIFICATE

It is certified that the work contained in the thesis titled "**Thermodynamic Modelling and Experimental Investigation of Two Bed Solar Vapour Adsorption Cooling System**," by **Asif Sha A.**, has been carried out under my supervision and that this work has not been submitted elsewhere for a degree.

Dr. Baiju V.

Assistant Professor

Department of Mechanical Engineering

TKM College of Engineering, Kollam

Date : 18-03-2023

Place : Kollam

Acknowledgement

Any initiative at any stage cannot be satisfactorily finished without the assistance and direction of knowledgeable people. I owe a significant amount of gratitude to all of the individuals whose unwavering encouragement and drive inspired me to conduct this research. I would like to express my most sincere appreciation towards my guide and mentor **Dr. Baiju V.**, Assistant Professor, Department of Mechanical Engineering, TKM College of Engineering for guiding me throughout the journey of the doctoral research. He has been a regular source of motivation and encouragement. Thank you will be the smallest word against the compassion and knowledge he conferred throughout. I express my deep sense of gratitude to **Dr. Shahul Hameed T. A.,** Principal, TKM College of Engineering and **Dr. Dileep P. N.**, Professor and Head of Department, Mechanical Engineering, from bottom of heart for lending me all facilities and support for completion of this research work.

I would like to thank **Dr. Salih A.**, Professor and Chairman of the Doctoral Committee and **Dr. Udayakumar J.,** Dean (Research), TKM College of Engineering for support to complete this project. I thank, **Dr. Mohammed Sajid N. K.,** Professor and former HOD of Mechanical Engineering and **Dr. Shafi K. A.**, Professor, TKM College of Engineering for giving their constant support for doing this research work. Special thanks to **Dr. Mahesh Kumar P.,** Professor, GEC Kannur (External DC member), **Dr. Joy Varghese V. M.,** Assistant Professor, CET (External DC member), **Dr. Mohammed Sadhikh**, Professor and **Dr. Reby Roy K. E.**, Professor, Department of Mechanical Engineering, TKM College of Engineering (Internal DC members), with their suggestion during the research work.

I would like to mention special thanks to **Mr. Yesudasan Johnson**, Instructor Gr.II, **Mr. Nazeer Khan A.**, Tradesman and other college staffs for the technical and nontechnical assistance given for the research work. I take this opportunity to extend my deep appreciation to my **loving Parents, Abdul Aziz M., Shahida Beegum** and **friends**, **Mr. Shajan S., Mr. Abhishek P., Mr. SyamKumar G., Mr. Krishna Raj V., Mrs. Salini S., Mr. Chindhu V. G.** and **Mr. Binil B.** for all that they meant to me during the crucial times of the completion of this project. I would like to express my gratitude towards my **loving wife**, **Shaleena Manafuddin** and my **daughters, Maleeha Sulthana and Haleema Sulthana** for encouraging me and providing endless support. Lastly, I thank **Almighty God** for being with me all the time and guiding me with their divine light.

ASIF SHA A.

Abstract

Adsorption cooling technology is an alternative to conventional cooling systems. The low heat transfer properties of the adsorbent-adsorbate pair utilised in adsorption cooling systems have an impact on the performance of the systems. Thus, researchers are concentrating on enhancing the performance of the system by introducing new composite adsorbent pairs. A transient model of a two-bed adsorption cooling system employing activated carbon-ethanol is presented to evaluate performance. The Coefficient of Performance (COP) and Specific Cooling Power (SCP), have been evaluated using SIMULINK platform. An adsorption chiller of 600 W capacity operating at an evaporator temperature of 5^0C with isothermal adsorption is used to improve the performance of system. The analysis envisages that a maximum heat input is used for the desorption of adsorbate from the bed and is 4543.44 kJ. The maximum COP is 0.68, for a desorption temperature of 95^0C. Moreover, the exergy destruction of the adsorbent bed has been evaluated as 0.19 kW. The next phase of the work is the design, development and performance study of the two-bed adsorption cooling system. The evaporator, condenser, adsorbent bed, energy storage tank and solar collector are designed and fabricated. The experimental COP of the system is 0.68 for the maximum hot water inlet temperature of 88^0C. The study also concentrated to investigate a composite adsorbent for the proposed system. The characteristic study of the composite suggests, composite B, having activated carbon 70% in weight, expanded graphite powder 10%, metal organic framework 10% and binder 10% as the favourable choice for adsorption cooling system. The thermal conductivity of the composite B and volumetric adsorption uptake of activated carbon-ethanol is determined as 0.29 $Wm^{-1}K^{-1}$ and 0.983 respectively. The thermodynamic modelling of the system as well as experimentally with the selected composite adsorbent-ethanol is carried out to evaluate its performance. The study reveals that COP of the system increases by 14.81% when using composite as compared with activated carbon-ethanol. The performance of the proposed system with the thermal energy storage material is also investigated. It is observed that the COP of the system increases by 20.69% as compared to the adsorption cooling system that uses activated carbon-ethanol.

Table of Contents

List of Figures

List of Tables

Abbreviations

AC	Activated carbon
B	Bed
CFC	Chlorofluorocarbon
COP	Coefficient of performance
CO_2	Carbon dioxide
CP	Cooling power
E	Valve
EG	Expanded graphite
GWP	Global warming potential
GI	Galvanised iron
HFC	Hydrofluorocarbon
IIR	International Institute of Refrigeration
MOF	Metal organic frame work
ODP	Ozone depletion potential
PTFE	Polytetrafluoroethylene
PVP	Polyvinylpyrolidone
SAC	Two-bed solar adsorption cooling
SCC	Specific cooling capacity
SCP	Specific cooling power
SGP	Silica gel powder
V	Valve

Nomenclature

A	area [m^2]
A_p	aperture [m]
B	mirror reflectivity [-]
C	specific heat [$J.kg^{-1}.K^{-1}$]
D	Structural constant [-]
Di	diameter [m]
D_0	receiver outer diameter [m]
D_e	exponential constant [K^{-1}]
D_{sp}	diffusion coefficient [$m^2.s^{-1}$]
D_{pf}	pre-exponential factor [$m^2.s^{-1}$]

E	adsorption characteristic parameter [J.mol]
E_x	exergy [W]
E_{ea}	energy for activation [$J.kg^{-1}$]
F_s	shape factor of particle [-]
H	isosteric heat of adsorption/desorption [$J.kg^{-1}$]
H_i	level height [m]
h	enthalpy [$J.kg^{-1}$]
I	radiation [W]
IR	irreversibility [W]
K	Thermal conductivity [$W.m^{-1}.K^{-1}$]
L_v	latent heat-vaporisation [$J.kg^{-1}$]
L_{co}	length of collector [m]
M	mass [kg]
$\dot{m}$	rate of mass flow [$kg.\ s^{-1}$]
P	pressure [Pa]
P_{sp}	pressure at saturated condition [Pa]
Q	sensible heat [J]
Q_{cp}	cooling power [W]
q	heat flux [$W.m^{-2}$]
R	gas constant [$J.kg^{-1}.K^{-1}$]
R_g	geometric factor [-]
R_r	radius of fibre [m]
s	entropy [$J.K^{-1}$]
T	temperature [K]
t	time [s]
t_o	atmospheric temperature [K]
t_2	rate of background temperature drift [s]
t_{phase}	phase time [s]
U_c	overall heat transfer coefficient [$W.m^2.K^{-1}$]
U	internal energy [W]
X_0	maximum adsorption capacity [$m^3.kg^{-1}$]
X	adsorbate concentration ratio at equilibrium [$kg.kg^{-1}$]
Y	intercept factor [-]
Y	wetness fraction [-]

Greek Symbols

Δ	change/difference [-]
Π	exergy destruction [W]
ρ	density [kg.m^{-3}]
η	efficiency [%]
ε	mass energy [W]
α	receiver absorptivity [-]
τ	cover transmission [-]
Ψ^*	adsorbate volume fraction [-]

Subscripts

ac	activated carbon
ads	adsorption
amb	ambient
b	bed
br	beam radiation
chil	chiller
co	collector
cold	cold water
com	composite
con	condenser
cons	constant
cu	copper
cwa	cooling water in adsorption
cw	cooling water
cy	cycle
des	desorption
eva	evaporator
ex	exergy
f	final
ga	gas
gen	generator
h	hot
hw	hot water
hwd	hot water in desorption

i	input/initial
liq	liquid
max	maximum
min	minimum
mc	metal cover
ref	refrigerant
re	receiver
sa	saturation
sat	saturation
sc	source or hot water
so	solar
sr	sunrise
ss	sunset
st	switching time
w	water
wi	water in
wo	water out
0	datum
1, 2, 3, 4, 5	state points

Superscripts

1, 2, 3, 4, 5	state points

Chapter 1

Introduction

In Indian culture, the sun is widely acknowledged as the source of all life on Earth and the origin of all forms of energy. Solar energy extracted directly or indirectly is used to generate power. “SURYA NAMASKAR” is also regarded as the best methodology for mental peace and physical energy well-being in yoga and meditation. The use of solar energy for practical applications is one of the important topics of research area. This chapter describes the background of the research, energy scenario in India, solar cooling options, developments of adsorption cooling systems, aim and scope of the present study.

1.1 Background of the Research

The concept of balancing environmental preservation and development is referred to as “sustainability”. Thus, the notion of sustainability is now widely accepted across all industries, and a number of engineering management techniques have been developed to address a variety of environmental issues. Sustainable engineering is an example of an interdisciplinary management technique concerned with the sustainable utilisation of natural resources. Sustainable growth is predicated upon the efficient utilisation of energy. In view of the fact that energy consumption is a necessary part of daily life, it is important to take care the environment [1]. Therefore, balancing the use of energy, economic growth,

and environmental protection is the most crucial aspect for long-term development plan. Considering environmental protection, the depletion of the ozone sphere by Chloro Fluoro Carbons (CFC), the most widely used organic refrigerant, is of primary importance. In vapour compression refrigeration systems, CFC was utilised as the most essential refrigerant. But due to environmental regulation in the Montreal Protocol in 1987, it has been decided to phase out the production and consumption of Ozone Depleting Substances (ODS) such as CFCs and halons from 1995. In addition, the 1997 Kyoto Protocol agreement aims to reduce or phase-out hydrofluorocarbon use by 2030 [2]. The Kigali agreement to the Montreal Protocol [3,4], which has been accepted by 91 nations as of October 2016, is an international agreement to gradually decrease the use and production of Hydro Fluoro Carbons (HFCs). Figure 1.1 depicts the Global HFC use as a share of the total on Global Warming Potential (GWP) weighted basis for refrigeration and air conditioning [5].

Utilisation of high-grade energy is the primary concern in refrigeration and space heating application. The conventional refrigeration and air conditioning systems are often powered by electricity. The cooling systems driven by low grade energy sources can be an interesting option for reducing the ODP and GWP. Vapour Compression refrigeration systems (VCR), Vapour Absorption Refrigeration systems (VAB), and Thermo Electric Cooling (TEC) systems are the most commonly used refrigeration systems nowadays.

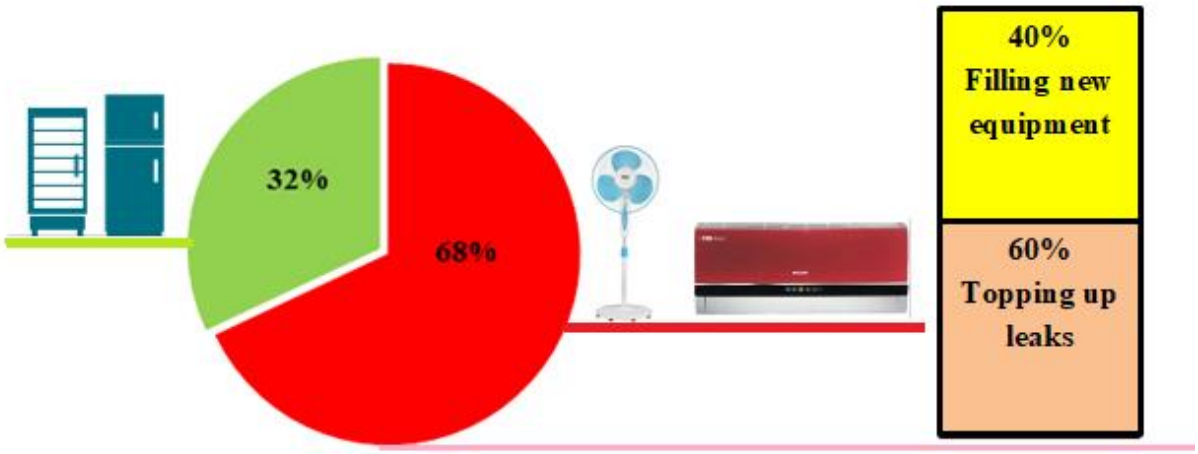

Fig. 1.1: Global HFC use as a share of the total on GWP-weighted basis for refrigeration and air conditioning [5]

The VCR system is considered to be the most efficient and useful for all practical applications. But the synthetic refrigerants like, CFCs, HCFCs or HFCs used in the VCR system causing for ozone layer depletion and/or contribute to the greenhouse effect. Additionally, the typical VCR cycles are electrically powered, consuming a significant amount of high-quality power, which increases the fossil fuel utilisation; and leads to the greenhouse effect. The VAB system utilizes the low-grade energy operated thermal compressor to change the pressure energy of the refrigerant. As a result, this system can be used in areas where electricity is scarce or prohibitively expensive. Another advantage of this system is the lack of moving parts, such as the pump or compressor, hence no wear or tear and easy control. The main disadvantage of the VAB system is its heavier size and very low Coefficient of Performance (COP). They are also not scalable to low and medium cooling capacity applications. The regenerative temperature of the electrolux VAB system is more than 200^0C, and the refrigerant NH_3 used in the system is highly poisonous and causes corrosion [6]. In the case of Lithium Bromide-Water VAB system, there is a minimum solution temperature below which the salt begins to crystallise, causes for the interruption of the system operation. Since, the absorbents of VAB are in the liquid state, they cannot be employed in systems that are subject to intense vibration, such as in boats, automotive, etc. TEC systems are Peltier-effect-powered solid-state heat pumps. The devices can be cooled or heated when an electrical current is applied and can undergo thermal cycling at pulse width modulator frequencies. The key advantage of the TEC system is that it contains no moving parts, can operate in any direction, more versatile, simple to operate, and more dependable. The primary problem of these types of devices is their comparatively low COP, high required power, and lack of suitable materials with a high fatigue of merit.

An adsorption cooling system which can effectively operate with solar energy, biomass, waste heat, and other low-grade sources is an interesting option for cooling applications. Adsorption cooling system is a nascent technology has gained attention as a possible alternative to vapour compression cooling system [6]. Many benefits of adsorption chillers include less moving parts, simple construction, and the ability to be powered by low-grade energy sources. Moreover, the refrigerant used in the Solar Adsorption Cooling (SAC) system is environmentally friendly and has zero ODP and low GWP. The deployment of SAC system in non-electric grids, where milk, food, and medicine spoilage occur, is also imperative.

1.1.1 Energy scenario in India

India has the 5th largest capacity for electricity generation and the 6th largest energy utilization, accounting for approximately 3.4% of global energy consumption. Due to rising energy consumption, population growth, and economic development, India faces a severe electricity and energy shortage. With a predicted yearly growth rate of 8 to 9 %, increased urbanisation, and rising living standards for millions of Indian households, demand of energy use is increased dramatically. This leads to the use of solar energy in the search for more sustainable energy sources for the Indian environment. In terms of non-conventional energy resources, India has a vast solar potential, as the majority of the country is blessed with abundant sunshine. There are approximately 300 clear sunny days each year in the majority of the country, and the average incident solar radiation over India ranges from 4 kWh to 7 kWh per day [5]. Solar radiation received by the Indian Territory is estimated to be approximately 5,000 quadrillion-TWh per year. The National Action Plan on Climate Change, launched in June 2008, includes eight key national missions, the largest of which focuses on solar energy. The project envisions a significant advance in the use of solar energy for electricity production and other applications. Figure 1.2 depicts renewable energy goal of India for 2022.

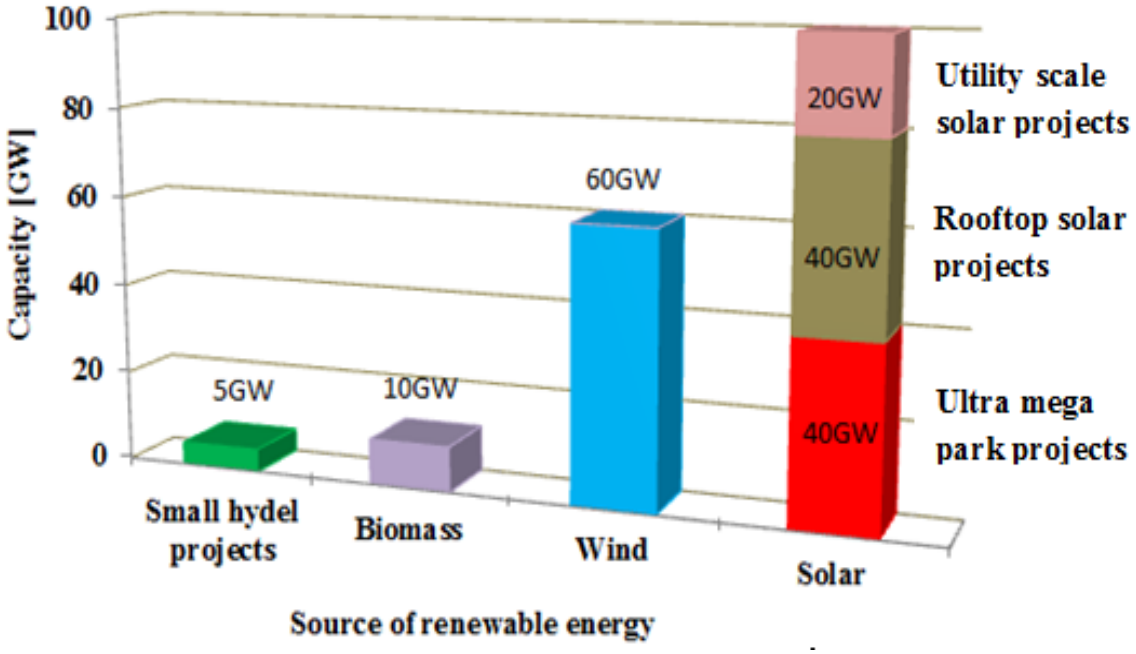

Fig. 1.2: Renewable energy goal of India for 2022 [5]

1.2 Solar Cooling Options

According to BEE in India, 45% of the total energy installed in India (1383 TWh approximately) is used for refrigeration and air-conditioning purposes. Hence it is important to find the alternative way of operating the conventional cooling systems or develop alternative cooling systems that can be effectively run by the solar energy. One of the most important applications of solar thermal utilisation is solar cooling, and like other solar thermal utilisation systems, the solar cooling system also needs solar collection and storage units in order to operate continuously with solar energy. The solar cooling systems are more attractive because of the following factors:

i. Solar energy is an alternate, abundantly available and renewable energy.
ii. Refrigeration accounts for a large portion of electricity consumption.
iii. The supply of solar radiation and the need for cooling are aligned. The change of solar energy with day time is depicted in Figure 1.3, illustrating that the demand for cooling is greatest during periods of maximum solar radiation availability. Cooling is far more important in warm temperatures than in cooler climes.
iv. Food production (agriculture, milk, fish) in rural areas without access to electricity, but open unused land space is more. Thus, the wastage of food products can be avoided.
v. Preservation of life-saving medicines in the remote area.

In the rural areas due to the shortage of power, there is acute shortage of cold storage facilities. The surveys clearly demand the need for cold storage facilities in the rural areas, where electricity is a major concern. Thousands of tonnes of perishable materials like fruits, vegetables, fruits, fish and related other food products are being wasted every year. The rural medical care centres facing the difficulty of the preservation of essential medicines for emergency use, because of the unavailability of cold storage facilities. Similar to this, due to the lack of electrical power in rural areas, people find it difficult because of the non-availability of the human comfort air-conditioning facilities during extreme hot and cold seasons. Solar cooling systems can provide these facilities since solar energy is freely available all over the country. In India, food production centres are

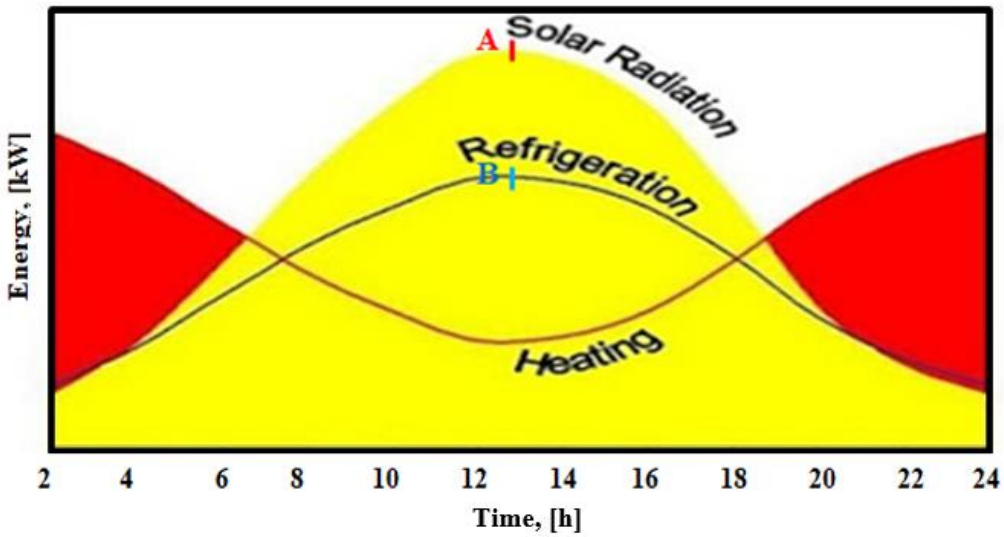

Fig. 1.3: The variation of solar energy with day time

typically located in areas where electric supply for running large refrigeration plants is not available. Therefore, a cooling system, which does not depend completely on electricity for its operation will be the most ideal under such circumstances.

In India, agricultural products plays an important role in the national economy. Some of the products could yield substantial foreign exchange, potatoes and onions, for instance. Steps are being taken to increase the production and export of these commodities. Preserving food in cold storage facilities is the most crucial method used to stop spoilage. A large amount of solar radiation with an average value of 600 $calcm^{-2}$ day for the entire country falls in India. Even in December, the value is around 500 $calcm^{-2}$ day for some cities in India During summer, the interior parts of the country become very hot with the maximum ambient air temperature reaching around 48^0C. Northern parts experience dry heatwave while the coastal regions are slightly cooler but due to extreme humidity, it becomes uncomfortable for human beings. Due to the extreme conditions in India, cooling of houses in summer and heating in winter is imperative, particularly in the interior areas and away from the coast. In addition to increasing human comfort, space conditioning increases commercial production and makes it possible to establish high-tech industries, which need a controlled environment. The existing cold storage and air-conditioning units in India are not quite satisfactory.

1.2.1 Types of Solar Cooling Systems

There is a great scope for the utilisation of solar energy and its application because the availability of solar energy is in phase with the demand for cooling, which is highest in summer and lowest in winter. Moreover, the solar collector efficiency is relatively high in summer because of the high ambient air temperature as compared to winter. The development of solar cooling devices has been dwarfed due to the availability of relatively low temperatures from solar collectors. However, with modern collectors, there is new hope for solar cooling systems. The solar cooling systems are the significant invention of utilising solar energy.

A solar refrigerator is a device that is operated completely by the solar energy harnessed from the Sun. For decades, peoples have used vapour compression refrigeration systems to store their medicines, food and other products. In 1935, Otto Mohr developed a cooling system operated with solar energy. He was able to outline each part required to assemble and operate the solar cooler. Even though the idea of a solar refrigerator was created by Otto Mohr in 1935, peoples were, however, more likely to choose highly efficient VCR systems. Hence, the research and development of solar thermal driven refrigeration system were noticeably reduced. Subsequently, electricity-driven vapour compression systems have played a significant role in the market. In 1970's, energy crisis became an issue and people started to work on PV-based systems. During that time, the cost of photovoltaic technology was expensive and had low efficiency. In 1990's, the research and development in the area of solar cooling became more familiar and popular. Figure 1.4 illustrates the possible refrigeration systems and their applications and Table 1.1 gives the existing solar-driven refrigeration technologies.

In solar thermal cooling systems, solar collectors capture solar energy, transform it into thermal energy, and it is used to power thermal compressors, specifically adsorbent beds. Solar electric cooling systems, on the other hand, use solar photovoltaic (PV) panels to power a traditional electric vapour compressor air-conditioning system. The solar-powered adsorption cooling system is proved to be an efficient method of achieving cooling with low cost, high-efficient and simple manufacture. In solar vapour compression refrigeration systems, solar energy converted into mechanical energy using a solar collector. The compressor of VCR system can be driven by this mechanical energy. This is

called the Rankine cycle cooling. The other version based on the inverse Rankine cycle for producing cooling using solar energy, where, solar energy is converted into mechanical energy with which the refrigerant air is compressed. Subsequently, it is cooled to remove the heat from it. The cold air is then expanded through the turbine where work may be extracted. The cold exhaust air is discharged into the air conditioning space. In the steam jet compression version of the system, the mechanical compressor is removed by the convergent/divergent nozzle known as jet ejector pump. The primary fluid, which receives heat as input from the solar collectors is expanded within the jet pump thereby affecting compression of the refrigerant, and suction is obtained in an evaporator where the cooling occurs. Thus, a jet ejector can be used to reduce the pressure over a liquid refrigerant. This causes evaporation and hence cooling of the liquid. Refrigerant cooled in this manner is circulated through a heat exchanger to affect the desired space cooling. Operation of the ejector is accomplished by high-temperature and pressure refrigerant vapour from a boiler through the ejector and passing to the condenser. Pumps are required to maintain the proper refrigerant volumes in the evapouriser, condenser and the evaporator.

Solar energy can also be used to generate cooling by using closed/open cycle adsorption cooling systems and/or absorption dehumidification cycles based on the solar regeneration of sorbents and liquid desiccants. In vapour absorption cooling systems, a mixture of absorbent and refrigerant is used to substitute the mechanical compression by thermal compression through the absorber-generator assembly and the solar heated water is used to supply low-grade heat input in the generator. Cooling is produced in the evaporator and heat is produced from the condenser and absorber. The COP of absorption systems is relatively less since the input energy is heat rather than work. The adsorption refrigeration cooling process is similar to that of the absorption cooling except with the difference that the refrigerant is adsorbed into the surface layer of the adsorbing material rather than being taken into the chemical solution. The refrigerant is then driven out by solar heating, the refrigerant evolved is then subject to condensation and throttled to produce the refrigeration effect. The refrigerant is then re-adsorbed to the carrier material to have a closed cycle.

Generally, with the thermodynamic cycles, it is advisable to have few energy conversions as possible. Thus, more direct conversion devices are preferable. A vapour absorption and adsorption cooling system require more heat energy input to produce

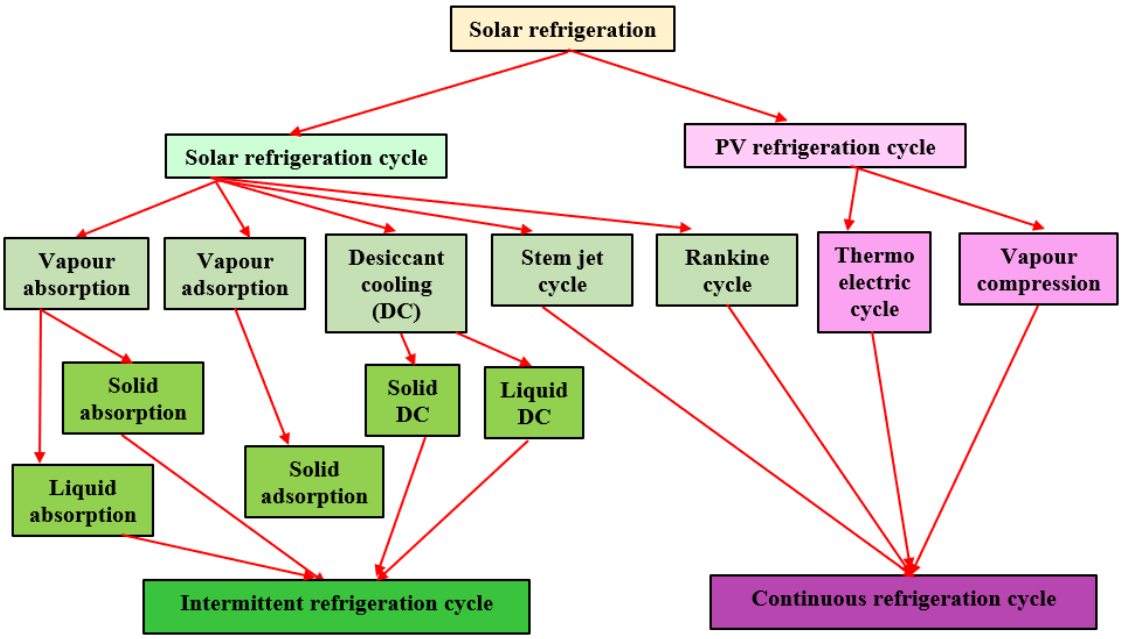

Fig. 1.4: Classification of the solar refrigeration cycle

Table 1.1 Existing solar-driven refrigeration technologies

Refrigeration Cycle	Solar Technology		COP	Available application		
	Thermal collectors (T_{gen}/T_{reg}) ^0C	PV cells powered (power for 30L cooling box in W)		R	AC	Example applications
Electricity/work driven cycles						
Vapour compression		(15-40)	3-5	√		HC, SC, CB
Thermo electric		A few in mW	0.5	√		VT, CB
Stirling		(8-50)	3	√		CB, LT
Heat driven cycles						
Absorption	(80-190)		0.6-0.8	√	√	AC, IP
Adsorption	(80-300)		0.3-0.6	√		CB, IP, VS
Chemical reaction	(80-300)		0.1-0.2	√		IP, VS, FS
Duplex Rankine	>120		0.3-0.5		√	AC
Desiccant Cooling	(40-80)		0.5-1.5		√	AC

AC: air-conditioning CB: cooling box, FS: food storage, IP: ice production, HR: household cooler, LT: low temperature applications, SC: small cooler VS: vaccine storage, VT: vaccine transportation, C: Cooler

cooling effect than the vapour compression refrigeration cycle. However, the energy inputto the former is primarily in the form of heat, whereas in the VCR systems, it works. According to the second law of thermodynamics, heat and work are not equivalent forms of energy. Heat is low-grade energy. Only a part of it is available, whereas work is high-grade energy because all of it is available. As a result, it is impossible to compare the COP of the VCR and VAB/VAD systems fairly. The basic consideration in refrigeration and cooling systems should have a high COP or lower cooling temperature or higher cooling capacity. This depends on specific applications and localised conditions. Achieving an ideal COP is not possible because of the irreversibility involved in processes. Another important factor for the cooling systems is economic. It is also possible to improve the COP of VAB/VAD systems by multi stage cycles and advanced absorption/adsorption cycles based on double effect generation/condensation/evaporation processes.

A non-conventional method of cooling is thermoelectric cooling. The main distinction between the thermoelectric cooling and other cooling devices is that the all cooling devices make use of mechanical shafts or thermal energy as input source while in the thermo electric cooling electric energy is directly utilsed for cooling. Light weight and low cost are some of the advantages of thermo electric cooling systems.

1.2.2 Difference between absorption and adsorption phenomenon

The processes absorption and adsorption are different. Absorption is the process through which a liquid or solid dissolves a fluid by absorbing it. When atoms, ions, or molecules from a material adhere to the surface of an adsorbent, adsorption occurs. During absorption, atoms flow through or enter a large material. When molecules are held loosely on the surface of an adsorbent and thus the vapour adsorbate can be easily removed by an external heat source. Consequently, adsorption is a surface phenomenon, whereas absorption is a bulk phenomenon in which the assimilate is distributed throughout a solid or liquid to produce a solution or a compound. The phenomena of absorption and adsorption are depicted in Fig. 1.5.

The adsorption properties of a specific pair are determined by the nature of the adsorbate, adsorbent, the surface reactivity, surface area, and the temperature and pressure

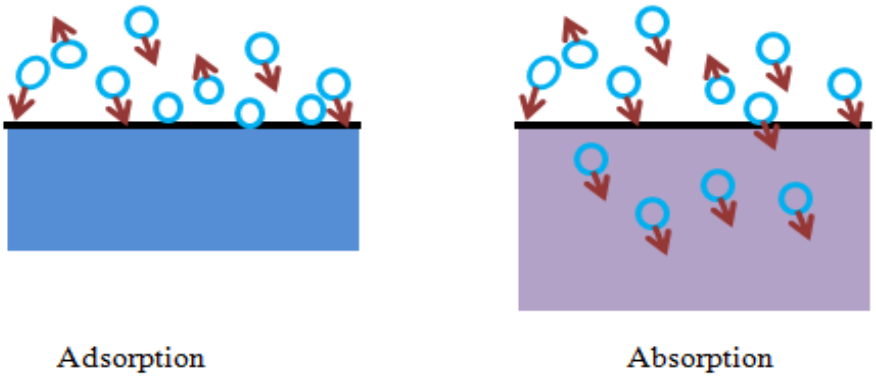

Fig. 1.5: Adsorption and absorption phenomenon

at which the adsorption process occurs. When a solid surface is in contact with a gas, the gas molecules embedded into the solid surface. Adsorption occurs when some of the intriguing molecules adhere to the solid surface and the adsorption equilibrium dynamics is shown in Fig.1.6. Initially, the adsorption quantity is high because the whole outer-surface area of adsorbent is not covered. Then, the adsorption rate gets reduced since more and more adsorbate vapour is being covered on the solid surface of the adsorbent. The range of heat source is mainly depends on the type of adsorbent-adsorbate pair used.

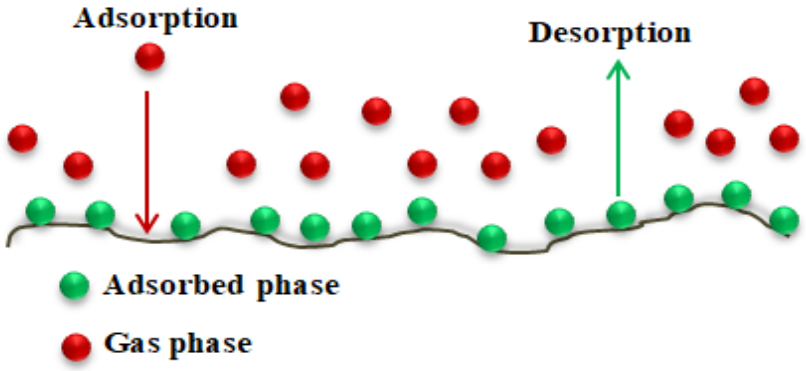

Fig. 1.6: Adsorption equilibrium dynamics [6]

1.2.3 Comparison of absorption and adsorption cooling system

The Table 1.2 summarises the major differences between vapour adsorption or absorption cooling system.

1.3 Developments in Adsorption Cooling Technology

The section describes the history of adsorption cooling systems, working of the system, and its classification. Additionally, the goal and scope of the work as well as the energy storage materials for adsorption cooling systems are also described in this section.

1.3.1 History of adsorption cooling system

Faraday discovered ammonia adsorption on silver chloride in 1848, which is the first document of the adsorption cooling phenomenon. G. E. Hulse introduced an adsorption cooling system to preserve food and beverages in train in 1920, using silica gel powder-sulphur dioxide as the adsorbent/adsorbate pair [6]. The evaporator temperature attained by this system is 12^0C. In 1940, an adsorption cooling system using calcium chloride-ammonia as the adsorbent-adsorbate pair was employed for preserving food and beverage on a train travelling from Liverpool to London. Plank (1960) developed an adsorption cooling system based on the adsorbent-adsorbate pair activated carbon-methanol.

Low-grade energy sources like solar energy, biomass, and waste heat from flue gas are used to power adsorption refrigeration systems. Moreover, the oil crisis of the 1970s served as a great catalyst for the development of adsorption cooling systems. Based on the environmental regulations established by the Montreal Protocol in 1987, it was decided to gradually cease the production and use of ozone-depleting substances including CFCs and halons. Further, the use of HFCs, which causes the greenhouse effect, can be reduced or phased out from 2030 by the agreement of Kyoto protocol in 1997. In the case of air conditioning and cooling applications, it is important to find a green technology that operates on low-grade energy, such as an adsorption cooling system, in order to address the issue caused by conventional compression refrigeration technology. In addition, the absence of moving elements makes the system more suitable for maritime, aircraft, and vehicle cooling applications. In order to overcome the current technological and financial challenges, researchers are focusing on improving the performance of adsorption cooling systems. Adsorption research primarily focuses on the analysis of the adsorption/desorption process, the physical and chemical properties of working pairs, the development of predictive models of their behaviour when operating in various environments, and the study of various cycles to enhance the functionality of the system.

Table 1.2 Differences between vapour adsorption /absorption cooling system

Absorption cooling systems	**Adsorption cooling systems**
In absorption, the substance is distributed throughout the solid or liquid to form a solution.	Adsorption takes place only at the surface, not in the body of the adsorbent.
The refrigerant vapour is drawn from the evaporator by absorption by the liquid with a high affinity for the refrigerant in an absorption cooling system. Application of heat to the solution raises its temperature level and the refrigerant vapour is driven off so that it can pass to the condenser to get liquefied	In adsorption refrigeration systems, adsorbent bed is used to adsorb or desorb the refrigerant vapour based on the temperature of the adsorbent. The bed of adsorbent cooling system is heated by hot water circulated through it to drive off the refrigerant vapour and is passed to the condenser.
Heat source temperature variations are minimal.	The adsorption system may be powered by a large range of heat source temperature from 50 to 500^0C.
A liquid pump is provided between the absorber and the generator of the system. It is used to improve the pressure of the solution from the absorber to the generator pressure.	Liquid pump is not needed for the system, since the pressure of the refrigerant increases due to isosteric heating.
The liquid absorption cooling systems requires a rectifier for its operation when working with NH_3-Water.	It does not require any such devices for its operation as the possibility of removal of solid adsorbent during the desorption stage is less.
The chance of corrosion for the components exists.	The working pairs commonly used in the system does not produce any corrosion problems for the components.
The solid absorbents need special treatment to obtain hard porous granules that increases the initial cost of the system.	Solid adsorbents used in the adsorption refrigeration do not need special treatments.
In comparison to adsorption cooling systems, the COP is high.	The COP and SCP of the adsorption refrigeration systems are less.

1.3.2 Working principle of adsorption cooling system

The adsorption cooling cycle is composed of two sorption elements (adsorber or desorber), a condenser, an evaporator, and an expansion device. The sorption element that serves as the thermal compressor substitutes the mechanical compressor in an adsorption cooling system. Figure 1.7 depicts the ideal thermodynamic adsorption cycle, with the adsorption cooling cycle divided into two independent cycles: the heat engine cycle and the refrigeration cycle. The refrigerant fluid is vapourised in the evaporator by absorbing heat from the space to be cooled throughout the refrigeration cycle; the heat is then transferred to the secondary fluid in the adsorber at room temperature. This cycle represents the adsorption phase. Adsorbed working fluid is desorbed in the heat engine cycle by collecting heat from the solar collector. The secondary fluid in the condenser transfers heat from the desorbed working fluid to the ambient temperature. This cycle depicts desorption phase of the system.

1.4 Classification of Adsorption Cooling System

This section describes the types of adsorption cooling systems and their working. Adsorption cooling systems are classified as single-bed, two-bed, multi-bed and convective thermal wave cycle.

1.4.1. Single-bed adsorption cooling system

The single bed adsorption cycle consists of a single sorption chamber filled with adsorbent, a condenser, an expansion tube, a refrigerant receiver, an evaporator and a parabolic solar concentrator, as illustrated in Fig. 1.8. The hot fluid from the heat source/ parabolic concentrator enters the adsorbent bed which causes an increase in the bed temperature. The rise in the adsorbent bed temperature causes the vaporisation of the refrigerant from the adsorbent bed. The desorbed vapour from the adsorbent bed is fed to the condenser, where the vapour refrigerant gets liquefied. The expansion device then expands this high-pressure liquid refrigerant to lower the pressure from condenser pressure to evaporator pressure. In the evaporator, the liquid adsorbate evaporates by absorbing the latent heat of evaporation from the cooling medium. This hot vapour adsorbate is then adsorbed by the adsorbent bed, completing the cycle. The main drawbacks of a single bed

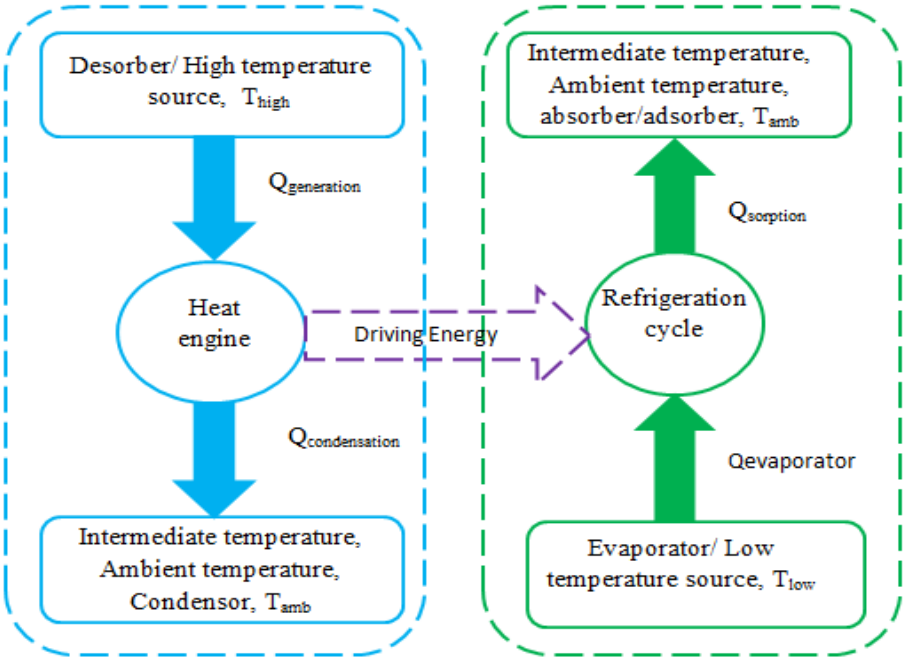

Fig. 1.7: Ideal thermodynamic adsorption cycle configuration

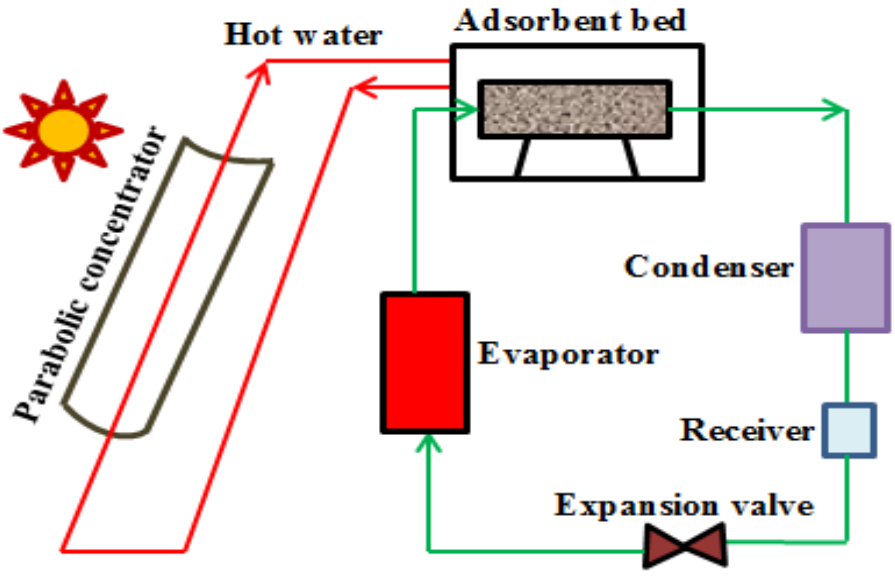

Fig. 1.8: Single-bed adsorption cooling system

adsorption cooling system is its intermittent nature, as the bed switches between adsorption and desorption. This disadvantage of a single-bed adsorption cooling system can be overcome by incorporating multiple beds into the system to provide a continuous cooling process.

1.4.2 Two-bed adsorption cooling system

The two-bed adsorption cooling system mainly consists of two adsorbent beds (either a desorber or an adsorber, depending on the mode of operation), a condenser, an expansion valve, an evaporator and a parabolic concentrator. During the desorption or adsorption process, the sorbent beds are packed with adsorbent material effective of desorbing or adsorbing the refrigerant or adsorbate. The valves are used to regulate the flow of refrigerant through the system as seen in Fig. 1.9. The adsorption of refrigerant during the adsorption process is an exothermic process; therefore, a continuous cooling of the adsorbent bed is required to eliminate the excess heat produced in the bed. To desorb the adsorbate from the adsorbent pores, external heating is required during the desorption process of the bed.

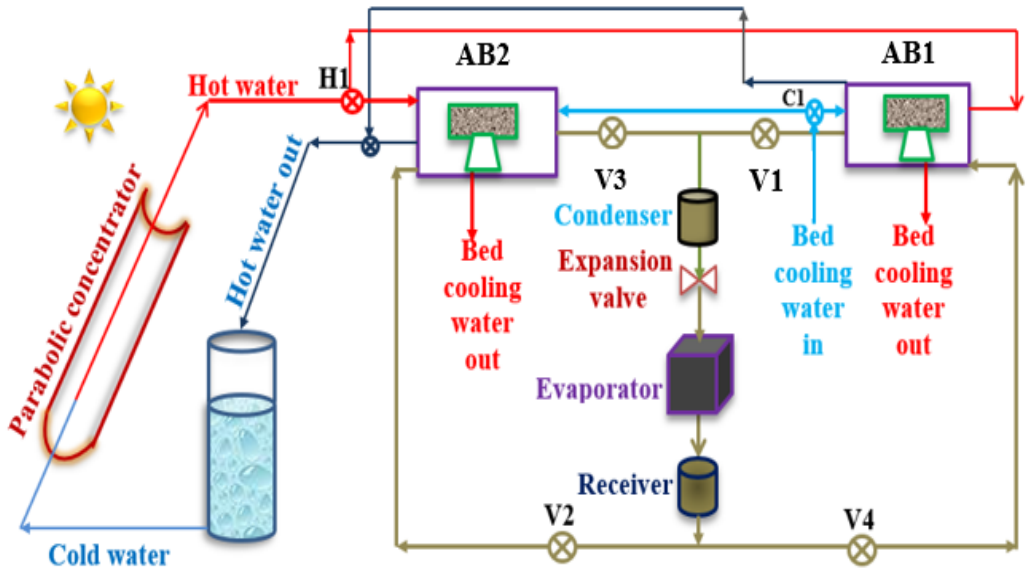

Fig. 1.9: Two-bed adsorption cooling system

Initially, the adsorbent bed 1 (AB1) is heated by flowing hot water through it while all the valves are fully closed (V1, V2, V3 and V4). When AB1 reaches the condenser pressure, the valves V1 and V2 open and the refrigerant vapour is transferred from AB1 to AB2. The adsorption of AB2 ceases when the maximum adsorbate from AB1 is desorbed. The vapour refrigerant condenses during the flow of vapour adsorbent from AB1 to AB2 through the common condenser. By reducing the pressure of the refrigerant from condenser

pressure to evaporator pressure, the liquid adsorbate is then entering to the evaporator through the expansion valve. The refrigerant absorbs the latent heat of the medium to be cooled and vapourises in the evaporator. Thus, the vapour adsorbate is finally fed to AB2 and one cycle of operation is completed. By circulating cooling water through AB2 during the adsorption process, its temperature can be decreased. During the subsequent cycle, the valves V3/V4 are fully opened while the other valves V1/V2 remains in closed position. The valve operating sequence of the two-bed adsorption cooling system is given in Table 1.3.

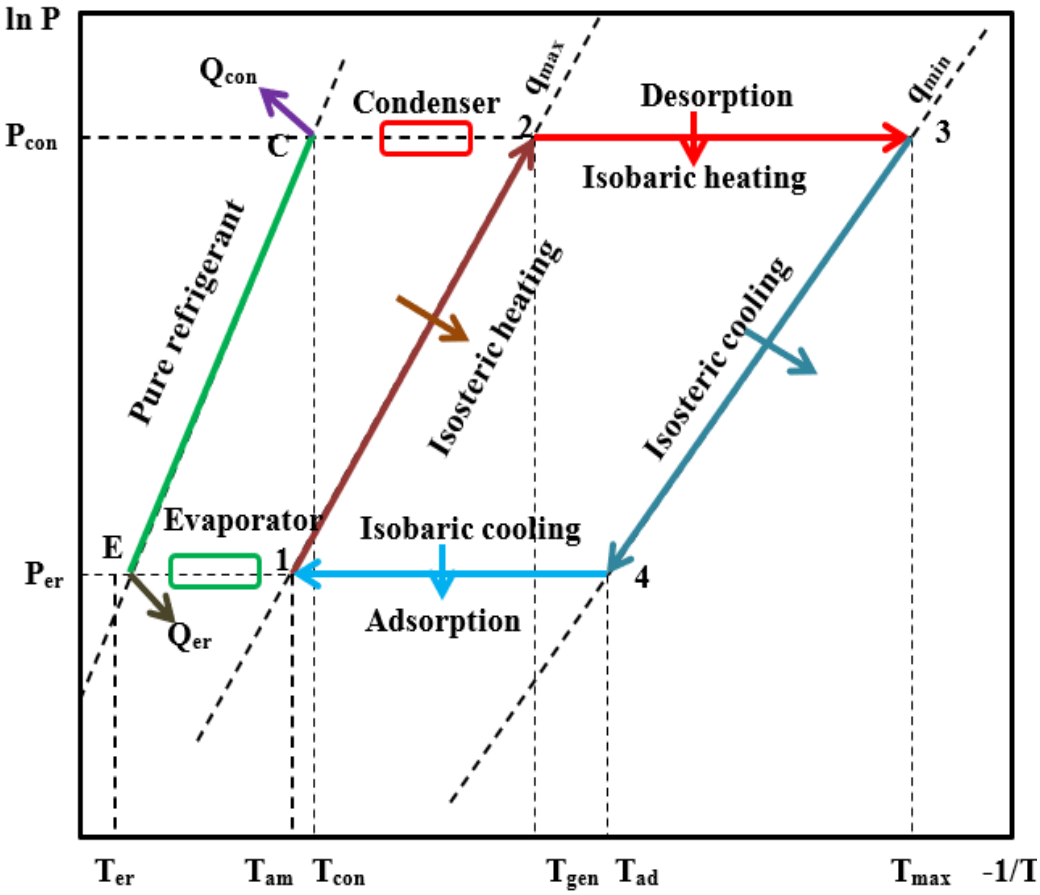

Fig. 1.10: Mode of operation of a two-bed adsorption cooling system

1.4.3 Multi-bed adsorption cooling system

The adsorption system having three or more beds with common condenser and evaporator is called multi-bed adsorption cooling system. The aim of using three adsorbent beds are to attain continuous evaporation of refrigerant, and thus continuous cooling

Table 1.3 Valve operating sequence of the two-bed adsorption cooling system

Component / Process	Bed$_1$ (AB$_1$)	Bed$_2$ (AB$_2$)	V$_1$	V$_2$	V$_3$	V$_4$
Isosteric heating (1→2)	Heating	Cooling	C	C	C	C
Isobaric heating (2→3)	Heating	Cooling	O	O	C	C
Isosteric cooling (3→4)	Cooling	Heating	C	C	C	C
Isobaric heating (4→1)	Cooling	Heating	C	C	O	O

C - Closed, O - Open

process can be obtained. The three-bed adsorption system includes four types of process such as- preheating, isobaric heating, precooling and isobaric cooling [8]. Figure 1.11 depicts a three-bed adsorption cooling system with a condenser and an evaporator, and Table 1.4 details the various operations of this system. During precooling and preheating modes, the interconnecting valves between the condenser and evaporator are closed to switch the pressure level of the reactor from pressure of condenser to evaporator pressure and vice versa. During the adsorption mode, the adsorbent bed gets cooled by circulated water through the bed, which causes for the adsorption of the vapour refrigerant coming from the evaporator. In this operation, the valve V1 between the adsorbent bed and evaporator is opened. Similarly, the valve V4 between the condenser and bed is closed to prevent the refrigerant from flowing backwards. During desorption mode, the valve connecting the adsorbent bed to the condenser is opened, allowing the refrigerant vapour to condense in the condenser and transfer to the evaporator. Mass recovery is also employed to enhance system performance.

1.4.4 Other configurations of adsorption cooling system

In addition to multi-bed adsorption cooling systems, the other configurations of adsorption cooling systems developed in the past twenty years in order to make the operation of the system continuous and to improve the performance are listed below:

i. Integrated adsorption cooling system
ii. Three-bed with dual evaporator adsorption cooling system
iii. Multi-stages adsorption cooling system

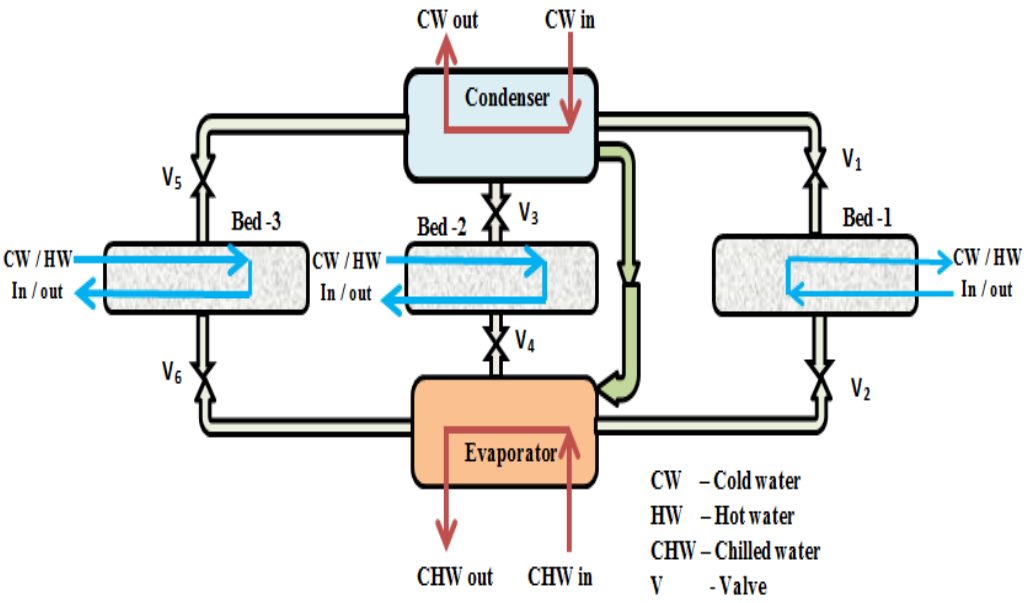

Fig. 1.11: Multi-bed **(**three bed) adsorption cooling system [8]

Table 1.4 Steps of three-bed adsorption cooling cycle and its operating modes

Component / Steps	Bed -1	Bed -2	Bed -3
Steps-01	Desorption	Adsorption	Desorption
Steps-02	Desorption	Adsorption	**Precooling**
Steps-03	Desorption	Adsorption	Adsorption
Steps-04	Desorption	**Preheating**	Adsorption
Steps-05	Desorption	Desorption	Adsorption
Steps-06	**Precooling**	Desorption	Adsorption
Steps-07	Adsorption	Desorption	Adsorption
Steps-08	Adsorption	Desorption	**Preheating**
Steps-09	Adsorption	Desorption	Desorption
Steps-10	Adsorption	**Precooling**	Desorption
Steps-11	Adsorption	Adsorption	Desorption
Steps-12	**Preheating**	Adsorption	Desorption

1.4.5 Advantages and disadvantages of adsorption cooling system

The following are the key benefits of adsorption cooling systems: [9];

i. The employed refrigerant is environmentally friendly.

ii. Low-grade energy sources like geothermal energy, waste heat, and solar energy can be used as a heat source.
iii. Since there are few moving parts, the operation is smooth and low vibration.
iv. It can be utilised on fishing vessels and trains.
v. Simple working principle.
vi. Relatively longer lifetime
vii. It can operate at lower temperature level (as below as 50^0C).

The following are some of the drawbacks of adsorption cooling systems:

i. Relatively lower COP as compared to the conventional cooling systems.
ii. Low heat and mass transfer characteristics.
iii. Intermittency of the cooling system.
iv. Lack of information on adsorption/desorption process.
v. High heat of adsorption and desorption of the commonly employed working pairs.

1.5 Types of Working Pairs Used in Adsorption Cooling System

The adsorption or desorption characterises of the working pair play an important role in the performance of the adsorption cooling system. The selection of working pairs is the most important task in the design of adsorption cooling systems. The most widely employed combinations for the adsorption cooling system includes: silica gel-water, zeolite-water, activated carbon-ammonia, metal hydrates-hydrogen, calcium chloride-ammonia, olive waste-methanol, $SrCl_2$-ammonia. Recent research indicates that consolidated adsorbent is a viable option for the adsorption cooling system due to its excellent porosity characteristics, thermal conductivity, strong affinity to the adsorbate, and high heat and mass transfer, all of which assist to enhance the performance of the cooling system. The selection of the working pair for this present study is detailed in the chapter 4.

1.6 Types of Thermal Energy Storage Materials

Since solar radiation is intermittent, fluctuating, and unexpected, there is often a mismatch between the rate and time of solar energy collection and the load requirements

for thermal application. As a result, it is frequently required to use an intermediate energy storage system. The storage system stores energy when the accumulated amount is greater than the requirement of the application and discharges it when it is required. The size of the storage system is usually decided on the basis of its use. Based on the thermal mechanism used to store energy the thermal energy storage materials are divided into three types, namely, sensible heat storage, latent heat storage and thermo-chemical heat storage materials. The most fundamental kind of heat storage system is sensible heat storage. It stores heat energy in the form of sensible heat. During this process of energy storage, there is no change in the phase of liquid or solid. Water and oil are examples of fluid storage media.

In a latent heat storage system, heat is stored in the material when its melts and extracted from the material as it freezes. A variety of such materials called phase change materials (PCM), have been studied in terms of their suitability for solar energy applications [10]. Basically, the PCM may be considered as organic materials and inorganic materials. Examples for organic type energy storage materials are Paraffin, Capric acid, etc. and inorganic type energy storage materials are Calcium chloride hexahydrate, Sodium sulphate decahydrate, etc. In a thermo-chemical heat storage material system, the solar energy is stored in the material by endothermic chemical reaction. This energy can be released when required by the reverse exothermic reaction. Both reactions occur at different temperatures, with the forward reaction taking place at a higher temperature than the reverse reaction. Thermochemical storage methods are only appropriate for medium or high temperatures.

1.7 Aim and Scope of the Research

Using fossil-fuel-based energy to power cooling equipment causes emissions of HFCs, CO_2, and black carbon, they significantly contribute to global warming. This prompts the development of a new cooling system that uses renewable energy sources and environmentally friendly refrigerant. Due to the availability of solar radiation, solar cooling technologies are more attractive. Recently, researchers have studied two-bed SAC systems to mitigate the problem of intermittency of single bed cooling systems. It is, however, possible to achieve better performance of the two-bed SAC systems only if their operating

parameters are optimised appropriately. Additionally, a consolidated working pair with enhanced heat transfer characteristics, can improve the performance of SAC systems.

A critical review of the literature indicates that there has been little research on the transient analysis and thermodynamic modelling of two bed adsorption cooling systems. To investigate the transient effect of the adsorption cooling systems, a Simulink model has not yet been developed in detail. Therefore, in this investigation, the development of a simulation model of the two-bed SAC system is conducted to determine the effect of various operating parameters on the SAC system performance. The preparation and characterisation of the consolidated adsorbent is also carried out to find the optimum working pair. Finally, the experimental performance evaluation on the two-bed adsorption system is done with and without energy storage material. The system uses solar energy as its heat source; thus, it can be used in remote areas where electricity is unavailable. Energy storage materials are incorporated into the system to store excess solar energy. When solar energy is scarce, this stored energy can be used to run the adsorption cooling system. Thus, the SAC system can be used in rural areas to cool/preserve food items, beverages, medicines, vegetables, etc. Furthermore, the absence of moving parts in the adsorption cooling system makes it a good choice in boats, locomotives and moving vehicles.

Summary

The chapter implies that vapour adsorption cooling system are a better alternative to other solar cooling technology that is currently in use. A thorough overview of the various types of adsorption cooling system, their working principles, different types working pair, energy storage materials, and the scope of the research are also included in the section. The second chapter discusses the history and present situation of adsorption cooling in India and worldwide.

Chapter 2

Literature Review

The literature review of various types of adsorption cooling system and its recent advancements are presented in this chapter. The chapter also envisages different types of working pairs and energy storage materials effective for adsorption cooling systems. The research gaps identified and the problem formulation are also discussed.

2.1 Single-Bed Adsorption Cooling System

Adsorption cooling systems with a single-bed are simple in construction and are more popular. Most of the work focuses on design and development, simulation studies, and numerical modelling of single bed system. The literature shows, most of the systems themselves use physical adsorbent materials as the working pair in the adsorbent bed.

In 1982, Dalgado *et al.* [11] invented a solar adsorption cooling operating ice machine. They performed a numerical analysis of the solar adsorption refrigeration system with a solar collector of 4 m^2 which is used to produce 25 kg of ice in each day. In the early 1990's, Exell [12] introduced an adsorption cooling system having a solar flat plate

collector of area 0.97 m^2 containing an array of copper tube. It contains a condenser, an evaporator and a cold box having a liquid receiver. The system produced 4 kg of ice in each day with a solar COP of 0.10 to 0.123.

In 2003, an adsorption chiller was developed in Burkina Faso by Buchter *et al.* [13] with carbon-methanol as the adsorbent-adsorbate pair having ventilation dampers in the adsorbent bed for improving the performance. Figure 2.1 shows the SAC system operated with ventilation dampers. The COP of the entire system ranges from 0.09 to 0.13, with daily solar radiation values varies from 22 to 25 MJm^{-2}. In the middle of 2004, Khattab [14] also introduced a SAC system module using charcoal as the solid adsorbent bed and methanol as refrigerant which is shown in Fig. 2.2. The COP of the system in the cold and hot climates, are 0.136 and 0.159, respectively. The study proved that the selection of proper adsorbent and adsorbate plays an important role in the performance of the SAC systems. The charcoal is preferred as adsorbent, since it has better adsorption capacity, easily available and low cost.

In order to improve the performance of the solar adsorption cooling system, Himsar Ambaritai *et al.* [15] carried out an experimental study with activated alumina and activated carbon as adsorbents on adsorption cooling cycle. It was reported that the presence of

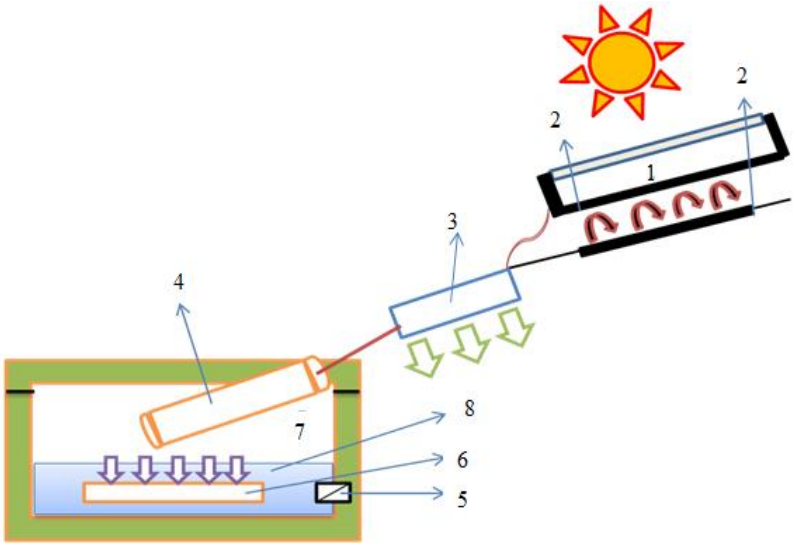

Fig. 2.1: Solar adsorption cooling system with ventilation dampers: 1. solar collector-adsorber 2. Dampers for regulating air flow 3.Condenser 4. Graduated bottle 5. Check valve 6. Evaporator 7. Cold box and 8. Ice storage [11]

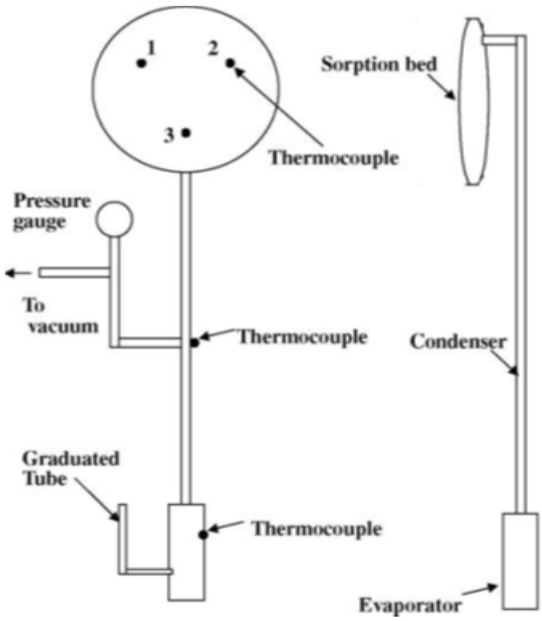

Fig. 2.2: Low cost solar powered adsorption module [14]

activated alumina increases the adsorption capacity. In this study, solar-powered adsorption cycle was tested with generator filled with different adsorbents in various proportions by exposing it to solar radiation in the Indonesian climatic condition. The experiment was divided into four cases and each of the four instances, the generator was filled with activated alumina (100 AA), a combination of 75% activated alumina and 25% activated carbon (75 AA), a combination of 25% active alumina and 75% activated carbon (25 AA), and activated carbon (100% AC). The COP of the system is 0.074 for 100% activated carbon with solar radiation that fluctuates between 11.3 and 17.9 MJm^{-2}.

Anupam *et al.* [16] conducted an experimental analysis of a pressure swing adsorption cooling system using a single-bed adsorber-desorber at six pressures ranging from 588 to 1,766 kNm^{-2}. This study focuses primarily on testing the effectiveness of an adsorption cooling system with granular activated carbon and nitrogen as the adsorbent-adsorbate pair. The present adsorption cooling system generated chilled water with a temperature of 1.70^0C from water with an ambient temperature of 28.20^0C. The main drawback of this type of pressure swing adsorption cooling system is that, it needs a mechanical compressor. Therefore, the system is not cost effective and cannot be deployed in remote areas without any power source. Moreover, the pressure swing adsorption or desorption process is suitable for a solid adsorbent-gas adsorbate is used as the working pair.

In 2018, Yunfeng Wang *et al*. [17] proposed an innovative SAC system that uses an active augmenting mass transfer approach based on the conventional basic cycle as depicted in Fig. 2.3. The working pair of the single-bed adsorption cooling system is composed of activated carbon and methanol and the comparative test were evaluated in the Kunming, China region. The experiment was conducted in a desorption process with and without enhancing mass transfer components. The system operating with the enhanced desorption process has a COP of 0.12, which is 21.6% greater than the system operated with the natural desorption process. The main disadvantages is that, the operation of the system is intermintent in nature and thus the performance is very low. The methanol used in the system is highly toxic and inflammable. The methanol has problem of the dissociation above 120^0C in the presence of copper. Therefore, the search for a new adsorbate which is non-toxic in nature, eco-friendly, and better desorption or adsorption characteristics is predominant in the adsorption cooling system.

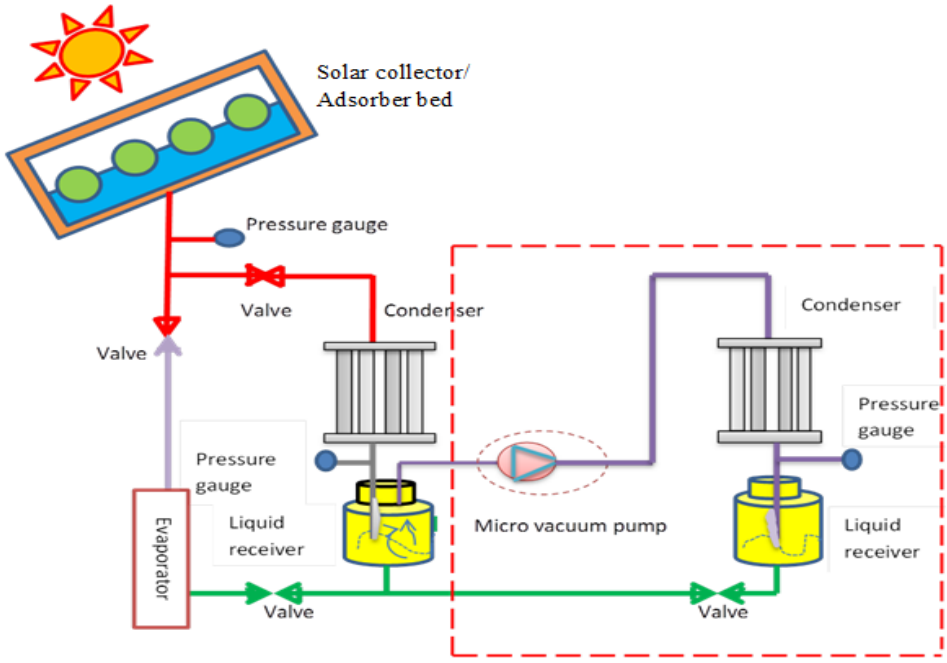

Fig. 2.3: Solar adsorption refrigeration system with and without enhancing mass transfer [17]

From the literature, it is clear that single-bed adsorption cooling systems with conventional working pairs are inadequate. This is due to the intermittent nature of the working cycle of the single-bed adsorption cooling system, as well as the low adsorption or desorption characteristics of the adsorbent towards adsorbate.

2.2 Two-bed Adsorption Cooling System

Single-bed adsorption cooling systems have only one adsorbent bed, resulting in an intermittent cooling effect. By employing two adsorbent beds, a continuous cooling effect can be produced, as indicated by Li's Patent [18], it is two beds cooling system, which produces continuous cooling effects, leading to better performance. It was observed that the performance of the two bed adsorption cooling systems significantly depending on its operating parameters and selection of working pair. Thus, the present section focuses on development in the two-bed adsorption cooling systems.

In 2009, Chang *et al.* [19] introduced a two-bed adsorption cooling system operated with solar energy for cooling application with silica gel-water as operating pair. At an average cooling capacity of 9 kW, the system achieved a COP of 0.37. They reported a SCP of around 72 Wkg^{-1} when operating with hot water at 80^0C and cooling water at 30^0C. Li and Wu [20] presented a cooling, heating, and power adsorption system that employed a two-bed adsorption chiller. Silica gel and water used as the adsorbent-adsorbate working pair. A transient model has been used to explain the system characteristics, which include one gas generator, a 10 kW adsorption cooling system, and water pumps. The maximum COP and cooling capacity of the system has been 0.44 and 7.9 kW respectively. Sadeghlu *et al.* [21] presented a simulation model of a two-bed adsorption cooling device that uses water as its adsorbate. The conservation of mass and energy balance equations were used to evaluate the performance of the system. Simulation shows that the cooling capacity of the system mainly depends on heat source temperature.

Ramesh *et al.* [22] developed a simulation model of a two-bed absorption refrigeration system operated with silica gel-water with lumped parameter method. They studied the importance of cycle time and system switching time for the enhancement of chiller efficiency. For a cycle time of 1600 s, the chiller cooling capacity of 5.95 kW was reported. Mahmoud *et al.* [23] designed an experimental set up of two-bed adsorption cooler operated by solar energy. The working pair used in the system was silica gel - water. Here the COP and SCP obtained has been 0.42 and 75 Wkg^{-1} for the hot water inlet temperature of 80^0C, the cooling water temperature of 25^0C and the chilled water temperature of 14^0C.

A standard two-bed adsorption cooling system with a storage tank has been studied by Rouf *et al.* [24]. The cooling system is connected to a storage tank, increasing cooling output by 24% with an increase of solar collector area by 57% when compared to direct solar collectors. The maximum cooling capacity of the system was 11.5 kW with the chilled fluid flow rate of 0.7 kgs^{-1} for the storage tank with a volume of 1 m^3 and cycle time of 1000 s. The cooling capacity of the system is also increased to a maximum of 16.1 kW, while the storage tank volume increases from 1 m^3 to 2.19 m^3, resulting in an 8% increase in overall daily cooling production when the solar collector area was 75.68 m^2.

The literature survey mentioned above is mainly focused on the system performance of single-bed and two-bed adsorption cooling systems. Two-bed SAC system is proved to be a better alternative for the single-bed system. Low COP, SCP, and heat and mass transfer are the primary barriers to the commercialization of two-bed SAC systems. Detailed research must be undertaken on the modification of the existing two-bed solar adsorption cooling system and the suitable selection and use of composite adsorbent.

2.3 Research Work in India

Various studies on solar adsorption cooling systems have been conducted in India. Various initiatives on adsorption cooling technology are currently underway in numerous regions of India, despite the fact that adsorption cooling systems did not receive the attention of Indian researchers. Kaushik *et al.* [25] conducted a comprehensive analysis of the solar adsorption cooling systems materials and collectors. Banker *et al.* [26] performed a performance study on the SAC system operated by using activated carbon and HFC-134a as working pair. The maximum COP attained in the study was 0.16. Anupam *et al.* [27] presented a model of a single bed adsorption cooling system, which uses activated carbon-carbon dioxide as the working media. Observations shows that the efficiency of the system depends on the pore volume and adsorption uptake of the adsorbent. The highest COP reported was 0.14. Even though there is a slight improvement in the performance of the SAC system further modifications are still needed for getting better performance related with conventional cooling system. Bry-air (Asia) Pvt. Ltd. introduced the first silica-gel water adsorption chiller system in India in 2015, with a cooling capacity of 40 kW and a low-grade heat source of 50^0C-100^0C. New Leaf Dynamic Technologies, India constructed

bulk milk coolers with $SrCl_2$-NH_3 as the working pairs of the system, paving the way for the innovation of an adsorption cooling system in the country.

2.4 Thermodynamic Modelling of Adsorption Cooling System

The first and second law of thermodynamics-based modelling of SAC systems are important to study the effect of various parameters on performance of the system. In recent years, a number of theoretical and experimental studies on SAC systems have been published. The simulation tools are used to empower in fixing the optimum conditions of the two-bed adsorption cooling system so as to obtain the best performance. Boelman *et al.* [28] presented a simulation model of an adsorption refrigeration cycle operated with waste heat at a near ambient temperature. The effects of operating temperatures (hot and cooling water), water flow rates, and adsorption-desorption cycle times were confirmed by the simulation programme. The most important parameter which effect the performance of the system is the operating temperatures, followed by water flow rates. In 2007, Saha *at al.* [29] established a simulation model to ascertain the effects of operating parameters on cooling effect and COP. The simulation study indicates the effect of operating temperatures (hot and cooling water), water flow rates, and adsorption-desorption time on the system's performance. The finding of the work shows that the operating temperatures plays a major role on the performance of the system.

Umair *et al.* [30] established a detailed simulation model for a continuous solar adsorption cooling system operated with a parabolic concentrator. The aim of the study was to investigate the system dynamic nature and compare the results to the performance of conventional refrigeration systems. The mathematical model for various components of the cooling system has been developed in MATLAB R2010b. They found that as the heat transfer coefficient between the compound parabolic concentrator and the adsorbent bed increases, so does the system efficiency. Fong *et al.* [31] studied the optimal parameters of the SAC system by simulation-optimisation method. For optimisation, the dynamic modelling of each part of the system was carried out using TRANSYS framework. The optimised model of SAC system has been determined, and the main energy consumption of the system was found to be 7.0%, which is lower than that of established in the general design method. An analytical model of an adsorption cooling system has been introduced

by Hassan *et al.* [32]. The system COP and SCP reported in the simulation work were 0.211 and 2.236 $kWkg^{-1}$, respectively.

Anyanwu [33] introduced a thermodynamic design procedure for the analysis of solid adsorption cooling system which uses the activated carbon-methanol, carbon-ammonia and zeolite-water as adsorbent-adsorbate pairs. The performance of the adsorption system in air-conditioning is primarily affected by condensation temperatures and evaporator temperatures. The experimental results indicate that zeolite-water can be the best working pair for air conditioning system because it has the lowest evaporator temperature in the air conditioning system. However, the maximum possible COP for activated carbon-methanol, activated carbon-ammonia, and zeolite-water were found to be 0.16, 0.19, and 0.30, respectively, which was very low when compared to conventional refrigeration systems.

Hussan [34] published a steady state thermodynamic differential analysis of the adsorption cooling system in late 2013. The system employs activated carbon and methanol as a working pair. The thermodynamic model of the system is based on first law differential analysis, which was used to analyse all energy interactions occurring in an ice maker which produces ice at -5^0C. In this system, the majority of the input energy, approximately 92%, was used as desorption energy. In 2017, Najeh Ghilen *et al.* [35] performed a numerical study of a cooling system operated with silica gel-water with mass recovery for an adsorption refrigeration chiller. The numerical simulation result has been found to be in good agreement with the experimental result.

Alahmer *et al.* [36] introduced a precise simulation model of a solar-powered adsorption refrigeration system utilising meteorological data from cities like Perth (Australia), and Amman (Jordan). The results shows that a 36.22 m^2 solar collector offers the COP of 0.49 and 0.47 for weather conditions at Perth and Amman, respectively. This maximum COP is achieved with a hot water inlet temperature of 80^0C and a flow rate of 0.33 kgs^{-1}. Rouf *et al.* [37] investigated the benefits of multiple bed adsorption refrigeration systems with limited solar energy. The investigation began with a three-bed adsorption refrigeration system functioning in series and then focused on a four-bed adsorption bed parallel system. The cooling capacity attained by the 3-bed distributed mass is 8.47 kW

with a cycle time of 800 s. Here the maximum SCP attained for the 4-bed parallel system is 150 Wkg^{-1} at its peak working hours.

Nikbakhti *et al.* [38] presented a lumped-parameter thermodynamic model for evaluating the performance of a newly integrated adsorption-absorption refrigeration system driven by low-grade heat sources. The COP and cooling capacity of the system was determined as 0.4 and 13.7 kW, respectively, which is higher when compared with the conventional adsorption cooling system operated with a hot water temperature of 65 ^{0}C. Alahmer *et al.* [39] evaluated the life cycle cost of adsorption cooling system with Payback Period and Life-Cycle Saving methodology. It is mainly used for evaluating the economics and to optimise the solar collector area for a two-bed silica gel-water adsorption cooling system in Perth, Australia. The cooling capacity of the chiller was determined as 11 kW at the peak hour 13 h. The solar COP and system COP are found to be 0.3 and 0.5, respectively.

From the above literature review, it is clear that there exists a few thermodynamic modelling of adsorption cooling system to study the effect of various influencing parameters on the performance of the system such as COP, SCP and cooling effect which plays a vital role for the design of the systems. However, there hasn't been any significant research on the transient analysis of two-bed ethanol-activated carbon adsorption cooling systems. Along with the detailed transient analysis of the system, the selection of proper working pairs also plays a vital role in the improvement of performance of the system. Detailed literature on the selection of working pairs, characteristics etc. are described in the following section 2.5.

2.5 Working Pairs of Adsorption Cooling System

Many investigations have been done in the last decades on the adsorbent-adsorbate working pairs effective for adsorption cooling systems, pointing out adsorption quality, their properties, and performance of the system. The popular working pair combinations are activated carbon-ammonia, activated carbon-methanol, zeolite-water, and silica gel-water. Table 2.1 gives the summary of SAC system operating with basic working pair. In 2003, Wang *et al.* [40] performed research on a specifically treated activated carbon - methanol and concluded that the solid bed with activated carbon had higher methanol

adsorption capacity than granular activated carbon and also required less time to adsorb. Guilleminot *et al.* [41] reported a COP of 0.12 for a SAC system that used activated carbon-methanol as working pair. Sumathy and Zhongfu [42] presented an experimental and theoretical investigation of an adsorption system working with an activated carbon-methanol pair. The system employed a solar collector (flat plate) with an exposed area of 0.92 m^2, produces the COP of approximately 0.1-0.12. Mortaza *et al.* [43] introduced a simulation model of a two-bed adsorption cooling system that utilised Zeolite 13X-water as the adsorbent-adsorbate pair. The adsorption cooling was evaluated by applying the conservation of mass and energy to various system components. The result obtained from this simulation showed that the cooling capacity of the system mainly depends on heat source temperature.

Palodkar *et al.* [44] investigated activated carbon and nitrogen adsorption conditions over a wide range of temperature and pressure. As the surface concentration increased, the heat of adsorption found to be decreases from 12.65 to 6.98 $kJmol^{-1}$ at 303K. Robbins *et al.* [45] presented an externally air-cooled adsorption cooling system that employs activated carbon as the adsorbent and ammonia as the refrigerant. The system's COP and SCP were determined to be 0.1 and 80 Wkg^{-1}, respectively. Chaudhari *et al.* [46] conducted experiments on a single bed adsorption system which uses activated carbon and ammonia as the working medium. The adsorption uptake of activated carbon was calculated as 0.22 $kgkg^{-1}$. At a maximum hot fluid temperature of 120^0C, the system produces a maximum cooling capacity of 50.67 W. The COP attained by the system was 0.097 during 62 mins of working time.

Dzigbor *et al.* [47] investigated a composite adsorbent that includes activated carbon and salt chloride. The performance of the composite adsorbent has been evaluated using a low and high grade ethanol and water working pair. For composite adsorbent with ethanol as refrigerant, they reported COP as 0.146 and SCP as 150 Wkg^{-1}. Cacciola *et al.* [48] introduced a new composite for adsorption cooling system made of activated carbon and polytetrafluoroethylene (PTFE) to improve the performance of the activated carbon with methanol. The carbon brick has been made by utilising PTFE as a binder and three different types of activated carbon were used. The specimen exhibited excellent mechanical qualities, a high adsorption capacity and a good thermal conductivity ranging from 0.13 to 0.20 $Wm^{-1}K^{-1}$.

Table 2.1 Summary of SAC system operating with basic working pair [5]

Working Pair	Author	Year	Application	COP	T_e (^{0}C)	Type
Activated carbon - Methanol	Delgado *et al.*	1982	Ice maker	0.16		Simulation
	Boubakri *et al.*	2000	Ice maker	0.05		Simulation
	Khattab	2004	Water cooler	0.16	-10	Simulation
	Anyanwu *el al.*	2005	Ice maker	0.18		Experimental
	Vasta et al.	2008	Ice maker	0.21		Simulation
	Hassan et al.	2011		0.02		Simulation
	Earle A Wilson *et al.*	2014				Simulation
	Himsar Ambarita	2016	Refrigerator			Experimental
	Noureddine Cherrad	2017	Ice maker			Experimental
	Sulaiman *et al.*	2012	Hybrid	0.62		Simulation
	Yunfeng Wang	2018	Refrigerator			Simulation
	Gaofei Yen *et al.*	2022	Refrigerator	0.12		Simulation
Activated carbon - Ethanol	Mhd Umair *et al.*	2014	Refrigerator			Simulation
	Palomba *et al.*	2017	Refrigerator			Experimental
	Astina *et al.*	2019	Ice maker	0.19		Experimental
Activated carbon- Ammonia	El Fadar et al.	2009	Refrigerator	0.18		Simulation
	Louajari et al.	2011	Refrigerator	0.11		Simulation
	Robbins *et al.*	2020	Ice maker	0.10		Experimental
	Ghazy *et al.*	2021		0.41		Experimental
Silica gel – water	Gurgel *et al.*	2000	Water cooler	0.18	12	Experimental
	Mayor *et al.*	2002	Ice maker	0.15	5	Simulation
	Brites	2013	Ice maker	0.07		Experimental
	Dechang Wang *et al.*	2014				Simulation
	Ntsonar *et al.*	2018	Water cooler	0.28		Experimental
	Ramy H Mohd. *et al.*	2018		0.23		Experimental
	Hongxuam Li *et al.*	2022	Refrigerator	0.36		Experimental
Zeolite - Water	Li *et al.*	2003	Refrigerator	0.27		Simulation
	Omisanya *et al.*	2012	Water Cooler	0.13	11	Experimental
	Diwaker Srivastava	2016		0.21		Simulation
	Cuneyt Ezgi	2021	Ice maker	0.38		Experimental
$SrCl_2$- Ammonia	Bansal *et al.*	1997	Refrigerator	0.81		Experimental
	Erhad *et al.*	1998		0.07		Experimental
	Qi	2005	Hybrid	0.07		Experimental

Animesh Pal *et al.* [49] experimentally investigated the adsorption of CO_2 by a consolidated composite of AC, Expanded Graphite Powder (EGP) and PolyVinyl Alcohol (PVA). The adsorption cooling system operated with the consolidated adsorbent produced a cooling effect per unit volume of 29 MJm^{-3} at 15^0C and 90^0C, respectively, which is 32% greater than the system operated with Maxsorb III-CO_2 as the working pair. Tso *et al.* [50] synthesised composite adsorbent from activated carbon, silica gel and $CaCl_2$. This composite adsorbent has the capacity of adsorbing 0.23 g of water per gram of the dry adsorbent at 900 Pa, which shows 933% improvement over parent material activated carbon. Calcium chloride is a chemical adsorbent, which helps to enhance the performance of the system because the change in enthalpy of hydration for $CaCl_2$ is much higher than the heat of adsorption of water on solid adsorbents. Chan *et al.* [51] investigated the effect of multi-walled carbon nanotubes (MWCNTs) in a zeolite 13X/$CaCl_2$ composite with a cycle time of 51 mins. When compared to the parent adsorbent, Zeolite 13X, the thermal conductivity of the composite adsorbent with multi-walled carbon nanotubes (MWCNT) (0.27-0.38 $Wm^{-1}K^{-1}$) increases significantly. This research will result in the development of composite adsorbents for the adsorption cooling system in order to improve its performance.

Wang *et al.* [52] introduced a new composite adsorbent made of $CaCl_2$ and expanded graphite powder for adsorption cooling system for making ice in the fishing boat. The composite adsorbent was found to be effective for the system because of its high thermal conductivity when compared with the parent adsorbent $CaCl_2$. This consolidate adsorbent has a thermal conductivity of 6.5-9.8 $Wm^{-1}K^{-1}$, which is 32 times greater than the parent adsorbate. The adsorption property of low grade ethanol onto the MIL-101Cr, metal-organic framework was explored theoretically and empirically by Saha *et al.* [53]. At 300^0C, the adsorbent has an uptake of 1.1 $kgkg^{-1}$ with ethanol, making it appropriate for the adsorption cooling system. It is clear from the literature that activated carbon and ethanol are the most effective combination for the adsorption cooling system. In addition, composite adsorbent can enhance both the absorption capacity and thermal conductivity of the parent material. The metal-organic framework (MOF) has a higher adsorption capacity due to its large surface area and pore volume. Despite their low thermal conductivity and high cost, metal-organic frameworks are new option for increasing refrigerant adsorption capacity. As a result, a suitable composite adsorbent-ethanol is required to design a composite adsorbent with increased adsorption capacity and thermal conductivity for

adsorption cooling systems. To make SAC system more compact and efficient, researchers are currently searching to develop composite adsorbent with better thermal conductivity and good volumetric adsorption uptake [54, 55].

2.6 Thermal Energy Storage Materials (TESM)

The occasional and unexpected occurrence of solar radiation leads to an imbalance between the rate and time of solar energy collection. This impacts the smooth operation of a continuous SAC system, thereby reducing the efficiency of the system. It is preferable to include TSEM in the system for the continuous operation and enhance its performance. The storage materials store excess energy and utilise it whenever heat energy is essential for the adsorption cooling system to operate. Eduard Oro *et al.* [57] introduced a newly developed high-temperature thermal energy storage with latent heat materials at the pilot plant built at University of Lleida, Spain for solar cooling applications. The pilot plant uses synthetic oil as the Heat Transfer Fluid (HTF) in the heat exchanger. The first stage of the work has been the selection of a suitable PCMs based on the temperature range. The chosen PCM was composed of hydroquinone and d-mannitol. The effective heat transfer when hydroquinone was used as PCM was 0.86, while d-mannitol achieved 0.88.

Nattaporn Chaiyat *et al.* [58] introduced the concept of using phase change material for improving cooling efficiency of an air conditioner system in the Thailand climatic condition. The thermal performance of Paraffin waxes with a melting point of 20^0C was evaluated by lowering the temperature at the evaporator coil. Using experimental data, a mathematical model of an air conditioner with PCM in the form of celluloid balls has been developed and validated. The model was used to evaluate the economic viability of the air conditioner and it was determined that the modified device utilised 3.09 kW less electricity. Amin Haighighi Poshtiri *et al.* [59] developed a PCM-integrated adsorption system for 24 hr cooling. The energy stored by the PCM during the day time is used to drive the system at night. A cooling channel has been utilised to decrease air temperature of the system. The airflow through the channel has been controlled by fans and differing ratios of fresh air (FR). Different parameters, including room temperature and maximum cooling demand, are estimated to determine whether thermal comfort can be attained. It is discovered that the system with PCM performs better than the system without PCM.

After reviewing the existing literature, it is observed that most studies are based on a single-bed adsorption cooling system utilising silica gel-water, zeolite-water, activated carbon-ammonia, or activated carbon-methanol. The refrigerant, water is considered to be a perfect adsorbate for the system but cannot be used in the chilling process below 0^0C. In the case of ammonia, it is considered to be highly toxic. Methanol is also considered to be highly toxic and inflammable and also indicates a dissociation problem at temperatures above 120^0C in the presence of copper. The continuous adsorption of water in the silica gel leads to the formation of hydroxyl group on the silica gel, which decreases the adsorption capacity of the adsorbent. The uptake quantity of water by silica gel is very low. The disadvantage of zeolite as adsorbent is its low adsorption uptake of water and the desorption temperature is higher than 200^0C. These deficiencies of the working pair urge a thorough investigation into new working pairs for the adsorption cooling system. Ethanol having low freezing point, non-toxic and zero ozone depletion potential is considered to be a better choice for solar adsorption cooling systems.

Mainly used adsorbent in the adsorption cooling system is activated carbon due to its attracting characteristics like good adsorption properties, high microporous structure, bulk density, specific heat, hardness, iodine number, ash content. Moreover, the affinity of activated carbon towards ethanol vapour make it more attractive as adsorbent in the adsorption cooling system when ethanol is used as the adsorbate. Ethanol can be easily desorbed by using low-grade energy sources such as solar energy or low-temperature waste heat. Its desorption temperature is also very low (60^0C to 100^0C). Here, the intermittent working nature of the single-bed adsorption cooling system reduced the performance of the system. This leads for developing a continuous operating or two-bed adsorption cooling system. Also, the work related to continuously operating cooling system is less when compared with single bed adsorption cooling system.

Transient study of the adsorption cooling system is a reliable way to investigate the effects of various parameters on the coefficient of performance, specific cooling power, and the refrigerating effect on the two-bed adsorption cooling system. No significant study on the transient analysis of the two-bed adsorption cooling systems operated with activated carbon-ethanol has been reported. The Simulink model of the adsorption cooling systems to investigate the transient effect are not yet studied in detail. Therefore, in this study, a theoretical model of continuous operating adsorption cooler has been developed and

simulated in the MATLAB Simulink environment to analyse the effect on adsorbent bed-cooling water, hot water temperature and mass inflow rate in the adsorption system. Simulink is a user-friendly software and involves only minimal simulation time compared to other software commonly used in adsorption cooling system. Numerous research on the energy analysis of single bed adsorption refrigeration systems by using various adsorbent-adsorbate pairs have been published recently. Although a few studies on the energy-efficiency of a two-bed solar adsorption refrigeration system with various working pairs have been published, the exergy analysis of a two-bed solar adsorption cooling system with activated carbon-ethanol has not been exhaustively studied. The study aids in determining the irreversibility of system components and helps in improving the efficient energy utilisation of a two-bed adsorption refrigeration system powered by solar energy. Hence there is a potential need to assess the energy-exergy of various critical system components in order to maximize energy utilisation. Thus, the primary objective of this research is to use the MATLAB platform to create a simulation model that can be used to determine the system performance based on the energy method and exergy destruction of various system components.

Nowadays, scientists are exploring composite adsorbent materials with improved thermal conductivity and high volumetric adsorption in order to enhance the performance of the adsorption cooling system and to make SAC more compact and efficient. According to the literature, the extremely porous adsorbent activated carbon powder exhibited superior ethanol adsorption capabilities, and there is an absence of accurate data on the ethanol adsorption characteristics of composite activated carbon. Therefore, another objective of this study is to develop and test composite adsorbents made from commercially available activated carbon. This work investigates the adsorption or desorption characteristics of activated carbon and composites constructed with MOF, expanded graphite powder, Silica gel, and PVP. The primary objective of this research is to create a more efficient consolidated adsorbent with a high adsorption capacity and thermal conductivity for use in solar adsorption cooling systems. The results will promote the use of SAC in areas with limited resources and pave the path for SAC to become more cost-effective and resource-efficient. In the meantime, energy storage for the solar adsorption cooling system for its continuous operation has been a challenge; therefore, the search for new energy storage materials for the system should be facilitated. It is believed that integrating the system with a solar collector and storing solar energy that may be used when solar energy is limited is

an alternate method for maintaining the continuous output from the system. Thus, selecting a suitable consolidated adsorbent–refrigerant pair coupled with a suitable energy storage material in the developed two bed adsorption cooling system is beneficial for improving the system's performance, such as COP, SCP, energy efficiency, and reducing the manufacturing cost.

Summary

This chapter presents an in-depth analysis of the state of solar adsorption cooling systems using various working pairs. The multi-bed adsorption cooling systems are more advantageous for improving the performance of the system. The next chapter envisages the objectives and methodology of the present work.

Chapter-3

Objectives and Methodology

The objectives and methodology of the present study are discussed in this chapter. The main goal of this research is to design and develop a two bed adsorption cooling system operated by solar energy. The work also focuses on the development of a new composite adsorbate for the current two bed adsorption cooling system.

3.1 Broad Objective

To design and develop a two-bed SAC system and select a suitable composite adsorbent for the better performance of the system.

3.2 Specific Objectives

The specific objectives of the present study are summarised as follows:

1. To carry out modelling of the two-bed SAC system with AC-ethanol as working pair to determine its performance.
2. To design, fabricate and conduct performance investigations of two-bed SAC system.
3. To select suitable consolidated adsorbent-adsorbate working pair through experimental investigation.

4. To investigate the performance of the system using consolidated adsorbent - refrigerant combination.

3.3 Conceptual Framework

The conceptual framework mainly consists of three sections, namely, study of adsorbent-adsorbate pair, working of SAC system and energy storage materials. Figure 3.1 depicts the conceptual framework of this study in detail. The present work primarily focuses on selection of adsorbent-refrigerant pair effective for the SAC system. The study includes simulation and an extensive experimental investigation to analyse the systems performance. Another goal of the study is to select a new consolidated composite adsorbent suitable for the two-bed adsorption system. The third section deals with the selection and integration of suitable energy storage materials for the SAC system.

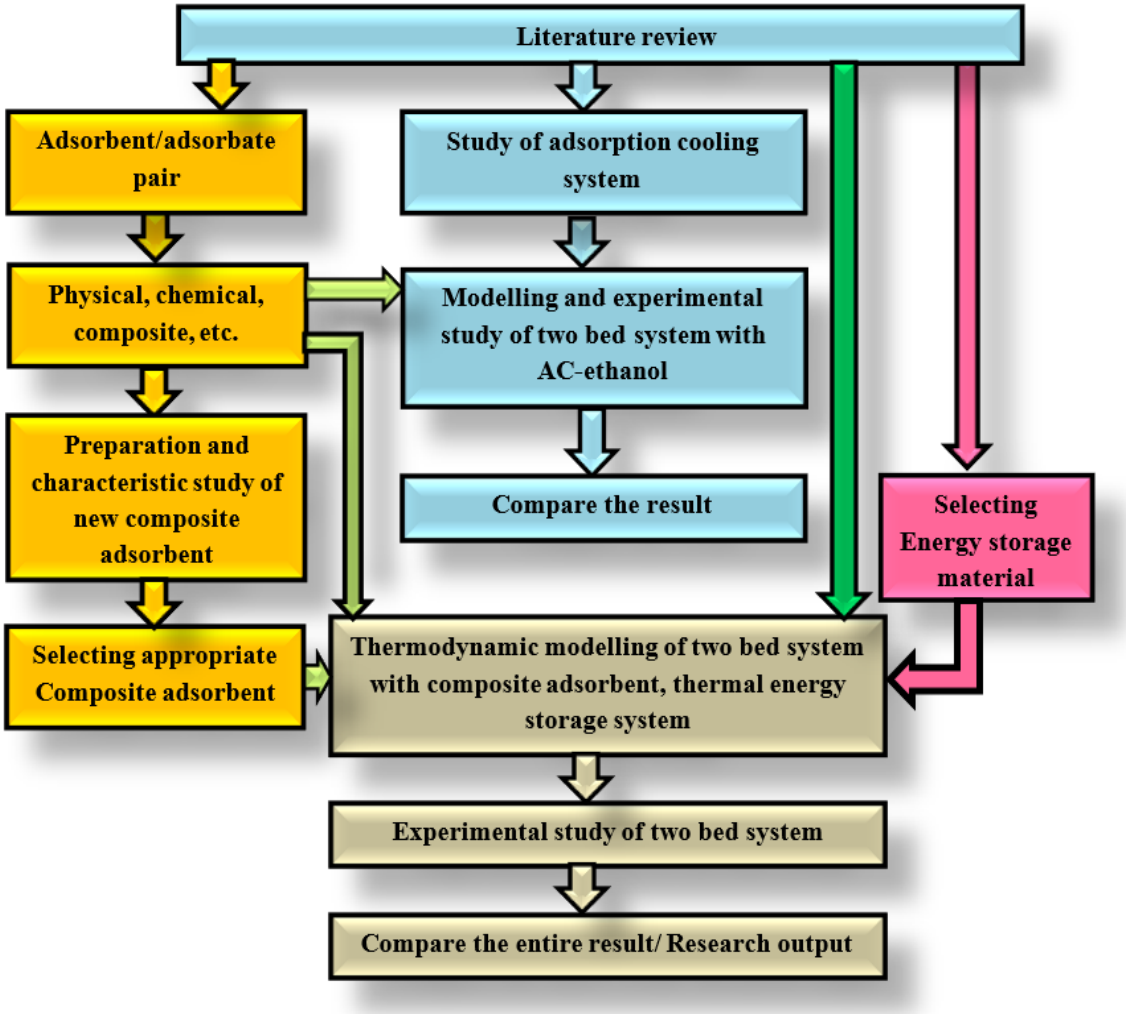

Fig. 3.1: Conceptual frame work of the present study

3.4 Methodology of the Present Work

The methodology of the current work is presented in this section and is depicted in the Fig 3.2. The preliminary part of the work is the selection of better working pair for the SAC system based on its adsorption capacity and affinity of the adsorbent towards the vapour adsorbate. Then transient and thermodynamic modelling of two-bed solar vapour adsorption cooling system is performed in SIMULINK. The inlet hot water mass flow rate and other varying conditions are mostly used to decide the performance of the system. The temperature profile of the adsorbent beds, condenser and evaporator are determined by using this model. The design and fabrication of components of the vapour adsorption cooling system, such as, an evaporator, condenser, adsorbent bed, and energy storage material tank, are also done. Experimental analysis and performance study of the system operating with activated carbon–ethanol is performed by varying the desorption temperatures.

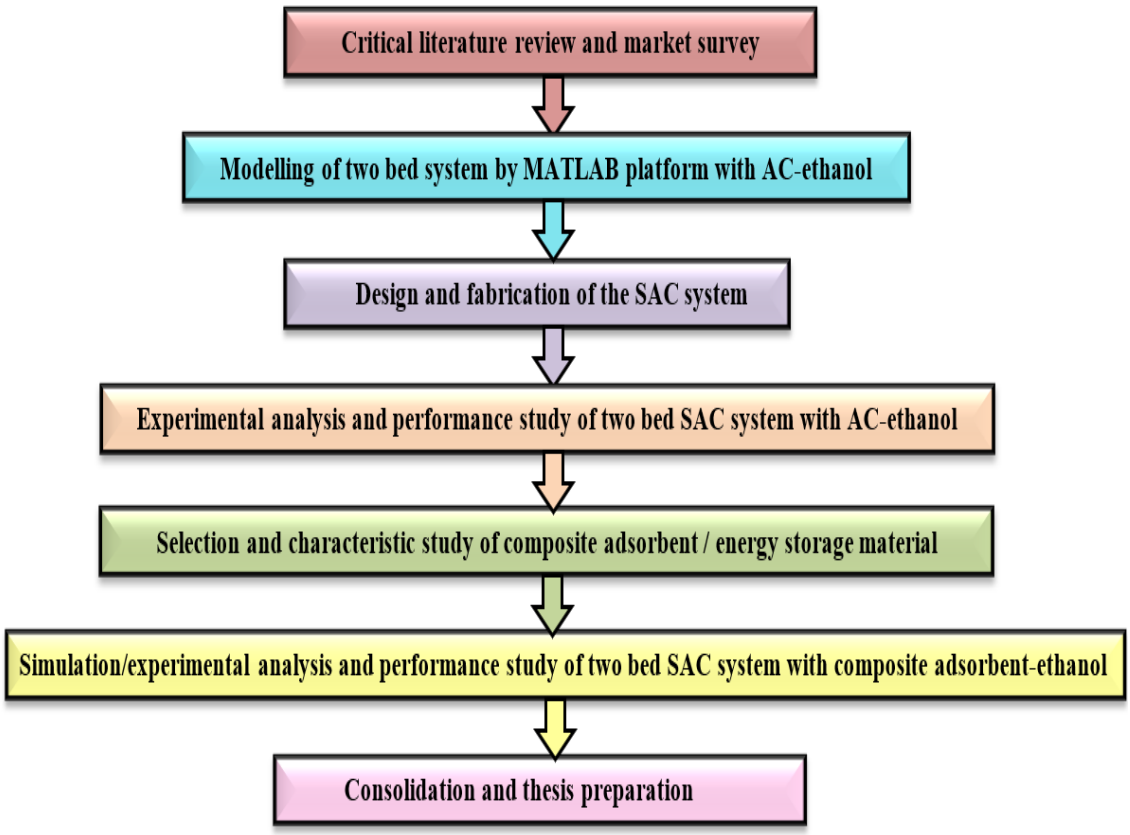

Fig. 3.2: Methodology of the work

The core part of this research work is to select proper additive materials to combine with the parent material to develop consolidated adsorbent. The selection of the material is done based on the pore volume, thermal conductivity, and adsorption rate. The composites are then subjected to a detailed characterisation study involving Brunauer-Emmett-Teller (BET) surface area, total pore volume, Thermo Gravimetric Analyser (TGA) to analyse the sample stability, Carbon-Hydrogen-Nitrogen-Sulphur (CHNS) organic elemental analyser. KD2PRO is the name of the instrument used to determine the thermal conductivity of the sample studied. The suitable energy storage material is also selected based on the desorption temperature of the system, negligible volume change, and chemical stability. In addition to that, it must have high thermal conductivity, better heat transfer rate, and low cost. The detailed performance investigations of SAC are conducted with selected composite and PCM to determine the performance parameters such as COP, specific cooling power (SCP), uptake, the effect of adsorption or desorption pressure, adsorbent bed pressure and the temperature, mass flow rate and heat source temperature. A comparative study is also performed to assess the performance enhancement in the SAC with PCM and consolidated adsorbent working pair.

3.5 Outline of the Thesis

The entire work of the thesis has been organized into nine chapters. The chapter wise summary of the proposed thesis as follows. The first chapter introduces the current energy scenario in the world and in India. The importance of solar energy as a heat source for cooling applications is also discussed in the chapter. The chapter also focuses on the significance and operation of an adsorption cooling system compared to a conventional refrigeration system. The aim and scope of the work is also detailed in this chapter. The second chapter presents the literature review on adsorption cooling systems. The section also details the development of single-bed and two-bed adsorption cooling system, and the national status of the adsorption cooling system. The chapter also tells the literature of different types of modelling used in the adsorption cooling system and working pairs used in the adsorption cooling system nowadays. The chapter outlines the study of the thermal energy storage system used for the low temperature application. The third chapter emphasises the objectives and methodology of the current work. The chapter includes a pictorial representation of the conceptual framework and thesis outline of the current study. The thesis's outline is also included in this chapter.

The fourth chapter highlights the selection of working pairs by studying the properties of various types of adsorbents, composite adsorbents, adsorbate, adsorbent or adsorbate pairs and their benefits and drawbacks. The chapter presents the selection of energy storage for the aforementioned system. The fifth chapter details the modelling of the adsorption cooling system which includes the transient as well as thermodynamic modelling of the SAC system operating with AC-ethanol. The results of the modelling are addressed in detail in this chapter. A comparative study of the SAC system operating with AC-ethanol with literature is also included in the chapter. The design, development and performance of the SAC system operating with AC-ethanol has been explained in the sixth chapter. The chapter details the various steps for designing the components of adsorption cooling system. The details of experimental work and the results obtained from the work is also included in this chapter.

Chapter seven presents the characteristics study of consolidated adsorbents in order to select a suitable composite adsorbent for the work. The chapter explains different methods used for determining the best composite material for the SAC system. The chapter also details the method for finding thermal conductivity of the material. The adsorption isotherm of the suitable composite adsorbent-ethanol pair with varying equilibrium pressure over the adsorption temperature is also included in this chapter. The chapter eight discusses the performance investigation of the SAC system operated with composite adsorbent-ethanol as working pair. The result obtained by thermodynamic modelling as well as the experimental results are included in this chapter. Moreover, a comparative study is detailed in this section. The chapter nine is the conclusion of the work which gives the outlook of the research work. The important outcomes of the present work and scope of the future work are also included in this chapter. The chapter describe the limitation of the system and further recommendations required to enhance the performance of the system.

Chapter 4

Working Pairs and Energy Storage Material

This chapter presents the selection of adsorbent-refrigerant pair of the adsorption cooling system. The different types of adsorbates, adsorbents and working pairs are explained in this chapter. The chapter also detail about various kinds of phase change materials that is effective for adsorption cooling systems and also envisages the procedure for selecting a suitable working pair and phase change material for the present study.

4.1 Choice of Adsorbents

When a liquid or gas attaches to the surface of a solid, the term "adsorb" is used. In this instance, the solid is referred to as an adsorbent. However, when one substance ingests another, the word “absorb” is used. Adsorbents can adsorb gases, chemicals, or vapour adsorbate and are primarily used in gas purification, gas separation, and adsorption cooling systems. The desirable characteristics of an adsorbent for adsorption cooling systems are outlined below [60, 61]:

i. The adsorbent must be able to adsorb a large quantity of vapour refrigerant

ii. Specific heat is low.
iii. High thermal conductivity to reduce cycle time.
iv. Better desorption property when heated with available heat source.
v. Safe to use chemically and physically with the chosen refrigerant.
vi. The adsorbents are non-toxic in nature, non-corrosive, low cost and easily available.

The most of the adsorbents are highly porous in nature, but this high porous structure produces very low thermal conductivity which limits the performance of the adsorption-based cooling system. The high porosity in turn causes the adsorption of refrigerant vapours in the porous part of the adsorbent [62]. Physical adsorbents, chemical adsorbents, metal organic frameworks (MOF), and composite adsorbents are the four types of adsorbents generally used in adsorption cooling systems. Adsorbents are classified according to the nature of the forces involved in the adsorption process, porosity, surface area.

4.1.1 Physical adsorbents

In physical adsorption or physisorption process the vapour refrigerant is adsorbed to the solid adsorbent matrix. A multilayer of adsorbate forms on the adsorbent primarily due to the Van der Waals forces that develop between the surface of the adsorbent and the molecules of the vapour. The heat of adsorption is of the order of i.e., ΔH_{ads} is 20-40 $kJmol^{-1}$. This force is weaker, less energy is required to desorb the adsorbate from the reactor bed (adsorbent). Figure 4.1 depicts the effect of temperature on adsorption uptake. Activated carbon, zeolite and silica gel are the most common physical adsorbents effective in adsorption cooling systems. This section describes the various types of physical adsorbents that are frequently employed.

(i) Silica gel

The silica gel appears to be an amorphous synthetic silica made of very tiny grains of hydrated SiO_4 [63]. Silica gel (Fig. 4.2) holds chemically bonded having small amounts of water between 2% and 3%, and it loses its absorptivity at temperatures above 120^0C, so it is generally used in systems with an operating temperature as low as 200^0C. Figure 4.3 depicts the structure of silica gel.

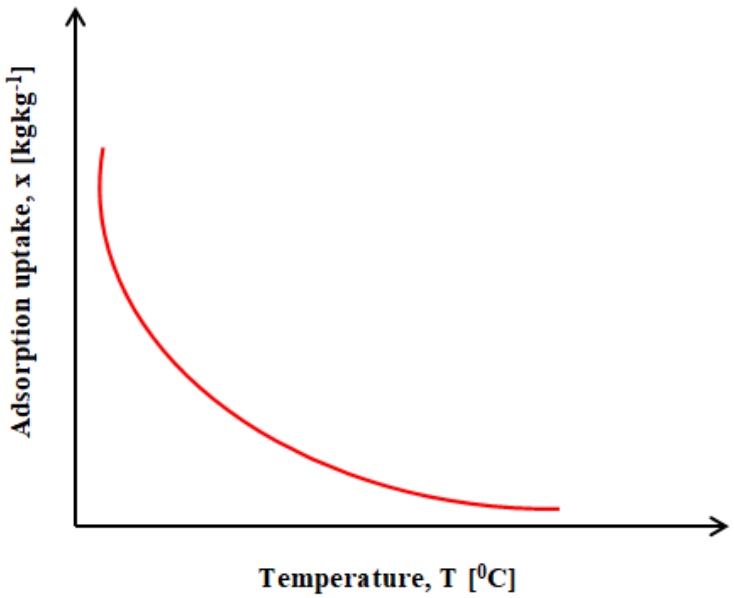

Fig. 4.1: Effect of temperature on the adsorption uptake in physisorption [6]

Fig. 4.2: Photograph of silica gel

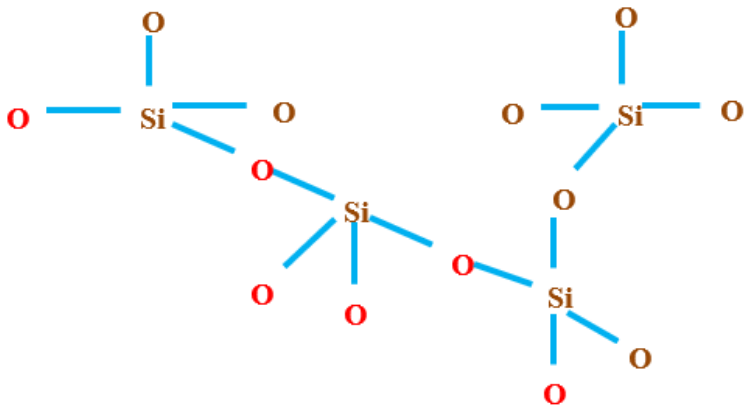

Fig. 4.3: Structure of the silica gel [6]

Silica gel is divided into type A and B based on pore size. Type A has pores of about 2 to 3 nm, and B gel has pores of about 0.7 nm, with a specific surface area of about 100 - 1000 m^2g^{-1} . The adsorption heat of silica gel is about 2800 $kJkg^{-1}$. In most cases, type A of silica gel is used in the desiccant systems applications, whereas type B is utilised in the places where the relative humidity exceeds 50%.

(ii) Activated carbon

Activated carbon is normally made as a powder or small pellets. It is an amorphous solid composed of micro crystallites with a graphite lattice and has a high porosity. It is non-polar and affordable. It is extremely combustible, which is one of its biggest drawbacks. Activated carbon can be manufactured from carbonaceous sources like coal (bituminous, subbituminous, and lignite), wood, peat, and nutshells (e.g., coconut – Fig. 4.4). The two stages of production of activated carbon are carbonization and activation. Drying and heating are required during carbonization in order to eliminate the byproducts from the raw material, such as tars and other hydrocarbons, and to drive off any gases created. The material is heated to between 400 and 600^0C during carbonization, and combustion is prevented by the lack of oxygen in the atmosphere. The carbonised particles are "activated" by subjecting them to a high-temperature oxidising agent, typically steam or carbon dioxide. During the carbonization phase, this agent burns away the pore-blocking structures, resulting in a porous, three-dimensional graphite lattice.

Fig. 4.4: Photograph of coconut shell based granular activated carbon

The shape of the pores is determined by the length of time they spend during the activation process. Pore sizes expand with increasing exposure time. The most commonly used aqueous phase carbons have excellent abrasion resistance, pore size distribution, and low cost, but their efficiency in each application must be evaluated to determine the best product. Activated carbon is generally used for the adsorption of organic substances and non-polar adsorbates, as well as for waste gas treatment [63]. It is the most widely used adsorbent. Its utility stems primarily from its high surface area, large micropore and mesopore volumes. The microcrystal for activated carbon generates a hexagonal carboatomic ring, and the functional groups connected to the carboatomic ring influence adsorption performance.

Following are the main forms of activated carbon (Fig. 4.5):

i. Granular Activated Carbon (GAC) is the irregularly shaped particles between 0.2 and 5 mm in size. This type is employed in liquid purification and gas separation applications.
ii. Powder Activated Carbon (PAC) is a type of carbon powder with most of its particles being less than 0.18 mm in size. These are utilised primarily for liquid and flue gas treatment applications.
iii. Pelleted Activated Carbon is extruded and cylindrical in shape with diameters between 0.8 and 5 mm. These are typically used in gas phase applications due to their low pressure drop, high mechanical strength, and low dust content.
iv.

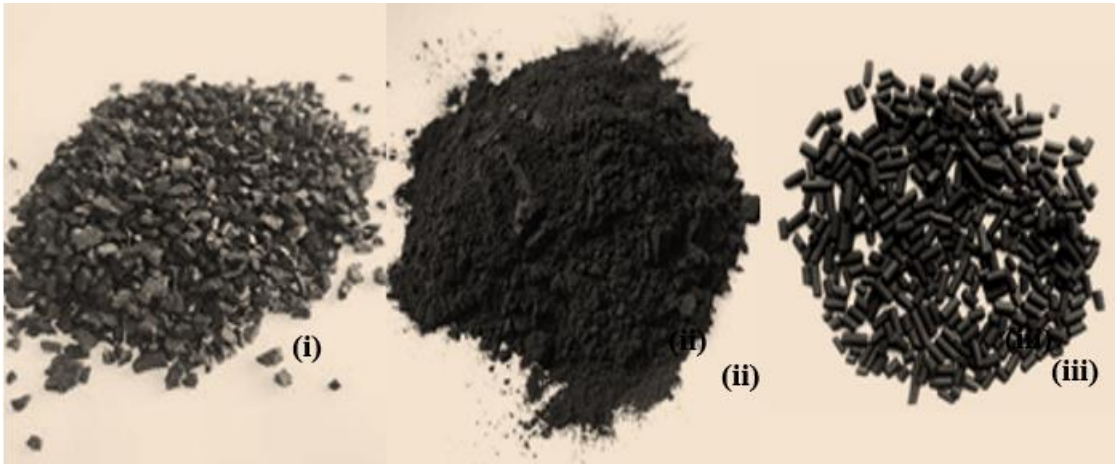

Fig. 4.5: Forms of activated carbon - (i) Granular activated carbon (ii) Powder activated carbon and (iii) Pelleted type activated carbon

(iii) Zeolite

Zeolite is an alumina silicate crystal with a porosity of 0.2 to 0.5 cm^3g^{-1} that forms in alkaline/alkaline soil. The adsorption capacity of zeolite is determined by the relative amounts of aluminium and silicon in the material. The tetrahedral structure of the zeolite is shown in Fig. 4.6. Natural zeolites is available in 40 different types, while as the synthetic zeolites is available in 150 different types. The synthetic zeolite transfers heat more effectively and has a relatively high specific weight. The zeolite has a cage structure with six casement sections connecting them, which enables it to adsorb lots of extra molecules [64]. Most zeolites sustain their adsorption and regeneration characteristics up to 500^0C, while synthesised zeolites can resist temperatures as high as 800^0C. Zeolite has an adsorption heat of 3300 - 4200 $kJkg^{-1}$ and is frequently used in adsorption air cooling systems that require regenerating temperatures of 200 - 300^0C.

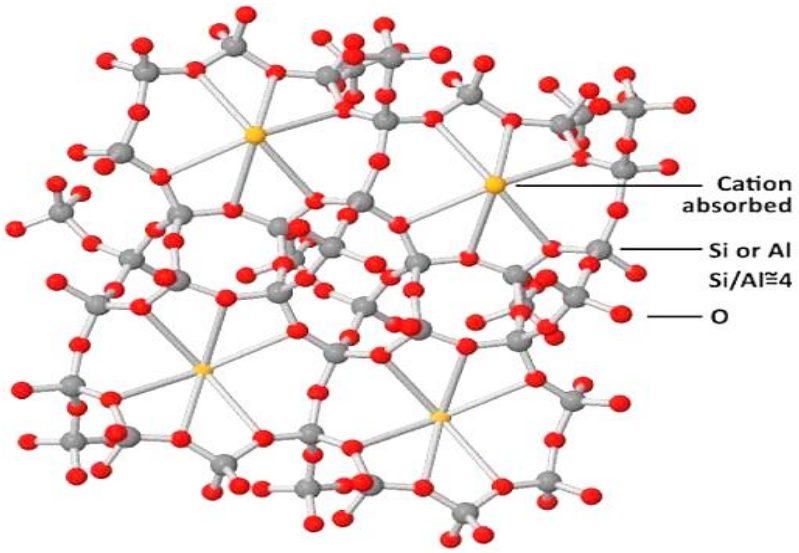

Fig. 4.6: The tetrahedral framework of zeolite [65]

4.1.2 Chemical adsorbents

In chemical adsorption or chemisorption, the refrigerant molecules are held to the surface of the adsorbents by chemical bonds. Chemical adsorption involves atom rearrangement, electron transfer, oxidation, hydrogenation, and the formation or fracture of a chemical bond. The chemical adsorbent and the refrigerant make a stronger connection,

and the adsorbent forms a monolayer on the adsorbate. It has high enthalpy of adsorption i.e., ΔH_{ads} is 200-400 kJmol^{-1}. Since the bond is stronger, more heat energy is needed to break the bond to desorb the refrigerant particles. Chemisorption increases first and then decreases as temperature rises and are illustrated in Fig. 4.7. In comparison to physical adsorbent, this type of metal chloride possesses a greater adsorption capacity. However, it may have disadvantages, such as requiring more energy to remove the adsorbent than physical adsorbent. In addition, its performance degrades due to salt swelling on the bed as a result of repeated adsorption or desorption processes. Table 4.1 gives comparison between the physical and chemical adsorption for the adsorption chiller application.

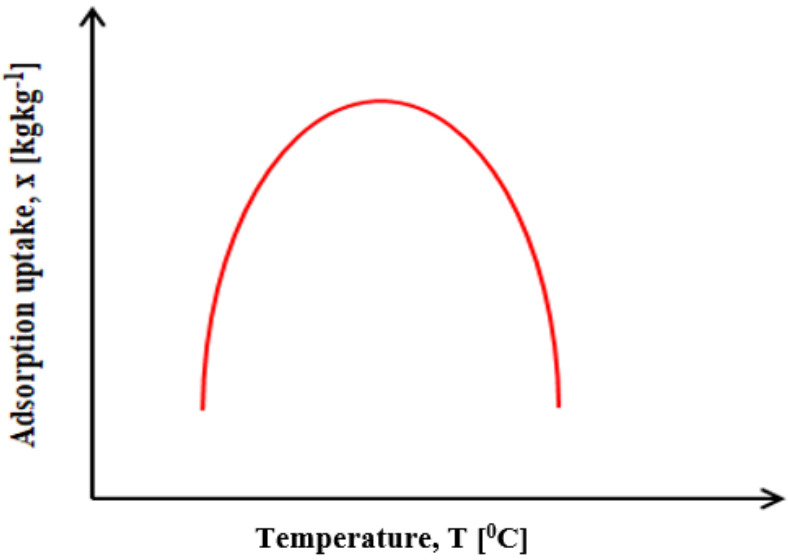

Fig. 4.7: Effect of temperature on the adsorption uptake in chemisorption [6]

(i) Metal chlorides

Calcium chloride ($CaCl_2$), magnesium chloride ($MaCl_2$), strontium chloride ($SrCl_2$), barium chloride ($BaCl_2$), manganese chloride ($MnCl_2$), and cobalt chloride ($CoCl_2$) are frequently used in adsorption cooling systems. Although metal chloride has a strong adsorption uptake of up to 1 kgkg^{-1}, the swelling and agglomeration that occur during adsorption have a detrimental effect on heat and mass transfer [66,67].

(ii) Salt and metal hydrides

Salt and metal hydrides, like lithium hydrides , calcium hydrides, and covalent high polymerized hydrides, have promising uses in hydrogen-based adsorption cooling systems [5].

Table 4.1 Comparison of Physical and Chemical adsorption

	Physical adsorption	**Chemical adsorption**
Forces	Physical (weak Van der Waals H bonds)	Covalent bond
Adsorption Heat	20 - 40 $kJmol^{-1}$	200 - 400 $kJmol^{-1}$
Number of layers	Several layers are possible during condensation	One layer
Reversibility	Easy (vacuum, temperature)	Reversibility is difficult
Adsorption rate	Adsorption rate is very high (s)	Adsorption rate is slow at low temperature and are fast at high temperature

(iii) Metal oxides

Metal oxides are frequently used as catalysts in oxidation and deoxidation reactions, as well as adsorbents in adsorption heat pumps that use oxygen as a refrigerant. Due to the high enthalpy of reaction between oxides and oxygen, metal oxide-oxygen pairs are appropriate for cryogenic heat pump applications at temperatures below $-153.15^{0}C$ [66].

4.1.3 Metal Organic Frameworks (MOF)

The metal-organic framework (MOF) is a novel adsorbent for use in adsorption refrigeration. The property of large surface area, large porosity, and favourable internal geometry, the MOF was selected as an adsorbent. MOFs have a high surface area (1000-10,000 m^2g^{-1}) and a porosity (void volume) that is often greater than 50% as compared to

physical adsorbent, making them superior adsorbents. MOFs are open crystalline structures made of inorganic metal ions and organic linkers. The most frequently used organic bonds are organic carbo-Xylates, whereas the inorganic component is the metal-containing unit defined as second building unit of the MOF. The available MOF for the adsorption cooling system are MIL-101Cr, MIL-100Fe, MIL-53Cr, MIL-100Al, MIL-53Al, Cu-BTC, Fe-BTC and CPO-27Ni [67].

4.1.4 Composite adsorbents

Adsorbents that can be obtained by the combining two or more adsorbents , such as a combination of metal chloride and expanded graphite, zeolite, or silica gel, are referred to as composite adsorbents. Simple mixture, impregnation methods, and mixture/impregnation and consolidation are the methods used to develop the composite [68]. The resulting mixture is heated and dried to remove water, yielding composite adsorbent. The primary objectives achieved by preparing composite adsorbent are as follows:

i. Enhance the heat and mass transfer capacities of the expanding chemical adsorbent during the adsorption process.
ii. The additives added to the composite adsorbent primarily improves the porous structure and thermal conductivity of parent material.
iii. Increase the physical adsorbents adsorption quantity.

4.2 Choice of Adsorbate

For a better outcome, the refrigerant or adsorbate of the adsorption cooling systems should meet the following criteria [69]:

i. In the liquid state, the adsorbent should have high latent heat of vapourisation
ii. Very high thermal conductivity
iii. It specific volume is low
iv. Adsorption effect can be improved by reducing the molecular size
v. Viscosity is very low
vi. Chemically stable at all operating temperature

vii. The adsorbate does not cause toxicity, flammability, or corrosion

viii. Environmentally friendly

The adsorbate or refrigerant of the adsorption system ought to have no negative environmental effects. The frequently employed refrigerants are water, methanol or ammonia which have low specific volume in the order of 10^{-3} m^3kg^{-1} and high latent heat values of 2260, 1368 and 1160 $kJkg^{-1}$, respectively. Water is the easily available adsorbate, but it is not used for cooling below 0^0C [70, 71]. Water, followed by methanol and ammonia, is the most thermally stable adsorbate. Comparing it to water and methanol, ammonia is more toxic and corrosive. At the required operating temperature, methanol can operate at sub atmospheric pressure, so any infiltration of ambient air into the system causes it to malfunction. Ethanol is another promising refrigerant for adsorption cooling systems. Furthermore, the high affinity of activated carbon for ethanol makes it more appealing to use ethanol as an adsorbate in adsorption cooling system.

4.3 Working Pairs

Several experimental and theoretical research have been undertaken over the past few decades to find improved adsorbent-adsorbate materials for adsorption refrigeration systems. Activated carbon-methanol, activated carbon-ammonia, zeolite-water, and silica gel-water are the most commonly used adsorbent-adsorbate pairs of the adsorption cooling system [71]. The adsorbent-adsorbate pair for the SAC system must have the following properties:

i. Adsorbate has a high latent heat of evaporation

ii. A thermodynamic operating pair with excellent efficiency

iii. There is a low heat of desorption at the operating pressure and temperature

iv. The absorbent material doesn't conduct heat very well

The most frequently used operating pairs in SAC system are detailed here. Table 4.2 shows various working pairs commonly used in adsorption cooling systems.

4.3.1 Silica gel-water

The silica gel is thermally stable, highly porous and non-hazardous, with the low desorption temperature of 50^0C, making it suitable for solar adsorption cooling applications

Table 4.2 Various working pairs used in adsorption cooling system [5]

Adsorbent	Refrigerant	ODP	GWP
Activated carbon	Water	0	0
	Ammonia	0	0
	H_2	0	5.8
	N_2	0	-
	Methanol	0	0
	R113	0.8	5000
	R114a	0.11	630
	R143a	0	1300
Silica gel	Water	-	-
Zeolite	Water	-	-
	Ammonia	-	-
	Methanol	-	-
	CO_2	-	-
$CaCl_2$	Ammonia	-	-
	Water	-	-
$SrCl_2$	Ammonia	-	-
Zeolite+$CaCl_2$	Water	-	-
Graphite+$CaCl_2$	Ammonia	-	-

[70]. The primary disadvantage of this working pair is that the adsorbate loses 4% to 6% (by weight) of water during each adsorption process. If this hydroxyl group is removed from the silica gel and its adsorption capacity reduces. As a result, the desorption temperature of the system cannot be higher than 120^0C. Another disadvantage of this pair is its low adsorption quantity of approximately 0.2 $kgkg^{-1}$. Furthermore, due to the freezing point of water, the evaporator cannot be used at temperatures below 0^0C [5].

4.3.2 Zeolite-water

The zeolite-water combination is used for dehumidification and adsorption cooling [70]. This pair has a higher heat of adsorption than silica gel-water. Since this working pair is more stable at high temperatures, the system can recover heat at temperatures greater than 200^0C. Due to the high adsorption heat and adsorption or desorption temperatures, this cannot be employed in low-temperature heat source applications. Zeolite-water desorption temperature varies between 250 and 300^0C. Desorption performance is adequate within this temperature range. The range of the heat of adsorption is 3300–4200 $kJkg^{-1}$.

4.3.3 Activated carbon (AC)-ammonia

At 30^0C, the latent heat of ammonia is approximately 1,365 $kJkg^{-1}$. The operating pressure of the cooling system with this operational pair is approximately 1,600 kPa [70] at a condensing temperature of 40^0C. Pipe diameter and heat exchanger size are small due to the high working pressure. AC–ammonia pairs have an adsorption heat in the range of 2,000 to 3,000 $kJkg^{-1}$ and can be utilised at temperatures exceeding 200^0C. Ammonia is poisonous, has a distinct odour, and is naturally corrosive.

4.3.4 Activated carbon (AC)-methanol

Methanol has a maximum adsorption quantity of 0.45 $kgkg^{-1}$ on activated carbon, and the latent heat at 33^0C is approximately 1429 $kJkg^{-1}K^{-1}$. At or above 120^0C, activated carbon acts as a catalyst to decompose methanol to dimethyl ether. Furthermore, because the system is operating at sub-atmospheric pressure thus the outer vessel of the bed must be hermetically sealed [5].

4.3.5 Metal chlorides-ammonia

The principal disadvantage of the metal chlorides-ammonia working pair is that it requires more heat energy to desorb the adsorbate from the adsorbent when compared with physical adsorbents. Continuous adsorption or desorption of metal hydrates diminishes their adsorption property due to salt swelling and agglomeration, which is an additional disadvantage of this type of working pair.

4.3.6 MOF-water

The MOF, MIL-101Cr shows a higher water adsorption rate for a relative pressure of 0.9 and is about 1.43 $kgkg^{-1}$. The Branauer-Emmett-Teller (BET) surface area of MIL-101Cr is 3017 m^2g^{-1} and it shows better thermal stability towards water [67]. The water adsorption rate MOFs of aluminium fumarate and CPO-27(Ni) has been 0.53 $kgkg^{-1}$ and 0.47 $kgkg^{-1}$ respectively for a relative pressure of 0.9.

4.3.7 Composite adsorbents-water

$CaCl_2$ and silica gel have been employed as a composite adsorbent for the adsorption of refrigerant water in the adsorption refrigeration system [67]. This combination has achieved a maximum uptake of 0.5 $kgkg^{-1}$ at 31^0C and 2 kPa, which helps to increase the COP and SCP of the system. In the instance of water adsorption, a mesoporous adsorbent is an excellent candidate for the adsorption process. Due to its mesoporous structure, the combination of type B silica gel with LiCl is now a viable alternative for the absorption of water when compared to other types of silica gel and hygroscopic salts. The composite adsorbent Alumina+Zeolite 13X absorbs 0.35 kg kg^{-1} of water.

4.4 Selection of Working Pair for the Experimental Work

The efficiency of the SAC system is dependent not only on the design of the adsorbent bed, but also on the choice of working pair. Therefore, judicious selection of the working pair improves system performance. The common working pairs of the SAC system have their own advantages and disadvantages. This section considers the proper selection of working pairs for the present study. The selection of working pair for the composite adsorbents are also detailed in this section.

4.4.1 Activated carbon (AC)-ethanol

The size of the molecules in the adsorbent bed, high latent heat of vapourisation, high thermal conductivity, nontoxic, non-corrosive, non-flammable, and environmentally friendly are all factors in the selection of adsorbate for the adsorption cooling system.

Water, ammonia and methanol are considered to be perfect adsorbates for adsorption cooling systems. Water cannot be used for the applications below 0^0C, whereas ammonia is highly toxic. Methanol is highly toxic and inflammable and it also has the dissociation problem above 120^0C in the presence of copper. Therefore, an environment friendly refrigerant with better adsorption or desorption characteristics needs to be explored in detail.

Among natural refrigerants/adsorbates such as ammonia, water, methanol, ethanol is interesting to be applied due to friendly environment effect on global warming and ozone depletion potentials. Ethanol is a flammable, colourless liquid with a faint odour. It burns with a blue flame that is smokeless and sometimes difficult to see in daylight. Moreover, ethanol has the boiling point of 78.24^0C and good adsorption property with activated carbon make this working pair more attractive for the SAC system. Most cases the solar adsorption cooling system are operating below 100^0C makes the said operating pair for solar adsorption refrigeration system nowadays. The easy availability and low cost make activated carbon as good option as the adsorbate for the adsorption cooling system. According to the American Society of Heating Refrigeration and Air-Conditioning Engineers (ASHRAE) the refrigerant ethanol lies in the A2L group which have lower flammability, non-toxic in nature, can be operates below 0^0C and high affinity of activated carbon towards vapour ethanol make more attractive as the operating pair for the SAC system [72].

The most frequently used adsorbents nowadays are silica gel, zeolite and activated carbon. When natural zeolite as the adsorbent, the system needs a large quantity because at operating temperature the desorption quality of the vapour refrigerant from the adsorbent is very less. However, it is used for the solar cooling application because of its non-linear pressure dependence. But the silica gel and activated carbon shows almost linear pressure dependent isotherms. Here the silica gel satisfies the above criteria of deterioration phenomenon of the adsorption capacities and aging causes to rethink for using the silica gel as the adsorbent. The activated carbon is a commonly used adsorbent for the SAC system due to its extremely good porous property and large surface properties. The activated carbon is a physical adsorbent and hence a lesser quantity of heat is required for the desorption of vapour refrigerant from the adsorbent. Moreover, the easy availability and low cost makes activated carbon as a favourable choice in the SAC system. Also, the

adsorption and desorption capacities of activated carbon are good compared to ordinary carbon and the high affinity of activated carbon towards ethanol vapour makes it selected as the adsorbent-refrigerant pair for the initial study of the research work. The ethanol and activated carbon have the following properties:

Adsorbate: Ethanol

i. Good adsorption rate with activated carbon
ii. High latent heat of vaporization
iii. Low freezing point (-114^0C)
iv. Zero ODP and low GWP
v. It can be quickly removed from the surface with a low-grade heat source

Based on ASHRAE ethanol lies in A2L Group with lower flammability and nontoxic in nature.

Adsorbent: Activated carbon

i. Ease of availability
ii. Large surface area
iii. Extremely high pore size and pore volume
iv. Stable and inert to alcoholic agents
v. High adsorption capacity

4.4.2 Selection of component materials for composite adsorbent

The consolidated or composite adsorbent is a mixture of two or three adsorbents with suitable binder in correct proportion. The presence of component materials in the right proportion will enhance the thermo-physical properties, leads to the improvement in the performance of SAC system. The improvement in the heat transmission of the adsorbent materials employed in the adsorbent bed is the most effective ways of enhancement of the performance of the SAC systems. Consolidated/composite adsorbents is one of the best method to improve the heat transfer in adsorber or desorber reactors. When compared to the parent adsorbents, the composite adsorbent has better surface features, thermo-physical properties and higher adsorption rate than single adsorbents which improves the surface as well as physical characteristics of parent adsorbate and thus to improve the performance

indices of the SAC system. The poor thermal conductivity of activated carbon and the low performance of the system helps to search for new component materials for developing new consolidated adsorbent for the proposed system with activated carbon as the parent adsorbent. Thus, the defects of the parent material can overcome by forming composite by adding Metal Organic Framework (MOF) MIL-53Al, EGP, Silica gel (SG) and Polyvinyl Pyrrolidone (PVP) as the additives. The property of the selected materials for the composite preparation are detailed in Table 4.3.

Table 4.3 Property of selected material for composite adsorbent preparation

Sl.No.	Material	Property
1	Expanded Graphite Powder [EGP]	Porosity is very high Density is very low Good thermal conductivity
2	Metal Organic Framework [MOF] MIL-53Al	High specific surface area Pore volume is large High chemical stability
3	Silica gel [SG]	High specific surface area
4	Polyvinyl Pyrrolidone [PVP] (Binder)	High thermal conductivity when compared with other types of binders

The MOF-MIL-53Al, one of the components for the composite adsorbent, is made of infinite trans chains of corner-sharing $AlO_4(OH)_2$ octahedra connected by 1,4-benzenedicarboxylate ligands (Fig. 4.8). This MOF have diamond-shaped frame work of one-dimensional channels which helps to adsorb small molecules into the structure. MIL-53 (Al) shows good stability and it can resist hydrolysis both in neutral and acidic conditions. MIL-53 (Al) is proved to be as the better MOFs for having good structural stability in aqueous solutions. Additionally, this MOF has significant pore volume, excellent chemical stability, high thermal stability, and the good surface area, contributes to the selection of the MOF as a component material for the AC in this composite production [73,74]. EGP is utilized to improve thermal conductivity of the parent adsorbent, since it possesses high porosity and low-density features [75].

Silica gel is a non-toxic, odourless, non-corrosive substance with excellent thermal stability and less heat of adsorption as compared to the activated carbon. The advantage of

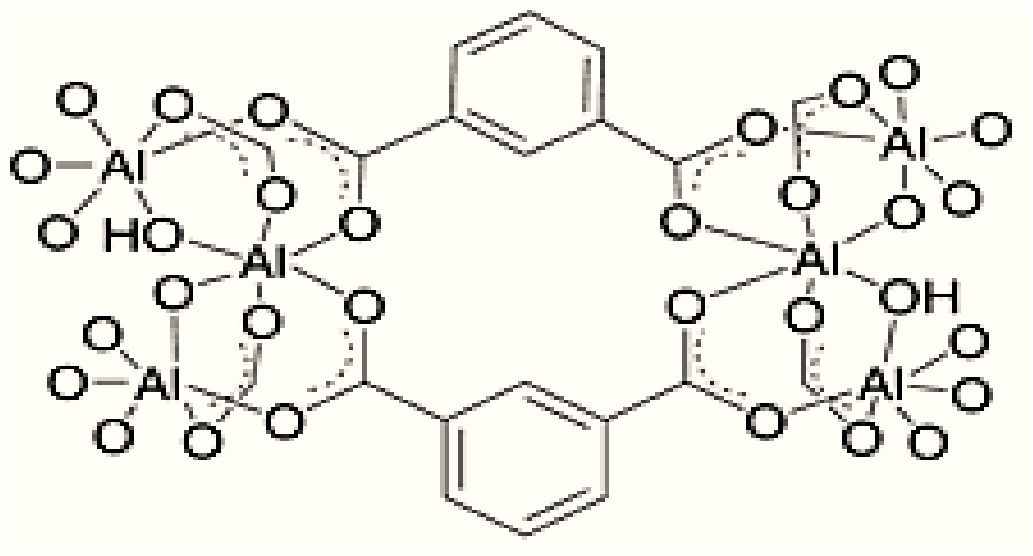

Fig. 4.8: Structure of MIL-53Al [76]

SG over AC is its lower adsorption heat, which increases the adsorption rate. Furthermore, SG has a greater adsorption rate than AC in high concentration refrigeration for adsorption cooling applications [78,79]. Polyvinylpyrolidone (PVP), which has a good thermal conductivity as compared to other types of binders, is employed in this preparation [80]. Table 4.4 lists the physical properties of the additive materials, and Table 4.5 outlines the BET surface area and pore volume of the base material and the other materials used to make the composite adsorbents for this study.

4.5 Energy Storage Material - Phase Change Material (PCM)

A preliminary study on the utilisation of PCM with SAC devices are proposed here to overcome the sporadic nature of SAC systems. This section describes the different types of PCMs and their characteristics. Energy storage not only decreases supply-demand mismatches, but it enhances the efficiency and contributes significantly to energy conservation. The PCM are heat storing materials that are "latent". PCMs are divided into four types: solid-solid, solid-liquid, liquid-vapour, and solid-vapour. Solid-liquid PCMs initially behave like conventional materials, with temperatures rising as heat is absorbed. Unlike typical (sensible) storage materials, PCM absorbs and releases heat at relatively consistent temperatures. Compared to common storage materials like water, masonry, or rock, they are able to store 5 to 15 times more heat per unit volume. A PCM can store and

Table 4.4 Physical parameters of additive materials

Material	Thermal conductivity ($Wm^{-1}K^{-1}$)	Density (kgm^{-3})	Specific heat capacity ($kJkg^{-1}K^{-1}$)	Thermal diffusivity (mm^2s^{-1})
Expanded Graphite	1.25	2260	0.79	0.7
MIL-53 Al	0.46	400	0.96	1.2
Silica gel	0.01	700	0.85 to 1.10	0.01 to 0.02
PVP (Binder)	1500	1200	-	-

Table 4.5 BET surface area and pore volume of the base material and materials used in producing the composite adsorbents for the present study

Base material	Total BET surface area [m^2g^{-1}]	Total pore volume [cm^3g^{-1}]
Activated carbon	1050 ± 25	0.62
Expanded graphite powder	37 ± 2	0.04
Silica gel	802 ± 15	0.27
MIL-53 Al	1830 ± 29	0.74
PVP	146 ± 3	0.12

release a lot more energy than sensible heat storage by melting and solidifying at the phase change temperature (PCT). When a substance undergoes a phase change, such as from solidto liquid or vice versa, or when its internal structure alters, heat is absorbed or released [81, 82]. The processes that occur in the PCM material during the energy storage and energy removal are depicted in Fig. 4.9. The storage capacity of the PCM based on temperature is represented in Fig. 4.10. The PCM is classified based on the melting temperature, as illustrated in Fig. 4.11.

4.5.1 Properties of PCM

The PCM is used to design the thermal-storage systems with the thermal, physical and chemical properties.

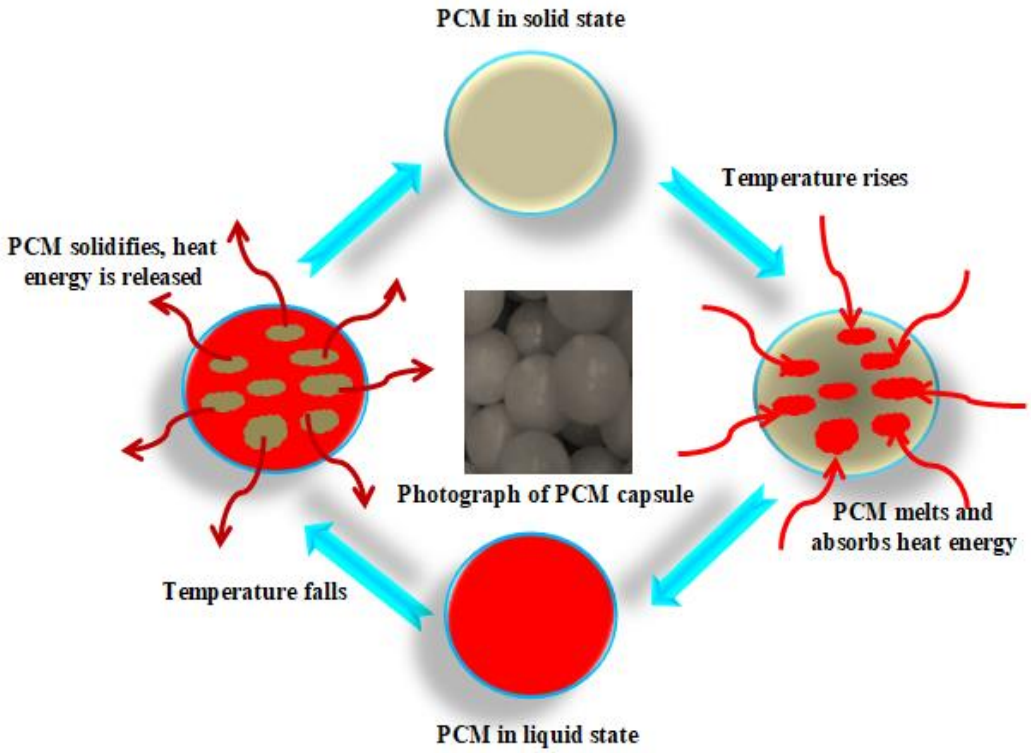

Fig. 4.9: Different processes during the phase change in PCM [82]

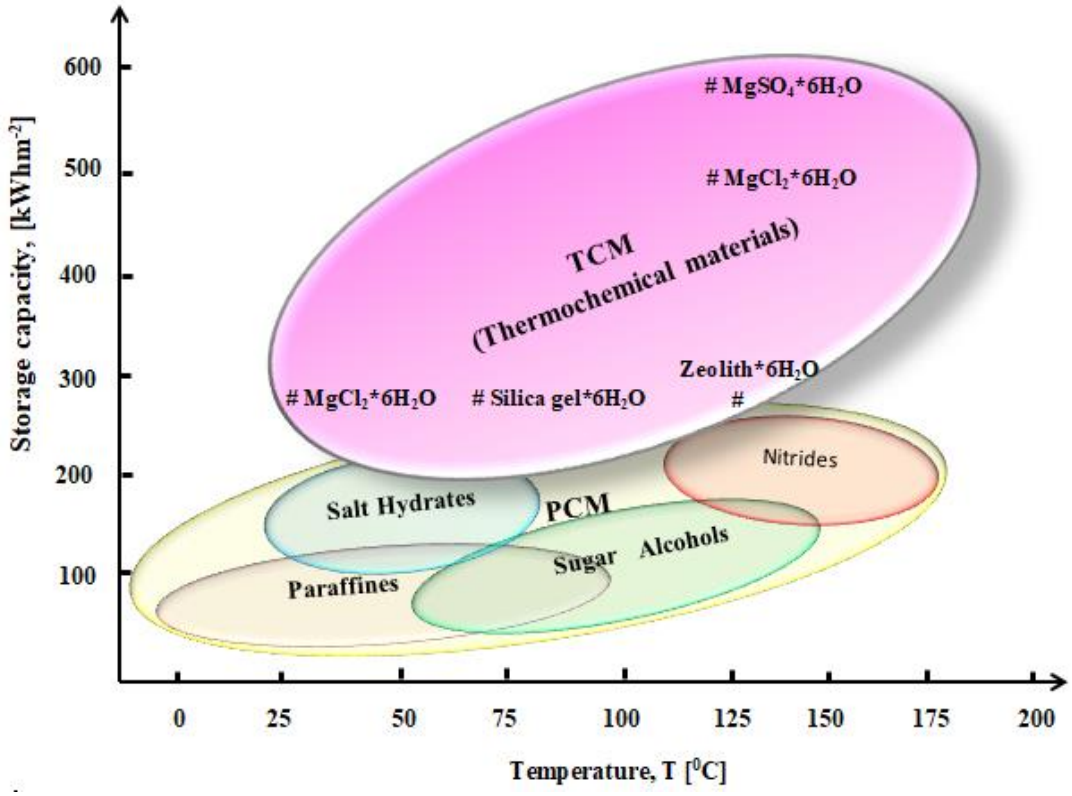

Fig. 4.10: Storage capacity of the PCM based on the temperature [82]

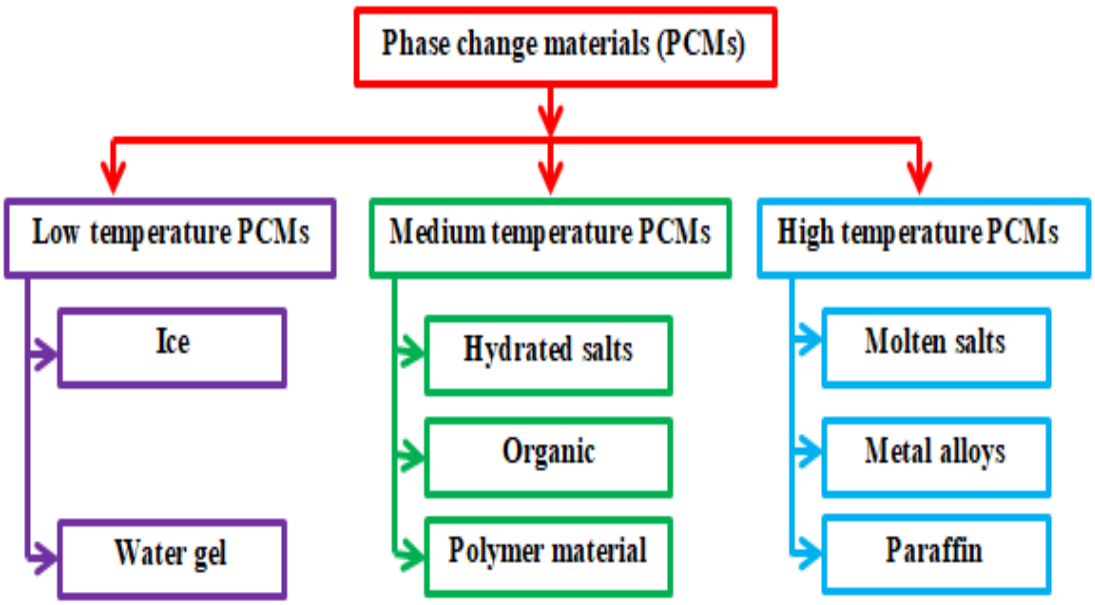

Fig. 4.11: Classification of PCM based on the melting temperature [82]

(i) Thermal properties

To select the appropriate PCM, the temperature range of the heating or cooling system must in line with the transition temperature of the PCM.

i. The proper temperature for phase transitions
ii. Latent heat of transition of PCM is very high
iii. Excellent heat transfer
iv. Good thermal conductivity

The high latent heat and high thermal conductivity of the PCM are the other decisive factors.

(ii) Physical properties

The following are the desirable physical features of PCMs:

i. Phase equilibrium is favourable

ii. Fairly dense

iii. Minor volume adjustment

iv. Insufficient vapour pressure

v. Adequate crystallisation rate

vi. Reduced superheating

Latent heat would benefit from phase stability during freezing and melting, while high density would allow for a smaller storage container. To reduce the containment problem, small volume fluctuations during phase transformation and low vapour pressure at working temperatures are used.

(iii) Kinetic properties

Super cooling has proven to be a challenging factor of PCM design, especially for salt hydrates. As a result, PCM must have the following kinetic properties:

i. No super cooling

ii. An adequate crystallisation rate

(iv) Chemical properties

The desirable chemical properties are listed below;

i. High nucleation rate to avoid liquid phase supercooling
ii. Chemical stability over time
iii. Compatibility with basic materials
iv. There is no toxicity
v. It is non-corrosive

PCM can deteriorate as a result of water loss during hydration, chemical breakdown, or incompatibility with building elements. In order to guarantee safety, PCMs should not be explosive, flammable, or toxic.

(v) Economics

The main economics factor that PCM have:

i. It is abundant

ii. Easily accessible

iii. It is inexpensive

The low cost and widespread availability of PCM are also important.

4.6 Types of PCM

Figure 4.12 shows the classification of PCM in detail.

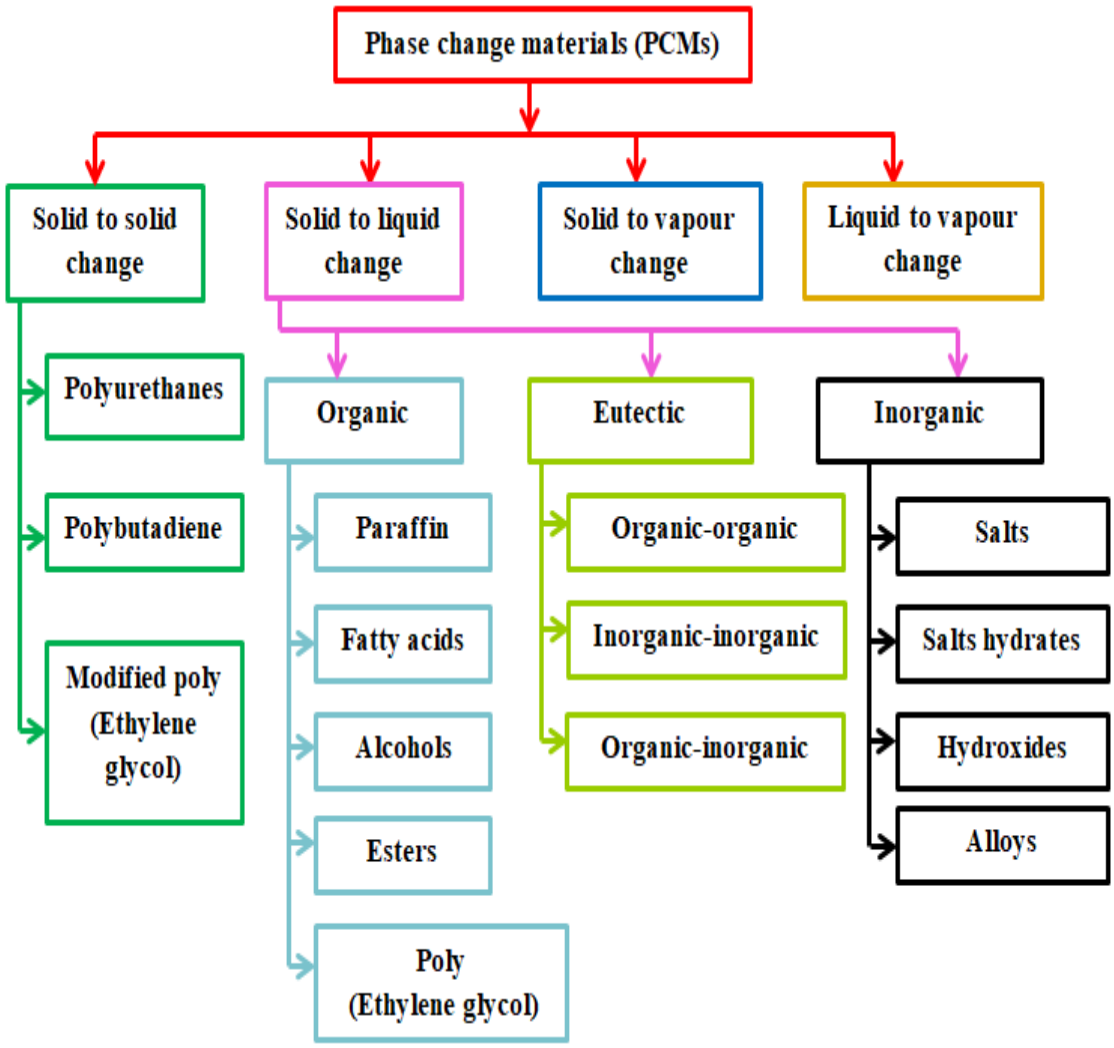

Fig. 4.12: Classification of PCM [83]

4.6.1 Organic type PCMs

Paraffins and non-paraffins are two types of organic compounds. Self-nucleation and congruent melting allow organic materials to crystallise with minimal or no supercooling, and phase segregation-free melting and freezing causes the loss of latent heat of fusion are the important property of organic PCMs. They are also frequently non-corrosive.

(i) Paraffins

Paraffin wax consists of a mixture of mostly straight chain n-alkanes $CH_3–(CH_2)–CH_3$. As the length of the chain increases, both the melting point and the latent heat of fusion also get increases. The paraffin is quite stable and when it is exposed to oxygen, they oxidise slowly. Thus, closed containers are a must for the storage of Paraffins. In the solid state, it has a greater heat of fusion but having a low thermal conductivity.

(ii) Non-paraffins

Most popular are non-paraffin organic phase change compounds with widely variable properties [82]. Each of these materials will have distinctive characteristics, unlike paraffin, moreover which has characteristics that are fairly similar. The majority of potential phase change storage materials fall into this category. Other non-paraffin organic chemicals and fatty acids are two categories of organic materials. These materials should not be exposed to high heat, flames, or oxidising chemicals because they are combustible. These organic compounds exhibit (i) high melting point, (ii) flammability, (iii) it has a low thermal conductivity and a low flash point (v) varying degrees of toxicity, and (vi) stabilility. Alcohol and fatty acids are two examples of non-paraffins.

4.6.2 Eutectics

A mixture of two or more substances that alternately melt and freeze as they crystallise is known as a eutectic. This mixture produces a mixture of the component crystals. Eutectic never segregates because it freezes to an intimate combination of crystals, making it impossible for the substance to separate. When both substance melt, they liquefy at the same time, making separation unlikely. Antimony eutectic is an example of a eutectic.

4.6.3 Inorganic type phase change materials

Inorganic substances are split as the salt hydrates, metallic substances, and alloys. Inorganic phase change materials do not supercool considerably. Salt hydrates are inorganic salt and water alloys that form a crystalline solid with the formula AB_nH_2O. Although the solid-liquid transformation of salt hydrates is thermodynamically analogous

to melting or freezing, it is in fact a dehydration of the salt hydration. The most important class of PCMs has been widely investigated for use in latent heat thermal energy storage devices are noncorrosive, plastic-compatible, and only moderately toxic. The storage of numerous salt hydrates are inexpensive. The primary disadvantage of adopting salt hydrates as PCMs is that the majority of those deemed suitable for heat storage disintegrate incongruously. Due to its greater density, solid salt sinks to the bottom of the container during the reverse freezing process and cannot be recombined with water. Each charge-discharge cycle reduces the irreversible melting-freezing of salt hydrate. Sodium sulphate decahydrate is an example.

4.6.4 Selection of energy storage material for the present study

The intermittent nature of solar energy, as well as the need to use solar energy in a consistent and static load, require the storage systems in the majority of potential solar energy uses. Thus, storage material is required in the present study to make the SAC system operate continuously. The PCM selection is primarily focused on low temperature applications, which leads to the selection of eutectic. The material used is the composition of 64% by weight $AlCl_3$ and 36% by weight NaCl having a melting point and latent heat of 93^0C and 201 $kJkg^{-1}$, respectively [82]. Now, by considering the present SAC system, based on the temperature range, high thermal diffusivity, cost of the material and availability, $AlCl_3$+NaCl is selected as the energy storage material for the present work (Material: 64% $AlCl_3$ + 36%NaCl [by weight]). The operating temperature range influences the option of PCM, and the following factors are also taken:

i. High thermal diffusivity
ii. Negligible volume change
iii. No super cooling
iv. High latent heat of transition
v. Better rate of heat transfer
vi. High thermal conductivity
vii. Non-toxic and non-corrosive
viii. The material must be chemically stable at the operating temperature for heating and cooling
ix. Non flammable

Apart from these properties an ideal heat storage material should have low cost and it should be easily available.

Summary

The different types of adsorbents, adsorbates, and working pairs used in the adsorption cooling system are presented in this chapter. The characteristics of the working pair used have a significant impact on the performance of the adsorption cooling system. The high affinity of ethanol vapour towards activated carbon, as well as its low cost, easy availability, and eco-friendly nature, are the primary factors that led to select activated carbon-ethanol as the working pair for the present study. In addition, the adsorption capacity, high surface area, affinity towards the adsorbate, thermal conductivity, and cost are the determining factors in selecting the composite adsorbent. The next chapter presents the modelling of two-bed adsorption cooling system to assess the performance.

Chapter 5

Modelling of Solar Adsorption Cooling System

The modelling of a solar adsorption cooling system is presented in this chapter. The transient Simulink modelling and thermodynamic analysis of the SAC system is detailed in this chapter. The development of the mathematical models of the system is based on the adsorption isotherm, kinetics energy balances between the adsorption elements, the evaporator and the condenser.

5.1 Two-Bed Adsorption Solar Cooling System Description

The schematic of the proposed two-bed adsorption cooling system is represented in Fig. 5.1. The system consists of an evaporator, a condenser, adsorbent bed 1 (AB_1) and adsorbent bed 2 (AB_2) which act as heat exchanger of the system and is working under four different operating process, namely, H, I, J and K. In the Process H, the valve L3 and L2 are opened whereas L4 and L1 are closed as shown in Fig. 5.1. In this Process, AB_1 and the evaporator are in the adsorption stage and AB_2 and the condenser are in the desorption

stage. The refrigerant concentration in the AB_1 in adsorption process increases and the sorption element 2 (AB_2) in the desorption process decreases. After completion of process H, the system is ready for isosteric heating or isosteric cooling (Process I). This process occurs for a short period of 10 to 30 s. In Process I, the direct flow of hot water and cold water to the beds ensures the isosteric heating and isosteric cooling of AB_1 and AB_2, respectively. When the desorber bed pressure and the condenser pressure are equal, the valve between the evaporator and AB2 is opened. When the adsorbent bed pressure and evaporator pressure are equal, the valve between the condenser and AB1 is opened. During the Process J, the valves L3 and L2 are closed and valves L4 and L1 are in opened position. The flow of hot water in AB_1 causes the desorption of adsorbate from this bed and gets absorbed by AB_2. During the Process J, the refrigerant valve's operation is just reverse of as in the Process H. At the end of the Process J, isosteric cooling of AB_1 and the isosteric heating of AB_2 starts (process K). After completion of the Process K, the system returns to Process H. The position of valves during this cycle is as shown in Table 5.1.

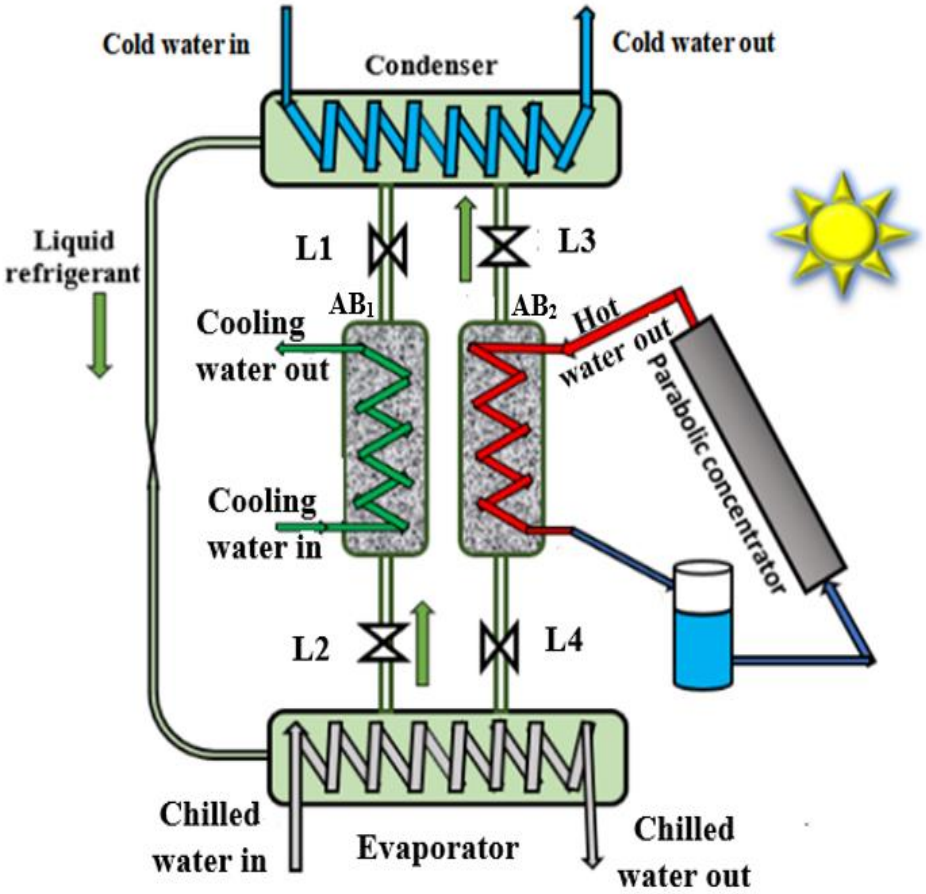

Fig. 5.1: Schematic of a two-bed adsorption cooling system

Table 5.1 Program of operation of valves and sorption bed in the two-bed adsorption cooling system

Process	Process H	Process I	Process J	Process K
(Duration)	(600 s)	(20 s)	(600 s)	(20 s)
V-L1	C	C	O	C
V-L3	O	C	C	C
AB_1	CW	HW	HW	CW
V-L4	C	C	O	C
V-L2	O	C	C	C
AB_2	HW	CW	CW	HW

C – Closed, O – Open, HW – Hot water, CW – Cold water, V - Valve

5.2 Transient Model of a Two-Bed Solar Adsorption Cooling System

The present section details the transient model of a two-bed adsorption cooling system performed in the SIMULINK platform. The transient analysis of SAC system to study the variations of parameters such as COP, SCP and cooling effect is important for the design of the systems. In this study, a theoretical model of two bed adsorption cooler including the effect on adsorbent bed-cooling water, hot water temperature and mass inflow rate in the adsorption cooler have been developed theoretically and then simulated in the MATLAB Simulink environment. Simulink is a user-friendly software and it involves only minimal simulation time compared to other software commonly used in adsorption cooling system.

5.2.1 Mathematical modelling

To evaluate the performance of an adsorption cooling system, a dynamic simulation model based on mass and energy balance equations has been developed. The working pair used in the system is activated carbon-ethanol. The following assumptions are made:

i. Throughout the operation, the pressure, temperature, and refrigerant adsorbed by the adsorbent bed are uniform
ii. The heat loss to the surroundings is neglected
iii. The adsorbed gas is considered to be calorically perfect
iv. The adsorbent bed's heat resistance to the metal tube is neglected
v. Metal tube, adsorbate vapour and the fluid properties are considered as constant

5.2.2 Adsorption or desorption isotherm and kinetics

The most frequently used adsorption equilibrium model for the adsorption of refrigerant vapour of ethanol in the solid adsorbent bed of activated carbon fibre is Dubinin-Astakhov (D-A) equation [83-85]. The pressure and temperature have a crucial part in the adsorption mode of vapour refrigerant in the activated carbon and is given by the following D-A model equation

$$X = \rho_l(T) X_0 \, exp\left[-\mathrm{D}\left(T \, ln\left[\frac{P_{sa}(\mathrm{T})}{P}\right]\right)^n\right] \tag{5.1}$$

where the value of D, X_0 and n is 1.716 x10^{-6} K^{-2}, 0. 797x10^{-3} m^3kg^{-1} and 2, respectively. Moreover, $\rho_l(T)$ and $P_{sa}(T)$ are the density and saturation pressure of ethanol related with the adsorption bed temperature. Saturation state properties of ethanol is taken from REFPROP 10-NIST [86].

The rate of adsorption or desorption in an adsorbent bed is mainly controlled by the macroscopic diffusion determined by Linear Driving Force (LDF) equation. The performance indices of the system are modelled using the energy and mass conservation equation and it depends on the relation established for the equilibrium uptake of refrigerant as well as the adsorption or desorption rate of the bed. The LDF equation has been proposed by Glucckauf [87, 88] and the rate of adsorption or desorption of the bed can be written as:

$$\frac{\partial x}{\partial t} = k_s a_v (X - x) \tag{5.2}$$

The successful mass transmit coefficient $k_s a_v$ interior of the activated carbon is given by the following expression:

$$k_s a_v = F_s \frac{D_{sp}}{R_r^2} \tag{5.3}$$

where, R_r is the radius of fibre and D_{sp} the diffusion coefficient which is described by the equation of Arrhenius, where D_{sp} is defined as [89]

$$D_{sp} = D_{pf} \, exp\left(-\frac{E_e}{R_g T_e}\right) \tag{5.4}$$

where D_{pf} , E_e and R_g represents the pre-exponential factor, energy for activation and ideal gas constant, respectively.

5.2.3 Energy balance equations

The following section provides an explanation of the energy balance equation for various SAC components.

(i) Desorber energy balance

$$\frac{d(T_{des})}{dt}\left[\left(M_{bed}C_{sp,bed}\right)+\left(M_{bed}x_{des}C_{sp,ref}\right)+\left(M_{cu,bed}C_{sp,cu}\right)\right]= \psi\,\Delta H_e M_{bed}\frac{d(x_{des})}{dt}+\dot{m}_{hwd}C_{sp,hwd}(T_{hw,in}-T_{hw,out}) \quad (5.5)$$

In the above equation, the value of Ψ is 'zero' for shifting time and is 'one' for desorption. The first part (LHS) of Eq. (5.5) indicates heating of the adsorbent bed, adsorbate and the copper tube of the heat exchanger due to the change in temperature during the desorption process. The equation on the right-hand side shows the system's desorption and sensible heat generated by hot or warm water during the desorption cycle. The Log Mean Temperature Difference (LMTD) is used to determine the exit temperature of hot fluid.

$$T_{hw,out}=T_{des}+(T_{hw,in}-T_{des})\exp\left(-\frac{U_{c,des}A_{des}}{m_{hwd}C_{sp,hwd}}\right) \quad (5.6)$$

(ii) Adsorber energy balance

$$\frac{d(T_{ads})}{dt}\left[\left(M_{bed}C_{sp,bed}\right)+\left(M_{bed}x_{ads}C_{sp,ref}\right)+\left(M_{cu,bed}C_{sp,cu}\right)\right]= \psi\,\Delta H_r M_{bed}\frac{d(x_{ads})}{dt}+\dot{m}_{cwa}C_{sp,cwa}\left(T_{cw,in}-T_{cw,out}\right) \quad (5.7)$$

For shifting time, the value of Ψ is 'zero' and is 'one' for the adsorption process in the bed. The first section (left side) of Eq. (5.7) indicates heating (sensible) of the adsorbent bed filled with activated carbon, adsorbate, and heat exchanger metals when bed adsorption occurs. During the adsorption mode of the bed, the right-hand side of Eq. (5.7) represents the heat rejection in the path of the vapour adsorbate and the cumulative heat released to the cooling water. The exit temperature of the water used to cool the bed is determined by:

$$T_{cw,out} = T_{ads} + \left(T_{cw,in} - T_{ads}\right)\exp\left(-\frac{U_{c,ads}A_{ads}}{m_{cwa}C_{sp,cwa}}\right) \quad (5.8)$$

(iii) Energy balance of condenser

The coolant used in shell and tube condenser is cold water. This coolant is utilized to liquefy the vapour adsorbate coming from the bed during the desorption process. Equation (5.9) gives the energy balance equation of the condenser.

$$\frac{d(T_{con})}{dt}\left[\left(M_{cu,con}C_{sp,cu}\right) + \left(M_{ref,con}C_{sp,ref}\right)\right] = \psi\left[-L_{V,ref}\,M_{bed}\frac{d(x_{des})}{dt} + M_{bed}C_{sp,ref}(T_{con} - T_{\text{des}})\frac{d(x_{des})}{dt}\right] + \dot{m_{cold}}C_{sp,cold}(T_{cold,in} - T_{cold,out}) \quad (5.9)$$

The expression given in the left-hand side of Eq. (5.9) shows the heating (sensible) of the metal tube of the heat exchanger and adsorbate condensed in the shell and tube condenser. The initial term in the right-hand side of Eq. (5.9) shows the latent heat of condensation and sensible heating of vapour adsorbate arriving from the adsorber bed during desorption and the last term in the same side indicates the heat energy carried away by the cooling medium. The cold water exit temperature of the condenser is obtained by using LMTD method as given below.

$$T_{cold,out} = T_{con} + (T_{cold,in} - T_{con})\exp\left(-\frac{U_{c,con}A_{con}}{m_{cold}\,C_{sp,cold}}\right) \quad (5.10)$$

(iv) Energy balance of evaporator

The Eq. (5.11) gives the evaporator energy balance equation.

$$\frac{d(T_{eva})}{dt}\left[\left(M_{cu,eva}C_{sp,cu}\right) + \left(M_{ref,eva}C_{sp,ref}\right)\right] = -\psi\left[L_{V,ref}M_{bed}\frac{d(x_{ads})}{dt} + M_{bed}C_{sp,ref}(\mathrm{T_{con}} - \mathrm{T_{eva}})\frac{d(x_{des})}{dt}\right] + \dot{m_{chil}}C_{sp,chil}(T_{chil,in} - T_{chil,out}) \quad (5.11)$$

The left-hand side of the Eq. (5.11) denotes the sensible heating of metal tube used in heat exchanger and adsorbate flowing through the evaporator. The first term in the right-hand side of Eq. (5.11) indicates the latent heat of adsorbent along with the sensible energy included with adsorbate coming from the condenser and the end term of this side is

associated with the refrigeration capacity. The chilled water outlet temperature is obtained by using LMTD method

$$T_{chil,out} = T_{eva} + (T_{chil,in} - T_{eva})\exp\left(-\frac{U_{c,eva}A_{eva}}{m_{chil}C_{sp,chil}}\right) \quad (5.12)$$

In the present study, the various physical parameters of activated carbon – ethanol working pair used in the simulation are summarized in the Table 5. 2.

(v) Conservation of mass

The mass interaction during desorption/adsorption operation period and switching period are considered. The rate of variation of refrigerant (ethanol) mass is the same as the quantity of refrigerant desorbed in the desorption period as well as the amount of refrigerant adsorbed in the adsorption period of the system.

$$\frac{dM_{ref}}{dt} = -M_{bed}\left[\frac{dx_{des}}{dt} + \frac{dx_{ads}}{dt}\right] \quad (5.13)$$

5.3 Performance Evaluation of the System

Parameters such as the COP and SCP are used to evaluate the performance of the system. The ratio of cooling power to the whole mass of the adsorbent bed is referred to as the SCP of the system as given below,

$$\text{SCP} = \frac{\dot{m}_{chil}\, C_{sp,chil} \int_0^{t_{phase}} (T_{chil,in} - T_{chil,out})dt}{M_{bed} t_{phase}} \quad (5.14)$$

The system COP is defined as the rate of the refrigerating effect of the system (Q_{Ref}) to the overall heat input to the cooler by the generator (Q_{in}).

$$\text{COP} = \frac{Q_{Ref}}{Q_{in}} \quad (5.15)$$

where the refrigerating effect of the system is given by,

$$Q_{Ref} = \dot{m}_{chil}\, C_{sp,chil} \int_0^{t_{phase}} \left(T_{chil,in} - T_{chil,out}\right)dt \quad (5.16)$$

Table 5.2 Numerical values adopted in the simulation model [90-94]

Parameter	Symbols	Numerical Values	Unit
Adsorption isotherm			
Activation energy	E_e	306.7 x 10^3	Jkg^{-1}
Constant	n	2	-
Exponential constant	D	1.716 x 10^{-6}	K^{-2}
Maximum uptake	X_o	0.797 x 10^{-3}	m^3kg^{-1}
Particle shape factor	F_s	11	-
Pre-exponential factor	D_{pf}	1.8 x10^{-12}	m^2s^{-1}
Radius of fibre	R_r	6.5 x10^{-6}	m
Adsorbent bed			
Area of bed	A_{bed}	2.5	m^2
Mass of bed	M_{bed}	45	kg
Mass of copper tube in bed	$M_{cu,bed}$	54	kg
Specific heat capacity of bed	$C_{sp,bed}$	941	$Jkg^{-1}K^{-1}$
Heat of desorption/adsorption	ΔH_r	1.2 x 10^6	Jkg^{-1}
Overall heat transfer coefficient of ads/des	$U_{c,ads/des}$	1724	$Wm^{-2}K^{-1}$
Condenser			
Area of condenser	A_{con}	3.5	m^2
Mass of copper tube in condenser	$M_{cu,con}$	12	kg
Overall heat transfer coefficient of condenser	$U_{c,con}$	4115	$Wm^{-2}K^{-1}$
Evaporator			
Area of evaporator	A_{eva}	1.5	m^2
Overall heat transfer coefficient of evaporation	$U_{c,eva}$	2557	$Wm^{-2}K^{-1}$
Refrigerant			
Specific heat capacity – refrigerant	$C_{sp,ref}$	2400	$Jkg^{-1}K^{-1}$
Latent heat of vaporization of refrigerant	$L_{V,ref}$	8.46 x 10^5	Jkg^{-1}
Specific heat capacity-copper	$C_{sp,cu}$	386	$Jkg^{-1}K^{-1}$
Mass of copper tube in evaporator	$M_{cu,eva}$	7	kg
Hot/Cold/Cooling water			
Specific heat capacity-cold/cooling water	$C_{sp,cwa/cold}$	4180	$Jkg^{-1}K^{-1}$
Specific heat capacity-hot water	$C_{sp,hwd}$	4197	$Jkg^{-1}K^{-1}$
Chilled water			
Specific heat capacity-chilled water	$C_{sp,chil}$	4193	$Jkg^{-1}K^{-1}$

and the overall heat input to the cooler by the generator is given by,

$$Q_{in} = \dot{m}_{hwd} C_{sp,hwd} \int_0^{t_{phase}} \left(T_{hw,in} - T_{hw,out}\right) dt \quad (5.17)$$

5.4 Simulink Modelling of Adsorption Cooling System

Simulink is an effective solver which utilizes the numerical and signal blocks with least coding requirements that provide useful information on the adsorption cooling system performance. Simulink model of the two-bed adsorption cooler system is depicted in Fig. 5.2, which consists of four major subsystems relating to the governing equations for desorption/adsorption of adsorbent beds, evaporator and condenser. Simulink, MATLAB R2019b platform is used for the modelling of a two-bed adsorption cooling system. The activated carbon-ethanol is used as the working pair. The performance parameters of the system are studied by varying heat transfer properties of the fluids, namely, temperature and mass inflow rate of warm, cold and chilled water used for heating and cooling of the adsorption system. Simulink block diagram shows the various components of the adsorption cooling system and they are connected by the switching sequences as shown in the Fig. 5.2. which connects and control the interactions between different blocks.

The condition of the system depends on the value of ψ. When ψ is 'one', the system is in operation mode, the beds are coupled to the condenser and evaporator for desorption and adsorption tasks accordingly. It has been understood that, when ψ is 'zero', the system shifts to the other mode and at this time there will be no mass transfer between evaporator and adsorbent bed. The system of differential equations of adsorber or desorber, condenser and evaporator are solved numerically using finite difference substitution. In this method, an exact strategy is used, where the key variables of the system are updated constantly by integration with time. The accuracy of output mainly depends on the time steps taken in the simulation of the system. Therefore, analysis is made with a smaller time step about 0.01 s. Like the other computational techniques, the stability of the solution mainly depends on time step. The system uses a sequence of subroutines to determine the kinetics of adsorption. An iterative scheme of the Simulink integral block is utilized to solve the combined ordinary differential equations or parameters of mass and energy balance equations. The tolerance criterion used in this system is $1x\ 10^{-3}$. When the cycle is operated in block manner, cold and hot water fluid flow between two beds is alternated. The Simulink model adopts a special tracking technique called "pointer" to transfer data from one cycle to another. Table 5.3 gives the specified operating condition of the system

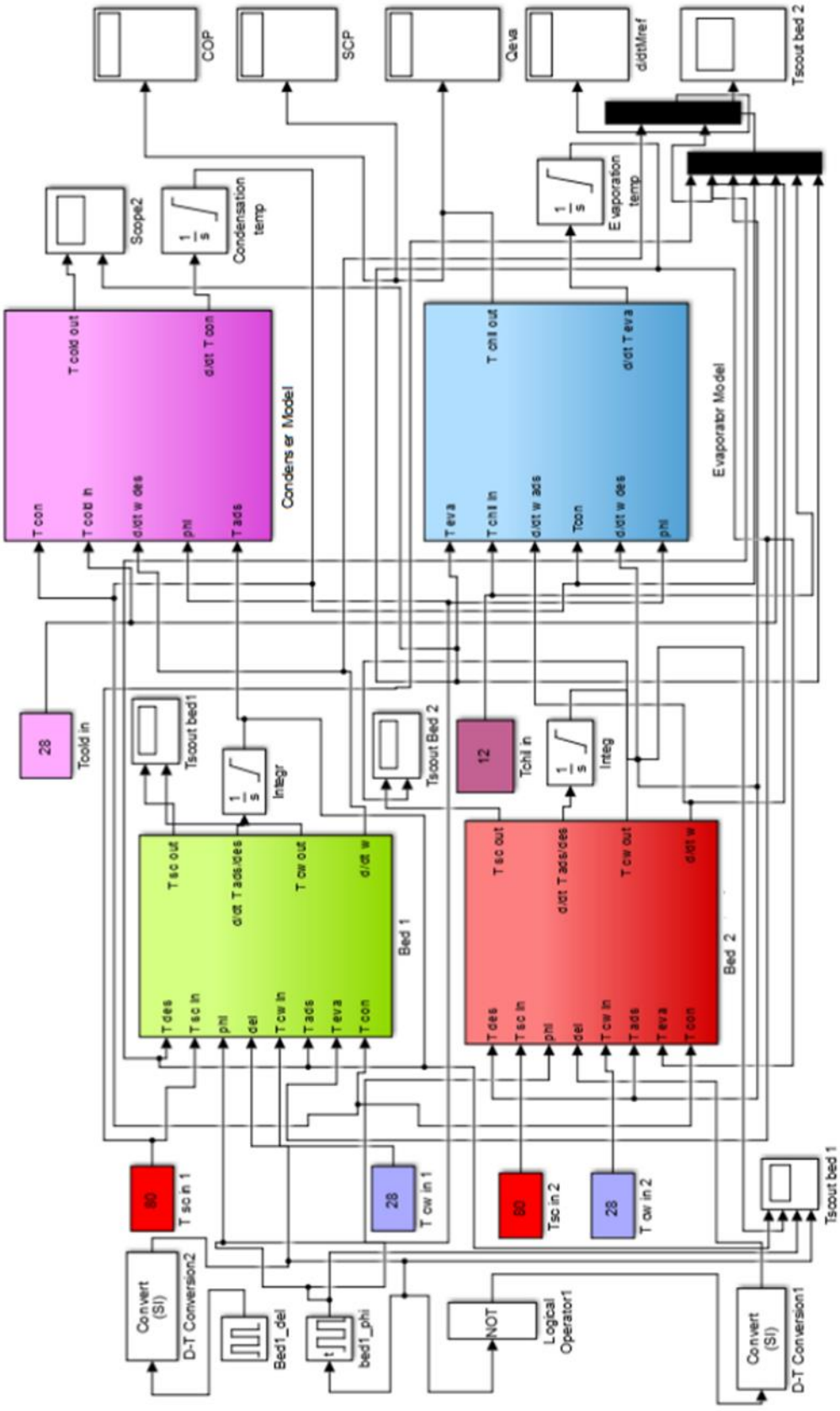

Fig. 5.2: Simulink model of the two-bed adsorption cooling system

producing an outlet chilled water temperature of 6^0C whose cooling capacity is 13.56 kW. The outside atmospheric temperature and solar radiation data has been taken from the weather station installed at Energy Research Lab, TKM College of Engineering, Kollam, Kerala. The maximum solar intensity reported is at around 11.00 h to 14.00 h and the maximum receiver output temperature obtained at that time is around 95^0C. Figure 5.3 shows the variation of solar intensity and receiver output temperature during the day time. The desorption rate is slow for hot water temperature is less than 50^0C and the process gets accelerated when the inlet temperature of hot water increases. The study focused on the regeneration temperature of 65^0C to 95^0C. The range of temperature is chosen depending on the boiling temperature of the ethanol, which is 78.5^0C. For the proper transferring of system's heat energy for desorption of refrigerant from the bed, sufficient rate of inlet mass flow of hot water is needed.

5.5 Results and Discussion

From the Eqs. (5.1) to (5.17) it is clear that the performance of the SAC is influenced by various parameters. The LDF model for gas adsorption kinetics in the solid adsorbate is commonly and efficiently used for adsorption process design study because of its simplicity. The LDF approach is substantially easier, since it eliminates the particle level

Table 5.3 Specified working environment

Inlet water					
Hot		**Cooling**		**Chilled**	
Temperature	80^0C	Temperature	28^0C	Temperature	12^0C
Mass inflow rate	2 kgs^{-1}	Mass inflow rate	2 kgs^{-1}	Mass inflow rate	0.6 kgs^{-1}
Half cycle time is 620 s					
Desorption/ adsorption phase time		600 s	Shifting time		20 s

Stages of inlet water temperature		
Hot water [^{0}C]	Cooling water [^{0}C]	Chilled water [^{0}C]
65-100	28	12
80	20-45	12
80	28	4-14

Heat transfer fluid flow rate conditions		
Hot water inflow rate [kgs^{-1}]	Cooling water inflow rate [kgs^{-1}]	Chilled water inflow rate [kgs^{-1}]
0.5 - 3.0	2	0.6
2	0.5 – 3.0	0.6
2	2	0.2 – 1.2

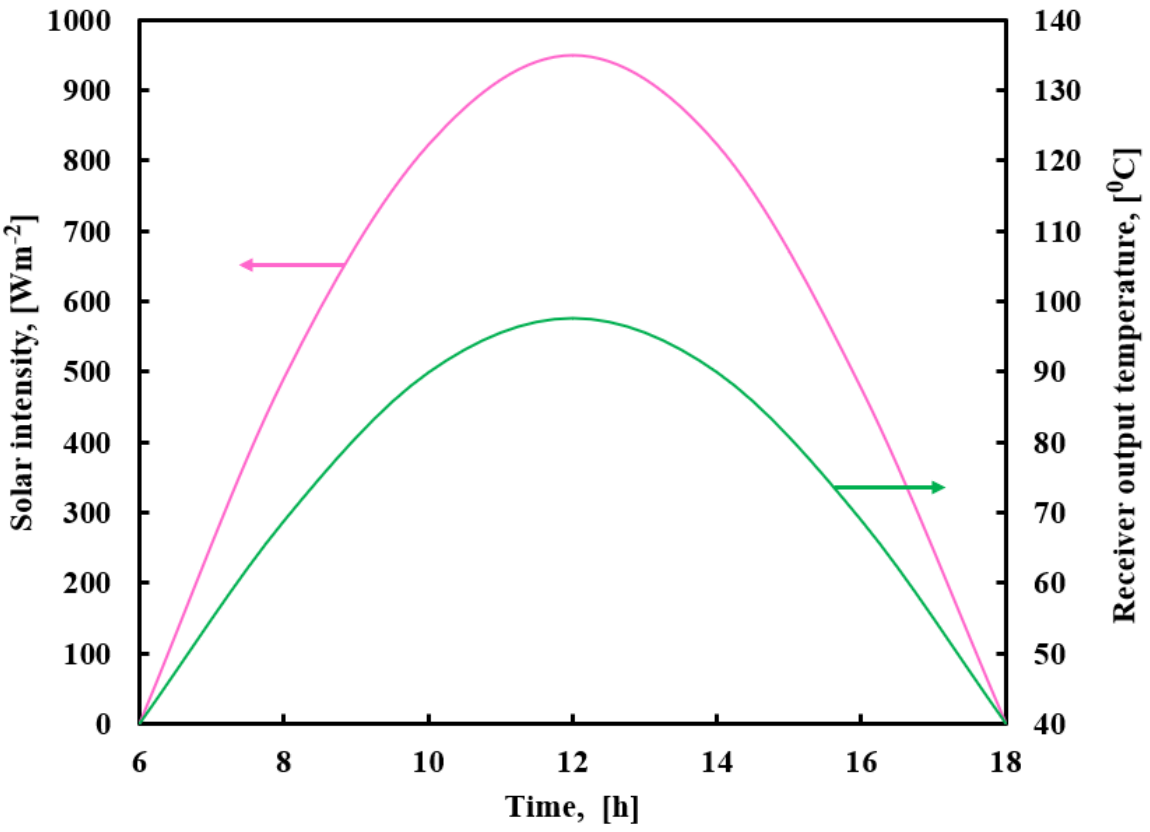

Fig. 5.3: Variation of solar intensity and receiver output temperature with day time

integration hence reducing the computational time needed for realistic process simulations. The parameters to be considered are mainly inlet hot water temperature, cold water temperature, desorption or adsorption time and also mass inflow rate of hot and cooling water. For simulation study, the various parameters given in Table 5.2 are used. Based on these input parameters, performance parameters such as COP, refrigerating effect and SCP are determined. The Simulink model of a continuous operating adsorption cooling operating with high grade activated carbon fibre-ethanol has been presented. The results obtained by simulation and its comparative study are detailed in the succeeding subsections.

5.5.1 Variation of COP and refrigerating effect with adsorption or desorption time

The variation of COP and refrigerating effect with adsorption or desorption time has been plotted in Fig.5.4, at the rated operating conditions. From Fig. 5.4, it can be seen that the COP of the system initially increases and then decreases around 600 s into the half-phase time. After the optimal range of desorption or adsorption time, the rate of increase of

refrigerating effect begins to decrease. When the adsorption or desorption time is less than 500 s, there is not enough time for the desorption or adsorption of the refrigerant, resulting in a very low COP and refrigerating effect. When the phase time exceeds 900 s, it can also be deduced from Fig. 5.4 that the rate of increase in refrigerating effect decreases due to the slower rate of adsorption. During this time period, the adsorbent beds have sufficient time for the adsorption and desorption of the refrigerant from the beds, which increases the COP and refrigerating effect of the system.

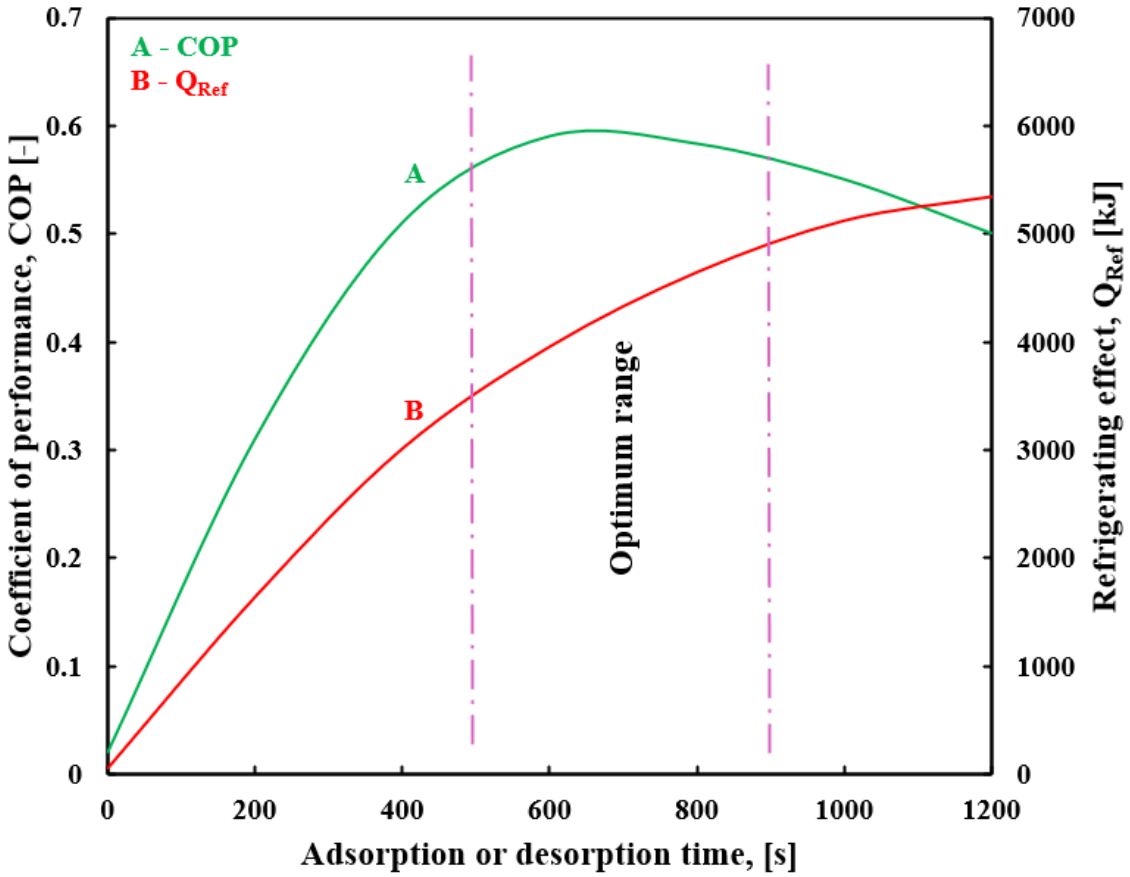

Fig. 5.4: Variation of COP and refrigerating effect with adsorption or desorption time

5.5.2 Variation of COP and refrigerating effect with switching time

The switching time is a significant parameter for the SAC and the variation of COP and refrigerating effect with switching time is shown in Fig. 5.5. In the system, instead of immediately connecting the condenser to the saturated bed in cold condition and the evaporator to the regenerated bed in hot condition, an isolated period or an isosteric thermal swing is required. But the immediate connection of condenser to saturated bed in cold condition does not annihilate the pressure at condenser, because the refrigerant in the

condenser may vapourised and maintain the pressure at saturated condition. Moreover, an unforeseen relationship between the evaporator and regenerated bed in hot condition has been rephrased into desorption of adsorbate and a gross reduction in refrigerating effect. Figure 5.5 envisages the influence of switching time on the system performance where the refrigerating effect of the system increases with increasing the switching time and beyond

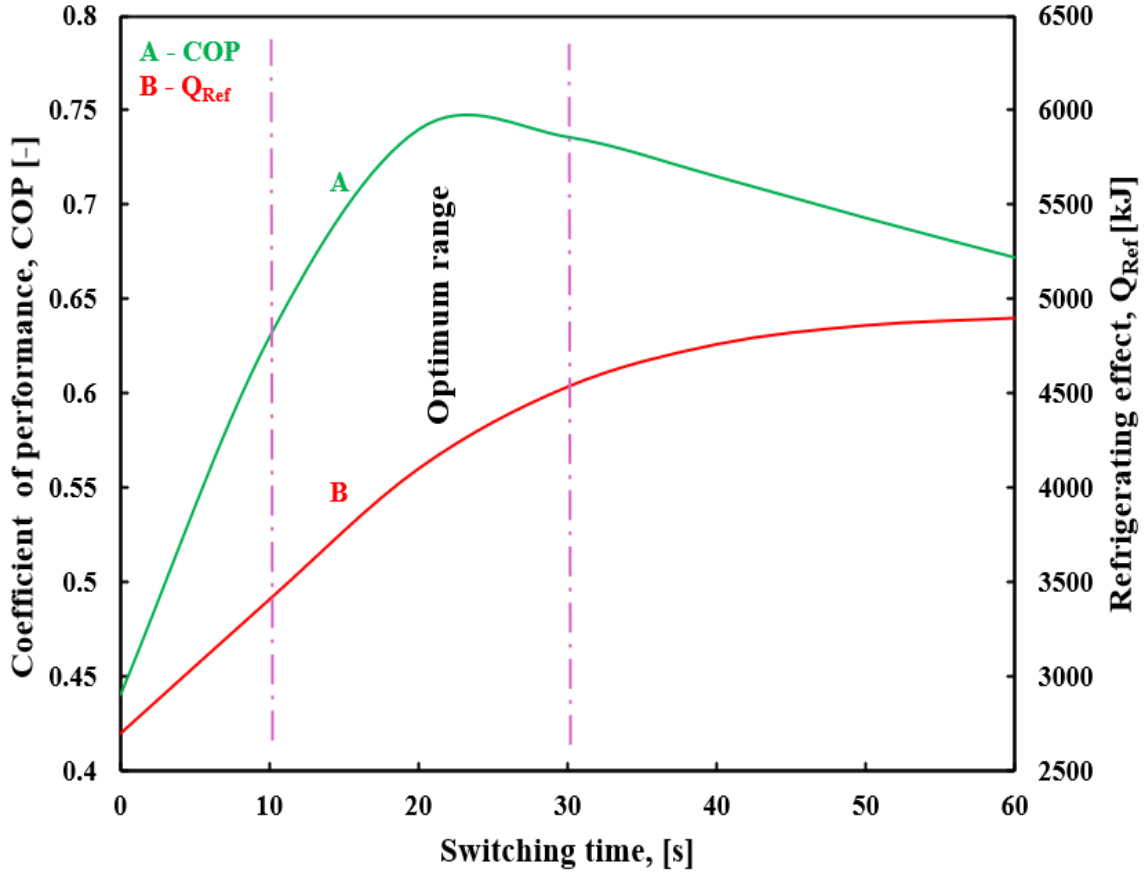

Fig. 5.5: Variation of COP and refrigerating effect with switching time

the optimum range of switching time the rate of increase of refrigerating effect gets decreases. It has been detected that the COP of the SAC system rises with switching time. The COP increases sharply up to the optimum range of switching time and after that it gets reduced. Thus, a prolonged switching time is not beneficial for this system.

5.5.3 Heat exchanger temperature profile of the SAC with adsorption or desorption time

Figure 5.6 shows the temperature profile of the SAC heat exchanger with adsorption or desorption time. The reference conditions taken are inlet hot water temperature of 80^0C,

cooling/cold water 28^{0}C, chilled water 12^{0}C and phase time 600 s. The simulation results show that the desorber bed temperature is equal to or less than 2 to 3^{0}C to that of the temperature of inlet hot water. The temperature in the adsorbent bed is greater than 4-5^{0}C of cooling water temperature at inlet condition. In the simulation both the desorption and adsorption processes are assumed to be take place with the same duration. But in practical case the adsorption process time can be reduced by increasing the mass flow rate of cooling water through the adsorption bed. The temperature history of the condenser shows that at the beginning of each cycle, reaches the peak value and then decreases. This is achieved by the rise in temperature of water for cooling during the switching of adsorbent beds from adsorption process to the desorption. Figure 5. 6 also shows that at the initial period of adsorption, there is a drop in the evaporator temperature, and it increases gradually.

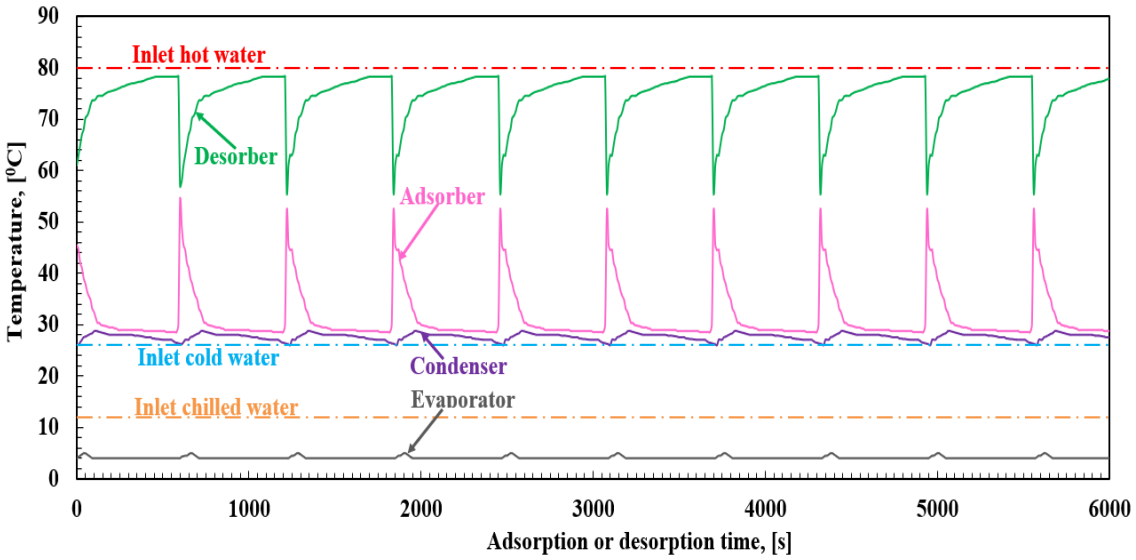

Fig. 5.6: Temperature profile of the SAC heat exchanger with adsorption or desorption time

5.5.4 Deviation of heat transfer fluid outlet temperature with adsorption or desorption time

Figure 5.7 indicates the deviation of heat transfer fluid outlet temperature with adsorption or desorption time. It is clear that after 600 s, the exit temperature is close to that of the inlet hot water temperature. It is found that, at 600 s the outlet temperature of cooling water is 4-7^{0}C and it is more than that of temperature at inlet condition. It is also clear that, at 600 s the chilled water exit temperature is nearly 4-6^{0}C which is less than the inlet temperature in the evaporator. After 600 s, it can be seen that there is a sharp change

in the exit temperature of hot water and adsorber cold water due to shifting of the adsorber to the desorber and in reverse for 10 to 30 s. The most suitable switching duration for the process is 20 s.

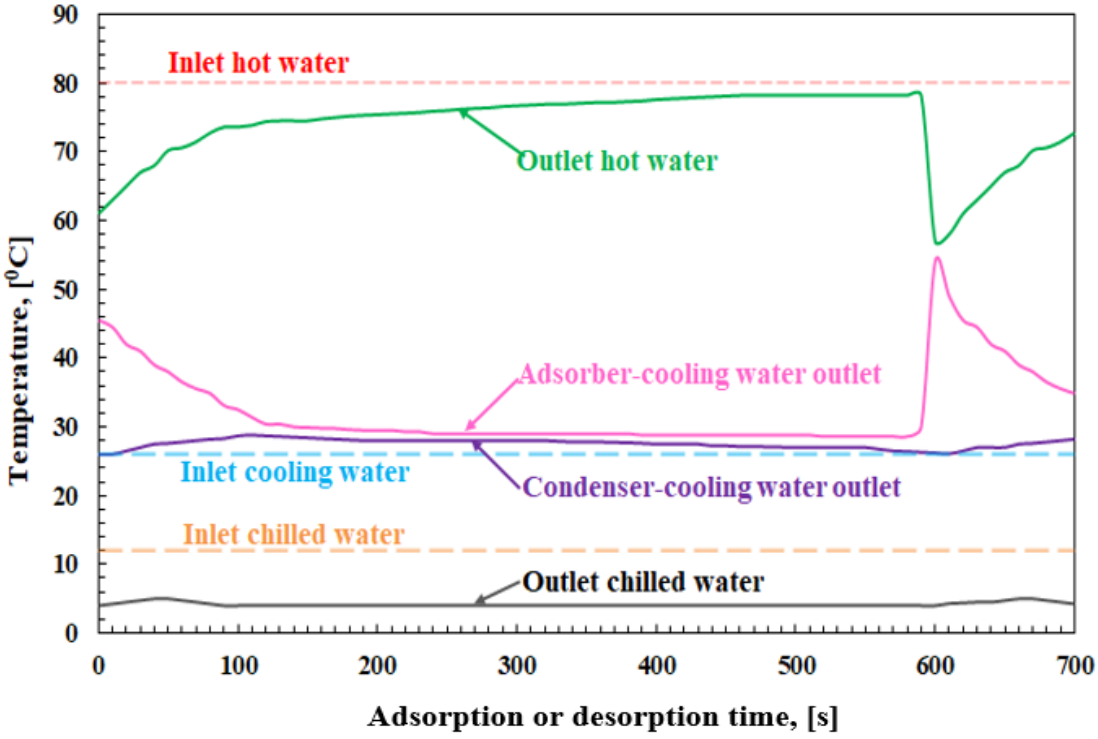

Fig. 5.7: The deviation of heat transfer fluid outlet temperature with adsorption or desorption time

5.5.5 Effect of operating temperature on the system performance

Figures 5.8 and 5.9 shows the variation in cycle COP, refrigerating effect, and SCP with different inlet temperatures. Figure 5.8 depicts the effect of hot water inlet temperature on COP and refrigerating effect of a two-bed adsorption cooler. The peak COP is obtained between 75^{0}C and 80^{0}C for the inlet hot water temperature range and is nearly constant between 80^{0}C and 100^{0}C. This is due to an increase in heat loss at higher desorption temperatures. If the inlet warm (hot) water temperature is less than 65^{0}C, the temperature in the desorption bed is insufficient, and the desorption of the refrigerant from the bed is low, resulting in a much lower COP. The undesorbed refrigerant affects the next adsorption process which adversely upset the refrigerating effect. The peak COP is found to be 0.57 whose inlet hot water and uniform cooling water temperatures are 80^{0}C and 28^{0}C, respectively. The COP is higher in the 75^{0}C to 80^{0}C temperature range and the ethanol boiling point falling within the

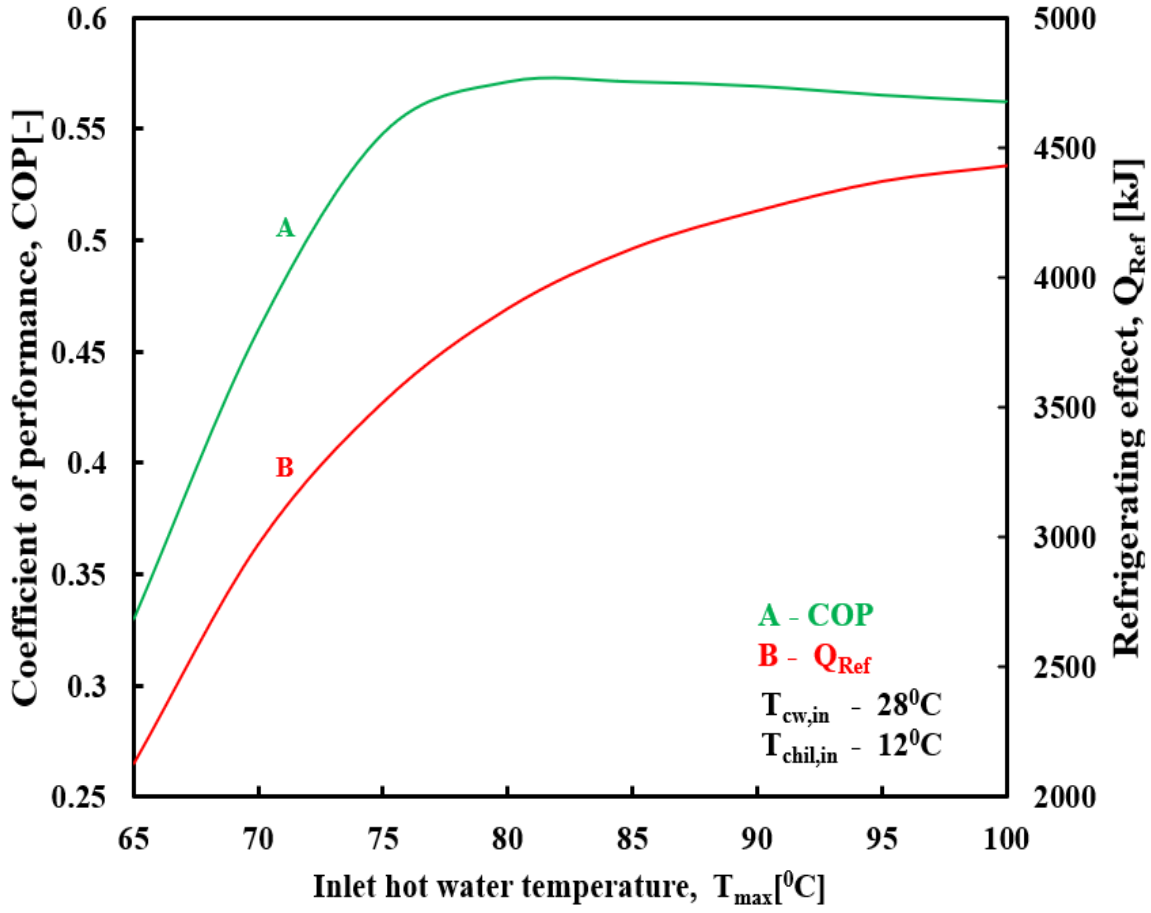

Fig. 5.8: Effect of inlet temperature of hot water on COP and refrigerating effect of two-bed adsorption cooler

range. This helps to choose an optimum heat source temperature when the system operates with the solar heating or waste heat energy. As the increment in the inlet hot water temperature is from 65^{0}C to 100^{0}C, the refrigerating effect of the system rises. The increase in inlet hot water temperature causes refrigerant to desorb at a faster rate from the adsorbent bed, which augments the refrigerating effect of the two-bed adsorption cooler.

Figure 5.9 depicts the influence of chilled water inlet temperature on the COP and refrigerating effect of a two-bed adsorption cooler. It is observed that the COP and refrigerating effect of a system increase considerably as the chilled water intake temperature rises. The rise in chilled water inlet temperature accelerates evaporation, causing the bed to absorb a substantial amount of refrigerant vapour. Consequently, the COP of the system increases. Since, the rise in inlet chilled water temperature leads to higher adsorbate evaporation, results in an increase in the refrigerating effect.

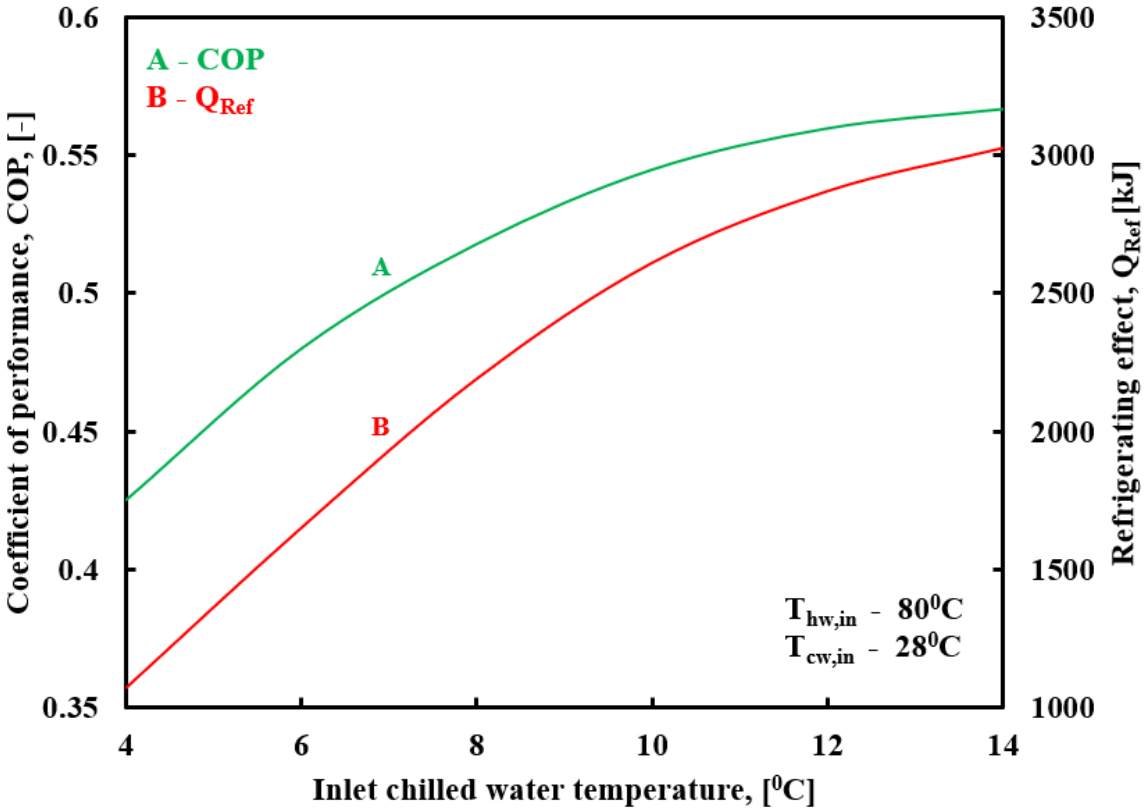

Fig. 5.9: Effect of inlet temperature of chilled water on COP and refrigerating effect of two-bed adsorption cooler

5.5.6 Variation of system performance with fluid flow rates

The variations in the system COP and refrigerating effect with hot water inflow rate is shown in Fig. 5.10. The desorption process of the system takes place due to the heating of the adsorbent bed with the inlet hot water temperature. Large amount of heat can be transferred to the adsorbent bed and refrigerant with a higher hot mass flow rate. The COP of the system increases with rise in hot water mass flow rate up to 2 kgs^{-1} and after that the increment is only marginal. This is because as the flow rate increases up to 2 kgs^{-1}, the COP increases as more adsorber is effectively desorbed from the bed. However, above 2 kgs^{-1}, the COP rise is small since more energy is lost to the atmosphere due to the higher mass flow rate of inlet hot water.

5.6 Thermodynamic Analysis of SAC System

Here, the steady thermodynamic behaviour of a two-bed solar adsorption system with a constant temperature adsorption process using activated carbon-ethanol as the adsorbent-adsorbate pair is shown. The adsorption isotherm shows how the amount of

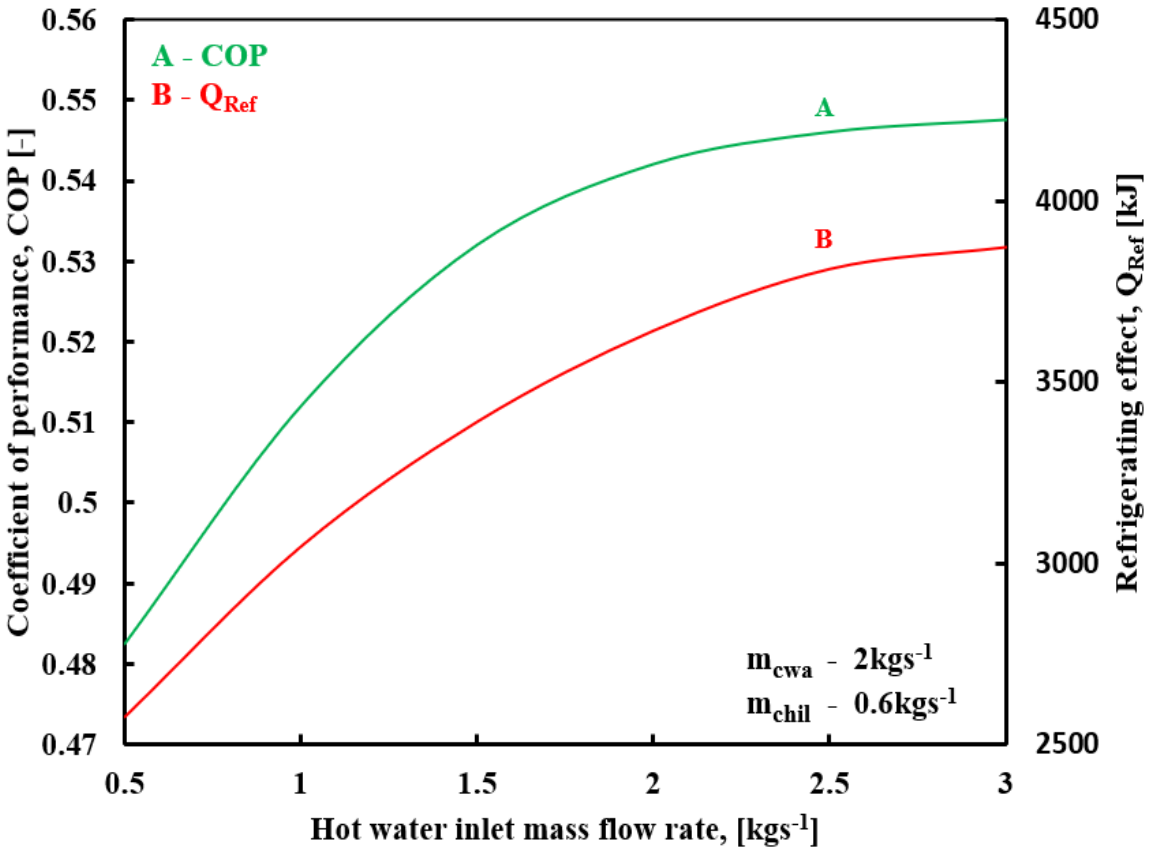

Fig. 5.10: Variation of system COP and refrigerating effect with hot water inflow rate

adsorbate that is absorbed per unit weight of adsorbent changes when the pressure stays the same. According to the Langmuir adsorption principle, if the process is done at a constant temperature, the adsorption rate will go up. This means that vapour refrigerant adsorption will be higher at a constant temperature than in the typical constant pressure adsorption method (process currently employed in adsorption cooling systems). During isothermal adsorption, the pressure increases from the minimum cycle pressure to the saturated vapour pressure. In contrast to the isobaric adsorption process, there is no visible heating of the bed component in the isothermal adsorption method. In addition, isothermal adsorption leads to a lower system cycle time [95]. When compared to conventional isobaric adsorption, isothermal adsorption releases less heat energy throughout the adsorption process. Heat released by the bed as a result of refrigerant vapour adsorption can be removed using tap water, which is sufficient for cooling the system in this method.

The adsorption is a pressure swing process, the cooling system needs a mechanical compressor, which needs electricity. So, the system is not economical and cannot be used

in remote areas where there is no power supply. Moreover, the pressure swing adsorption or desorption process is suitable for a solid adsorbent-gas adsorbate as a working pair. The present system uses a solid adsorbent-liquid adsorbate pair. This section envisages a mathematical simulation of an isothermal SAC system operating with activated carbon-ethanol as a working pair and the Fig 5.11 represents the proposed Clausius-Clapeyron diagram of the system. This model is used to evaluate the energy distribution in various processes of the cooling system (including isothermal adsorption process), effect of cycle temperature on adsorbate phase volume fraction, maximum desorption temperature on effective mass of refrigerant desorbed and chilled water outlet temperature and performance parameters, namely, COP, refrigeration effect and SCP are also analysed.

Dubinin-Astakhov (D-A) model is the most widely accepted adsorption equilibrium model, primarily used in activated carbon microporous adsorbents. Adsorbed mass in activated carbon mainly depends on adsorption temperature and pressure and is given by,

$$X\left(T,P\right)=\rho_{\mathrm{l}}(T)X_0\exp\left[-D\left(T\ ln\left[\frac{P_{\mathrm{sa}}(T)}{P}\right]\right)^n\right] \tag{5.18}$$

where D is the structural constant that mainly depends on adsorbent-refrigerant pairs, X_0 the maximum adsorption capacity, P the equilibrium pressure of adsorbent - refrigerant and $P_{\mathrm{sa}}(\mathrm{T})$ and $\rho_{\mathrm{l}}(\mathrm{T})$ are the adsorbate saturation pressure and density, respectively.

The refrigerant phase volume fragment at an equilibrium state ψ^* has been obtained by,

$$\psi^*=X(T,P)(1-\varepsilon)\frac{\rho_{\mathrm{ac}}}{\rho_{\mathrm{l}}(T)} \tag{5.19}$$

where ε and ρ_{ac} are the total adsorption bed porosity and material density of solid adsorbent, respectively.

The maximum or initial adsorbate concentration in the adsorbent bed is given by

$$X_{\max}=X(T_{\mathrm{am}},P_{\mathrm{eva}})=X\left(T_{\mathrm{gen}},P_{\mathrm{con}}\right) \tag{5.20}$$

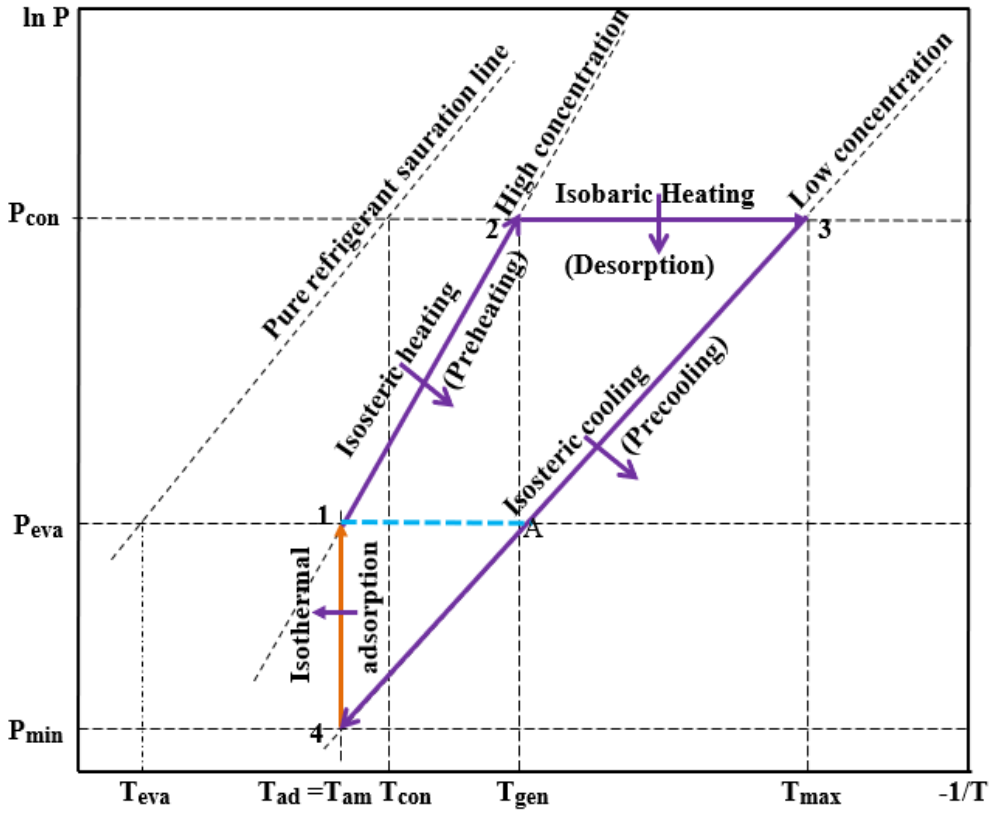

Fig. 5.11: Clausius - Clapeyron diagram of the proposed two-bed solar adsorption cooling cycle

The minimum or final adsorbate concentration in the adsorbent bed is determined from the following equation

$$X_{\min} = X(T_{\max}, P_{con}) = X\left(T_{ad}, P_{\min}\right) \tag{5.21}$$

where T_{gen} and T_{ad} are temperatures at the starting point of desorption and adsorption of refrigerant from the bed, respectively.

During the entire process of desorption or adsorption, the adsorbate concentration (ethanol) is given by

$$X_{\text{max-min}} = X_{\max} - X_{\min} \tag{5.22}$$

During adsorption process, the evaporator pressure is $P_{eva} = P_{sa}(T_{eva})$,and in desorption process, the condensing pressure is given by $P_{con} = P_{sa}(T_{con})$.

By rearranging the Eq. (5.18) the pressure *P* of the system is obtained by an explicit formula

$$ln\,P = ln\,P_{sa}(T) - \frac{1}{T}\left[\frac{1}{D}\,ln\left(\frac{X_0\rho_l(T)}{X}\right)\right]^{\frac{1}{n}} \tag{5.23}$$

Differentiating Eq. (5.18) (by keeping temperature constant and at varying pressure) gives

$$\left.\frac{\partial X}{\partial P}\right|_T = nXD\left(\frac{T}{P}\right)\left[T\,ln\left(\frac{P_{sa}(T)}{P}\right)\right]^{n-1} \tag{5.24}$$

Then differentiating Eq. (5.18) (by keeping the pressure constant and at varying temperature) gives

$$\left.\frac{\partial X}{\partial T}\right|_P = X\,\frac{d\,ln\rho_l(T)}{dT} - nXD\left[T\,ln\left(\frac{P_{sa}(T)}{P}\right)\right]^{n-1}\left[ln\left(\frac{P_{sa}(T)}{P}\right) + T\,\frac{d\,lnP_{sa}(T)}{dT}\right] \tag{5.25}$$

The process of desorption is endothermic, whereas adsorption is exothermic. The isosteric desorption or adsorption heat (ΔH) is defined as the amount of heat needed to desorb/adsorb a unit mass of the ethanol. The Clausis-Clapeyron equation is used to calculate the heat per unit mass of ethanol as follows:

$$\Delta H = R_e T^2\left(\frac{\partial\,lnP}{\partial T}\right)_{X=c} \tag{5.26}$$

Differentiating Eq. (5.23) gives

$$\frac{\partial\,lnP}{\partial T} = \frac{\partial\,lnP_{sa}}{\partial T} + ln\frac{P_{sa}}{P}\left(\frac{1}{T} - \frac{1}{nD}\frac{\partial\,ln\rho_l(T)}{\partial T}\left[T\,ln\frac{P_{sa}}{P}\right]\right)^{-n} \tag{5.27}$$

Substituting Eq. (5.27) in (5.26), the change in isosteric heat of adsorption or desorption is obtained as a function of temperature and is given by,

$$\Delta H = R_e T^2\,\frac{d\,lnP_{sa}}{dT} + R_e T\;ln\frac{P_{sa}(T)}{P} - \frac{R_e T}{nD}\,\frac{d\,ln\rho_l(T)}{dT}\left[T\;ln\frac{P_{sa}(T)}{P}\right]^{1-n} \tag{5.28}$$

Thermodynamics analysis of SAC system is carried out with the following assumptions:

i. Adsorption process takes place at constant temperature (ambient) and at varying adsorbent bed pressure
ii. Heat transfer coefficient and specific heat are constant
iii. The bed is well-insulated
iv. Refrigerant vapour behaves as a perfect gas

5.6.1 Isosteric heating (process 1→2)

During this process, adsorbent bed is preheated at a constant concentration of adsorbate in the bed. The total sensible heat $Q^{1\to2}$ added to the system is given by,

$$Q^{1\to2} = Q_{ac}^{1\to2} + Q_{mc}^{1\to2} + Q_{ref}^{1\to2} \tag{5.29}$$

where $Q_{ac}^{1\to2}$, $Q_{mc}^{1\to2}$ and $Q_{ref}^{1\to2}$ are sensible heats of adsorbent medium, metal cover, and adsorbate, respectively.

$$Q_{ac}^{1\to2} = \int_{T_{ad}}^{T_{gen}} m_{ac} C_{ac} dT = m_{ac} C_{ac} [T_{gen} - T_{ad}] \tag{5.30}$$

$$Q_{mc}^{1\to2} = \int_{T_{ad}}^{T_{gen}} m_{mc} C_{mc} dT = m_{mc} C_{mc} [T_{gen} - T_{ad}] \tag{5.31}$$

$$Q_{ref}^{1\to2} = \int_{T_{ad}}^{T_{gen}} m_{ac} X_{max} C_{ref} dT = m_{ac} X_{max} C_{ref} [T_{gen} - T_{ad}] \tag{5.32}$$

5.6.2 Isobaric heating - desorption (2→3)

In this phase, adsorption reactor undergoes desorption process at condenser pressure, where the concentration of adsorbate (X_{max}) in the activated carbon decreases to a minimum value (X_{min}).Total heat input$(Q^{2\to3})$during this process is given as the sum of heat given to the adsorbent medium$(Q_{ac}^{2\to3})$, metal cover$(Q_{mc}^{2\to3})$, adsorbate $(Q_{ref}^{2\to3})$and heat of desorption $(Q_{des}^{2\to3})$. It is an endothermic process.

Then,

$$Q^{2\to3} = Q_{ac}^{2\to3} + Q_{mc}^{2\to3} + Q_{ref}^{2\to3} + Q_{des}^{2\to3} \tag{5.33}$$

$$Q_{ac}^{2\to3} = \int_{T_{gen}}^{T_{max}} m_{ac} C_{ac} dT = m_{ac} C_{ac} [T_{max} - T_{gen}] \tag{5.34}$$

$$Q_{mc}^{2\to3} = \int_{T_{gen}}^{T_{max}} m_{mc} C_{mc} dT = m_{mc} C_{mc} [T_{max} - T_{gen}] \tag{5.35}$$

$$Q_{ref}^{2\to3} = \int_{T_{gen}}^{T_{max}} m_{ac} X C_{ref} dT = m_{ac} C_{ref} \int_{T_{gen}}^{T_{max}} X dT \tag{5.36}$$

$$Q_{des}^{2\to3} = -m_{ac} \int_{T_{gen}}^{T_{max}} \Delta H \left[\frac{\partial X}{\partial T}\right]_{P=C} dT \tag{5.37}$$

where $\left(Q_{\text{des}}^{2\to3}\right)$ is the heat required to desorb the differential amount of ethanol from the activated carbon.

During the process 1→2→3, heat input to the system is given by

$$Q_{\text{in}}^{1\to2\to3} = Q^{1\to2} + Q^{2\to3} \tag{5.38}$$

5.6.3 Isosteric cooling (3→4)

During this process, total heat liberated $\left(Q^{3\to4}\right)$ from the system is given by

$$Q^{3\to4} = Q_{\text{ac}}^{3\to4} + Q_{\text{mc}}^{3\to4} + Q_{\text{ref}}^{3\to4}$$

where $Q_{\text{ac}}^{3\to4}$, $Q_{\text{mc}}^{3\to4}$ and $Q_{\text{ref}}^{3\to4}$ are sensible heats of adsorbent medium, metal cover and adsorbate, respectively.

$$Q_{\text{ac}}^{3\to4} = \int_{T_{\text{ad}}}^{T_{\text{max}}} m_{\text{ac}} C_{\text{ac}} dT = m_{\text{ac}} C_{\text{ac}} [T_{\text{max}} - T_{\text{ad}}] \tag{5.39}$$

$$Q_{mc}^{3\to4} = \int_{T_{ad}}^{T_{max}} m_{mc}\, C_{mc} dT = m_{mc} C_{mc}\, [T_{max} - T_{ad}] \tag{5.40}$$

$$Q_{ref}^{3\to4} = \int_{T_{ad}}^{T_{max}} m_{ac}\, X_{min} C_{ref} dT = m_{ac} X_{min} C_{ref} [T_{max} - T_{ad}] \tag{5.41}$$

5.6.4 Isothermal adsorption (4→1)

In this process, AB_2 adsorbs the vapour refrigerant leaving the evaporator at constant temperature, hence, the mass of ethanol in AB_2 increases from X_{min} to X_{max}..Total heat rejected ($Q^{5\to1}$) is given by

$$Q^{5\to1} = Q_{ad} \tag{5.42}$$

$$Q_{ad}^{5\to1} = m_{ac} \int_{P_{min}}^{P_{ev}} \Delta H \left[\frac{\partial X}{\partial P}\right]_{T_{ad}} dP \tag{5.43}$$

where $Q_{ad}^{5\to1}$ is the heat required to accumulate the varying quantity of ethanol in the activated carbon.

Temperature at the beginning of desorption process (T_{gen}) of thermodynamic cycle can be obtained from

$$T_{gen} = \frac{T_{am}T_{con}}{T_{eva}} \quad (5.44)$$

5.6.5 Condenser

The desorbed refrigerant enters the condenser, where it is subjected to condensation by rejecting its latent heat of condensation. Initially, the refrigerant is de-superheated in the condenser and then latent heat of condensation is removed. Thus, for the condensation process, total heat rejected is given by

$$Q_{con} = m_{ac}(X_{max} - X_{min})L_{ref} + m_{ac}C_{ref}\int_{T_{con}}^{T_{max}}(T_{con} - T)\left[\frac{\partial X}{\partial T}\right]_{P_{con}} dT \quad (5.45)$$

5.6.6 Expansion process

In the expansion process, total energy is persevered by the adsorbate. Thus, after the expansion process, wetness fraction *y* of adsorbate is represented as

$$y = 1 - \frac{h_{fl}(T_{am}) - h_{fl}(T_{eva})}{L_{ref}(T_{eva})} \quad (5.46)$$

where $h_{fl}(T_{eva})$ and $h_{fl}(T_{am})$ are specific enthalpies of saturated liquid adsorbate at evaporator and atmospheric temperatures, respectively. $L_{ref}(T_{eva})$ the latent heat of vapourisation of adsorbate at the evaporator temperature.1-*y* represents the fraction of liquid adsorbate evaporated.

5.6.7 Evaporator

The refrigerating effect is given by,

$$Q_{Ref} = m_{ac}(X_{max} - X_{min})y\, L_{ref}(T_{eva}) \quad (5.47)$$

5.7 Energy Balance of the SAC System

Total heat energy added (Q_{add}) and rejected (Q_{reje}) from the entire system is given by

$$Q_{add} = Q^{1\to2} + Q^{2\to3} + Q_{Ref} \quad (5.48)$$

$$Q_{reje} = Q^{3\to5} + Q^{5\to1} + Q_{con} \quad (5.49)$$

5.8 Performance Indices of SAC system

Performance of SAC system is defined in terms of (a) coefficient of performance (COP), (b) cooling capacity (Q_{eva}), (c) specific cooling power (SCP), (d) effective refrigerant mass (m_{ef}) and (f) refrigerant mass consumption efficiency (η_{rm})

5.8.1 Coefficient of Performance (COP)

It describes how effectively the input energy is converted into useful refrigerating effect (Q_{Ref}).

$$COP = \frac{Q_{Ref}}{Q_{in}} \tag{5.50}$$

5.8.2 Cooling capacity (Q_{eva})

Performance of the system is assessed by its cooling capacity. It can be written as:

$$Q_{eva} = \frac{Q_{Ref}}{Operating\ time\ of\ an\ adsorption\ bed\ X\ 3600} \tag{5.51}$$

5.8.3 Specific cooling power (SCP)

Depending on the system capacity, the cooling capacity varies from one to the other system. Specific cooling power (SCP) is used to quantify the efficiency of adsorption cooling systems of different sizes. It is defined as the ratio of the system cooling capacity to the unit mass of adsorbent in the bed.

$$SCP = \frac{Q_{eva}}{m_{ac}} \tag{5.52}$$

5.8.4 Effective refrigerant mass (m_{ef})

It is the mass of adsorbate essential for contributing to the refrigerating effect within the evaporator. m_{ef} is defined as the total mass of adsorbate which is circulated through the condenser and evaporator. This is given by

$$m_{ef} = m_{ac}(X_{max} - X_{min}) \tag{5.53}$$

5.8.5 Refrigerant mass consumption efficiency (η_{rm})

It is defined as the ratio of effective mass of adsorbate to the gross adsorbate mass (m_{ac}) required to charge the system and can be written as

$$\eta_{rm} = \frac{m_{ef}}{m_{ac}X_{max}} = 1 - \frac{X_{min}}{X_{max}} \tag{5.54}$$

5.9 Results and Discussion

Results of First law analysis of SAC system operating at isothermal adsorption process is presented here. Energy balance Eqs. (5.29)-(5.49) are used to model the SAC system. Thermodynamic and transport properties of ethanol are taken from REFPROP-10 NIST reference fluid properties. Mathematical model of the proposed SAC system is carried out in MATLAB R2019b environment with the baseline parameters given in Table 5.4.

Table 5.4 The baseline parameters considered in the present work [34]

Parameter	Numerical value	Parameter	Numerical value
T_{max}	95^0C	C_{ac}	0.71 kJkg^{-1}K^{-1}
T_{con}	45^0C	C_{mc}	0.48 kJkg^{-1}K^{-1}
T_{ev}	5^0C	C_{re}	2.4 kJkg^{-1}K^{-1}
T_{am}	33^0C	C_{cwai}	4.2 kJkg^{-1}K^{-1}
T_{cwai}	33^0C	ϵ	0.74
D	1.716 x10^{-6} K^{-2}	m_{ac}	16 kg
X_0	0.797x 10^{-3} m^{3}kg^{-1}	m_{mc}	16 kg
n	2	ρ_{mc}	7000 kgm^{-3}
R	180.48 Jkg^{-1}K^{-1}	ρ_{ac}	2100 kgm^{-3}

5.9.1 Two bed adsorption cooling system operated with activated carbon-ethanol as working pair

Study aims in determining the energy developed in each component of the system when the adsorption takes place isothermally. It has been ascertained that total heat energy added (Q_{add}) to the entire system is 11057 kJ, whereas 10985 kJ of heat is rejected during the cycle. Therefore, relative error is 0.65%, which is very low and validates the accuracy

of analysis. Total heat input($Q_{in}^{1\rightarrow2\rightarrow3}$) to the SAC system is 6882.96 kJ and the distribution of heat within the adsorbent bed components during the heating processes is given as $Q_{\text{des}}^{2\rightarrow3}$ =4543.44 kJ, $Q_{\text{ref}}^{1\rightarrow2\rightarrow3}$=978.07 kJ, $Q_{\text{ac}}^{1\rightarrow2\rightarrow3}$= 865.88 kJ and $Q_{\text{mc}}^{1\rightarrow2\rightarrow3}$= 495.57 kJ, respectively. Figure 5.12 represents the input heat distribution within the adsorbent bed components. A major part of heat input is used for desorption of the refrigerant, i.e., 66.01%. About 14.21% of total heat added to the system is used for sensible heating of the refrigerant during the process 1→2→3, whereas 12.58% is used for heating of adsorbent bed and remaining 7.2% is used for sensible heating of the metal cover of bed. The maximum COP obtained is 0.68 for a maximum desorption temperature of 95^0C.

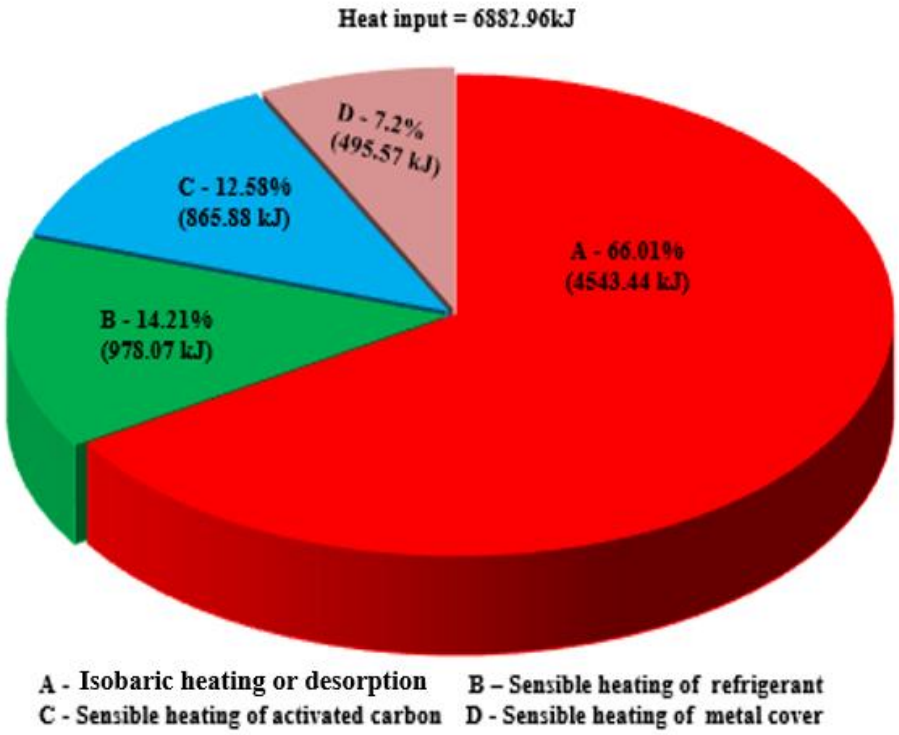

Fig. 5.12: Input heat distribution within the adsorbent bed components

5.9.2 Adsorbent bed pressure-temperature correlation

The variation of adsorbent bed pressure with cycle temperature is shown in Fig. 5.13 During isosteric heating (1→2) the pressure of adsorbent bed rises from an evaporator pressure (P_{eva}) of 2.01 kPa to the condenser pressure of 23.1 kPa. When the bed reaches at 78^0C, refrigerant starts desorption and the process continues till it reaches maximum cycle

temperature (T_{max}). The curve 3→4 (isosteric cooling) shows a declining pattern of pressure. Lowest cycle pressure obtained at the end of this process is 0.36 kPa. The curve 4→1 (isothermal adsorption) indicates adsorption process of the system at constant temperature.

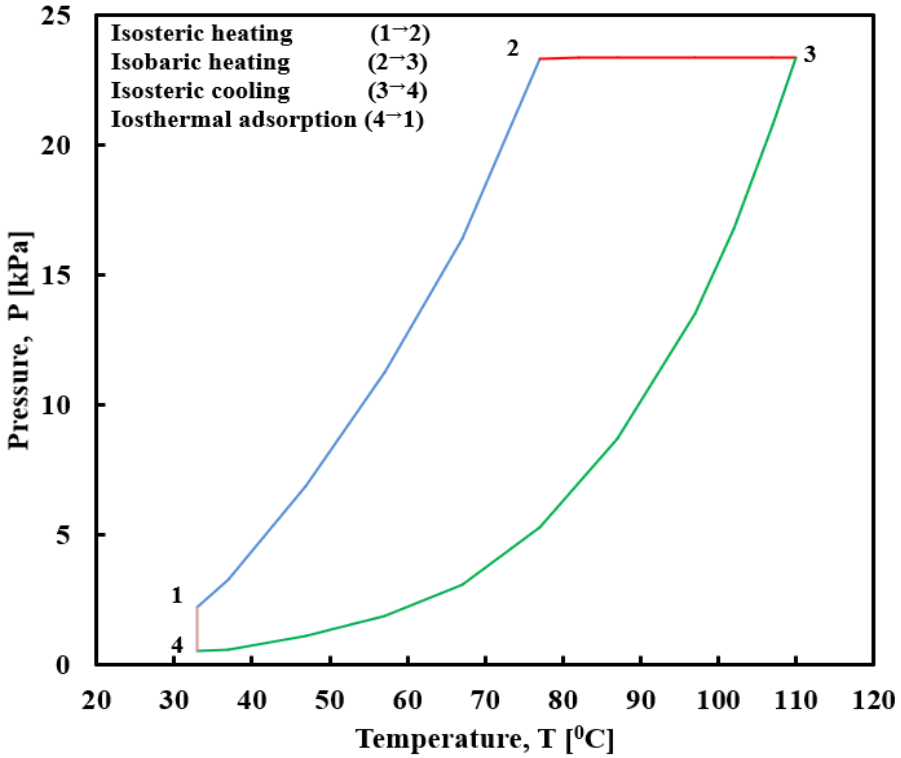

Fig. 5.13: Variation of adsorbent bed pressure with cycle temperature

5.9.3 Influence of adsorption bed temperature on the adsorbate concentration ratio and volume fraction

The adsorbate concentration ratio with cycle temperature at equilibrium are analysed by the Eq. (5.53) and its effect is shown in Fig. 5.14. During this cycle, the concentration ratio of adsorbate varies from the maximum of 0.39 kgkg^{-1} to a nadir value of 0.09 kgkg^{-1}, corresponding to adsorbed refrigerant phase mass 6.20 kg and 1.56 kg, respectively and refrigerant mass consumption efficiency (using Eq. (5.54)) as 74.85%. Figure 5.15 encapsulates adsorbate phase volume fraction with cycle temperature. As shown in Fig. 5.15, the fraction of adsorbed volume varies continuously during the adsorption process. In both isosteric heating and cooling a minor change of fraction of adsorbate refrigerant volume is noted. Due to the decrease in adsorbed refrigerant density in the adsorbent bed, the refrigerant volume fraction rises as the temperature rises in the

isosteric preheating process. Similarly, in the isosteric cooling process, volume fraction of the refrigerant decreases and hence the adsorbed refrigerant density increases with decreasing adsorbent bed temperature. Thus, from Eq. (5.19), the maximum and minimum volume fractions obtained in the above processes are determined as 0.30 and 0.07, respectively.

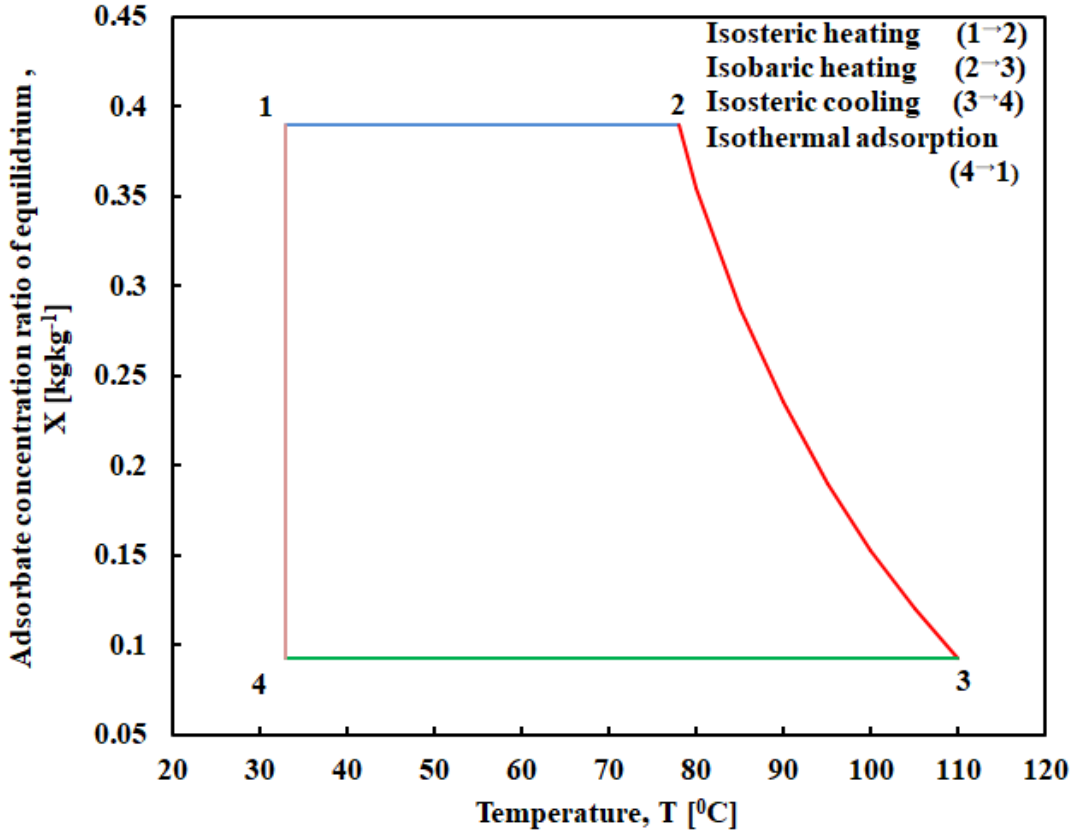

Fig. 5.14: Adsorbate concentration ratio with cycle temperature

5.9.4 Evolution of the effective mass of refrigerant desorbed/adsorbed during the isobaric heating /isothermal adsorption process

The effect of desorption temperature on effective mass of refrigerant desorbed during isobaric desorption process (2→3) is depicted in Fig. 5.16. It is obvious that during. isobaric heating, the rate of refrigerant desorbed from the adsorbent bed reaches at its peak valve. As the bed temperature increases, desorption rate increases continuously and at the end of this process, it reaches a lowest value that is sustained at minimum concentration and maximum cycle temperature. Figure 5.17 shows the effect of adsorbent bed pressure on the effective mass of refrigerant adsorbed during the isothermal adsorption process (4→1). In the isothermal adsorption, there is an upward trend in the rate of adsorption and

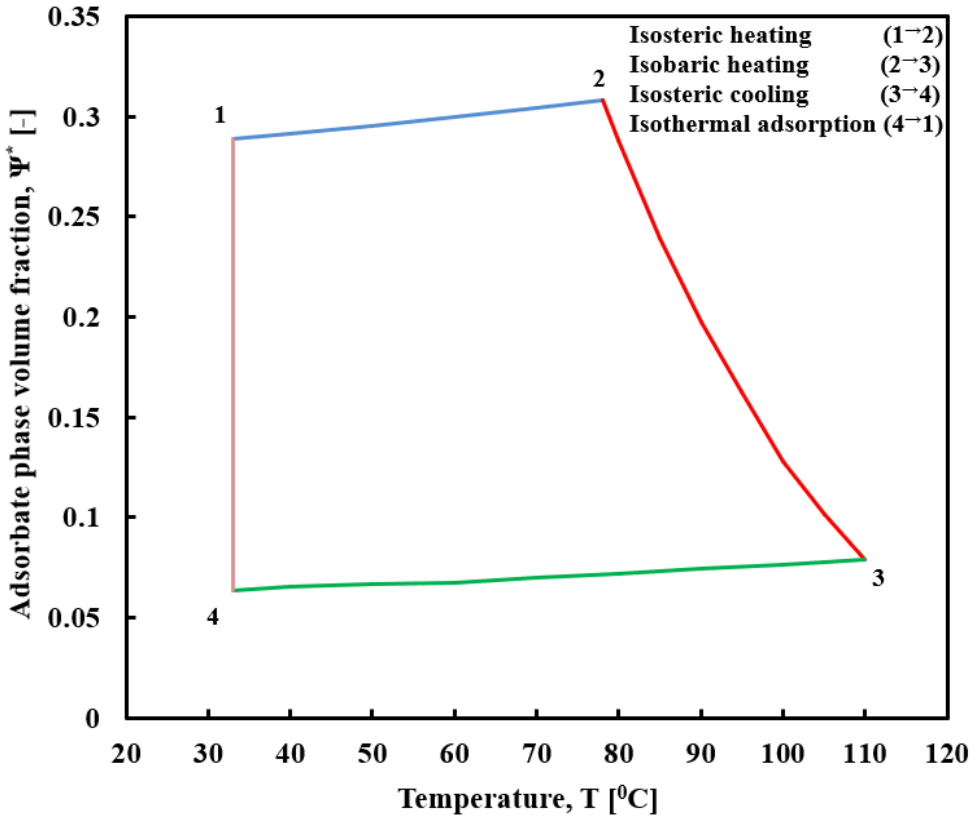

Fig. 5.15: Adsorbate phase volume fraction with cycle temperature

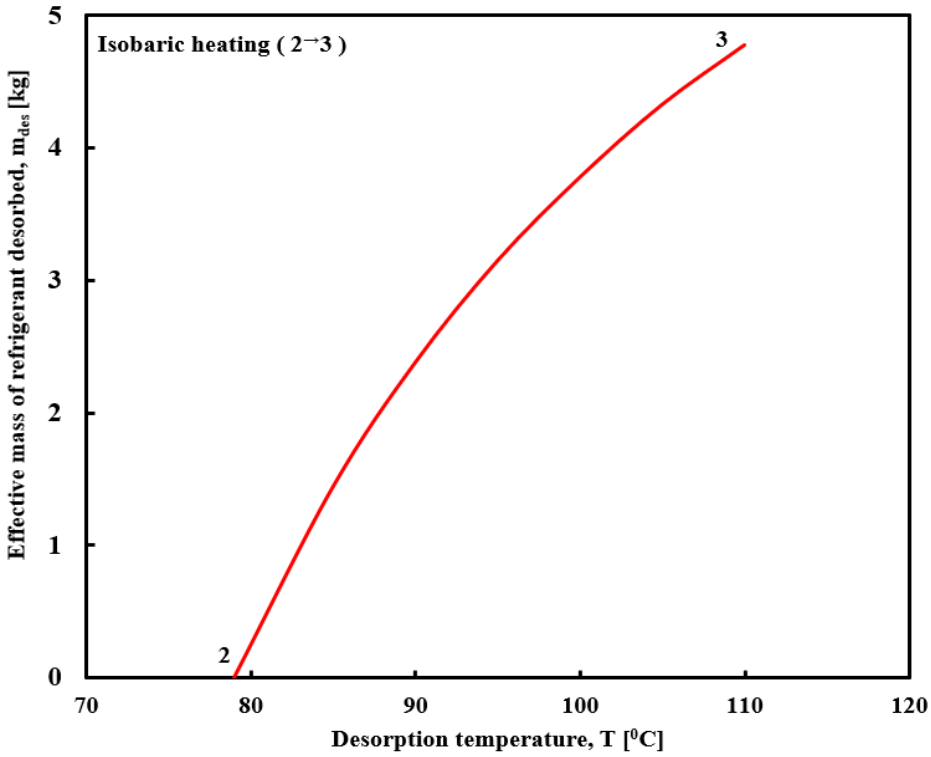

Fig. 5.16: Effect of desorption temperature on total mass of refrigerant desorbed during isobaric desorption process (2→3)

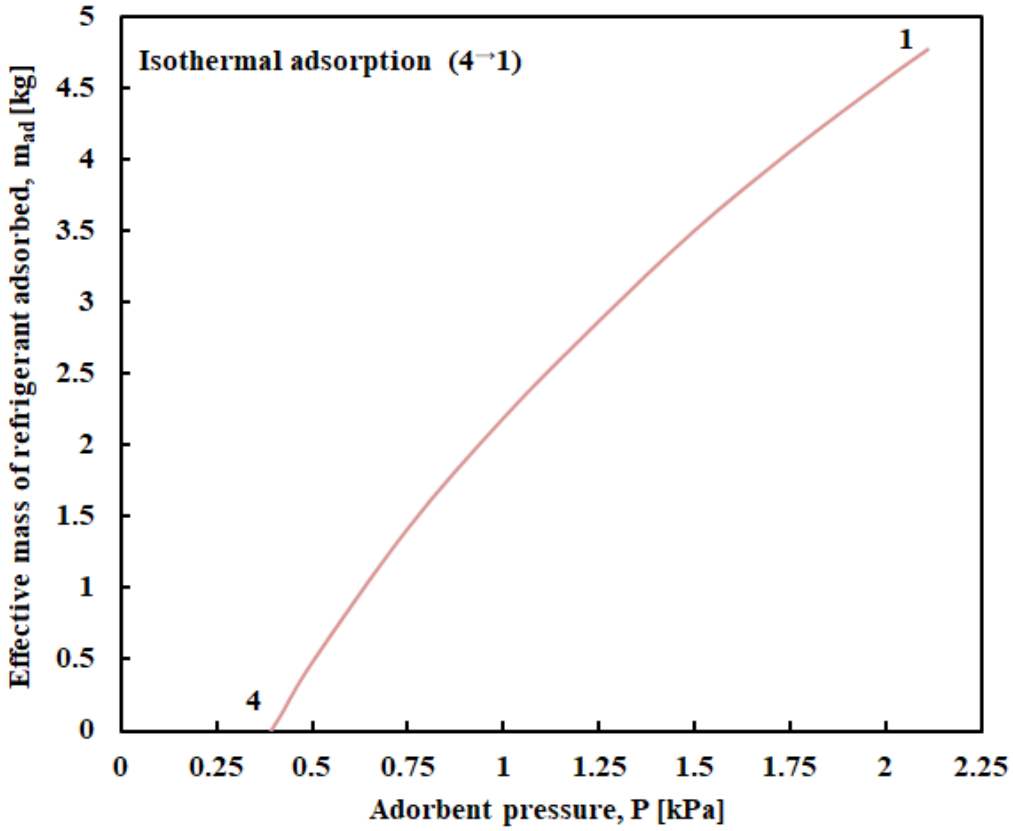

Fig. 5.17: Effect of adsorbent bed pressure on effective mass of refrigerant adsorbed during isothermal adsorption process (4→1)

the reason for the same is explained based on Langmuir adsorption isotherm. Langmuir adsorption isotherm defines the variation of adsorption with pressure and it is given by,

$$\emptyset = \frac{KP}{1+KP} \tag{5.55}$$

where $\emptyset$ is the fraction of total available adsorption area that is occupied by the adsorbent, P the pressure and K the adsorption equilibrium constant. At low-pressure, Langmuir adsorption isotherm approaches to KP and the fraction of refrigerant adsorbed varies linearly with pressure, known as the first–order region. Higher partial pressure of the bed tends to increase the adsorption tendency. However, as the pressure increases, available adsorption area decreases which leads to decrease in the adsorption process. At high-pressure, Langmuir adsorption isotherm approaches to 1, which means that the surface area available for adsorption is limited and area occupied by adsorbate are known as zero-order region. Thus, a rise in pressure has no effect on the rate of the adsorption process.

5.9.5 Accumulated amount of specific energy added or removed during heating or cooling process of adsorbent bed

The accumulated amount of specific energy applied to the adsorbent bed during the heating process is presented in Fig. 5.18. The adsorbent bed has been triggered by a total specific energy of 430.81 $kJkg^{-1}$. In the preheating process, a portion of total heat, i.e. 22.57% is used to raise the bed temperature from ambient to desorption. The remaining

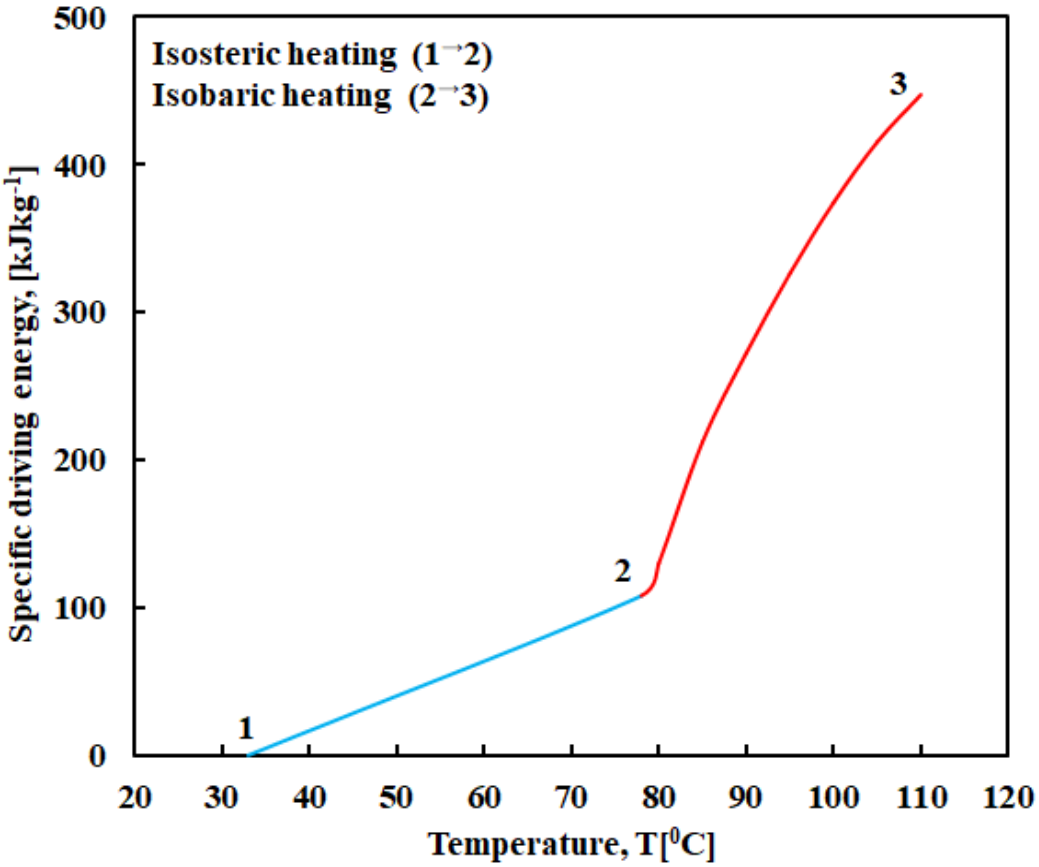

Fig. 5.18: Accumulated amount of specific energy applied to the adsorbent bed during the heating processes(1→2→3)

77.43% has been used for the constant pressure desorption process. Figure 5.18 illustrates the rate of increase of temperature in the course of isosteric heating (1→2), which is more rapid as compared with that of isobaric heating (2→3). During the isosteric heating process, the entire input energy has been used for sensible heating of the bed. A significant portion of the total heat input has been used for desorption of refrigerant during the isobaric heating process. Figure 5.19 depicts the aggregate amount of specific energy expelled from the

adsorbent bed during cooling process, where the total amount of heat energy rejected is 422.5 kJkg^{-1}. Initially, in the isosteric cooling (3→4), only a portion of this energy, about 26.11%, has been lost to the atmosphere and it is utilised by the bed to sustain its original ambient temperature. During the isothermal adsorption (4→1), the remaining portion of this energy has been discharged from the bed to the atmosphere.

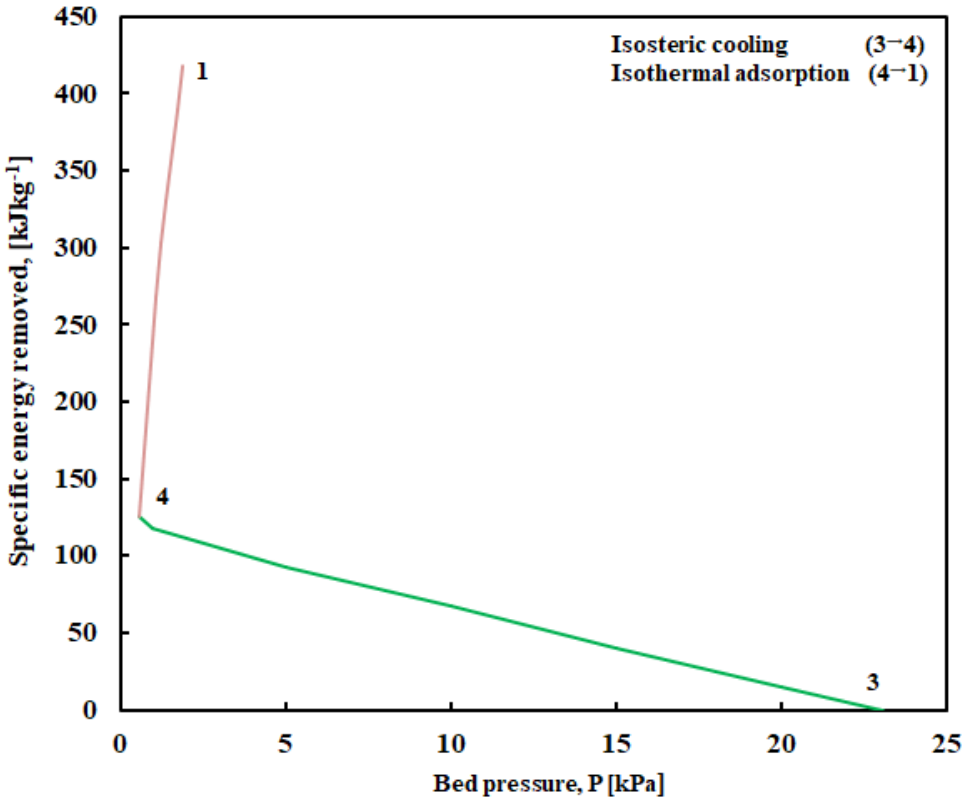

Fig. 5.19: Accumulated amount of specific energy expelled from the adsorbent bed during cooling processes (3→4→1)

5.9.6 Effect of maximum desorption temperature on the performance of the system

The effect of maximum desorption temperature on the cycle COP and refrigerating effect is presented in Fig. 5.20. Initially, the COP of the system increases with increase in desorption temperature and attains its maximum value and then slowly decreases when the system is operating at constant atmospheric temperature. As desorption temperature (T_{max}) increases, desorption of the refrigerant mass also increases internally, which causes an increase in the refrigerating effect. The COP of the system increases to an optimal value and it reduces further, beyond the optimal value of desorption temperature. During this process, the energy consumed by the adsorbent is used to improve sensible heat of the

system components. Thus, the change of COP beyond an optimal value is very small. The COP of the system obtained from the simulation study is 0.68 for the maximum desorption temperature of 95^0C as depicted in Fig 5.20. The effect of maximum desorption temperature on specific cooling power of the cycle is depicted in Fig. 5.21. The maximum desorption cycle temperature is one of the decisive factors on the SCP. The ascending dependency between the SCP and desorption temperature is due to the increase in desorption temperature resulting in good desorption, hence, improves the adsorption refrigeration performance.

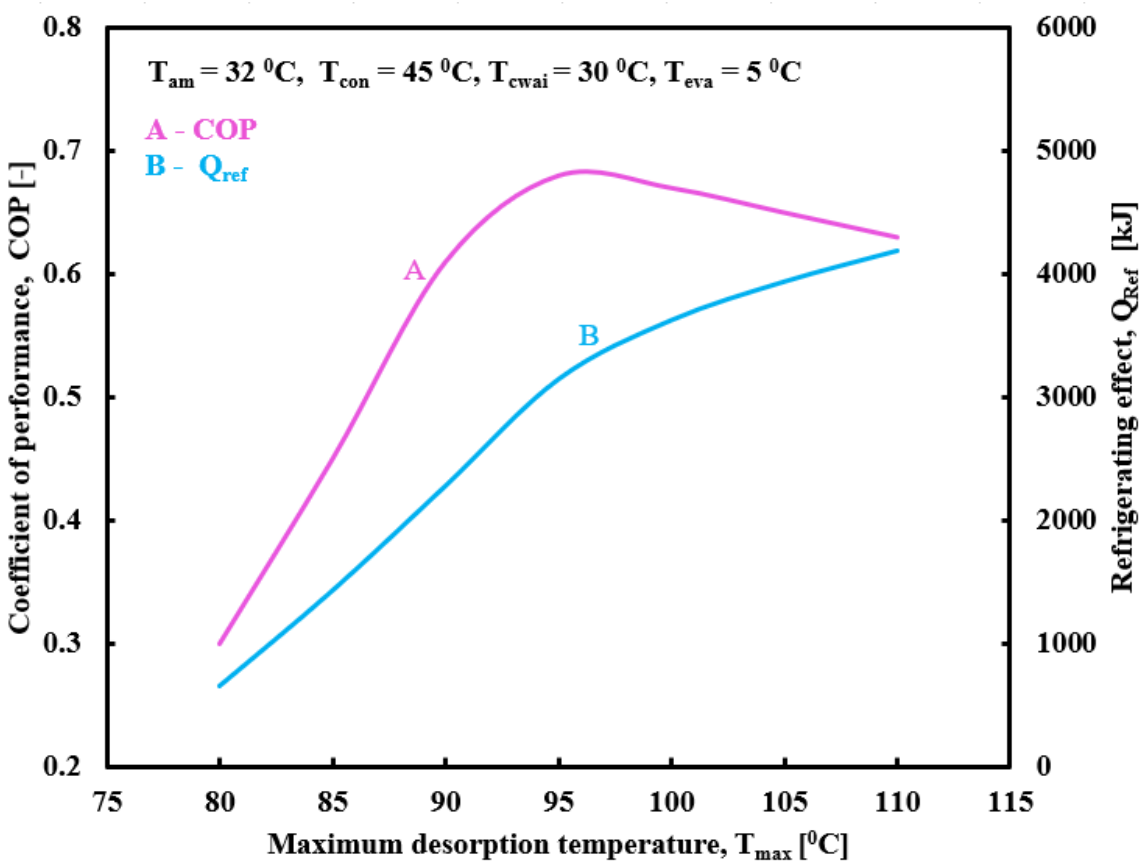

Fig. 5.20: Effect of maximum desorption temperature on COP and refrigerating effect

5.10 Comparison of Present Study with Works Reported in Literature

The Fig. 5.22 illustrates a comparison between present study and works reported in the literature. The COP of the system obtained in the present investigation is about 13.23% higher than that reported by Saha *et al.* [29]. Comparison with works reported by Sadeghlu

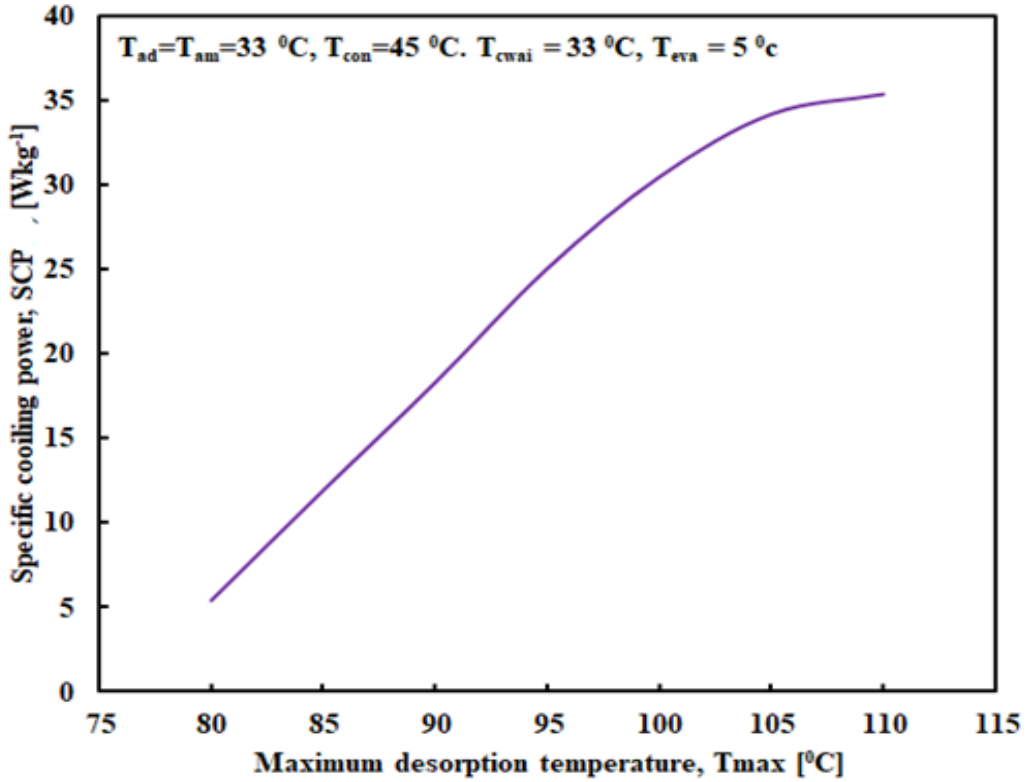

Fig. 5.21: Effect of maximum desorption temperature on specific cooling power of the cycle

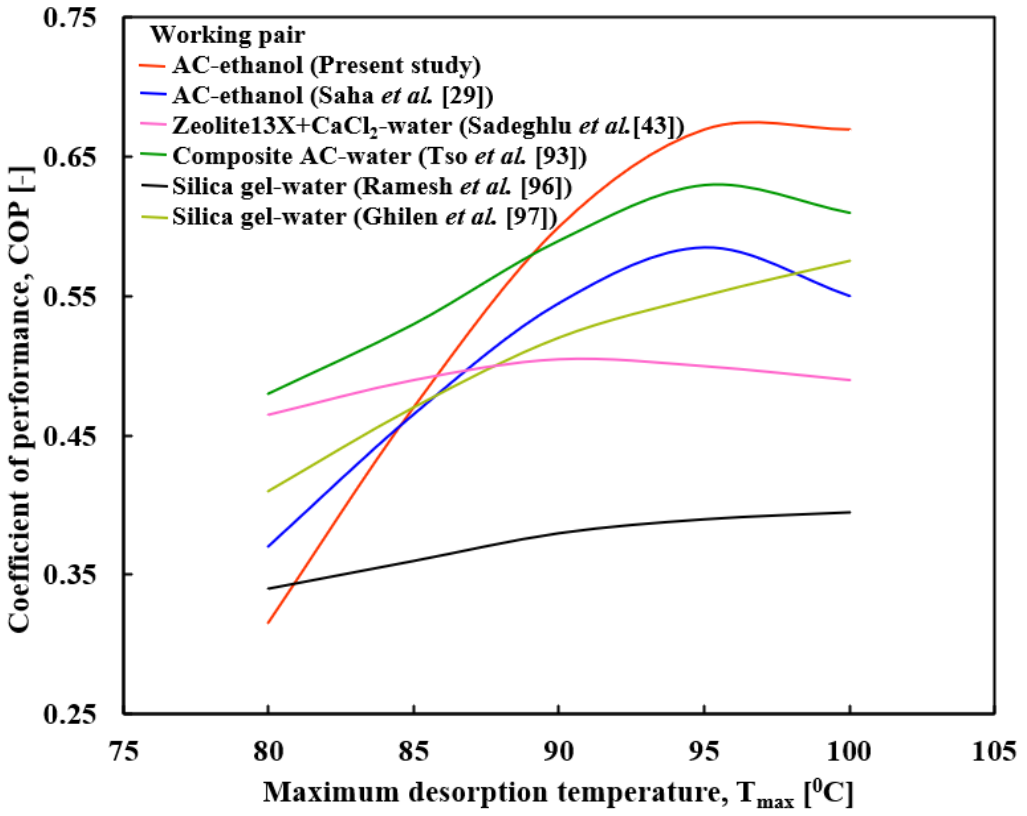

Fig. 5.22: Comparison between present study and works reported in the literature

al. [43], Tso *et al.* [93], Ramesh et al [96] and Ghilen *et al.* [97] are also presented in *et* Fig. 5.22.

5.11 Exergy Analysis of the SAC System

The energy balance equation of the SAC system and its studies does not provide a clear picture of losses in the system. Exergy assessment measures the destruction and losses In various components of the overall system. Thus, it is preferable to investigate the exergy analysis of the SAC system in order to improve performance by correcting the losses that occur in each component of the system.

To simplify mathematical formulation of the exergy models, the following assumptions are to be considered:

i. The SAC system operates at a very low vapour pressure; hence the interaction between the refrigerant particles is very less, resulting in the vapour refrigerant behaving like a perfect gas
ii. The adsorbent beds are well-insulated, and the system is adiabatic in nature, which means that there is no heat loss to the surrounding environment
iii. Physical exergy accounts for the majority of the system's exergy, as the fluid velocity in the SAC system is low and there is no datum head to account for kinetic and potential exergy. Furthermore, because to the weak Van der Waals forces, the adsorbent and adsorbate are solid and vapour, respectively, and the system is free of chemical reaction. Hence the chemical exergy is not considered for the present study.
iv. The throttling process is isenthalpic since no work is done or heat is transferred from or to the system. The kinetic energy terms are often minimal since the velocity of flow through the expansion valve is negligibly small
v. It is assumed that the physical parameters of the adsorbent bed do not change. During desorption and adsorption, the adsorption bed is heated and cooled. Most of the time, fluid convective heat transfer from the outside is used to heat the adsorbent bed. Since it is made of metal, the heat capacity of the adsorption bed is less than that of the external fluid. So, its physical characteristics are thought to be constant.

5.11.1 Exergy assessment of the collector-receiver system

The quality of energy is specified by the second law. It is more directly concerned with energy depletion, entropy creation, and lost work opportunities during the process, and it has a lot of room for improvement. The section describes the exergy assessment of the SAC system in a separate manner.

(i) Collector

A solar collector system consists of a parabolic trough with a fluid-passing absorber or receiver tube. This fluid transfers heat energy from the solar collector system to the bed. The energy received (Q_{in}) and absorbed (Q_a) by the solar collector is given by [98-101],

$$Q_{in} = \left(I_{br} R_g\right) A_p L \tag{5.56}$$

$$I_{br} = I_{max} sin\left[\frac{3.141(t - t_{sr})}{(t_{ss} - t_{sr})}\right] \tag{5.57}$$

$$Q_a = (I_{br} R_g)(\tau \propto)\left[BY + \frac{D_0}{A_P - D_0}\right] \tag{5.58}$$

$$\text{Energy loss}_{co} = Q_{in} - \ Q_a \tag{5.59}$$

$$\text{Percentage of Energy loss}_{co} = \left[\frac{Q_{in} - Q_a}{Q_{in}}\right] .100 \tag{5.60}$$

The solar collector energy efficiency is then defined as the ratio of energy absorbed to the energy received by the collector, and can be represented as:

$$\eta_{co} = \frac{Q_a}{Q_{in}} \tag{5.61}$$

Eqs. (5.62) and (5.63) are used for calculating the exergy received (Ex_{in}) and exergy adsorbed (Ex_a) by the solar collector and the Eq. (5.66) gives the exergy efficiency or second law efficiency ($\eta_{Ex,co}$) of the collector system.

$$Ex_{in} = Q_{in}\left(1 - \frac{T_0}{T_{so}}\right) \tag{5.62}$$

$$Ex_a = Q_a\left(1 - \frac{T_0}{T_{co}}\right) \tag{5.63}$$

The difference between the exergy received and absorbed by the solar collector is known as exergy loss or irreversibility of the collector and can be denoted as,

$$\text{Exergy loss}_{\text{co}}\ (\pi_{co}) = \text{Irreversibility}_{\text{co}}\ (IR_{co}) = Ex_{in} - Ex_a \tag{5.64}$$

$$\%\ \text{of Exergy loss}_{\text{co}} = \left[\frac{IR_{co}}{Ex_a}\right].100 \tag{5.65}$$

$$\eta_{Ex,co} = \frac{Ex_a}{Ex_{in}} \tag{5.66}$$

(ii) Receiver

Equation for exergy efficiency and exergy delivered to the liquid flowing through the receiver tubes are presented as follows. The usable energy to the fluid flowing through the receiver tube is given as,

$$Q_{use} = \dot{m_w}\, C_P(T_{wo} - T_{wi}) \tag{5.67}$$

$$\text{Energy loss}_{\text{re}} = Q_a - Q_{use} \tag{5.68}$$

$$\%\ \text{of Energy loss}_{\text{re}} = \left[\frac{Q_a - Q_{use}}{Q_a}\right].100 \tag{5.69}$$

The energy efficiency of the receiver system is defined as the ratio of energy transferred to the fluid flowing through the tube to energy absorbed by the collector of the solar collector system.

$$\eta_{re} = \frac{Q_{use}}{Q_a} \tag{5.70}$$

The useful exergy delivered by the receiver system is given by,

$$\text{Ex}_{\text{use}} = \dot{m_w}\,[(h_{wo} - h_{wi}) - T_0(s_{wo} - s_{wi}] \tag{5.71}$$

$$\text{Exergy loss}_{\text{re}}\ (\pi_{\text{re}}) = \text{Irreversibility}_{\text{re}}\ (\text{IR}_{\text{re}}) = Ex_a - Ex_{use} \tag{5.72}$$

$$\%\ \text{of Exergy loss}_{\text{re}} = \left[\frac{\text{IR}_{re}}{\text{Ex}_{use}}\right].100 \tag{5.73}$$

The ratio of the useful exergy delivered by the receiver system to the exergy absorbed by the solar collector is defined as the exergy efficiency of the receiver system of the solar collector. This can be written as,

$$\eta_{Ex,re} = \frac{Ex_{use}}{Ex_a} \quad (5.74)$$

(iii) Collector - receiver system

The product of the collector and receiver system efficiency can be used to define the overall system performance and can be denoted as:

$$\eta_{co-re} = \eta_{co}\, x\, \eta_{re} \quad (5.75)$$

$$\eta_{co-re} = \frac{Q_{use}}{Q_{in}} \quad (5.76)$$

The overall second law efficiency of the solar collector and receiver system is written as the product of the collector and receiver system efficiency.

$$\eta_{Ex,co-re} = \eta_{Ex,co}\, x\, \eta_{Ex,re} = \frac{Ex_{use}}{Ex_{in}} \quad (5.77)$$

5.11.2 Exergy analysis of the adsorption cooling system

Adsorption isotherms reveal the amount of refrigerant that can be absorbed in the micropores of the adsorbent under constant conditions. Numerous relationships have been utilised to determine the adsorption isotherms for numerous adsorbent-adsorbate combinations. The exergy balance of each of the system components to has been formulated from the general exergy balance equation. The exergy balance of each components of the system has been formulated from the general exergy balance equation as given below [102],

$$\Delta U - T_0 \Delta S = \sum \left(1 - \frac{T_0}{T_i}\right) Q_i - \left[\sum_f m(h - T_0 S) - \sum_i m(h - T_0 S)\right] - T_0 \Delta S_{gen} \quad (5.78)$$

where,

$$\sum \left(1 - \frac{T_0}{T_i}\right) Q_i = \sum Ex(Q_i) \quad (5.79)$$

$$\sum_f m(h - T_0 S) - \sum_i m(h - T_0 S) = \sum \varepsilon_f - \varepsilon_i \quad (5.80)$$

$$T_0 \Delta S_{gen} = \pi \quad (5.81)$$

rearranging the Eq. (5.78) in terms of exergy losses/destruction or irreversibility and can be written as;

$$\pi = \sum Ex(Q_i) - \left[\sum \varepsilon_f - \varepsilon_i\right] - [\Delta U - T_0 \Delta S] \quad (5.82)$$

The first law of thermodynamics is given as,

$$\Delta U = Q - W \quad (5.83)$$

Since the adsorbent bed does not move under pressure, work done is zero. Thus Eq. (5.83) can be written as:

$$\Delta U = Q \quad (5.84)$$

Figure 5.11 depicts the entire cycle of a SAC system, which includes four processes: isosteric heating, isobaric heating (desorption), isosteric cooling, and isothermal cooling (adsorption).

(i) Isosteric heating Process 1→2

During the isosteric heating of the adsorbent bed, one of the adsorbent beds is sensibly heated at a uniform adsorbate mass of X_{max}.

Thus $\sum \varepsilon_f - \sum \varepsilon_i$ is zero and then Eq. (5.82) reduces to

$$\Pi_{1\to2} = \sum Ex(Q_{1\to2}) - (\Delta U_{1\to2} - T_0 \Delta S_{1\to2}) \quad (5.85)$$

where,

$$Ex(Q_{1\to2}) = \left(1 - \frac{T_0}{T_H}\right) Q_{1\to2} = \left(1 - \frac{T_0}{T_H}\right) \left[(m_b c_b + m_{mc} c_{mc} + m_b c_{ref} X_{max}) \int_{T_{amb}}^{T_{gen}} dT \right] \quad (5.86)$$

The internal energy change of the process is determined from

$$\Delta U_{1\to2} = (m_b c_b + m_{mc} c_{mc} + m_b c_{ref} x_{max}) \int_{T_{amb}}^{T_{gen}} dT \quad (5.87)$$

while the change in entropy is obtained by Eq. (5.88)

$$\Delta S_{1\to2} = (m_b c_b + m_{mc} c_{mc} + m_b c_{ref} x_{max}) \int_{T_{amb}}^{T_{gen}} \frac{dT}{T} \quad (5.88)$$

(ii) Isobaric heating or desorption Process 2→3

During isobaric heating, the adsorbent bed undergoes a constant pressure desorption. The concentration of adsorbate (x) decreases to a minimum value x_{min}. The entire heat input to the system during process 2→3 is utilized for the desorption of the adsorbate from adsorbent and partly used for sensible heating of the bed, metal cover and adsorber. In this process, exergy loss is given as:

$$\Pi_{2\to3} = Ex(Q_{2\to3}) - (\varepsilon_f - \varepsilon_i) - (\Delta U_{2-3} - T_0 \Delta S_{2\to3}) \quad (5.89)$$

where,

$$Ex(Q_{2\to3}) = \left(1 - \frac{T_0}{T_H}\right) Q_{2\to3}$$
$$= \left(1 - \frac{T_0}{T_H}\right) \left[(m_b c_b + m_{mc} c_{mc}) \int_{T_{gen}}^{T_{max}} dT + m_b c_{ref} \int_{T_{gen}}^{T_{max}} X\, dT + m_b \int_{T_{gen}}^{T_{max}} \Delta H \left(\frac{dX}{dT}\right)_{P=c} dT\right] \quad (5.90)$$

The Clausis-Clapeyron equation can be used to calculate ΔH, which is the desorption or adsorption heat per unit mass of ethanol, which can be written as:

$$\Delta H = R T^2 \left(\frac{\partial \ln P}{\partial T}\right)_{X=C} \quad (5.91)$$

The change in mass, internal energy and entropy of the isosteric heating process are obtained from the Eqs. (5.92)-(5.94)

$$\varepsilon_f - \varepsilon_i = m_b \int_{T_{gen}}^{T_{max}} \Delta H \left(\frac{dX}{dT}\right)_{P=c} dT - T_0 \left(m_b \int_{T_{gen}}^{T_{max}} \frac{\Delta H}{T} \left(\frac{dX}{dT}\right)_{P=c} dT\right) \quad (5.92)$$

$$\Delta U_{2\to3} = (m_b c_b + m_{mc} c_{mc}) \int_{T_{gen}}^{T_{max}} dT + m_b c_{ref} \int_{T_{gen}}^{T_{max}} X\, dT + m_b \int_{T_{gen}}^{T_{max}} \Delta H \left(\frac{dX}{dT}\right)_{P=c} dT \quad (5.93)$$

$$\Delta S_{2\to3} = (m_b c_b + m_{mc} c_{mc}) \int_{T_{gen}}^{T_{max}} \frac{dT}{T} + m_b c_{ref} \int_{T_{gen}}^{T_{max}} \left(\frac{dX}{dT}\right)_{P=c} \frac{dT}{T} \quad (5.94)$$

(iii) Isosteric cooling Process 3→4

In the isosteric cooling process, heat rejects from the bed to the cooling media at constant adsorbate concentration, x_{min}. The mass of adsorbate in the adsorbent bed remains constant during this cooling process and cooling will continue until the dead state (T_0) is reached. Moreover $\sum \varepsilon_f - \sum \varepsilon_i$ is zero and the loss of exergy in this process becomes

$$\Pi_{3\to4} = Ex(Q_{3\to4}) - (\Delta U_{3\to4} - T_0 \Delta S_{3\to4}) \quad (5.95)$$

where $Ex(Q_{3\to4})$, $\Delta U_{3\to4}$ and $T_0 \Delta S_{3\to4}$ are the change in heat energy, internal energy and entropy of the isosteric cooling of the system in the process 3→4 , given by Eqs. (5.96)-(5.98)

$$Ex(Q_{3\to4}) = \left(1 - \frac{T_0}{T_0}\right) Q_{3\to4} = 0 \quad (5.96)$$

$$\Delta U_{3\to4} = (m_b c_b + m_{mc} c_{mc} + m_b x_{min} c_{ref}) \int_{T_{max}}^{T_{ad}} dT \quad (5.97)$$

$$\Delta S_{3\to4} = (m_b c_b + m_{mc} c_{mc} + m_b x_{min} c_{ref}) \int_{T_{max}}^{T_{ad}} \frac{dT}{T} \quad (5.98)$$

(iv) Isothermal adsorption Process 4→1

The bed begins to adsorb refrigerant vapour in the isothermal adsorption process. The concentration of adsorbate (x) rises to a maximum value x_{max}, and this increase in adsorbate mass at constant temperature and varying pressure. Therefore, the loss of exergy is given by,

$$\Pi_{4\to1} = Ex(Q_{4\to1}) - (\varepsilon_f - \varepsilon_i) - (\Delta U_{4\to1} - T_0 \Delta S_{4\to1}) \quad (5.99)$$

$$Ex(Q_{4\to1}) = 0 \quad (5.100)$$

Eq (46) gives change in mass energy of process 4→1.

$$\varepsilon_f - \varepsilon_i = m_b \int_{P_{min}}^{P_{ev}} \Delta H \left(\frac{dX}{dp}\right)_{T=c} dP - T_0 \left(m_b \int_{P_{min}}^{P_{ev}} \frac{\Delta H}{T} \left(\frac{dX}{dP}\right)_{T=c} dP\right) \quad (5.101)$$

Internal energy and entropy is given by Eqs. (5.102) and (5.103)

$$\Delta U_{4\to1} = m_b \int_{P_{min}}^{P_{ev}} \Delta H \left(\frac{dX}{dp}\right)_{T=c} dP \quad (5.102)$$

$$\Delta S_{4\to1} = 0 \quad (5.103)$$

5.11.3 Exergy balance of the condenser

The refrigerant vapour desorbed from the adsorbent bed enters the condenser. Figure 5.23 shows the control volume of condenser, expansion valve and evaporator. The refrigerant is firstly de-superheated in the condenser, and then reduces the latent heat of condensation. Since there is no internal energy or entropy formation in this process, the area considers it as a quasi-stationary operation regime where heat exchange happens slowly. Hence, the destruction of exergy at condenser can be written as:

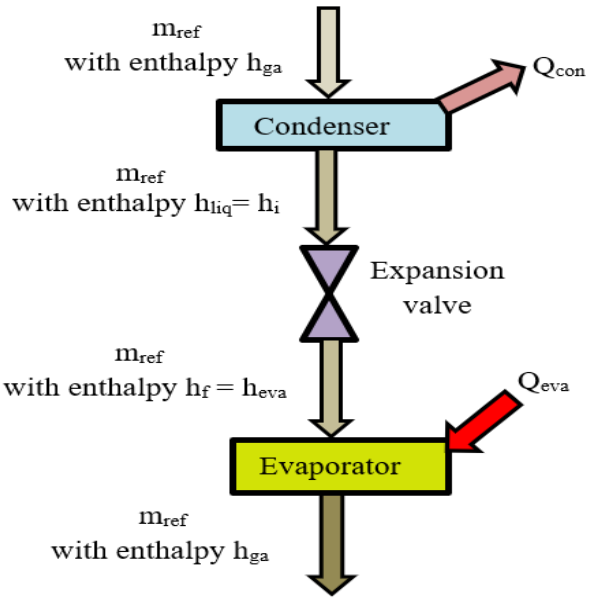

Fig. 5.23: Control volume of condenser, expansion valve and evaporator

$$\Pi_{con} = Ex(Q_{con}) - (\varepsilon_f - \varepsilon_i) \quad (5.104)$$

where

$$Ex(Q_{con}) = \left(1 - \frac{T_0}{T_0}\right) Q_{con} = 0 \quad (5.105)$$

$$(\varepsilon_f - \varepsilon_i) = m_{ref}[h_{ga} - h_{liq}] - m_{ref} T_0 [s_{ga} - s_{liq}] \quad (5.106)$$

$$m_{ref} = m_a (X_{max} - X_{min}) \quad (5.107)$$

5.11.4 Exergy balance of the throttling device

The throttling process is assumed to be isenthalpic which is shown in Fig. 5.23. The exergy destruction of throttling device can be written as,

$$\Pi_{Exp} = -(\varepsilon_f - \varepsilon_i) \quad (5.108)$$

where,

$$\varepsilon_f - \varepsilon_i = m_{ref} T_0 (s_f - s_i) \quad (5.109)$$

5.11.5 Exergy balance for the Evaporator

The evaporator produces cold water by evaporating the liquid adsorbate, whose control volume is depicted in Fig. 5.23. Since the adsorbate mass flow rate and vapour production during this process are very low, the evaporator is considered as a quasi-stationary operation regime. Furthermore, there is no adsorbate superheating in this process. Thus, the exergy destruction of the evaporator is given by,

$$\Pi_{ev} = Ex(Q_{Ref}) - (\varepsilon_f - \varepsilon_i) \quad (5.110)$$

where the heat exergy and mass exergy variation are obtained from Eqs. (5.111) and (5.112) respectively.

$$Ex(Q_{Ref}) = \left(1 - \frac{T_0}{T_{eva}}\right) Q_{Ref} = \left(1 - \frac{T_0}{T_{eva}}\right) m_{ref} L_{ref} \quad (5.111)$$

$$(\varepsilon_f - \varepsilon_i) = m_{ref}[h_{ga} - h_{eva}] - m_{ref}T_0[s_{ga} - s_{eva}] \quad (5.112)$$

5.11.6 Exergy efficiency

Exergy efficiency (η_{Ex}) is expressed as the fraction of exergy output to exergy input in a system and can be written as,

$$\eta_{Ex} = \frac{\text{Exergy output}}{\text{Exergy input}} = \frac{|Ex(Q_{eva})|}{Ex(Q_{In})} = 1 - \frac{\Pi_{Ex,loss}}{Ex(Q_{In})} \quad (5.113)$$

where,

$$\pi_{Ex,loss} = \pi_{1-2} + \pi_{2-3} + \pi_{3-4} + \pi_{4-1} + \pi_{con} + \pi_{exp} + \pi_{eva} \quad (5.114)$$

$$Ex(Q_{In}) = Ex(Q_{1-2}) + Ex(Q_{2-3}) \quad (5.115)$$

$$Ex(Q_{In}) = |Ex(Q_{Ref})| + \pi_{Ex,loss} \quad (5.116)$$

5.12 Results and Discussion

MATLAB R2019b environment is used for the mathematical modelling of the SAC system for the exergy analysis using the baseline parameters listed in Table 5.5 and Table 5.6. The variation of solar insolation and receiver temperature output with day time is shown in the Fig. 5.3. The highest solar irradiation and receiver output temperature are found to be between 11.00 h and 14.00 h during the day. Moreover, the properties of the ethanol used in this study are obtained from REFPROP-10 NIST (Johnson, 2013)

Table 5.5 Parameters for the analysis of the solar collector [103-104]

Parameter	Numerical Value	Parameter	Numerical Value
τ	0.76 [-]	L_c	2.5 m
Y	0.93 [-]	T_{so}	5505^0C
R_g	1.002 [-]	T_{co}	33^0C
α	0.94 [-]	T_o	33^0C
D_o	0.03 m	$\dot{m}_w$	0.03 kgs^{-1}
A_p	1.2 m	I_{max}	950 Wm^{-2}

Table 5.6 Parameters for exergy analysis of adsorption cooling system

Parameter	Numerical value	Parameter	Numerical Value
C_b	0.71 $kJkg^{-1}K^{-1}$	m_{mc}	16 kg
C_{mc}	0.48 $kJkg^{-1}K^{-1}$	T_{con}	33^0C
C_{ref}	2.48 $kJkg^{-1}K^{-1}$	T_{ev}	5^0C
m_b	16 kg	T_{gen}	78^0C

5.12.1 Influence of maximum cycle temperature on minimum cycle pressure with atmospheric temperature

The influence of maximum cycle temperature and ambient temperature on minimum cycle pressure is depicted in Fig. 5.24. It is evident that increasing in the maximum cycle or adsorbent temperature results in a decrease in the minimum cycle pressure in accordance with Eq. (5.18). Moreover, the minimum cycle pressure increases as the ambient temperature rises, resulting in a lower maximum cycle temperature. Furthermore, as seen in the Fig. 5.24 the influence of ambient temperature on minimum cycle pressure becomes negligible at highest maximum adsorbent temperature. As a result,

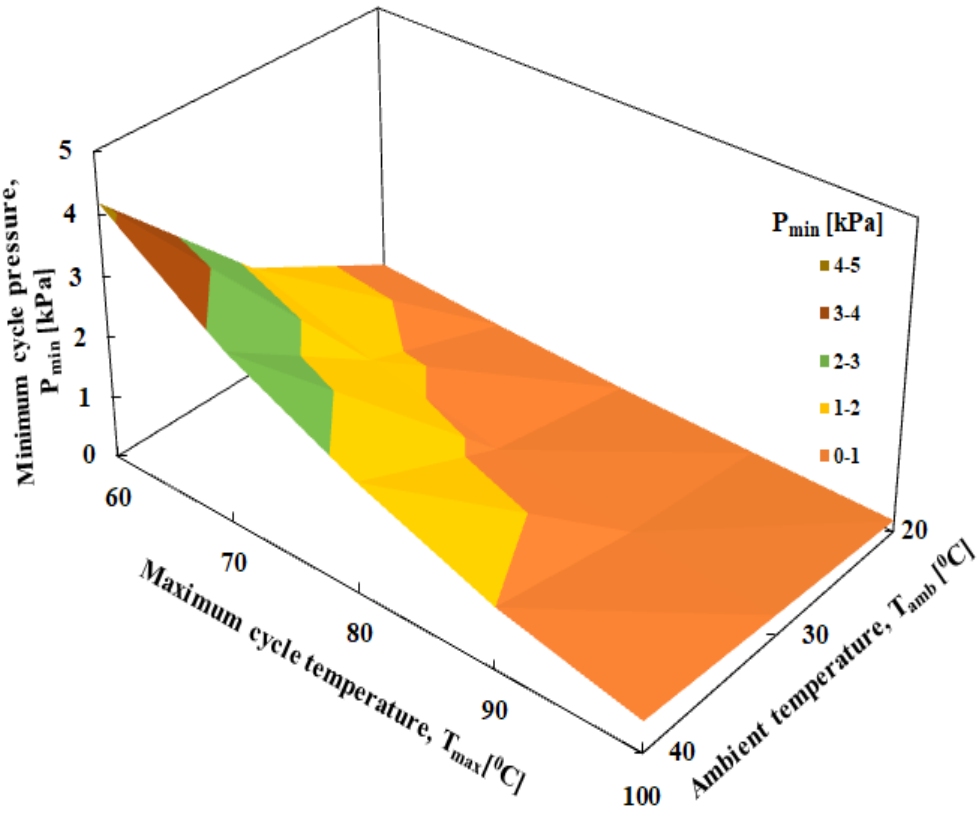

Fig. 5.24: Influence of maximum cycle temperature on minimum cycle pressure

in addition to the maximum cycle temperature; the ambient or atmospheric temperature has a significant impact on the minimum cycle pressure. The role of minimum cycle pressure in the adsorption process is to improve the total adsorption rate of the refrigerant by the adsorbent in the bed as the cycle pressure drops. This is because when the beds pressure drops, more desorbed refrigerant is able to adsorb in the voids, raising the temperature and slowing the adsorption process. This temperature rise can be reduced by flowing cold water through the bed, which improves the rate of adsorption. As a result, the minimal cycle pressure increases adsorption property of the bed, resulting in improved system performance.

5.12.2 Impact of maximum cycle or condenser temperature on exergy efficiency

The effect of maximum cycle temperature (T_{max}) on exergy efficiency is shown in Fig. 5.25. As the maximum cycle (heat source) temperature rises, exergy efficiency declines from 35.8% to 28.3%. The high heat source temperature leads to a faster

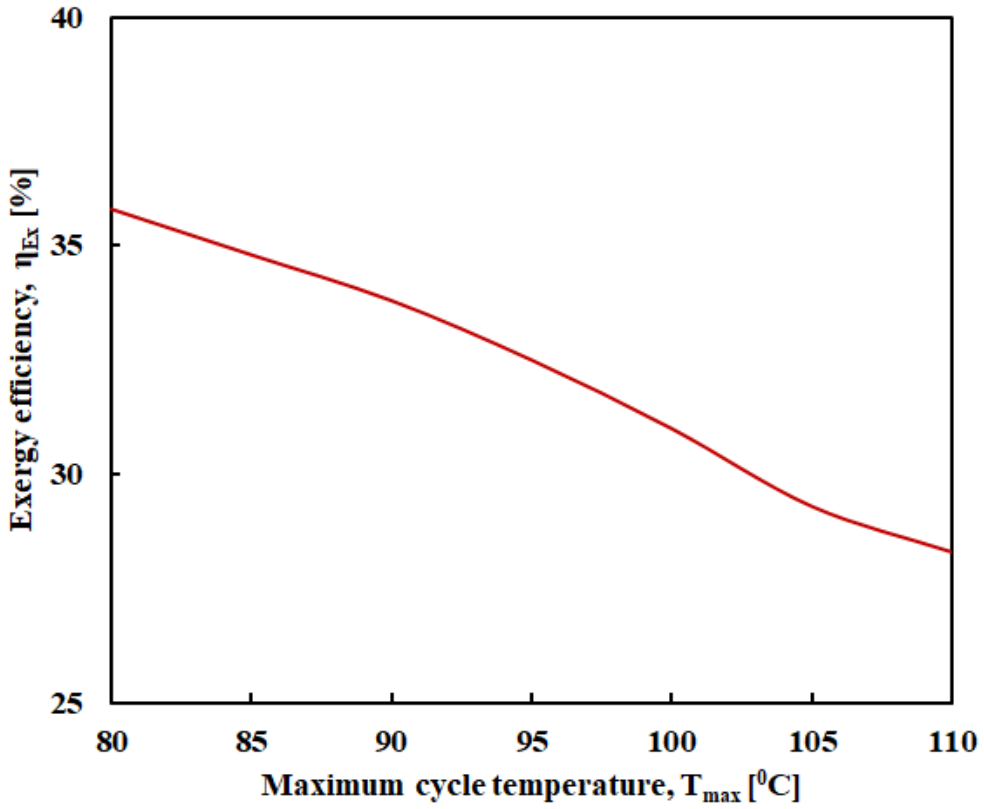

Fig. 5.25: Impact of maximum cycle temperature on exergy efficiency

adsorption in the adsorbent bed during the adsorption process. As the heat source temperature increases, significant exergy destruction inside the adsorption bed is expected, resulting in a decline in exergy efficiency. Figure 5.26 shows the impact of condenser temperature on exergy efficiency. The exergy efficiency decreases as the condenser temperature increases. As the temperature of the condenser rises, so does the pressure of the condenser, as well as the pressure difference between the evaporator and condenser subsystem increases. This necessarily needs higher isosteric heat and a longer switching time for adsorption or desorption. Thus, for a fixed cycle time and longer switching time, desorption or adsorption cycle time reduces which causes reduction in adsorbate circulation in the system. The above fact leads for increasing exergy degradation that causes lowering the exergy efficiency of the system.

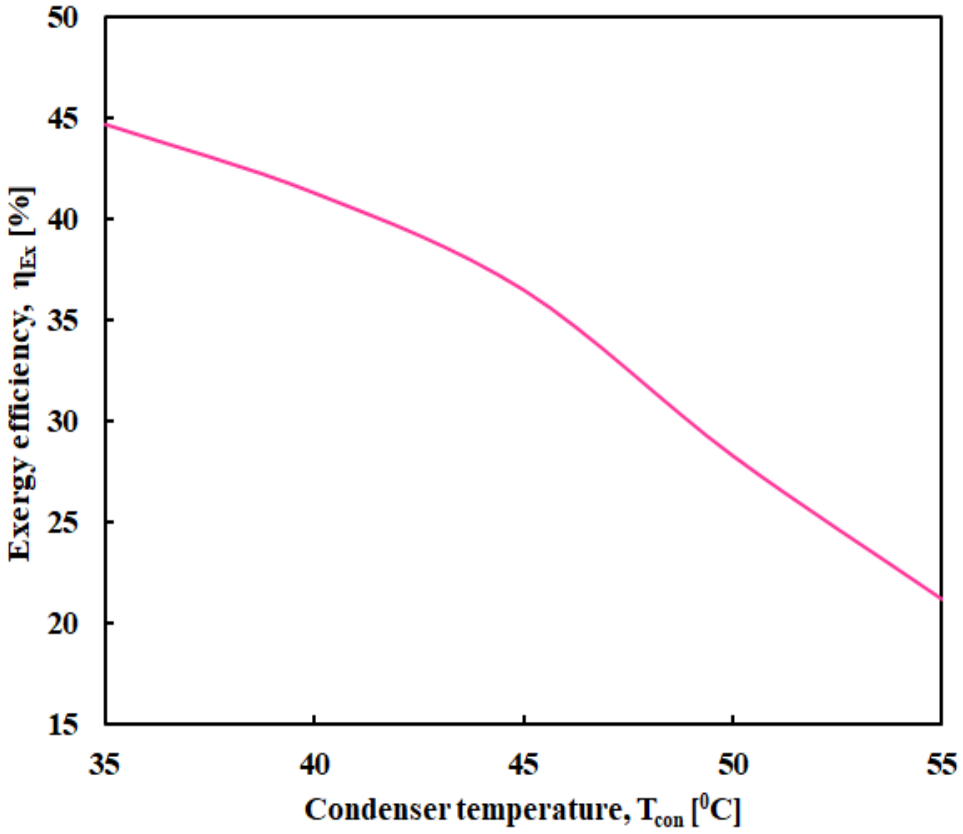

Fig. 5.26: Impact of condenser temperature on exergy efficiency

5.12.3 Impact of maximum cycle temperature on exergy destruction

The impact of maximum cycle temperature (T_{max}) on exergy destruction is shown in Fig. 5.27. It is obvious from Fig. 5.27 that the exergy destruction increases with increase in desorption temperature. This is attributable to the fact that increasing the maximum

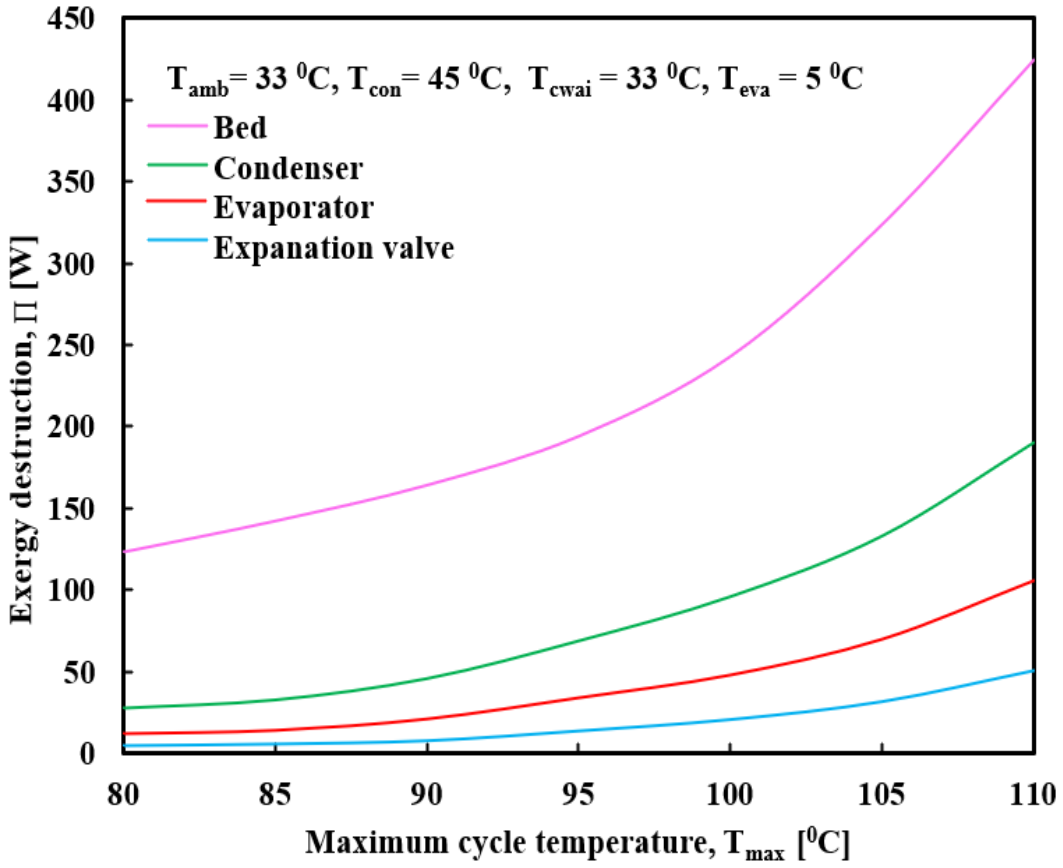

Fig. 5.27: Impact of maximum desorption temperature (T_{max}) on exergy destruction

desorption temperature results in a larger mass of adsorbate that can be desorbed. The amount of heat required for adsorption increases as the mass of the adsorbate grows, resulting in an increase in exergy destruction. The adsorbent bed is found to have the most exergy destruction, followed by the condenser, evaporator, and expansion valve in that order. The adsorbent beds exergy destruction increases as the maximum cycle temperature rises, with a maximum exergy destruction of 425 W. It is because increasing the heat source's temperature greatly influences the bed by increasing the temperature difference during heat transfer, and indirectly affects other components of the SAC system. Furthermore, increase in temperature causes entropy formation; this leads to increasing irreversibility and exergy destruction. The condenser highest exergy destruction at maximum cycle temperature of 110^{0}C is 192 W, which is low when compared to the adsorbent bed. The phase shift process of the refrigerant, which leads to condensation, is the primary causes of exergy degradation in the condenser. Similarly, exergy destruction in the evaporator is mainly caused by an irreversible refrigerant phase change process that results in the cooling effect. Figure 5.27 shows that the highest exergy destruction at the evaporator at maximum cycle temperature of 110^{0}C is 106 W. The maximum cycle

temperature has less effect on the exergy destruction at the expansion valve. As a result, exergy destruction of the expansion valve is 52 W, which is very low when compared to exergy destruction of the adsorbent bed at the maximum cycle temperature of 110^0C.

5.12.4 Results of thermodynamic analysis

The energy and exergy balance equation from Eq. (5.18) to Eq. (5.116) is used to quantify the SAC system. Table 5.7 provides the energy analysis of the SAC system. It depicts that the collector in the collector-receiver system experiences the maximum energy loss. While there is significant energy destruction in the refrigerator subsystem, the collector-receiver subsystem has a higher percentage of energy destruction than the refrigerant subsystem. The first law efficiency of the solar collector-receiver subsystem and the overall system is estimated as 35.24% and 23.99%, respectively. Exergy analysis of a solar collector receiver system is shown in Table 5.9. The exergy efficiency of solar-receiver subsystem is only 4.98%. Figure 5.28 shows a comparison of percentage loss in energy and exergy of solar collector subsystem. Conduction, convection and radiation are the main causes of exergy loss in the collector. It is primarily due to convection and radiation in the receiver. Reduction in losses improves the performance of the collector-receiver subsystem. The losses caused by re-radiation can be improved by using a selective surface, and the loss caused by convection can be reduced by creating a vacuum between the glass cover and the absorber.

Exergy loss of different components of a SAC system is given in Table 5.9. The results show that the adsorbent bed possess the maximum irreversibility. Figure 5.29 depicts the Grassmann exergy structural outline of the adsorption cooling system circuit, which illustrates the percentage distribution of exergy destruction in SAC system components. The large amount of energy is used for heating the adsorbent bed and its causes the high irreversibility. The irreversibility of the adsorbent bed has been quantified as 0.20 kW. During heating (isosteric heating and desorption process) of the bed, the pressure increases from 2.01 kPa to 23.1 kPa. Since a large fraction of heat input is required to heat the adsorbent and metal components of the bed, the irreversibility is higher in desorption process. The thermal conductivity of the adsorbent, adsorbate and heat transfer materials, the geometry factors of the adsorbent like porosity and contact between the particles affect the irreversibility of the SAC system. The use of composite adsorbent

improves the thermal conductivity of the adsorbent. Furthermore, the fluid friction and finite temperature difference in the condenser and evaporator causes the exergy destruction and is proportional to the pressure gradient generated by the fluid friction. As a result, heat transfer by conduction through the heat transfer material plays a significant role in exergy loss.

Table 5.7 Energy analysis of SAC System

Subsystem	**Energy acquired [kW]**	**Energy transferred [kW]**	**Energy loss [kW]**	**Energy loss [%]**	**First law efficiency [%]**
Collector	1.98	1.02	0.96	48.46	51.54
Receiver	1.02	0.69	0.32	31.60	68.39
Collector–receiver	1.98	0.69	1.28	64.75	35.24
Refrigerator	0.88	0.29	0.59	67.05	32.94
Overall circuit system	1.98	0.29	1.51	76.00	23.99

Table 5.8 Solar collector receiver system exergy analysis

Subsystem	**Exergy acquired (kW)**	**Exergy transferred (kW)**	**Exergy loss (kW)**	**Exergy loss (%)**	**Second law efficiency (%)**
Collector	1.88	0.46	1.42	75.57	24.42
Receiver	0.46	0.09	0.36	79.58	20.41
Collector–receiver	1.88	0.09	1.78	95.01	4.98

Table 5.9 Exergy loss - various components of SAC system

Components	**Exergy loss (Irreversibility) (kW)**	**Exergy loss (%)**
Condenser	0.07	21.90
Expansion device	0.01	4.45
Evaporator	0.03	10.79
Adsorbent Bed	0.20	62.86

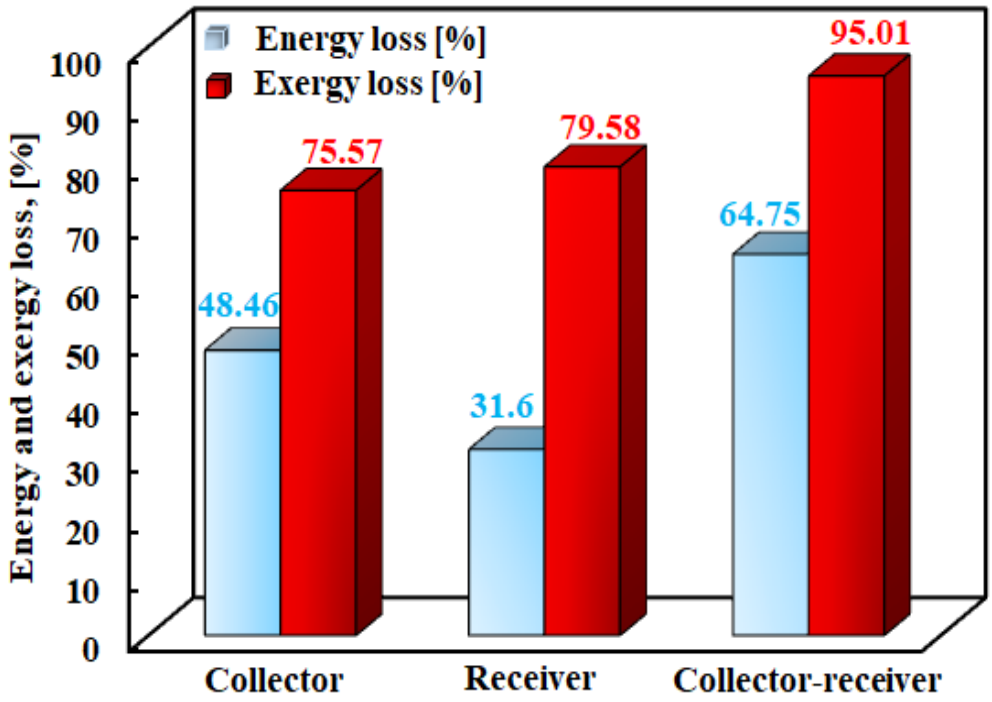

Fig. 5.28: Percentage loss in energy and exergy of solar collector subsystem

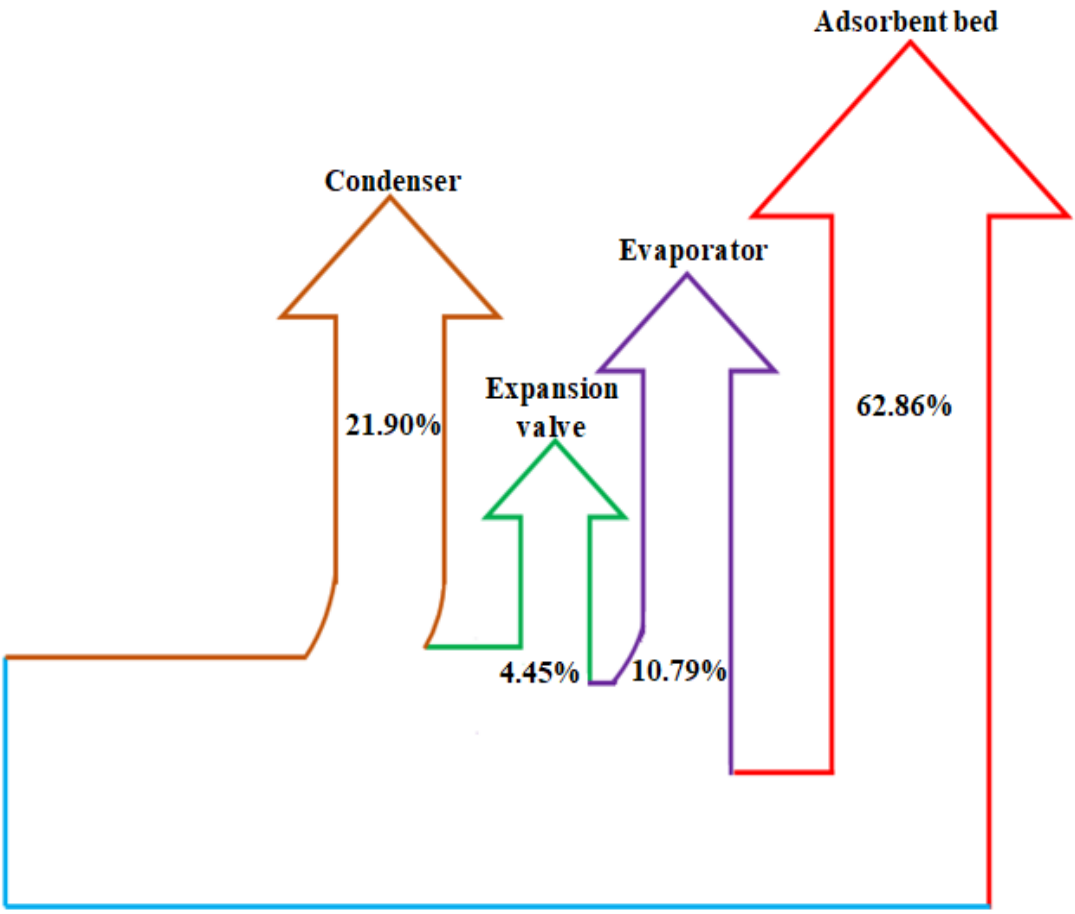

Fig. 5.29: Grassmann exergy structural outline for SAC system

Summary

The chapter concluded that the simulation platform is helpful for predicting the performance of the SAC system. The optimal range of adsorption or desorption time is between 500 and 900 s, while the optimal range of switching time for this process is between 10 and 30 s. The thermodynamic modelling of the SAC system gives a maximum COP of 0.68. The refrigerating effect and SCP of the system are determined as 3120 kJ and 25.4 Wkg^{-1}, respectively at the maximum desorption temperature of 95^0C. In addition, the energy-exergy analysis is carried out to assess the exergy destruction of the various components of the SAC system. The maximum desorption temperature plays an important role in the exergy destruction and it rises as the desorption temperature does. The maximum exergy destruction occurs in the adsorbent bed followed by condenser, evaporator and expansion valve. The maximum exergy loss related to solar collector-receiver system is 1.78 kW and that of the adsorbent bed is 0.20 kW. The first and second law efficiency of the collector-receiver system of the present study has been quantified as 35.24% and 4.98%, respectively. The design procedure of the SAC system and its experiment procedure, its results and discussion are outlined in the Chapter six.

Chapter 6

Design, Development and Performance Study of SAC System with Activated Carbon-Ethanol

The design, development and performance investigations of the SAC system is presented in this chapter. The design of components of SAC systems such as evaporator, adsorbent bed, condenser and thermal energy storage tank is presented here. The performance investigations of the system are conducted with AC-ethanol as the working pair.

6.1 System Description

The schematic of the proposed SAC system is shown in Fig. 6.1. The SAC system has a condenser, evaporator, expansion valve, two adsorbent beds, and a parabolic solar concentrator. Initially, the hot water from the solar concentrator raises the temperature of adsorbent bed 1 (AB1), causing the vapour pressure of the adsorbed refrigerant to achieve the condensing pressure (P_{con}). When AB1 reaches P_{con}, valve L1 is opened and the desorbed vapour enters the condenser, where it is condensed by cooling water. In the expansion device, this high-pressure liquid refrigerant is exposed to expansion. The low-pressure refrigerant travels from the expansion device to the evaporator, where it absorbs

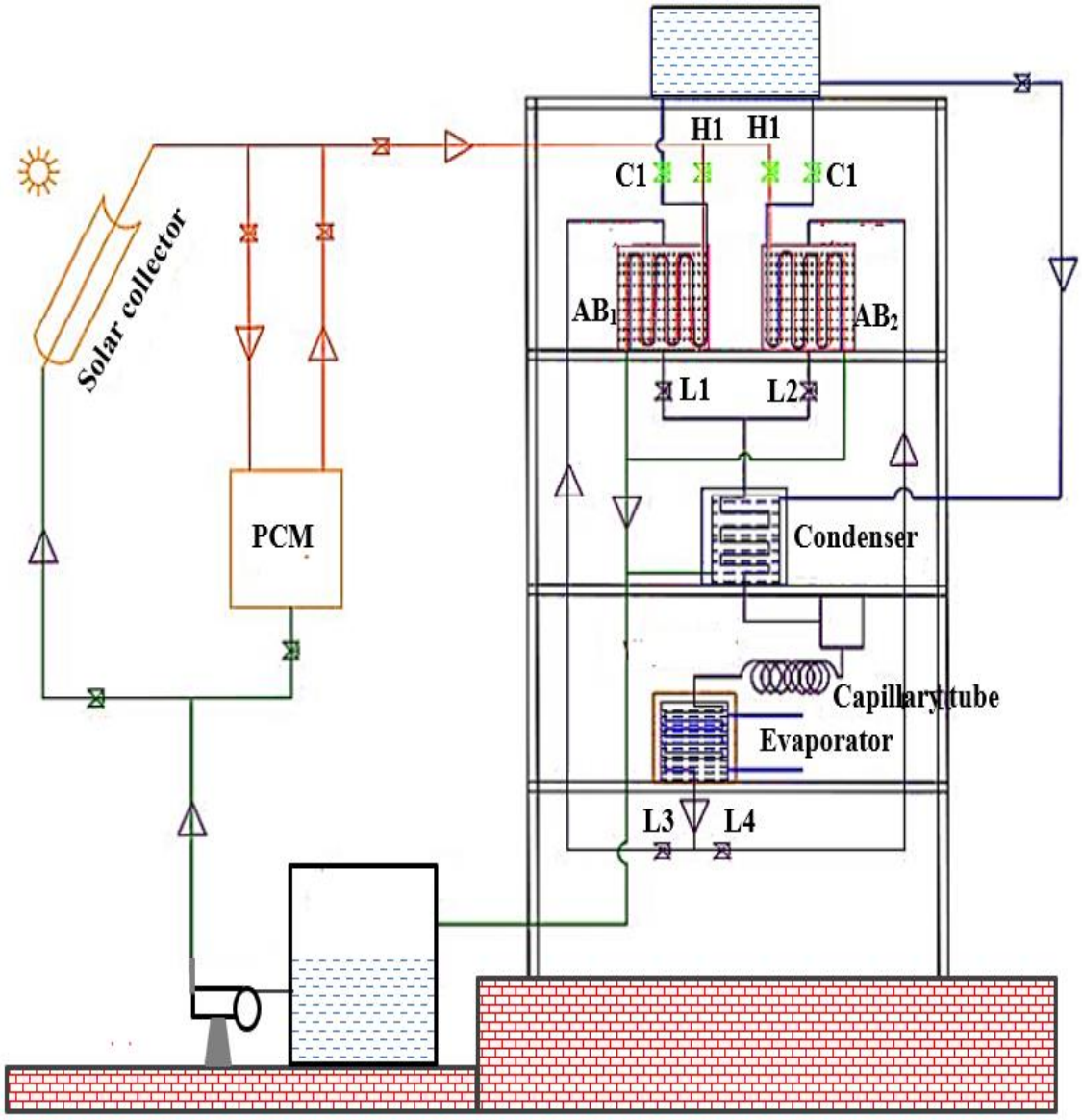

Fig. 6.1: Layout of the two-bed adsorption cooling system

latent heat from the water to be chilled and is transformed to vapour. The refrigerant vapour at low pressure enters the adsorbent bed 2 (AB_2) through valve L4. Thus, one cycle of the two-bed adsorption cooling cycle has been completed. During the next cycle, the above process gets revised by reversing the flow of hot and cold water through the adsorbent bed. Here, AB_2 undergoes desorption process and AB_1 executes adsorption process by opening the valves L_2/L_3 and closing L_1/L_4. Thus, the system produces a continuous refrigerating effect. The flow of hot and cold-water to the adsorbent bed is regulated by valves H1 and C1, respectively. The hot water is directly fed to the desorption bed for desorbing the refrigerant.

6.2 Design of SAC system

The section details about the steps involved in the design of different components of SAC system like, condenser, adsorbent bed, evaporator, storage tank and collector.

6.2.1 Design of evaporator

Evaporator is a cylindrical tank in which a copper tube of 3/8-inch size, spirally wound inside it. The SAC system is designed to cool the 20 kg of water from 30^0C to 5^0C in 1 h. This spiral coil is completely covered with the water which is to be cooled. The ethanol flows through the pipe and is vapourised by absorbing latent heat from the space to be cooled. Figure. 6.2 shows the evaporator assembly for the adsorption cooling system.

Fig. 6.2: (a) Photograph of the evaporator assembly and (b) Log Mean Temperature difference of the working fluid in evaporator

Assumptions:

i. Refrigerant inlet to the evaporator is saturated liquid
ii. Refrigerant outlet of the evaporator is saturated vapour

The refrigerating effect for the system is given by the Eq. (6.1)

$$Q_{Ref} = m\,Cp\,(T_{wf}-T_{wi}) \quad (6.1)$$

$$=2090\text{kJ}$$

where, m is the mass of water (kg), C_p the specific heat of water ($Jkg^{-1}K^{-1}$), T_{wi} the intial temperature of water (K) and T_{wf} the final temperature of water (K)

Cooling capacity of the system $(Q_{eva}) = \frac{\text{Refrigerating effect}}{\text{Time}}$ (6.2)

$Q_{eva} \approx 600$ W

So, the cooling capacity of the system is taken as 600 W

For internal flow (low pressure vapour ethanol coming from the expansion valve flowing through the copper tube of the evaporator)

Properties of ethanol are taken at -5^0C from REFPROP- 10 NIST and Data book [105]

For fully developed flow constant heat flux, Nu= 4.26

$$h = \frac{\text{Nu k}}{\text{d}} \quad (6.3)$$

$= 84.1125$ $Wm^{-2}K^{-1}$

If only internal flow is considered, U = h

The total area of the coil has been calculated by,

$$Q = \text{UA(LMTD)} \quad (6.4)$$

$$\text{LMTD} = \frac{\Delta T_1 - \Delta T_2}{\ln\left(\frac{\Delta T_1}{\Delta T_2}\right)}$$

$\Delta T_1 = 303\text{-}268 = 35$ K

$\Delta T_2 = 278\text{-}268 = 10$ K

LMTD =19.96 K

$$A = \frac{Q}{U\,.\,(\text{LMTD})}$$

$= 0.3573$ m

$A = \pi dl$

The total length of the coil is

$$l = \frac{A}{\pi\,.\,d}$$

$= 11.94\ m$

≈ 12 m

Total length of the coil is calculated as 12 m. Figure 6.3 shows the photograph of the evaporator covered with thermal insulator.

Fig. 6.3: Photograph of the evaporator

6.2.2 Design of condenser

The condenser used is a tank and tube type. The desorbed ethanol is flowing through the copper tube where it condenses by transferring the latent heat of vapourisation to the cooling water filled in the condenser and Fig. 6.4 shows the condenser assembly.

Assumptions:

The assumptions made for the design of the condenser of the system are

i. Refrigerant inlet to the condenser is saturated vapour
ii. Refrigerant outlet of the condenser is saturated liquid
iii. Flow direction- counter flow

The diameter of the coil is, d= 9.525 x 10^{-3} m

For calculating the length of coil, the Properties of ethanol at 50^0C is taken from REFPROP- 10 NIST.

For internal flow [105],

Fig. 6.4: Photograph of the condenser assembly

$$Re = \frac{4\dot{m}}{\pi D\mu} \quad (6.5)$$

$$= 10910.17$$

$$Nu = 0.023Re^{0.8}Pr^{0.3} \quad (6.6)$$

$$=36.82$$

$$Nu = \frac{hd}{k} \quad (6.7)$$

$$h = \frac{Nu\ k}{d}$$

$$= 616.25\ Wm^{-2}K^{-1}$$

If only internal flow is considered, U = h

$U = 616.25\ Wm^{-2}K^{-1}$

Then,

$$Q_{con} = \left(Q_{eva} + \frac{Q_{eva}}{\eta_{col}}\right)$$

$$= 2600\ W$$

$\Delta T = 10.82\ K$

$$Q = UA(LMTD) \quad (6.8)$$

$$A = \frac{Q}{U\ (LMTD)}$$

$$= 0.39m^2$$

Area of the coil, A = πdl

$$l = \frac{A}{\pi\ d}$$

= 13.03 m

≈ 13 m

Thus, the required length of the coil is 13 m. Figure 6.5 shows the photograph of the condenser used in the present study.

Fig. 6.5: Photograph of the condenser

6.2.3 Design of Adsorbent Bed

As the adsorbent bed is the most significant component of the system, the total performance of the system is strongly dependent on its physical features. The adsorbent bed should have enhanced heat and mass transmission capabilities. The adsorbent bed is filled with granular absorbents. Metallic mesh is stretched across the heat exchangers to prevent adsorbent spillage while allowing ethanol vapour to permeate. During the adsorption or desorption process, the adsorbent material is heated and cooled by transferring hot or cold water via the copper tubes of heat exchangers. As depicted in Fig. 6.6, heat exchangers are inserted inside the adsorbent tank.

Mass of ethanol evaporated = 2.8 $kghr^{-1}$

Fig. 6.6: Photograph of the adsorbent bed assembly

$$\text{Volume of ethanol} = \frac{\text{Mass of ethanol}}{\text{Density of ethanol}} \quad (6.9)$$

$$= 0.017\ m^3$$

The adsorption rate of ethanol in the selected activated carbon has been experimentally determined as 0.369 $kgkg^{-1}$.

$$\text{Mass of activated carbon for each bed} = \frac{\text{Mass of ethanol evaporated}}{\text{Concentraton ratio}}$$

$$= 7.58\ kg = 8\ kg$$

$$\text{Volume of activated carbon} = \frac{\text{Mass of activated carbon}}{\text{Density of activated carbon}} \quad (6.10)$$

$$= 3.81 \times 10^{-3}\ m^3$$

$$\text{Total volume of the adsorbent bed} = \text{Volume of ethanol} + \text{Volume of Activated Carbon} \quad (6.11)$$

$$= 0.021 m^3$$

Thus by fixing length and diameter as 36 cm and 28 cm, respectively, the adsorbent bed has been constructed. Figure 6.7 shows the photograph of the adsorbent bed.

6.3 Calculation of Volume of Energy Storage Material

The average solar energy obtained in a clear day time is 950 W (data obtained from ambient weather station, TKMCE). During the operation of the adsorption cooling system with solar energy, half of it is used to store in the energy storage material. This energy is used to operate the adsorption cooling system during the time when the availability of solar energy is comparably less or null by using a heating media like water.

Fig. 6.7: Photograph of the adsorbent bed

Total energy available for the energy storage material from the solar energy,

Q_{sun}= 475W

Time duration for storing solar energy in the energy storage material, t = 4 h

(From 11.00 h to14.00 h solar irradiance data from weather station showed maximum irradiance during this period)

Total energy stored in the energy storage material = Q_{sun} t

= 6840 kJ

Let m be the mass of energy storage material in kg

Latent heat of selected energy storage material [10] = 201 $kJkg^{-1}$

Melting point of the storage material = 93^0C

Inlet temperature of heating fluid, T_i = 88^0C

Outlet temperature of heating fluid, T_0 = 45^0C

Specific heat, C_p = 1.21 $kJkg^{-1}K^{-1}$

The total energy stored in the material = $m \times [L + C_p(T_i - T_o)]$ (6.12)

i.e., m = 27.03 kg

Density of energy storage material = 1835 kgm^{-3}

Volume of energy storage material tank required $= \frac{m}{\rho}$ (6.13)

$= 0.01\ m^3$

Diameter of tube for circulating heat transfer fluid $= 9.525 \times 10^{-3}$ m

Length of the tube = 5 m

Volume of the tube $= \pi d l$

$= 0.15\ m^3$

Total volume = 0.01 + 0.15

$= 0.16 m^3$

Volume of the storage tank = 80 cm x 80 cm x 26 cm

6.4 Design of Parabolic Solar Collector

The parabolic solar collector consists of parabolic concentrator or trough collector, collector supporting structure, receiver and reflecting surface. The following section details the design procedure of parabolic solar collector.

6.4.1 Parabolic trough collector

The parabolic trough collector for the adsorption cooling system has been designed based on the COP of the cooling system and is given as:

$$\text{COP} = \frac{\text{Cooling capacity}}{\text{Heat input}} \quad (6.14)$$

COP of a solar adsorption cooling system is 0.68 (from thermodynamic simulation) and the cooling capacity is 600 W

$$\text{Heat input} = \frac{\text{Cooling capacity}}{\text{COP}}$$

= 882 W

The efficiency of parabolic concentrator is given as the ratio of the output power of the parabolic concentrator to the input power of it and is given by Eq. (6.15)

$$\eta_{PTC} = \frac{Heatoutput_{PTC}}{Heatinput_{PTC}} \quad (6.15)$$

Heat input_{PTC} (Q_{PTC}) = 2940 W

Now, the area of parabolic trough collector is calculated by [106],

$$A_p = \frac{Q_{PTC}}{I} \quad (6.16)$$

$= 3\ m^2$

The common accessible reflective stainless steel sheets are used to create a pilot trough-receiver unit. The reflecting surface is made of stainless steel sheet with dimensions of 2.5 m x 1.3 m. The parabolic trough collector is designed based on simple parabolic equation. The cross section of the parabolic collector is shown in Fig. 6.8. The sheet is then curved into a parabolic trough module with a 3 m^2 aperture area, having 2.5 m length and 1.2 m aperture width. The simple parabolic equation in Cartesian coordinate is given by [106],

$$x^2 = 4fy \quad (6.17)$$

Rearranging Eq. (6.17) is yields the height of the parabola in terms of focal length and aperture,

$$\left(\frac{A_p}{2}\right)^2 = 4fh \quad (6.18)$$

$$h = \frac{A_p^2}{16f} \quad (6.19)$$

The rim angle is given by the Eq. (6.20),

$$tan\frac{\Psi}{2} = \frac{A_p}{4f} \quad (6.20)$$

The geometrical concentration ratio C_G is defined as the ratio of the collector aperture area, A_p to the surface area of the receiver, A_r

$$C_G = \frac{A_p}{A_r} \quad (6.21)$$

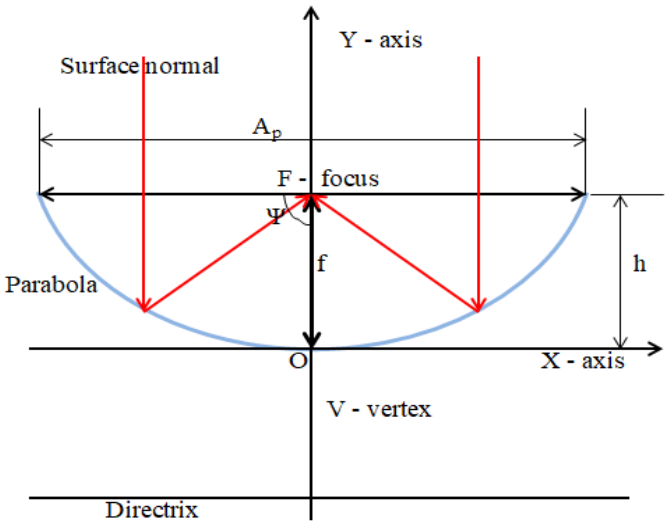

Fig.6.8: Cross section of the parabolic collector

The focal point of the present model is selected at the aperture line, thus the collector height *h* is same as focal length 'f ' with rim angle Ψ is 90^0. Table 6.1 gives the geometrical parameters of the designed parabolic trough model used for the present study.

6.4.2 Collector supporting structure

The collector is supported by a rigid supporting structure that ensures smooth operation of the entire system. It is being used to spin the horizontal axis in order to track the orientation of the sun. The unit is designed and developed to enable easy manual tracking for the test purpose and cost reduction.

6.4.3 Receiver

The receiver pipe is made of galvanized steel and it has relatively low absorptivity. A pipe of inner diameter D_i = 0.026 m and outer diameter D_0 = 0.03 m is used as the receiver tube. The absorber surface is black in color and it is erected in the East-West direction.

Table 6.1 Geometrical parameters of the designed parabolic trough model

Parameter	Numerical Value
L	2.5 m
A_p	1.2 m
f	0.3 m
C_G	31.84 [-]
D_0	0.03 m

6.4.4 Reflecting surface

The reflecting surface of the parabolic collector is parabolic in shape that linearly extended into trough shape to form curve area of 3.25 m^2 and aperture area of 3.0 m^2. The Fig. 6.9 shows the photograph of parabolic solar collector.

6.5 Procurement Details of Materials

The following information deals about the procurement details of materials used for the construction of the SAC system.

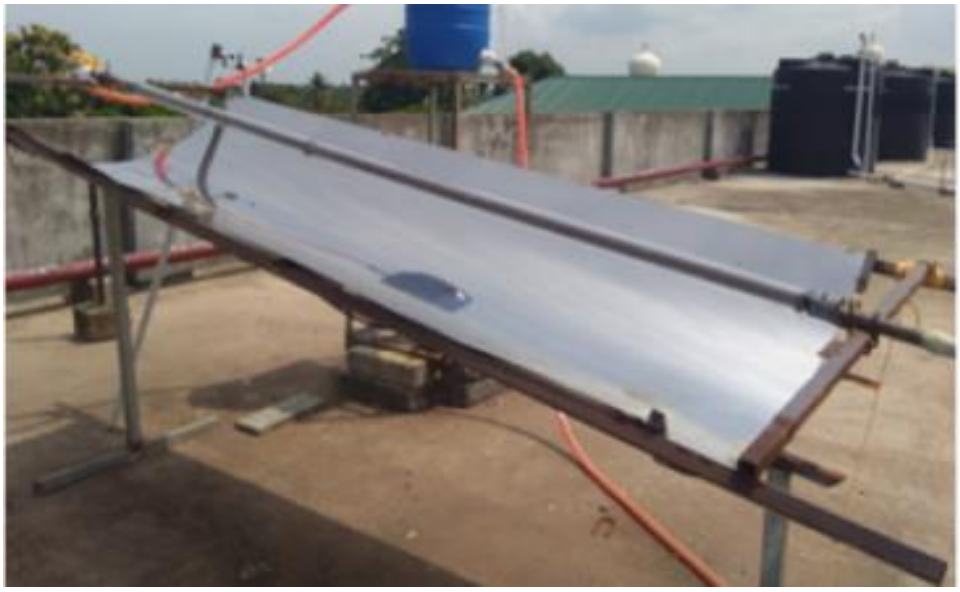

Fig. 6.9: Photograph of parabolic solar collector

6.5.1 Refrigerant duct/ pipe

Material: Copper (3/8 inch)

Copper is selected as the pipe material due to the following factors.

i. Resistant to corrosion
ii. High level of heat transfer (high thermal conductivity of 350 $Wm^{-1}K^{-1}$)
iii. Easy to bend and form desired shapes
iv. Available in a wide range of sizes starting from 3/8 inch
v. Easily available
vi. Ease of weldability

6.5.2 Condenser and outer layer of evaporator

Material: GI Sheet

GI sheet is selected as the pipe material due to the following factors.

i. Good weldability and formability
ii. Corrosion resistant
iii. Low cost with reasonable mechanical strength
iv. Thermal conductivity of 18 $Wm^{-1}K^{-1}$

6.5.3 Adsorbent bed, inner layer of evaporator and energy storage tank

Material: Stainless Steel

Stainless Steel is selected as the pipe material due to the following factors.

i. High strength and can withstand vacuum pressure
ii. Corrosion resistance and long life

Chemically stable and inert to acidic or basic or alcoholic medium.

6.6 Design Dimensions

Table 6.2 gives the dimensions of the various components like evaporator, adsorbent bed, condenser, energy storage tank and parabolic solar collector which is used for the fabrication of the adsorption cooling system.

6.7 Pressure and Vacuum Test

After integrating all the components in position, the whole system is tested for any possible leaks. The testing is done at pressures above the maximum working pressure of the system. For tracing the leaks, the system is filled with compressed air from an air compressor. The system is loaded to a pressure of 2 bar. Further leaks are tested by checking for the drop in the pressure of the system over 6 h (Fig. 6.10). After testing the entire system for high pressure, a vacuum test is performed on the adsorbent bed, achieving a 700 mmHg within the adsorbent beds. After ensuring that the vacuum is maintained for a predetermined time, the system is prepared for refrigerant charging. The final experimental setup is shown in Fig. 6.11. The pressure gauge readings are monitored to

Table 6.2 Design dimensions of SAC system

Components	**Material**	**Dimension/quantity**
Evaporator (Double walled: puff insulated)	Copper tube	Length: 12 m Diameter: 3/8 inch (9.53 mm)
	Stainless steel (Inner round chamber)	Diameter: 26 cm Height: 38 cm
	GI Sheet (Outer cubic chamber)	Suitable dimensions for covering inner vessel and insulation are used
Adsorption Bed (2 Nos.)	Copper tube	Length: 10 m Diameter: 3/8 inch (9.53 mm)
	Stainless steel (Cylindrical chamber)	Length: 36 cm Diameter: 28 cm
Condenser	Copper tube	Length: 13 m Diameter: 3/8 inch (9.53 mm)
	GI Sheet (Cubic chamber)	Length: 38 cm Height: 38 cm
Energy storage tank	Copper tube	Length: 5 m Diameter: 3/8 inch (9.53 mm)
	Stainless steel (Inner rectangular chamber)	Length: 80 cm Height: 26 cm
Parabolic solar collector	Stainless steel sheet	Length: 2.5 m Aperture: 1.2 m

check the leakproof of the vessels. The system is maintained under the same condition for 24 h, and no leakage in the system is noticed. Hot water is circulated through the adsorbent bed, and desorbed gases are evacuated using a vacuum pump. Heating and evacuation are done for 2 h.

6.8 Instrumentation

The instruments used to indicate, measure, and record physical quantities for the SAC system are detailed in this section. It consists of a rotary vane pump, a pressure gauge, a temperature measuring instrument, a weight measuring instrument, and a weather station for measuring temperature, pressure, solar insolation and other atmospheric conditions.

Fig. 6.10: Photograph of leakage testing of the system

Fig. 6.11: Photograph of the experimental setup

6.8.1 Rotary vane pump

The air cool made vacuum pump is used for evacuation of the adsorption setup and to maintain the system under the vacuum condition. Specifications of the pump are Power rating 0.25 HP, 225V AC and 1425 RPM.

6.8.2 Vacuum pressure gauge

The analog type vacuum pressure gauge is used to monitor the pressure of the adsorbent bed as well as the pressure of the refrigerant before and after expansion process. The specification of vacuum gauge is given below:

Dial size: 4 inch/100 mm

Display type: Analog

Pressure type: Gauge pressure

Range: -30 in.Hg/760 mmHg

6.8.3 Temperature measurement

K-type thermocouples with temperature indicator are used to measure the temperature of the inlet hot water and the outlet hot water temperature of the bed. The temperature of cooling water, condenser, evaporator and the temperature of the refrigerant before and after expansion process are also measured by thermocouples. The specifications of thermocouple is given below

Material: Chromel {90.1% nickel and 9.9% chromium}

Alumel {95.9% nickel, 1.1% manganese, 2% aluminium and 1% silicon.

Thermocouple range: 0-400^{0}C

Tolerance: ± 0.1^{0}C

6.8.4. Weight measuring instrument

The weighing machine QUINTIX-125D-10-IN, with a weight capacity of 150 gms and readability of 0.1 mg has been used to weigh the adsorbent samples. The weighing machine Voda with a weight capacity of 100 kg and 0.01 kg accuracy heavy duty platform has been used to weigh the adsorbent.

6.8.5 Weather station

The ambient weather station WS-2902C is used to monitor the indoor and outdoor conditions such as wind speed, wind direction, rainfall, outdoor temperature relative humidity, solar radiation, barometric pressure and UV index. Figure 6.12 shows the

Fig. 6.12: Photograph of weather station

weather station used for the present study, which is installed in Energy Research Lab, Department of Mechanical Engineering, TKM College of Engineering, Kollam.

6.9 Charging of the Refrigerant

The charging of the refrigerant is the next step in the preparation process. To evacuate the system, turn on the rotary pump. The vacuum pump is turned off once suitable vacuum conditions have been achieved. A sufficient amount of ethanol has been added to the system. The charging line of the adsorbent bed is connected to the ethanol cylinder. The refrigerant enters the adsorbent bed as the refrigerant cylinders open, and adsorption begins. Because the adsorption is an exothermic process, the system temperature rises. Pressure in the system rises to prevent further refrigerant adsorption. Hence, the system is cooled by circulating cold water around the adsorbent bed to reduce the temperature. The refrigerant is charged back into the system. After charging the unit, the system is ready for the experimental investigation.

6.10 Experimental Procedure

The procedure for carrying out the experiment is described in detail here. Initially, the experiment is carried out on a two-bed SAC system using activated carbon-ethanol as the working pair. The goal of this study is to determine the effect of evaporator and hot water temperatures on system performance. In this experiment, the system is only powered by hot water from the solar collector. When the temperature of the hot water from the solar

collector is completely inadequate to operate the system, an auxiliary heating source is used. The vacuum condition is ensured with a vacuum pump, and once the desired vacuum conditions are achieved, the system is ready for charging the refrigerant. The adsorbent bed (AB1) has now been charged with the sufficient quantity of ethanol. The following are the steps involved in the experimental study:

i. Initially, hot water temperature from the heating source, say 80^0C, is allowed to flow through H1 into the adsorbent bed AB1 for heating; during this process, all valves L1, L2, L3, and L4 are closed.
ii. Allow enough cold water to flow through the adsorbent bed AB2 to cool it and lower the pressure to below the evaporator pressure.
iii. Set the time period for heating and cooling the bed and the flow rate of hot water through the AB1, by measuring the mass flow rate of hot water with a cylinder beaker and stopwatch.
iv. When the pressure in AB1 rises to condenser pressure (say, 23.1 kPa), the valves L1 and L4 open, allowing vapour refrigerant to flow to the condenser.
v. Allow hot water to flow through AB1, with L1 in the open position, to maximise desorbed refrigerant transfer from AB1 to condenser.
vi. Note down the hot water temperature inlet and outlet as it circulates through the bed AB1.
vii. The vapour refrigerant leaves from the evaporator are adsorbed by the bed AB2 through the valve L4. The condenser temperature, evaporator temperature, and pressure of the system are recorded.
viii. The temperature of the bed AB2 increases due to the adsorption of the vapour refrigerant. As a result, maximum cooling water circulation is ensured via the bed AB2 to bring the temperature of the bed same as atmospheric temperature.
ix. This completes one cycle, and during the next cycle, the valves L1 and L4 are closed, and the entire process is revised to achieve continuous operation.
x. Where the solar intensity is low, supplementary heating of hot water is provided to desorb the refrigerant from the adsorbent bed.
xi. A number of observations are performed with different hot water temperature by maintaining the evaporator temperature as constant to investigate the influence of hot water on the performance of the SAC system. It is mostly used to determine the effect of hot water temperature on system performance.

xii. Similarly, the effect of evaporator temperature on system performance can be determined by repeating the procedure for different initial temperature of the evaporator.

6.11 Uncertainty Analysis

The standard uncertainty equation for the independent variable is given by [102]

$$\delta U_R = \sqrt{\left(\frac{\partial R}{\partial x_1} U_1\right)^2 + \left(\frac{\partial R}{\partial x_2} U_2\right)^2 + \cdots + \left(\frac{\partial R}{\partial x_n} U_n\right)^2} \tag{6.22}$$

The result R is a given as a function in the terms of independent variables. Let δU_R be the uncertainty in the result and U_1, U_2, …. , U_n be the uncertainties in the independent variables.

Errors and uncertainties in experiments typically arise from the selection and condition of the instruments used to measure different parameters, the environment, observation, and test plans. This section presents a precise approach for assessing the uncertainty of the current study. In the present study, the mass of the adsorbent, the temperature of working fluid, the diameter of the evaporator tube, the mass of the composite sample, and the concentration of ethanol in the uptake process are measured. The Q_{Ref}, Q_{gen}, and COP of the SAC system are functions of different parameters. The total uncertainty of the calculated parameters is shown in Table 6.3 and methods of evaluation is given in the Appendix IV.

$$\delta Q_{Ref} = \sqrt{\left(\frac{\partial Q_{Ref}}{\partial m}\delta dm\right)^2 + \left(\frac{\partial Q_{Ref}}{\partial C_p}\delta C_p\right)^2 + \left(\frac{\partial Q_{Ref}}{\partial \Delta T}\delta d\Delta T\right)^2} \tag{6.23}$$

$$\frac{\partial Q_{Ref}}{\partial m} = C_p\, \Delta T \tag{6.24}$$

$$\frac{\partial Q_{Ref}}{\partial \Delta T} = \mathrm{m}\, C_p \tag{6.25}$$

$$\delta Q_{gen} = \sqrt{\left(\frac{\partial Q_{gen}}{\partial \dot{m}}\delta d\dot{m}\right)^2 + \left(\frac{\partial Q_{gen}}{\partial C_p}\delta C_p\right)^2 + \left(\frac{\partial Q_{gen}}{\partial \Delta T}\delta d\Delta T\right)^2 + \left(\frac{\partial Q_{gen}}{\partial t}\delta t\right)^2} \quad (6.26)$$

$$\frac{\partial Q_{gen}}{\partial \dot{m}} = C_p\, \Delta T\, t \quad (6.27)$$

$$\frac{\partial Q_{gen}}{\Delta T} = \dot{m}\, C_p\, t \quad (6.28)$$

$$\delta COP = \sqrt{\left(\frac{\partial COP_{sy}}{\partial Q_{Ref}}\delta dQ_{Ref}\right)^2 + \left(\frac{\partial COP_{sy}}{\partial Q_{gen}}\delta dQ_{gen}\right)^2} \quad (6.29)$$

$$\frac{\partial COP}{\partial Q_{Ref}} = \frac{1}{Q_{gen}} \quad (6.30)$$

$$\frac{\partial COP}{\partial Q_{Ref}} = \frac{-Q_{Ref}}{Q_{gen}^2} \quad (6.31)$$

Table 6.3 Total uncertainty in different parameters

Description	Total uncertainty [%]
Refrigerating effect	±0.73%
Heat input to the system	±2.54%
COP	±2.67%

6.12 Results and Discussion

The performance of the system is evaluated experimentally under the meteorological conditions of the TKM college of Engineering in Kollam. Activated carbon and ethanol are used as the working pair in the experimental investigation. The experiments are performed between January and December of 2021. The hot water collected from the parabolic concentrator is then directed to the adsorbent bed. Here, both the hot water temperature and the evaporator inlet water temperature have a substantial effect on the performance of the SAC system, including the refrigerating effect, COP, and SCP, which is working with activated carbon-ethanol as the working pair.

6.12.1 Solar intensity and the ambient temperature with time

The solar irradiation and ambient temperature have been measured by the ambient weather station WS-2902C installed at the Energy Research Lab of TKMCE, Kollam. The solar intensity and the ambient temperature obtained for a whole year and its variation with time on a sunny day (18/04/2021) is shown in the Figs. 6.13 and 6.14. The receiver outlet fluid temperature with time on a sunny day is also shown in the Fig 6.15. The experimental results shows that the maximum solar intensity obtained is 1229 Wm^{-2} and the average solar intensity of about 950 Wm^{-2} for most of the day has been obtained. The availability of this high intensity solar radiation gives the high temperature to the receiver fluid. This high temperature receiver fluid is used as the heat source of SAC system for the present investigations.

6.12.2 Effect of hot water temperature on the COP of the system

The hot water obtained from the solar collector is transmitted to the SAC system, which acts as the heat source. The highest temperature of the hot water employed for the experimental investigation is limited to 88^0C. Figure 6.16 illustrates the impact of hot water temperature on the COP of the activated carbon-ethanol working pair. The comparison

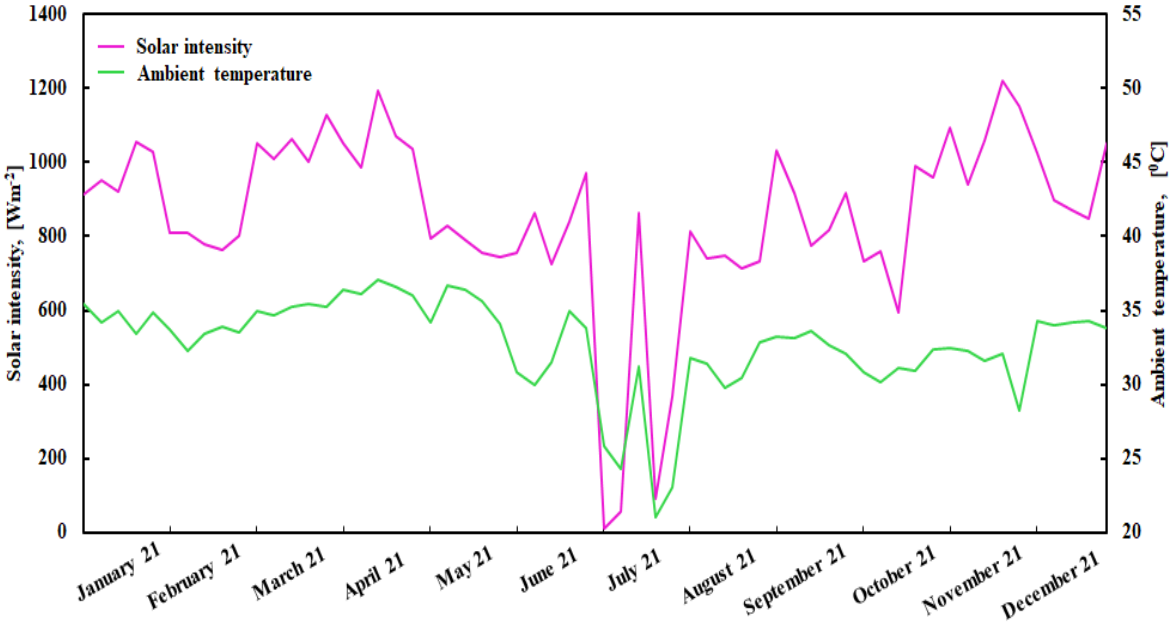

Fig. 6.13: Solar intensity and the ambient temperature for a year [January 2021-December 2021]

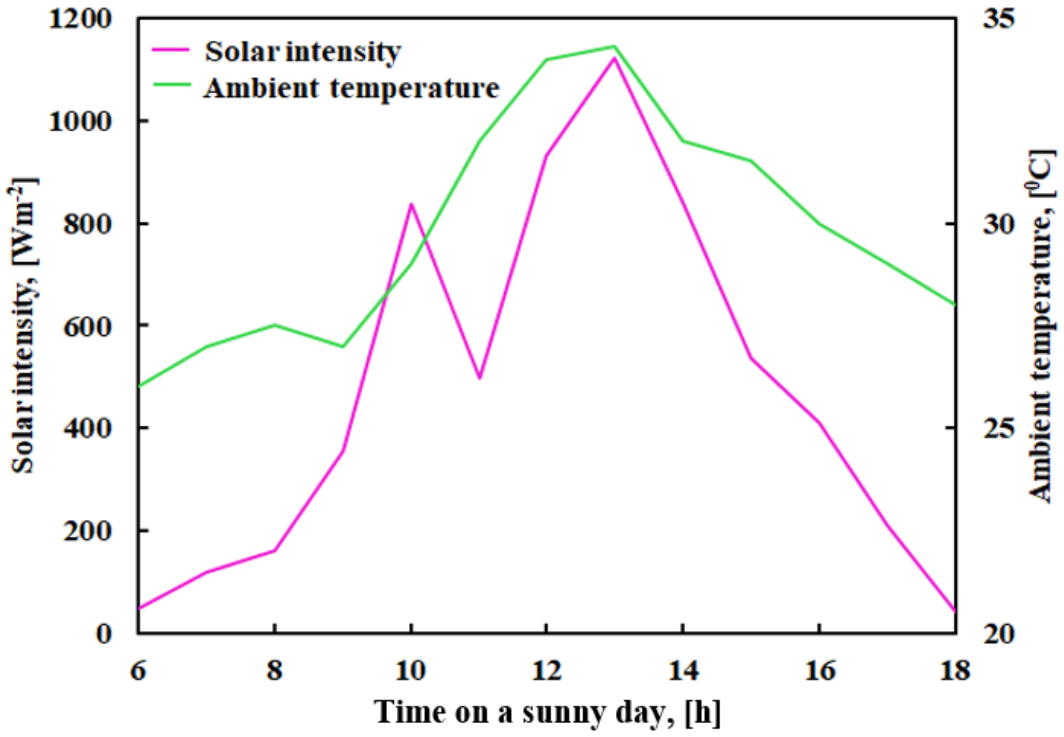

Fig. 6.14: Solar intensity and the ambient temperature with time on a sunny day [18/04/2021]

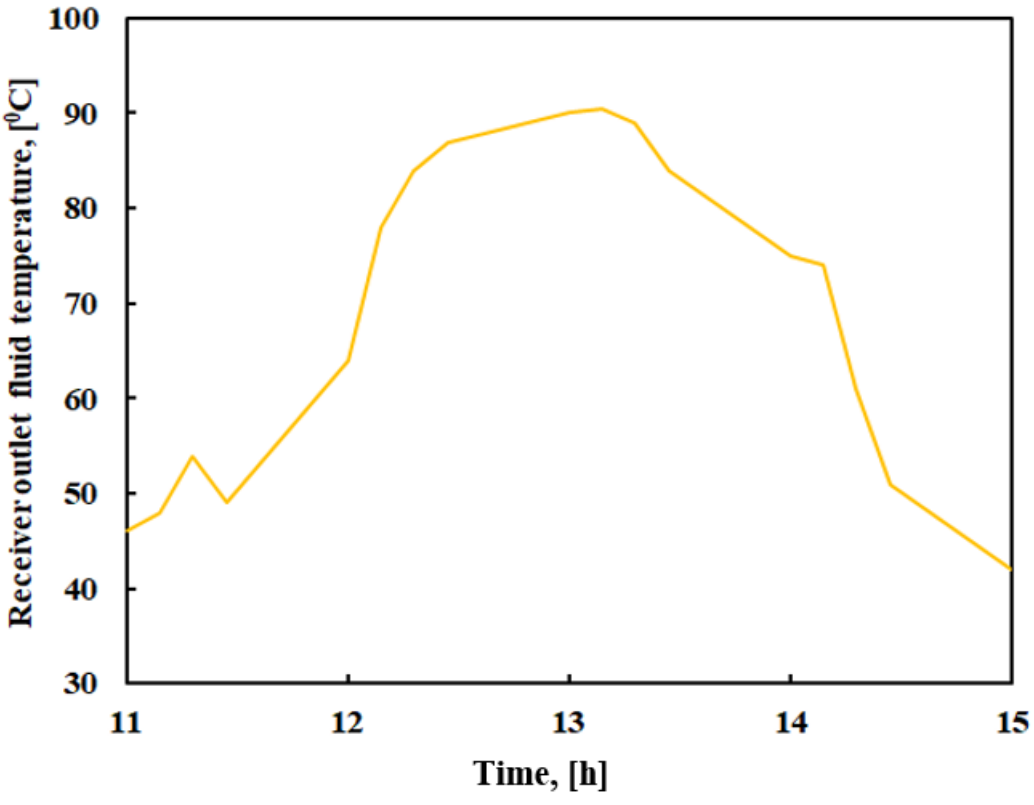

Fig. 6.15: Receiver outlet fluid temperature with time on a sunny day [18/04/2021]

between experimental and simulation study is also shown in Figure 6.16. The experimental profile follows a similar pattern to the simulated profile, suggesting that the simulation and experiment are in agreement. It is evident from Fig. 6.16 that the COP of the system increases as the hot water temperature rises. Due to the fact that as the temperature of the hot water rises, the mass of the refrigerant is desorbed at a faster rate. As the desorption of the refrigerant increases, the refrigerating effect also gets increases, and this increase is considerably greater than the change in heat input. Therefore, the COP of the system also enhances. The comparison demonstrates that the simulation results mostly reflect the variance of system performance under different working situations. But even so, in terms of specific values, the experimental results are slightly lower than the simulated results and are due to the following reasons: (i) heat loss to the environment may occur throughout the experiment (ii) during the experiment, the various system processes have not been conducted under perfect conditions (iii) the specific heat capacity of the favored pair is

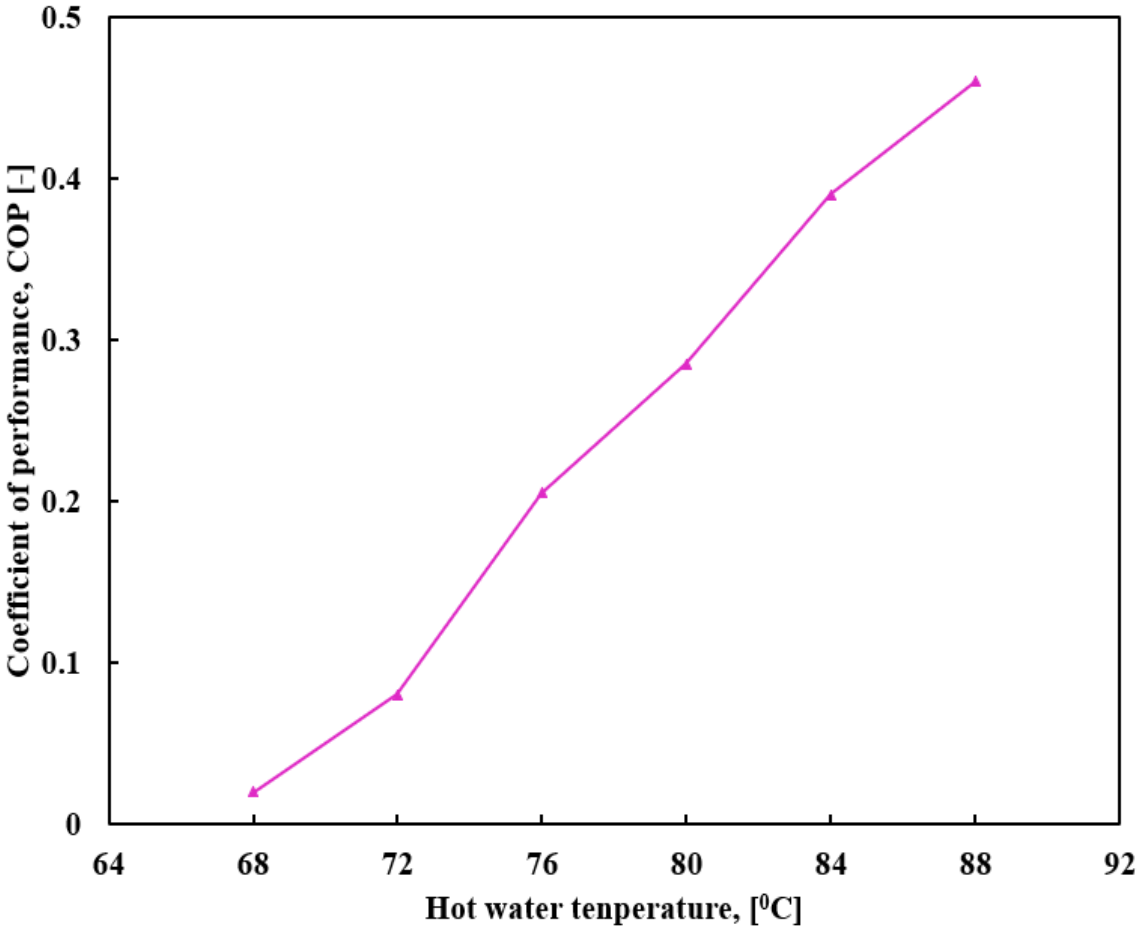

Fig. 6.16: Effect of hot water temperature on COP under experiment and simulation with activated carbon-ethanol as working pair

remains constant during the modelling process but varies according to temperature during the experiment. Simulation and experiment have yielded maximum COP values of 0.49 and 0.46, respectively. The difference between simulation and experiment is within the acceptable range.

6.12.3 Effect of hot water temperature on the refrigerating effect of the system

The hot water temperature or desorption temperature of the adsorption cooling system also plays an important role in the refrigerating effect and it is shown in Fig. 6.17. From the Fig. 6.17, it is clear that the refrigerating effect increases from 655 kJ to 1704 kJ in the simulation and from 601 kJ to 1542 kJ in the experimental values. In both the cases, as the hot water temperature or the desorption temperature of the SAC system increases the refrigerating effect also increases drastically. This is because the amount of desorbed refrigerant increases as the heat source temperature rises, and the evaporation of additional

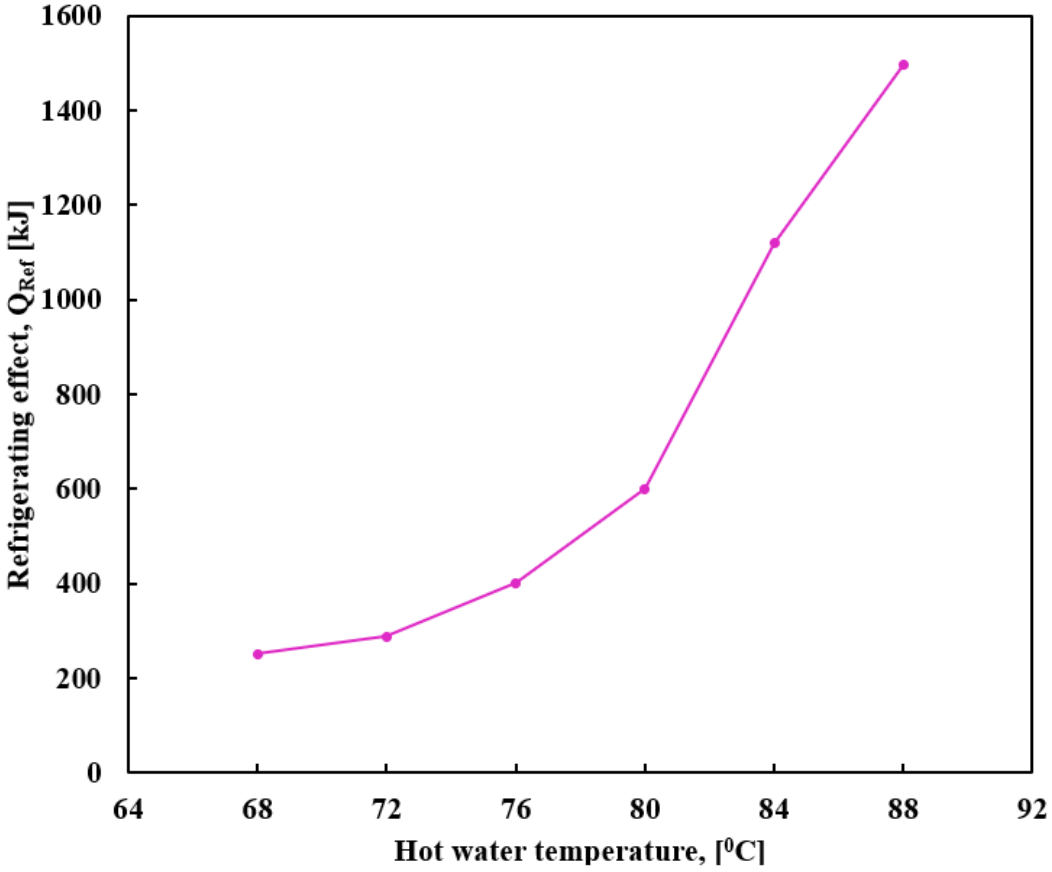

Fig. 6.17: Effect of hot water temperature on refrigerating effect under experiment and simulation with activated carbon-ethanol as working pair

Table 6.4: Refrigerating effect in Watts at different hot water temperature

Hot water temperature [^{0}C]	Refrigerating effect [W]
68	34.86
72	40.14
76	55.69
80	83.60
84	151.52
88	214.22

refrigerant increases the refrigerating effect. Due to the rise in heat losses, the divergence between the simulated and experimental values increases as the hot water temperature increases. The variation of the refrigerating effect in Watts at different hot water temperature is presented in Table 6.4.

6.12.4 Effect of hot water temperature on the specific cooling power of the system

The effect of hot water temperature on the specific cooling power of the system is depicted in Fig. 6.18. The temperature of the hot water has a significant impact on the SCP. With an increase in hot water temperature, the SCP of the system rises due to the increased desorption of refrigerant, which improves the refrigerating effect. This effect also causes for the improvement of performance of the SAC system.

6.12.5 Effect of evaporator water temperature (inlet) on the performance of the system

Figures 6.19 and 6.20 represent the effect of evaporator water temperature (inlet) on the performance of the system like COP, refrigerating effect and SCP of the system operated with activated carbon-ethanol as the working pair. As shown in Fig. 6.19, the COP of the system increases as the evaporator temperature rises. This is because a higher evaporator inlet temperature causes more refrigerant to evaporate from the evaporator system, hence improving the refrigerating effect and COP of the system. Figure 6.20 illustrates the influence of evaporator water temperature (inlet) on system SCP. In addition, increasing the evaporator water temperature improves the refrigerating effect, which reduces the cycle time and improves the SCP of the system.

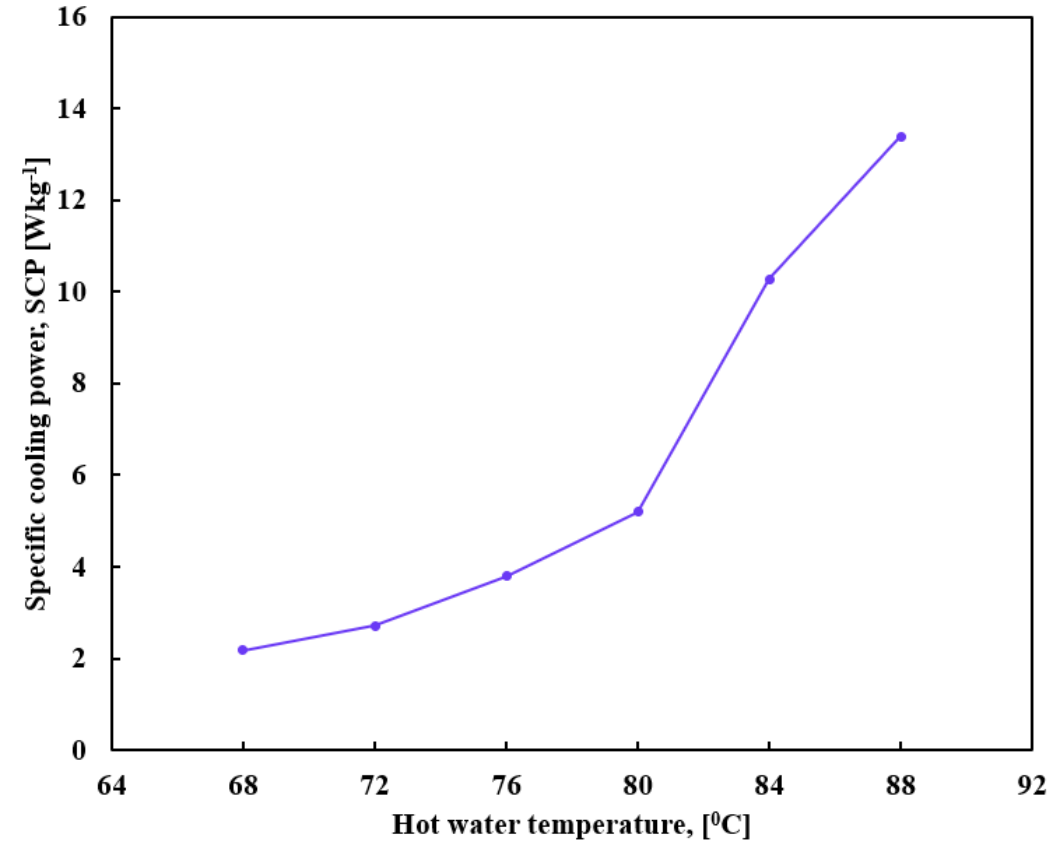

Fig. 6.18: Effect of hot water temperature on specific cooling power under experiment and simulation with activated carbon-ethanol as working pair

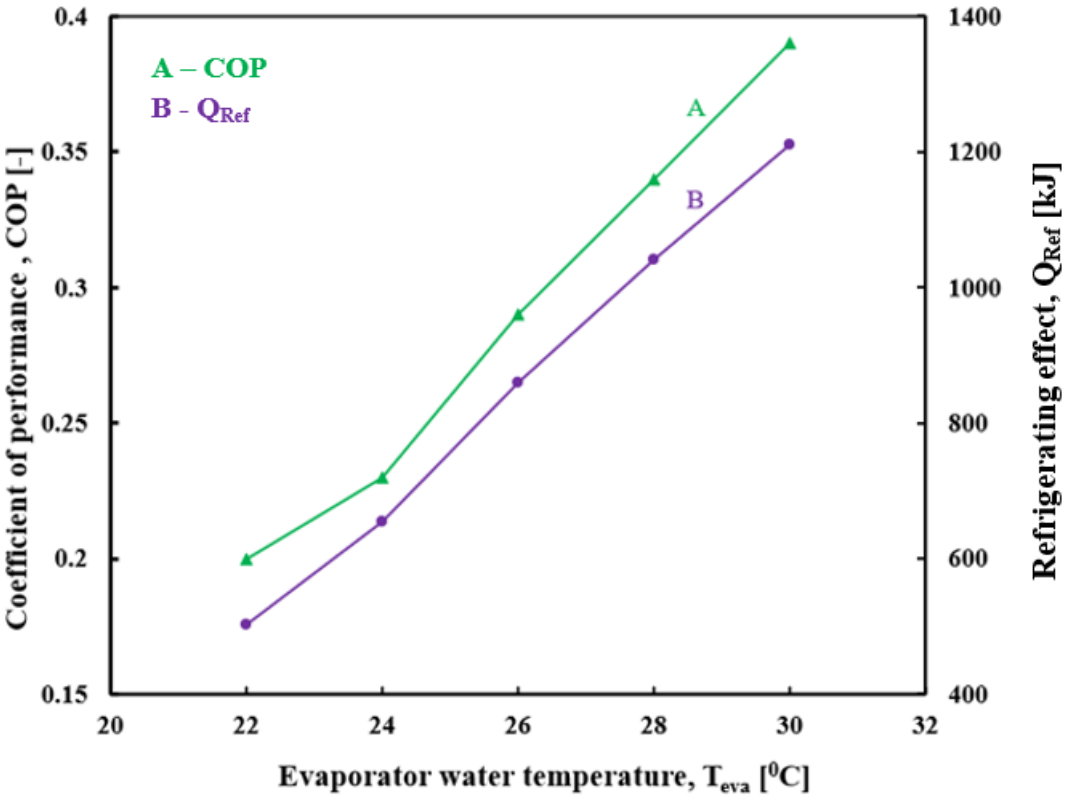

Fig. 6.19: Effect of inlet water temperature of evaporator on COP and refrigerating effect

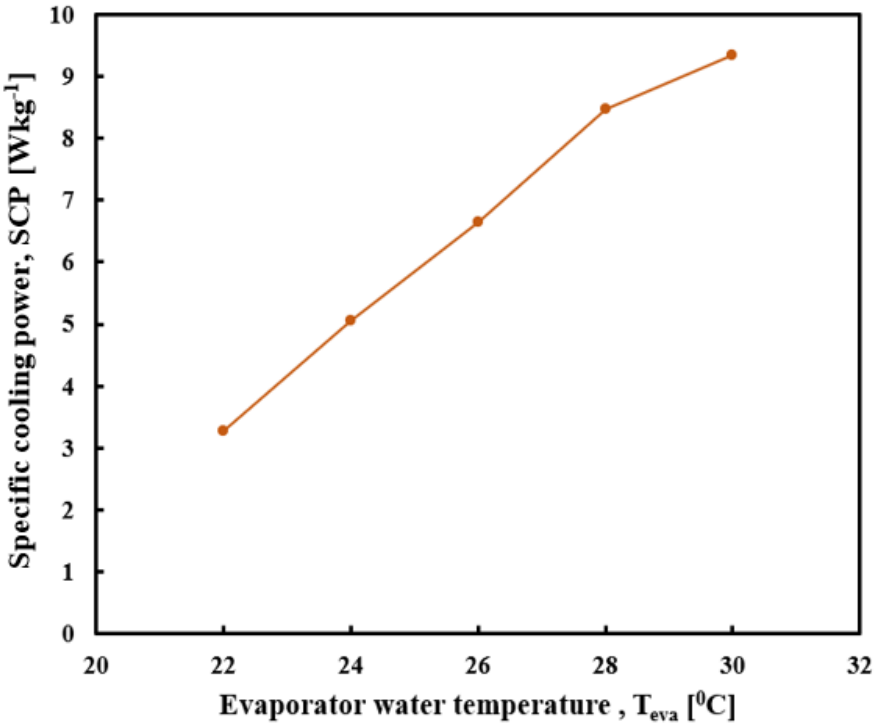

Fig. 6.20: Effect of inlet water temperature of evaporator on SCP of the system

Summary

The energy equation has been used to design the evaporator, condenser, adsorbent bed, energy storage tank, and solar collector of the SAC system. The performance of the system is investigated by varying the inlet hot water and evaporator temperatures. The COP, refrigerating effect, and SCP are found to be increasing with the increase in the hot water inlet temperature. The maximum COP, refrigerating effect and SCP obtained are 0.46, 1495 kJ and 13.72 Wkg^{-1}, respectively, for the maximum inlet hot water temperature of 88^0C. The performance parameters such as COP and SCP at the maximum evaporator temperature at 30^0C is determined as 0.39 and 9.1 Wkg^{-1}, respectively. The next chapter narrates the characteristic study of the composite adsorbent which is selected for the experimental work.

Chapter 7

Selection and Characteristic Study of Consolidated Adsorbent

This chapter details the selection and characterisation study of the consolidated adsorbent proposed in the present work. The preparation of the sample is also described in this chapter. The characteristic study comprises of pore volume, BET surface area, CHNS analysis, SEM image and stability analysis are described in this chapter.

7.1 Reasons of Low Heat and Mass Transfer Properties of Conventional adsorbent

As the bed of solid adsorbent is heated or cooled by an external fluid, the heat transfer process is governed by the equivalent thermal conductivity (k_{eff}) of the solid adsorbent and the bed wall heat transfer coefficient between the tube or finned tubes and the fixed adsorbent bed. Figure 7.1 shows the thermal resistances involved in heat transfer within a solid adsorbent bed.

The overall heat transfer coefficient of an adsorbent bed is calculated by simple heat conduction and is given by Eq. (7.1),

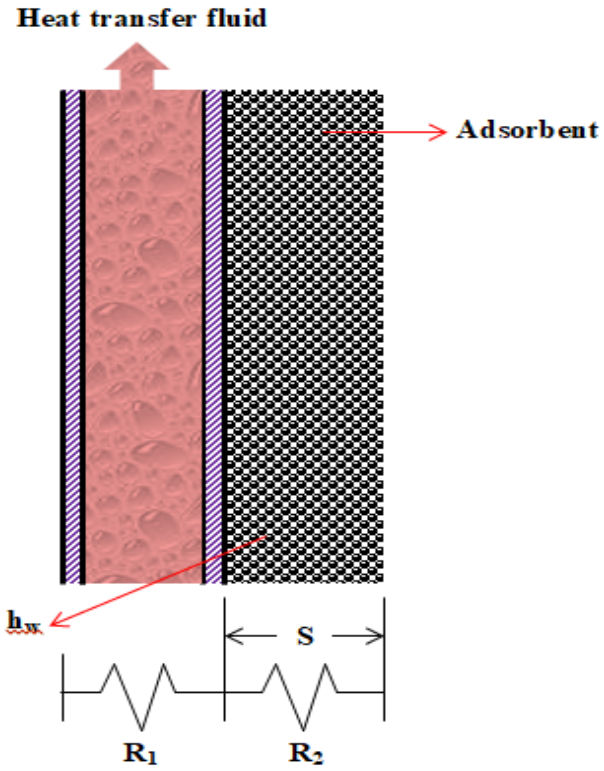

Fig. 7.1: The thermal resistances involved in heat transfer within a solid adsorbent bed

$$\frac{1}{UA_f} = \frac{1}{h_f A_f} + \frac{1}{h_w A_{eff}} + \frac{x_{eff}}{k_{eff} A_{eff}} \qquad (7.1)$$

where A_f and A_{eff} are the fluid and solid heat exchanger surfaces, h_f and h_w are the fluid and solid heat transfer coefficients, and x_{eff} and k_{eff} are the effective thickness and thermal conductivity of the adsorbent bed. To improve the heat transfer rate, U should have a very high value. However, in adsorption cooling systems, U is typically quite low for the following reasons:

i. The poor effective thermal conductivity of granular adsorbents is a result the large porosity and discontinuity of the solid material

ii. In solid-gas adsorption systems, thermal resistance is primarily of two types. The first resistance (R1) occurs at the interface between the metal tube wall and the adsorbent and is primarily determined by the physical contact between the adsorbent and the tube wall. The interface will have a poor contact heat transfer coefficient and a high temperature gradient if the thermal contact between the

iii. metal surface and the adsorbent materials is insufficient. In the case of working fluids with a low evaporator pressure, such as water or ethanol, the lack of gas convection at the interface also adds to the extremely low heat transfer coefficient. The second heat transfer resistance (R2) arises within the adsorption bed due to the poor thermal conductivity of the adsorbent. Laminar flow of the external heat transfer fluid within the tubes reduces the heat transfer coefficient

To minimise the cycle time and increase the heat transfer rate, the resistance, R1 and R2 values should be low, and the effective thermal conductivity should be high. This improves the performance of the system and makes the SAC system more economically viable. Adsorbate mass transfer is very low due to low adsorbent permeability and low refrigerant evaporator pressure. Long cycle times are caused by low mass transfer rates. As a result, for the system to work well, an appropriate level of gas permeability within the adsorbent bed is required. In a low pressure system using water or ethanol as the refrigerant, mass transfer is critical because kinetics influence adsorption or desorption. The mass transfer of an adsorbent bed containing activated carbon is not critical in a high pressure environment like ammonia. Because the suggested system is a low pressure system, mass transfer rate improvements are necessary to achieve the desired COP. As a result, composite adsorbents are proposed to increase the thermophysical properties. Composite adsorbents are typically created by combining a parent material with two or more physical adsorbents. The mixtures of activated carbon with other conceivable combinations of other adsorbents are investigated in this study. The following section details about the process of selection of composite adsorbents and their properties.

7.2 Selection of Materials for Composite Adsorbent Preparation

The detailed study related to the selection of material has been presented in the section 4.4 of chapter 4. Granular activated carbon (AC) with mesh size 12, apparent density of 0.69 gcm^{-3} (Grade - VP E122) and BET surface area in the ranges of 900-1150 m^2g^{-1}, used for the present study has been obtained from Indo German Carbon Limited, Cochin, Kerala, India. The secondary adsorbents are Expanded Graphite Powder (EGP), Silica Gel (SG), and MIL-53Al Metal Organic Framework (MOF). Akshar Chem (India) Limited, Mehsana, Gujarat, supplies EG with a mesh size of 20-60 and a purity of 99.5 %. QTrade Link, Mehsana, Gujarat, India, provided the SGP, which has a mesh size of 50-

80 mesh, a bulk density of 0.60-0.90 gcm^{-3}, and a BET surface area of 350 m^2g^{-1}. Intelligent Materials Pvt. Ltd, Dera Bassi, Punjab, India, has provided MOF of type MIL-53Al with a density of 0.40 gcm^{-3} and a surface area of 1500 m^2g^{-1} (BET). Polyvinylpyrolidone (PVP), which is manufactured by Bangalore Fine Chem. in Bangalore, Karnataka, India, is the binder used in the composite preparation. Ethanol having a purity of 99.5% is used as the adsorbate (supplied by Siddha Chemicals, Pune, Maharashtra, India).

In the present study, the consolidated adsorbent consisting of activated carbon as the parent material with MOF MIL-53Al, EGP, SG and PVP as the additives are considered. 21 combinations are tested to optimise the surface characteristics and its porous properties. After the detailed study, four of the samples having better performance such as higher BET surface area and effective pore volume are selected. The CHNS analysis, SEM analysis, TGA analysis, and the measured thermal conductivity are also considered for the selection of optimum samples. Then the adsorption rate of selected adsorbent with ethanol is measured for finding D-A constant. The instruments used to analyse the properties of the composites are details in Table 7.1. The porous properties of the composite adsorbent are determined of the N_2 adsorption data at 77 K investigated using Quantachrome Instruments NOVA Touch lx4 Model. The image of the synthesised samples is obtained by Scanning Electron Microscopy (SEM). The chemical compositions of the composite adsorbent are determined by Elemental Analyser. The thermal conductivity and thermal stability of the samples are evaluated by KD2 PRO and Thermogravimetric Analyzer (TGA), respectively.

Table 7.1 Instruments used to analyse the properties of the composite adsorbent

Properties of the composite adsorbent	**Instruments**
Porous properties	Quantachrome Instruments NOVA Touch lx4 Model
Image of the synthesised samples	Scanning Electron Microscopy (SEM)
Chemical compositions	Elemental Analyser
Thermal conductivity	KD2 PRO
Thermal stability	Thermogravimetric Analyzer (TGA)

7.3 Experimental Study

Preparation of composite adsorbents and its experimental investigations to determine the best consolidated adsorbent for the adsorption of ethanol and its characteristics properties are detailed in this section.

7.3.1 Preparation of composite adsorbent

The composite adsorbents are produced by using commercially available AC as the parent material with secondary sorbent (MIL-53Al, EG, SGP) and PVP as binder. The steps involved to make composite adsorbents are detailed here. To eliminate any leftover moisture content, the AC and secondary adsorbent (in a proper proportion by weight percentage) are heated at 130^0C for roughly 5 h. Then the powdered binder is mixed with water to produce a solution; the mass of water is roughly two times that of the composite adsorbent. The solution is then blended in particular ratios with the dry AC and secondary sorbent, then agitated to ensure uniform mixing. After that, it is squeezed with a mechanical compressor at a pressure of 3 to 7 MPa. The sample is then dried for about 8 h in a hot air oven at 130^0C to remove the excess water. A series of composite samples are prepared by varying the composition ratios of AC and secondary sorbent, in the form of dry mass of around 224 mg, 20 mm diameter and thickness 2mm. The Fig. 7.2 depicts the process of making AC consolidated composite samples. These samples are mainly used for determining the porosity and adsorption characterisation of the composites with N_2 and ethanol as adsorbates. The thermal conductivity of the composites has been determined by KD2 PRO thermal conductivity measuring instrument. Table 7.2 provides a list of composites prepared with activated carbon as parent material and Fig. 7.3 shows photograph of activated carbon samples prepared for the study.

7.3.2 Porous properties of composites

The adsorption or desorption of N_2 into adsorbate is defined as the standard method for determining the texture porous properties of composites such as specific surface area and incremental pore volume. The volumetric model is used to determine the composites adsorption or desorption isotherms of N_2 using a Quantachrome Instruments NOVA Touch

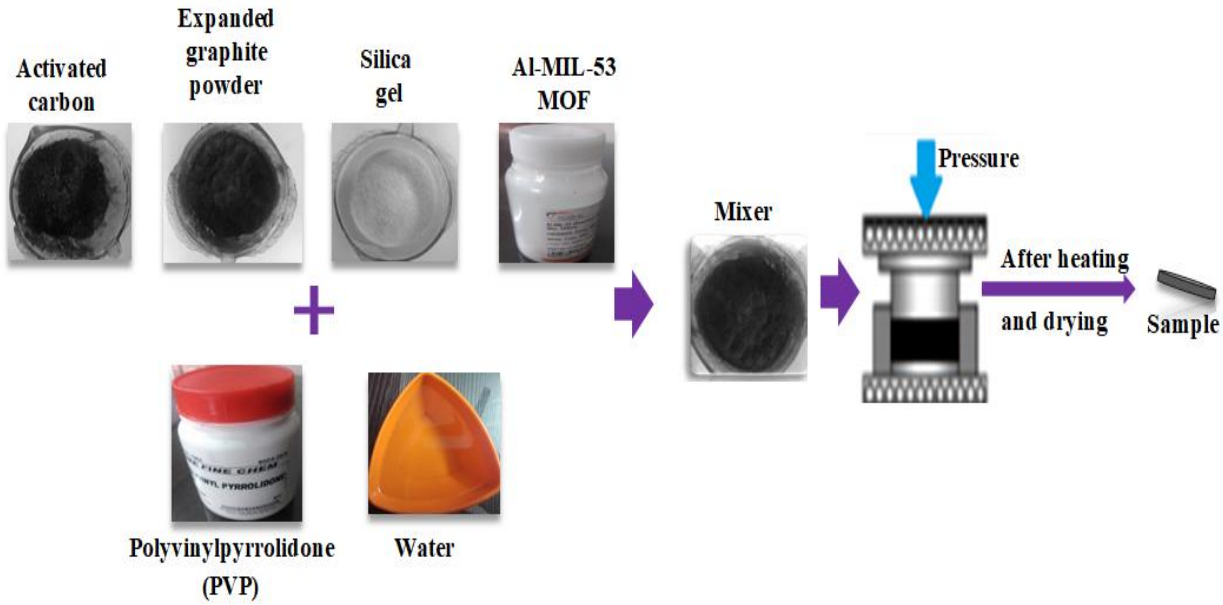

Fig. 7.2: Process of making AC consolidated composite samples

Fig. 7.3: Photograph of composite activated carbon samples prepared for the study

Table 7.2 List of composites prepared with activated carbon as parent material

Sample	Composite A	Composite B	Composite C	Composite D
AC (weight %)	70	70	70	70
MIL-53Al (weight %)	20	10	-	-
EGP (weight %)	-	10	-	20
SGP (weight %)	-	-	20	-
PVP (weight %)	10	10	10	10

lx4 Model BET surface analyser supplied by Anton-Paar Austria. The pressure of N_2 adsorption gas is evaluated using a pressure transducer with an accuracy of 0.1 % of the reading and a resolution of 10^{-5} mmHg. Figure 7.4 shows the N_2 adsorption/desorption isotherm curves of all produced composites as well as the parent activated carbon at 77K. There is no hysteresis in the adsorption and desorption of N_2, which is critical for adsorption cooling. This demonstrates that the adsorbate is mesopore-free. At low relative pressure, all of the adsorbents studied show a dramatic increase in N_2 adsorption. The composite A has a stronger N_2 adsorption than the other composites for the same weight percentage of activated carbon because it contains 20% MOF MIL-53Al. The composite A adsorbs N_2 at a faster rate due to the increased porous characteristics of the MOF MIL-53Al. The surface area of the composites is analysed using the BET model. Composite B, contains 10 % MOF MIL-53Al by weight, does have a stronger N_2 adsorption property than the other samples and basic materials, but less than composite A.

In the present study, Density Functional Theory (DFT) is used to compute the total pore volume and pore size distribution. The results demonstrate that the width of pores of the composites range from 1 to 3.8 nm. Figure 7.5 depicts the pore width distribution of activated carbon and its composites. The composite adsorbent prepared by the combination of physical adsorbent like activated carbon with metal organic frame work (MOF) helps to improve the BET surface area of the adsorbent than that of parent adsorbent as illustrated in Figs. 7.4 and 7.5 [107]. Composites A and B with MIL-53Al additives provide higher surface area and pore volume than composites C and D. It is presumed that additives with a higher surface area and pore volume significantly alter the porous properties of the base materials. Moreover, the weight percentage of the parent material also plays an important role in the properties for adsorption process [108].

Table 7.3 provides the BET surface area and total pore volume of the parent material and its components under evaluation. The BET surface area of the composite A and B is determined as 1704 $m^2 g^{-1}$ and 1597 $m^2 g^{-1}$, respectively, which is 38.38% and 34.25% greater than the base material. The presence of activated carbon and MOF MIL-53(Al) increases the surface area and pore volume of the consolidated adsorbent. The increase in surface properties of the composite materials such as pore volume, surface area are based on the fact that, by the addition of materials to the parent adsorbent causes for the well

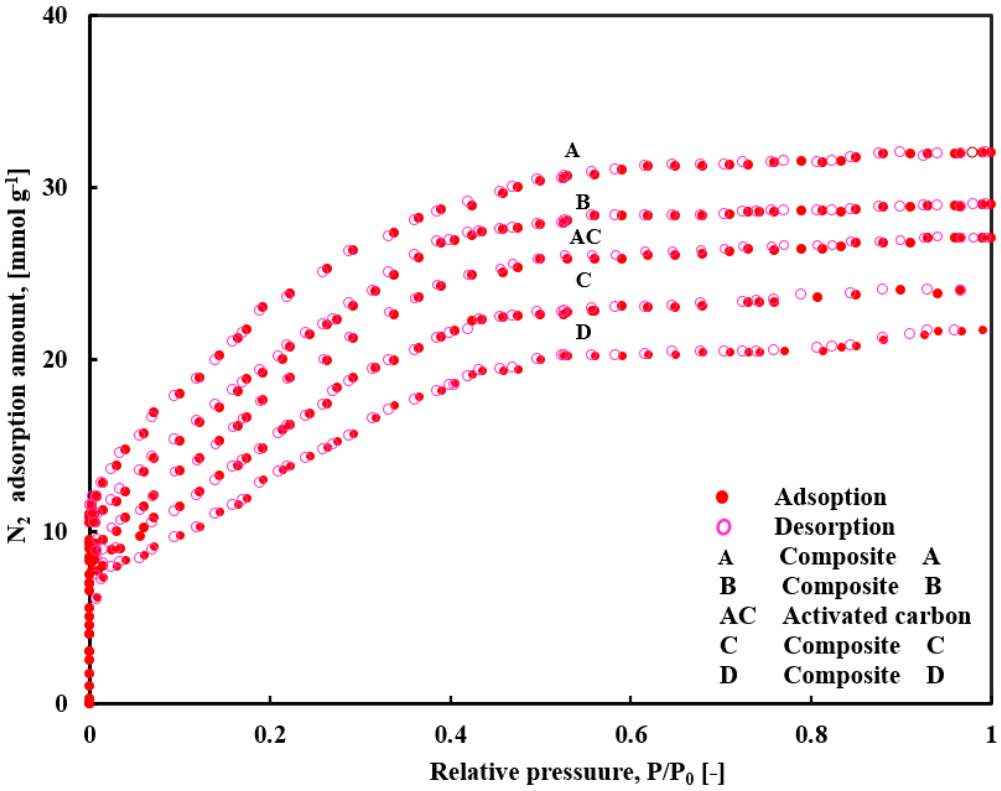

Fig. 7.4: Characterisation of parent material and its composite N_2 adsorption or desorption isotherm curves of all produced composites as well as the parent activated carbon at 77K

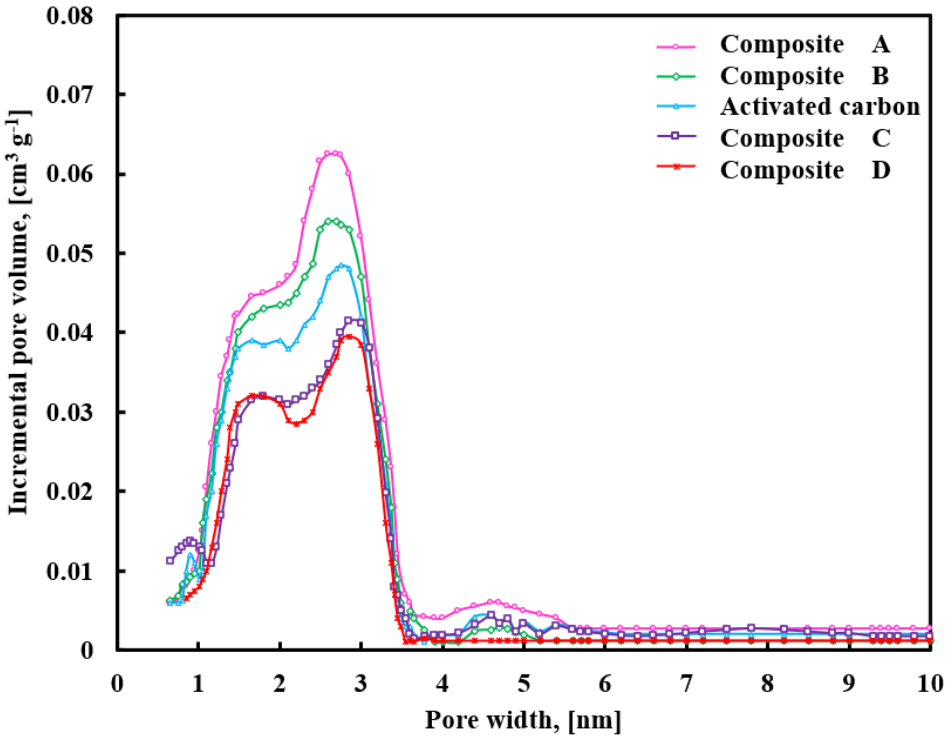

Fig. 7.5: Pore width distribution of activated carbon and its composites

Table 7.3 BET surface area and total pore volume of the parent material and its components under evaluation

Composite	BET surface area [$m^2 g^{-1}$]	Total pore volume [$cm^3 g^{-1}$]
Composite A	1704±29	1.01
Composite B	1597±26	0.93
Composite C	947±17	0.78
Composite D	792±20	0.49

formation of samples without intercepting pores or the opening of existing pores may be achieved [109]. This increase in specific surface area may be due to crystallographic flaws brought on by the addition of activated carbon, which causes the opening or creation of micropores. Additionally, the framework is less contaminated by unreacted particles, thereby the volume of the composite increases due to the presence of activated carbon [110].

7.3.3 SEM image

Surface morphology and orientations of the materials that make up the sample will be clearly visible in the SEM images and the images are consistent with the SEM images reported by Tso et al. and Mertsoy et al. [111, 112]. Figure 7.6 (a)-(d) show SEM images of activated carbon and composites A to D. A fully developed pore structure resembles honeycomb gaps in the micrograph of composite A, as seen in Fig. 7.6(b). The volatilisation of hemicellulose, cellulose, and other compounds causes carbonisation, which results in the creation of rudimentary pores. The space generated by the evaporation of moisture and other impurities in the base material results in certain cavities and well-developed pores.

In composite B, small pores, transitional pores, and large pores of varied shapes can be seen in Fig. 7.6 (c), indicating pore broadening and more developed pore structure. Porous materials detected by micrographs are consistent with BET surface area and pore volume in composite A and B. However, due to the low surface area of the added materials in composites C and D, the surface area and pore volume are reduced (Fig. 7.6. (d)-(e)). As a result, foreign particles in the base and additives, as well as the surface area and pore volume of the additives, have a significant impact on the formed composite's shape.

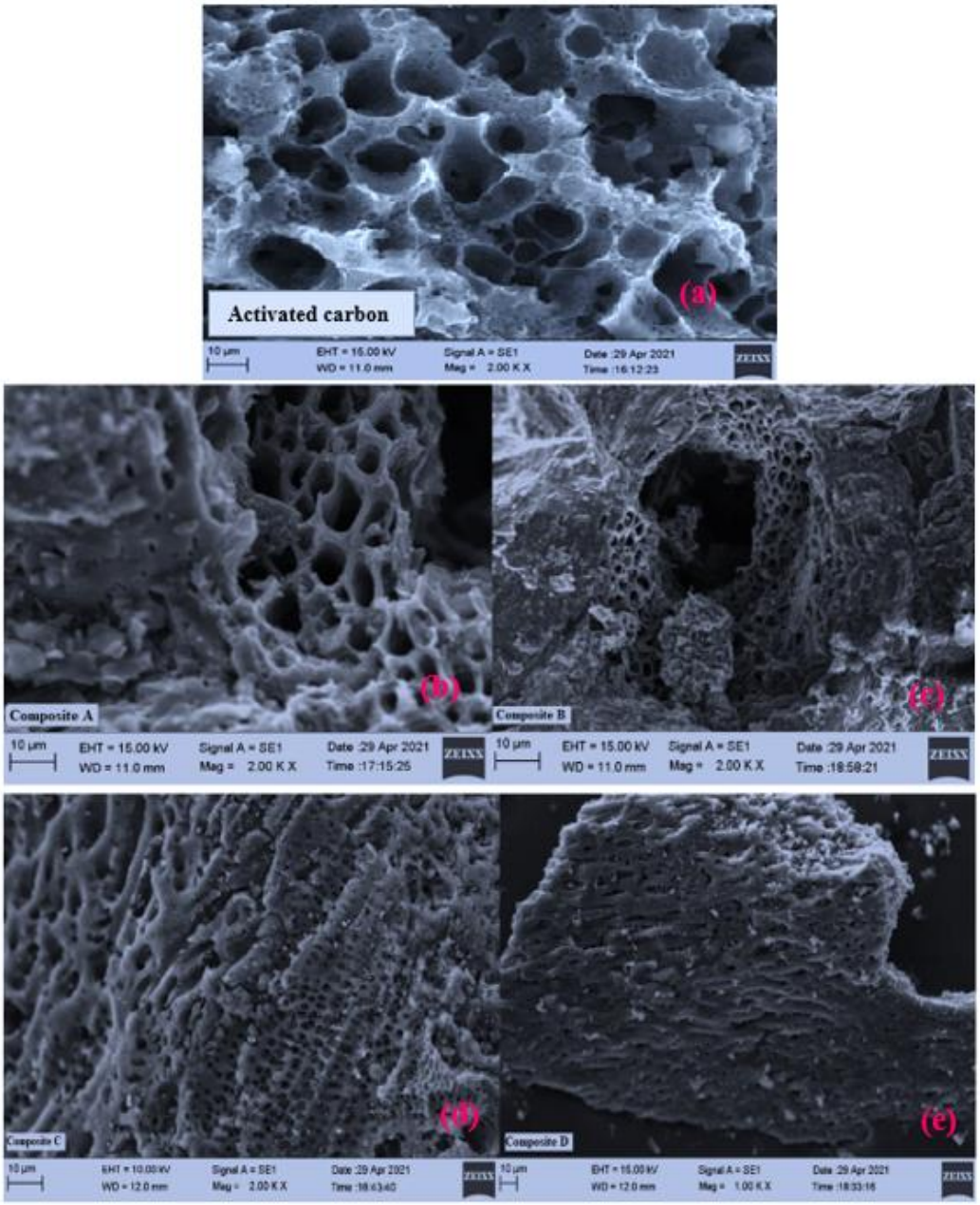

Fig. 7.6: Morphology or SEM image of (a) activated carbon, (b) composite A, (c) composite B, (d) composite C and (e) composite D

7.3.4 CHNS analysis of the sample

Using a Perkin Elmer 2400 Series II CHNS Organic Elemental Analyzer (EA) 100 V, the carbon (C), hydrogen (H), nitrogen (N), sulphur (S), and other volatile substances in the sample are analysed. EA determines the C, H, N, and S contents of the adsorbent, whereas the oxygen (O) and volatile contents are estimated by subtracting the quantities of

the aforementioned contents from 100. To have a high adsorption capacity, the adsorbent must have a high carbon concentration and a low ash content [113]. Due to weak Van der Walls forces, a high carbon concentration may increase the interaction between adsorbent and refrigerant. The composition of the base and composite materials utilised in this study are detailed in Table 7.4.

Table 7.4 Elementary contents of the base and composite materials

	C (%)	**H (%)**	**N (%)**	**S (%)**	**O and volatile matters (%)**	$\left(\frac{N}{C}\right) x\ 100$
AC	84.77	0.61	0.27	0.012	14.34	0.32
Composite A	86.21	0.52	0.19	0.0	13.08	0.22
Composite B	83.65	0.89	0.24	0.0	15.22	0.29
Composite C	73.85	1.24	0.38	0.02	24.51	0.51
Composite D	70.34	0.97	0.43	0.0	28.26	0.61

7.3.5 Thermal conductivity measurement

The thermal conductivity of the sample has been measured using KD2 PRO (Fig. 7.7) established by Decagon Devices [114]. It consists of a portable controller and a source to determine thermal conductivity by measuring heat dissipation from the needle probe. This probe can measure thermal conductivity with a precision of 10 % in the range of 0.1 to 6 $Wm^{-1}K^{-1}$. The measurement of thermal conductivity by KD2 PRO with single needle algorithm. Heat is applied to a single needle for t_t seconds, and the temperature in the needle is measured throughout the heating time and for an additional time equal to t_t seconds afterward. The temperature of the sample throughout the heating process is then determined by Eq. (7.2).

$$T = t_0 + t_2 t + t_3 \ln t \tag{7.2}$$

where t_0, t_2 and t_3 represents the atmospheric temperature during heating, rate of background temperature drift and the slope of line relating temperature rise to logarithm of temperature respectively. Eq. (7.3) represents the model of cooling process.

Fig. 7.7: Photograph of KD2 PRO

$$T = t_1 + t_2 t + t_3 \ln \frac{t}{t - t_t} \tag{7.3}$$

Eq. (7.4) is used to calculate the thermal conductivity, K of the sample

$$K = \frac{q}{4\pi t_3} \tag{7.4}$$

where, q denotes the heat flux applied to the needle probe over a given time period. This heat disappears differently along the sample, and as shown in Eq. (7.4). Moreover, the value is used by the equipment KD2 PRO to evaluate the thermal conductivity of the sample. The KD2 PRO, does not provide the heat flux applied and it only provides the final thermal conductivity value.

Figure 7.8 depicts the thermal conductivity plots of activated carbon and its composites. Experimental results demonstrate that composites B and D have higher thermal conductivity than composites A and C due to the presence of thermal enhancement materials such as natural expanded graphite. Furthermore, rather than pure powder, the analysis focuses on composite and granular forms of materials. Due to the greater inter-particle contact resistance, the powder form may have low thermal conductivity [115]. Because the parent adsorbent contains 20% (by weight) expanded graphite powder,

composite D has the maximum thermal conductivity of the composite adsorbents investigated. At ambient temperature, the sample has a thermal conductivity of 0.37 $Wm^{-1}K^{-1}$, which is 64.86 % higher than the parent adsorbent. Thermal conductivity and adsorption capacity are equally significant in this study because it is primarily concerned with adsorbents for low-temperature applications such as adsorption cooling systems. As a result, composite B is being examined as a possible composite candidate for SAC systems.

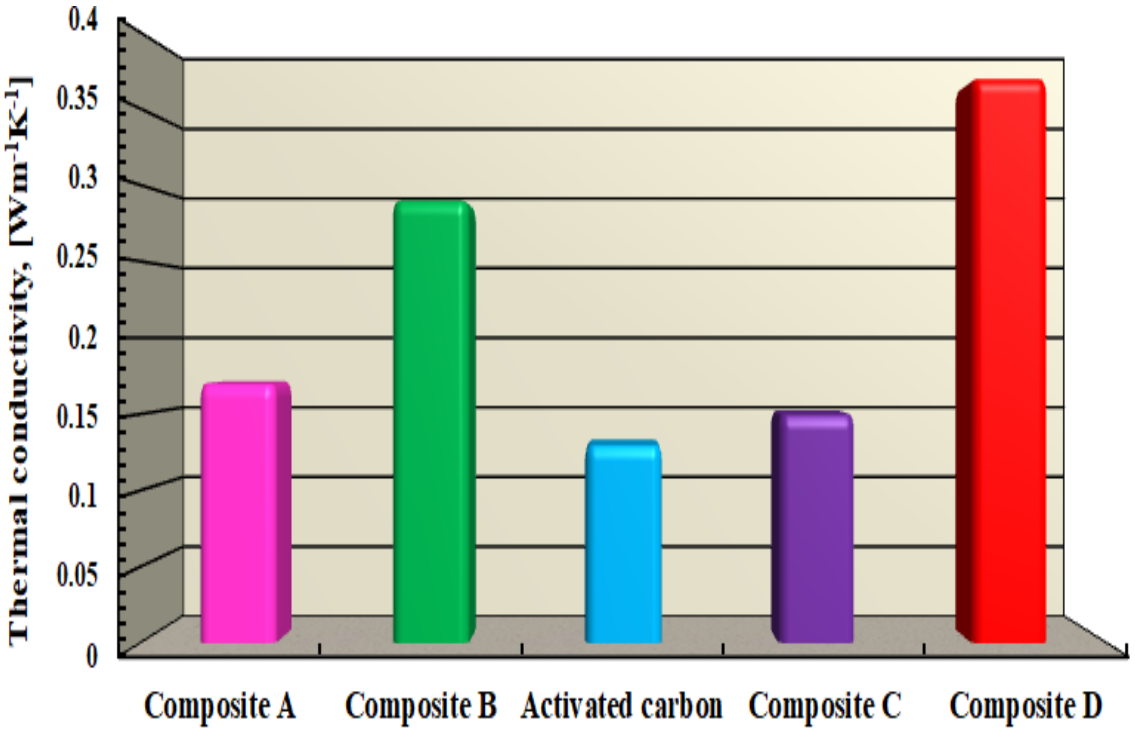

Fig. 7.8: Comparison of thermal conductivity of activated carbon and its composites

The composite B has a thermal conductivity of 0.29 $Wm^{-1}K^{-1}$, which is 55.17 % higher than the activated carbon base material at ambient temperature. The thermal conductivity is a temperature dependent property. In the present study, the thermal conductivity of the selected composite (composite B) has been measured at 40, 50, 60 and 70^0C. Figure 7.9 depicts the effect of temperature on thermal conductivity of composite B and it shows that the thermal conductivity of the material varies linearly with temperature. The relationship between the thermal conductivity and temperature of the composite B is given by:

$$k=0.2907 + 0.001035 (T - T_0) \quad (7.5)$$

where, T_0 be the atmospheric temperature which is taken as 30^0C.

Figure 7.10 presents the effect of packing density on the thermal conductivity of the selected composite B. Packing density mainly depends upon the mass of the adsorbent per unit volume. Figure 7.10 indicates that thermal conductivity and packing density have a strong correlation. At a composite packing density of 600 kgm^{-3}, the composite B has the maximum thermal conductivity of 0.45 $Wm^{-1}K^{-1}$, which is 17.8% higher than the base material activated carbon at the same packing density. The higher the packing density, greater the contact surface area, which improves the thermal conductivity of the material. However, at the start of the adsorption process, the increased packing density of the adsorbent affects its permeability and immediate adsorption capacity. As a result, choosing an adequate packing density for the adsorbent is critical when designing a small adsorption unit. Hence, Composite B is selected for the present study, which has a medium packing density of 421 kgm^{-3}. A Quantachrome Instruments Autopycnometer-PentaPyc 5000e is used to determine the packing density of the activated carbon and composite B.

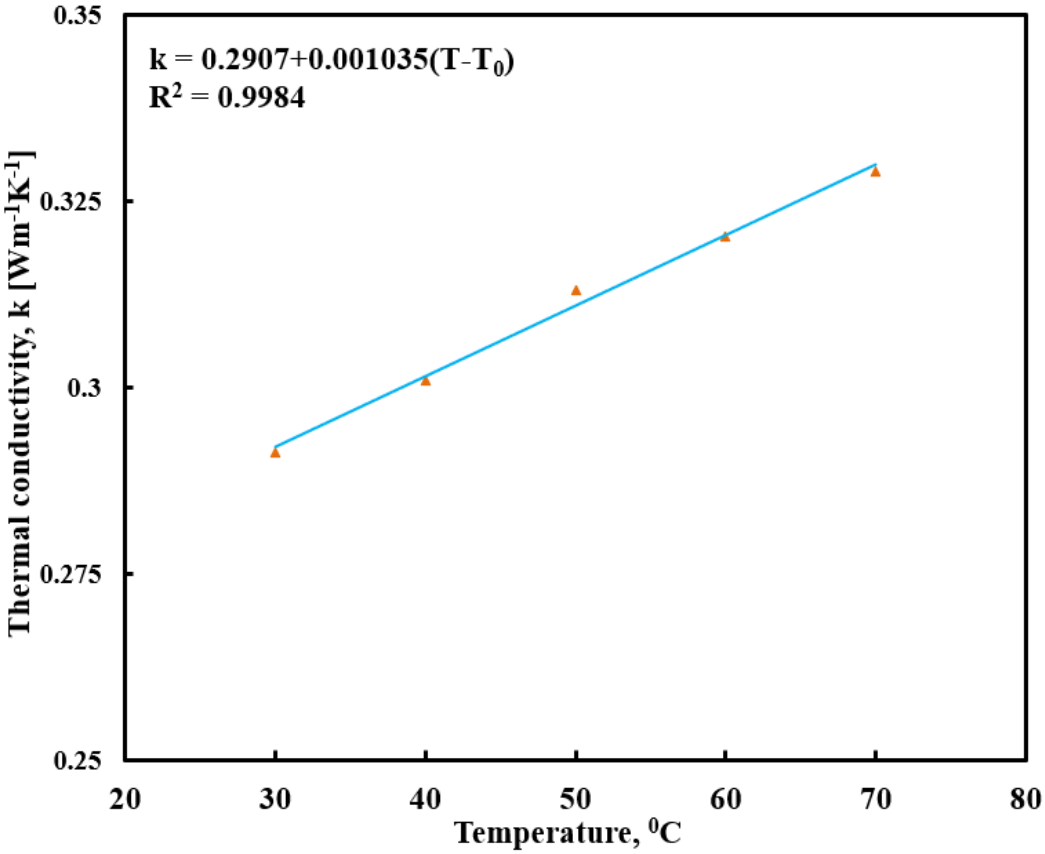

Fig. 7.9: Effect of temperature on thermal conductivity of composite B

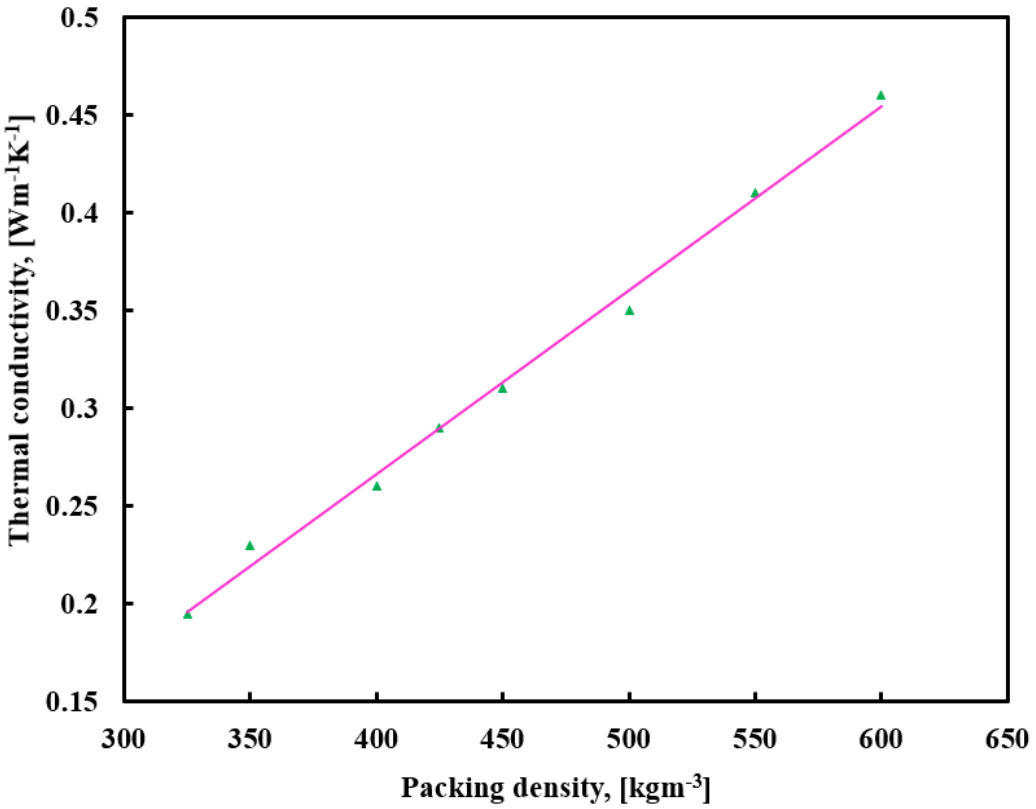

Fig. 7.10: Effect of packing density on the thermal conductivity of composite B

7.3.6 TGA analysis of Activated carbon and composites A and B

Thermo Gravimetric Analysis (TGA) provided by SDT Q 600 is used to evaluate the thermal behaviour of the adsorbents used. In this case, the activated carbon and composites A and B weighing 3 to 4 mg are analysed using a thermal analyser with nitrogen as a purge gas at a heating rate of $5^0 Cmin^{-1}$. Figure 7.11 depicts the comparative thermal analysis curves of the adsorbents used. The water evaporation and devolatilisation and decomposition, two phases of the heating pyrolysis process is highly visible in the Fig. 7.11 of TGA curves. Prior to the TGA analysis, the samples are first saturated with water vapour for 24 h. Then the TGA analysis is carried out at 90^0C and at low pressure in a nitrogen atmosphere to remove water vapour and inadvertently trapped volatile materials (especially moisture) that is adsorbed on the surface of adsorbents [116]. The weight loss is caused by the evaporation of absorbed water from the activated carbon and composites by isothermal heating at 90^0C for 30 mins (seen in Fig. 7.11 during the first phase of TGA curve). At different onset temperatures of 224^0C, 227^0C, and 221^0C, substantial mass degradation from the activated carbon sample, composite A and B, is seen. At this stage, the degradation of organics, which accounts for the majority of the pyrolysis of fixed

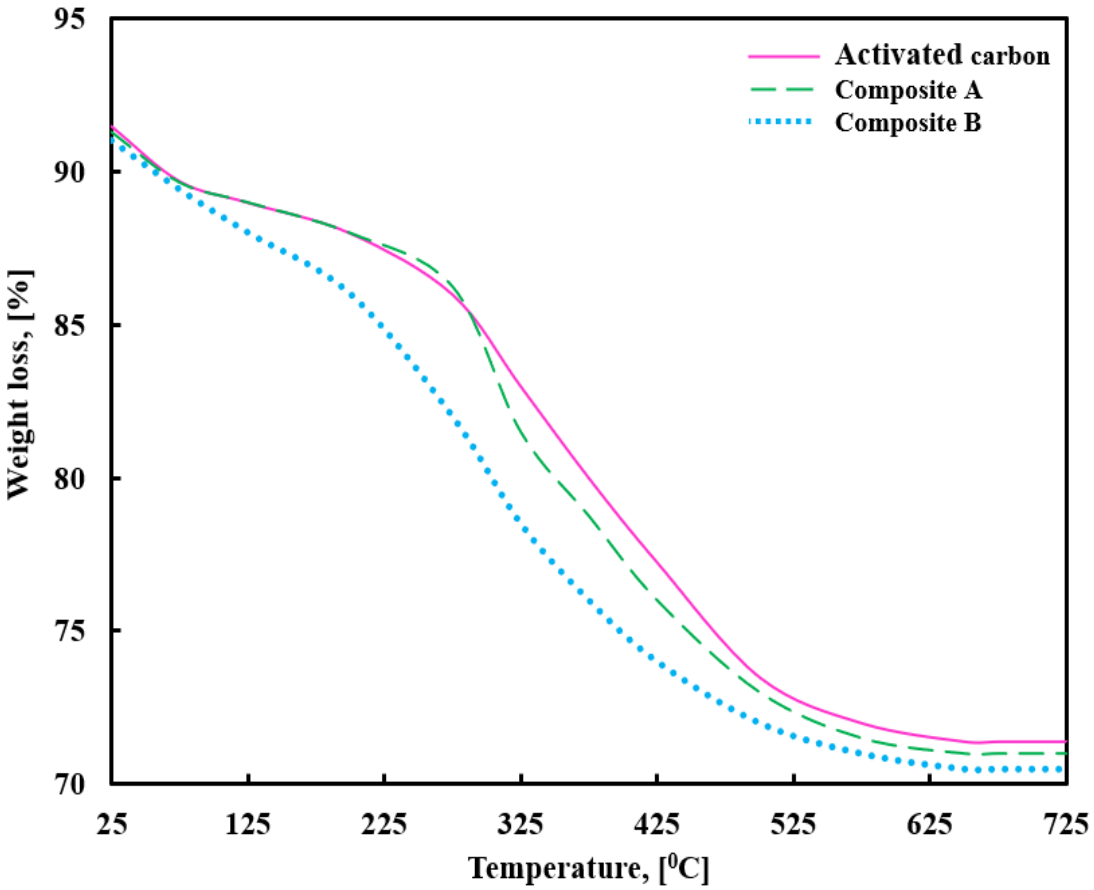

Fig. 7.11: TGA curve of activated carbon and selected composite A and B

carbon, results in massive mass loss. After 525^{0}C, the mass of the base material carbon did not change appreciably, indicating that pyrolysis is practically complete. Because the composites contain the same ingredients, such as activated carbon, expanded graphite powder, and MOF, the TGA patterns of the remaining composites will be substantially identical. As a result of this study, it's reasonable to conclude that the synthesised composites have good thermal stability and are thus suited for low-temperature adsorption cooling applications.

7.4 Ethanol Adsorption Uptake Measurement

From the characteristics study conducted, the composite B, comprising 70% (by weight) of parent material - activated carbon, 10% MOF MIL-53Al, 10% EGP and 10% PVP is selected as the suitable consolidated adsorbent for the present investigation. Figure 7.12 shows a schematic of the experimental setup utilised to investigate the ethanol adsorption process using the newly designed composite adsorbent B. An evaporator, an adsorbent bed, two continuous water baths and a water circulator, a vacuum pump, and a

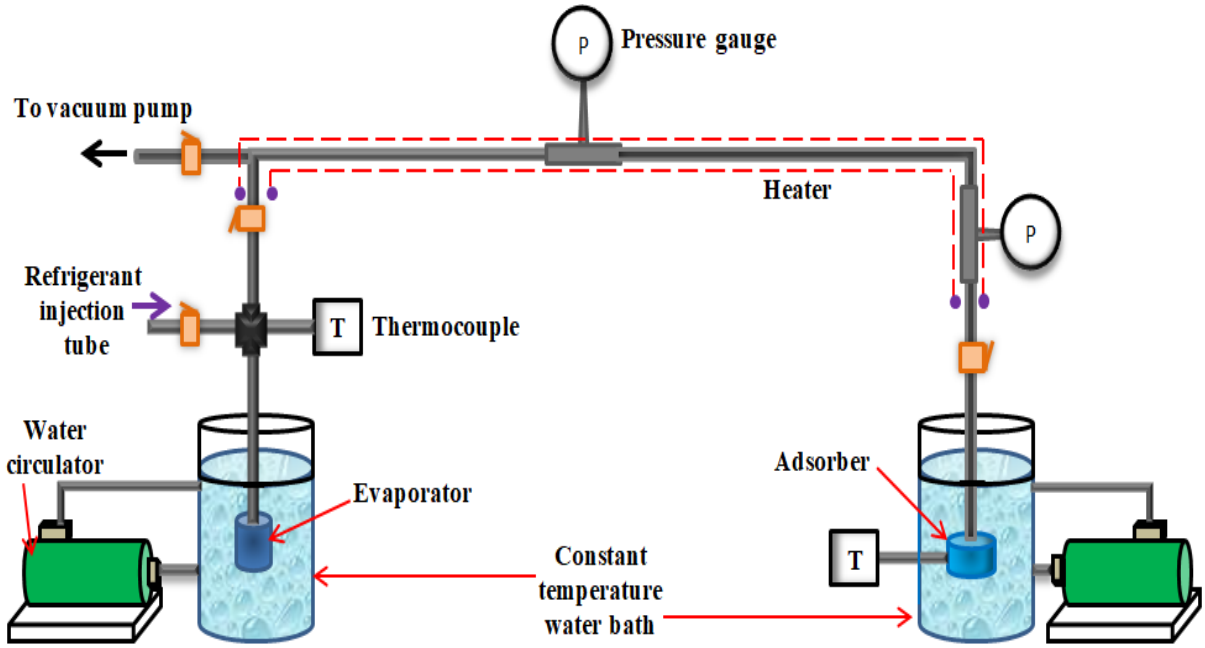

Fig. 7.12: Experimental system used to study the ethanol adsorption process onto the newly developed composite adsorbent (Composite B)

heat source are all included in the experimental setup. The evaporator is a cylindrical glass tube of 6.5 mm inside diameter and 168 mm height. The adsorbent bed is also cylindrical in shape made of stainless-steel tube having 38 mm in diameter and height. A K-type thermocouple is inserted to measure the temperature at the evaporator and at the adsorbent bed. The evaporator and adsorbent bed are set in a constant temperature water bath of type TSGP10, which is controlled by a water circulation pump of type HQB-3000. An Arish - VP245 type rotating vacuum pump has been used to evacuate the system. A PGH-011 digital type pirani gauge and a 316L stainless steel OEM pressure transducer are used to measure the vacuum and pressure of the system, respectively. The difference between the height of the ethanol level in the adsorbent bed before and after the adsorption has been monitored using an ISM-PM200SB digital microscope with a minimum resolution of 0.01 mm. The weighing machine QUINTIX-125D-10-IN with a weight capacity of 150 gms and readability of 0.1 mg has been used to weigh the adsorbent samples. The chance of arising condensation in the system can be avoided by using a tape heater placed in the tube which connects the evaporator and adsorbent bed components of the system. The composite is dried in the oven for about 10 hrs at 100^0C to remove the volatile and vapour content in it. Weigh the dried adsorbent before placing it in the adsorbent bed. Under vacuum at 90^0C, the composite is regenerated in the adsorbent bed for more than 4 h. The amount of ethanol

in the evaporator is measured using a digital microscope at 5^0C and 80^0C for the evaporator and adsorber temperature, respectively. The evaporator-adsorber valve is then opened, allowing ethanol vapour to flow to the adsorbent. After achieving equilibrium, the amount of ethanol inside the evaporator is measured again to determine the amount of ethanol adsorbed.

The evaporator-adsorbent bed valve is closed, and the adsorbent bed is cooled to 75^0C using a constant temperature water bath. The valve is then opened to allow the refrigerant to flow from the evaporator to the adsorbent bed, and the procedure is repeated at 70^0C, 65^0C, 60^0C, 55^0C, 50^0C, 45^0C, 40^0C, 35^0C, 30^0C, 25^0C and 20^0C adsorption temperatures. To get the matching isobaric adsorption curves, the procedure is repeated at 10^0C and 15^0C evaporator temperatures. Experimental data have been used to calculate the structural constants of the D-R equation of the novel composite-ethanol combination chosen for this study.

7.5 Uncertainty analysis

Equation (7.6) has been used to calculate the uncertainty in measuring ethanol adsorption accumulation (kgkg^{-1}) by the newly selected composite adsorbent using the experimental test rig shown in Fig. 7.12. Eqs. (7.6) to (7.10) represents the corresponding derivatives. Eq. (7.7) has been used to calculate ethanol adsorption accumulation (kgkg^{-1}) in the newly selected composite adsorbent using the experimental test rig shown in Fig. 7.12.

$$\delta X = \sqrt{\left(\frac{\partial X}{\partial Di_{eva}}\delta dDi_{eva}\right)^2 + \left(\frac{\partial X}{\partial M_{com}}\delta dM_{com}\right)^2 + \left(\frac{\partial X}{\partial Hi_{eva}}\delta dHi_{eva}\right)^2} \qquad (7.6)$$

$$X = \rho_{liq}\ Hi_{eva}\ \frac{\pi}{4}\left(\frac{Di_{eva}^2}{M_{com}}\right) \qquad (7.7)$$

$$\frac{\partial X}{\partial Di_{eva}} = \rho_{liq}\, Hi_{eva}\ \frac{\pi}{4}\left(\frac{2Di_{eva}}{M_{com}}\right) \qquad (7.8)$$

$$\frac{\partial X}{\partial M_{com}} = -\rho_{liq}\ Hi_{eva}\ \frac{\pi}{4}\left(\frac{Di_{eva}^2}{M_{com}^2}\right) \qquad (7.9)$$

$$\frac{\partial X}{\partial Hi_{eva}} = \rho_{liq} \frac{\pi}{4} \left(\frac{Di_{eva}^2}{M_{com}}\right) \quad (7.10)$$

where ethanol adsorption uptake measurement uncertainty is represented by δX. The uncertainty of the evaporator diameter, composite sample mass measurement and ethanol level measurement inside the evaporator glass tube by the digital microscope is given by δdDi_{eva}, δdM_{com} *and* δdHi_{eva}, respectively. The diameter of the evaporator glass tube, composite sample mass, and ethanol level height inside the evaporator are represented by Di_{eva}, M_{com} *and* Hi_{eva}, respectively. The following are the detailed specifications for calculating uncertainty analysis of the ethanol adsorption uptake, where Di_{eva} = 6.5 mm, δdDi_{eva} = 0.1 mm, M_{com} = 1.9 gms, δdM_{com} = 0.01 gms and δdHi_{eva} = 0.01 mm. The ethanol adsorption uptake measurements is found to be having an average value of 3.12% uncertainty.

7.6 Structural Constants of D-R Equation

The Dubinin-Rreduskevich equation is used to model the system, the equation has the following form:

$$X = X_0 \exp\left\{-D\left(T \ln\frac{P_{sa}}{P}\right)^n\right\} \quad (7.10)$$

The Eq. (7.10) can be expressed in a logarithmic form as:

$$\ln(X) = \ln(X_0) - D\left(T \ln\frac{P_{sa}}{P}\right)^n \quad (7.11)$$

where, numerical value of X_0 and D are specific coefficient for the selected combination-refrigerant pair, T is the adsorption temperature (K), and P_s the saturation pressure. $\left(T \ln\frac{P_{sa}}{P}\right)^n$ is then fitted against ln (X) yields the structural constant D and maximum adsorption X_0, as shown in Fig. 7.13. The best fitting of the experimental value has been obtained when n = 2. It is also worth mentioning that the maximum adsorption uptake of composite B is 0.983, which is approximately 19.63% of the maximum adsorption uptake of the activated carbon-ethanol pair. Table 7.5 provides the numerical values of X_0, D, and n of the proposed composite B. Figure 7.14 shows the adsorption isobars of the composite

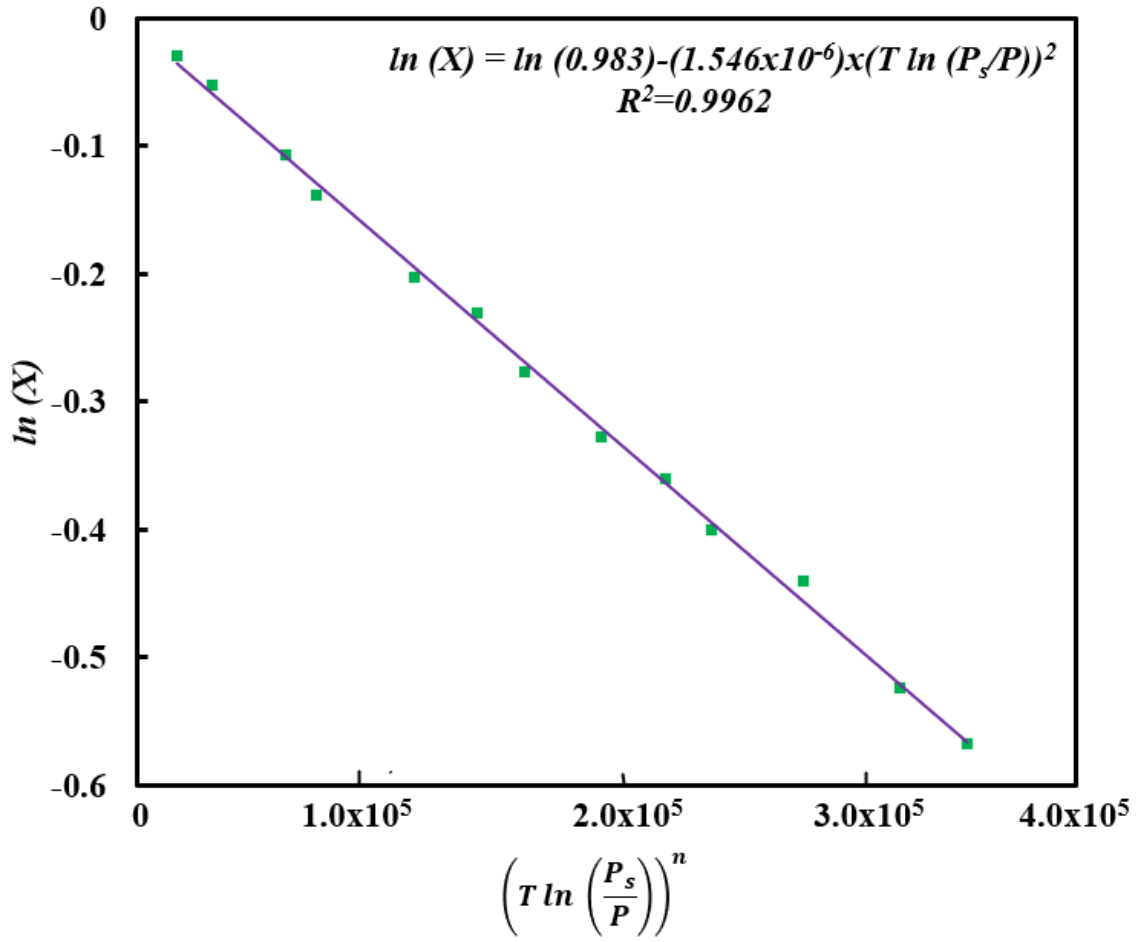

Fig. 7.13: Linear fitting (D-R) of equation for composite B-ethanol pair for n = 2

Table 7.5 Numerical values of X_0, D, and n of the proposed composite B

	X_0	**D**	**n**
Composite B	0.983	1.546×10^{-6}	2

B-ethanol at evaporator temperature of 5^0C (2.01kPa), 10^0C (3.11 kPa) and 15^0C (4.28 kPa). The D-R equation fitting for adsorption isotherm of composite B-ethanol is also represented in the Fig. 7.15. The predicted adsorption data using D-R equation agrees well with the measured value. This is ample proof that the doping and binder materials of the composite do not compromise the adsorption of the consolidated material. The composite B-ethanol adsorption isotherms are depicted in Fig. 7.16, which also demonstrates that as the relative pressure approaches unity, the working pairs become concave to the relative pressure, and the adsorption capacity approaches a limit value.

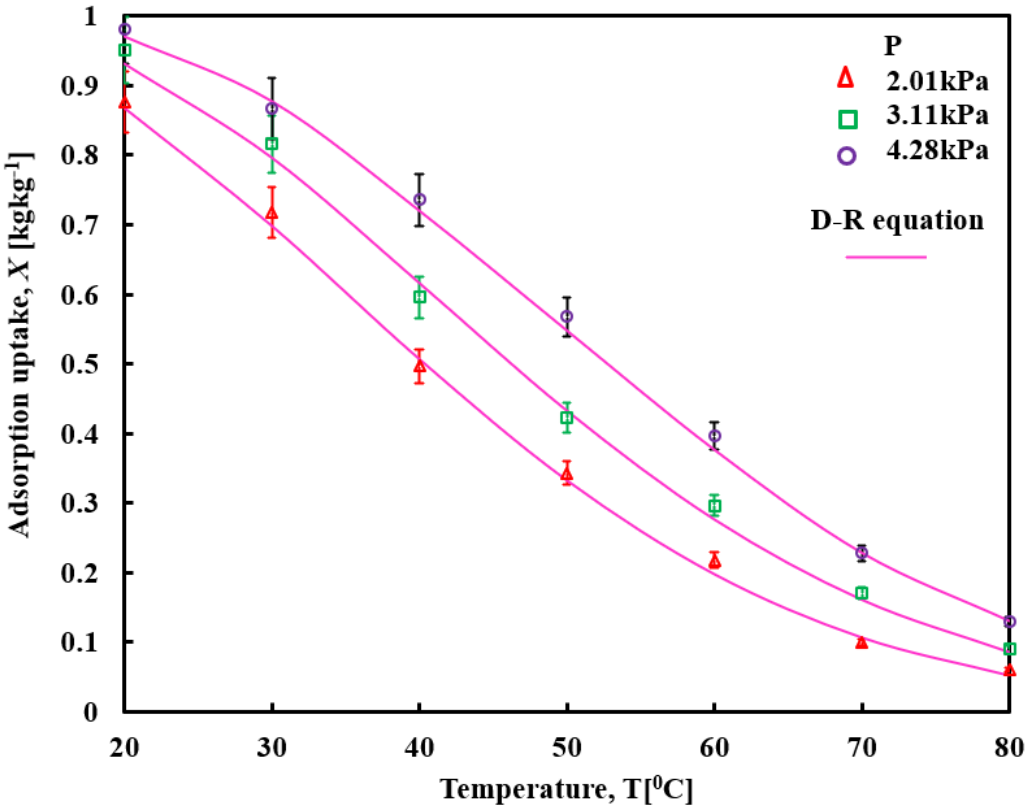

Fig. 7.14: Adsorption isobars of the composite B-ethanol at evaporator temperature of 5^0C (2.01 kPa), 10^0C (3.11 kPa) and 15^0C (4.28 kPa)

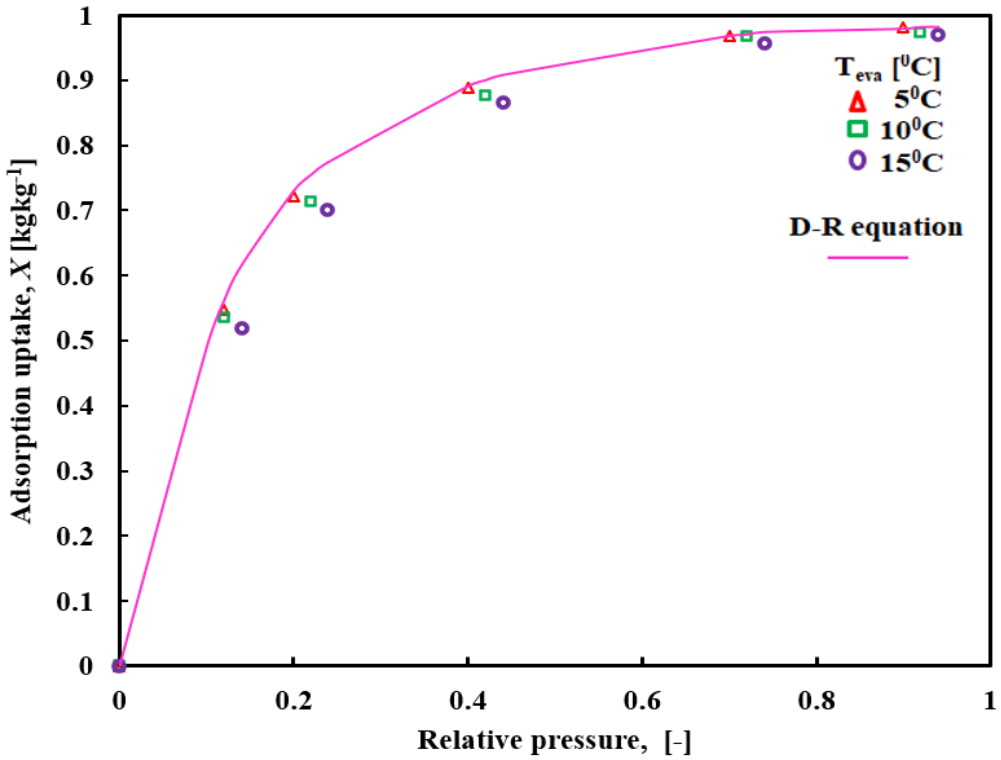

Fig. 7.15: Adsorption isotherm of Composite B-ethanol pair

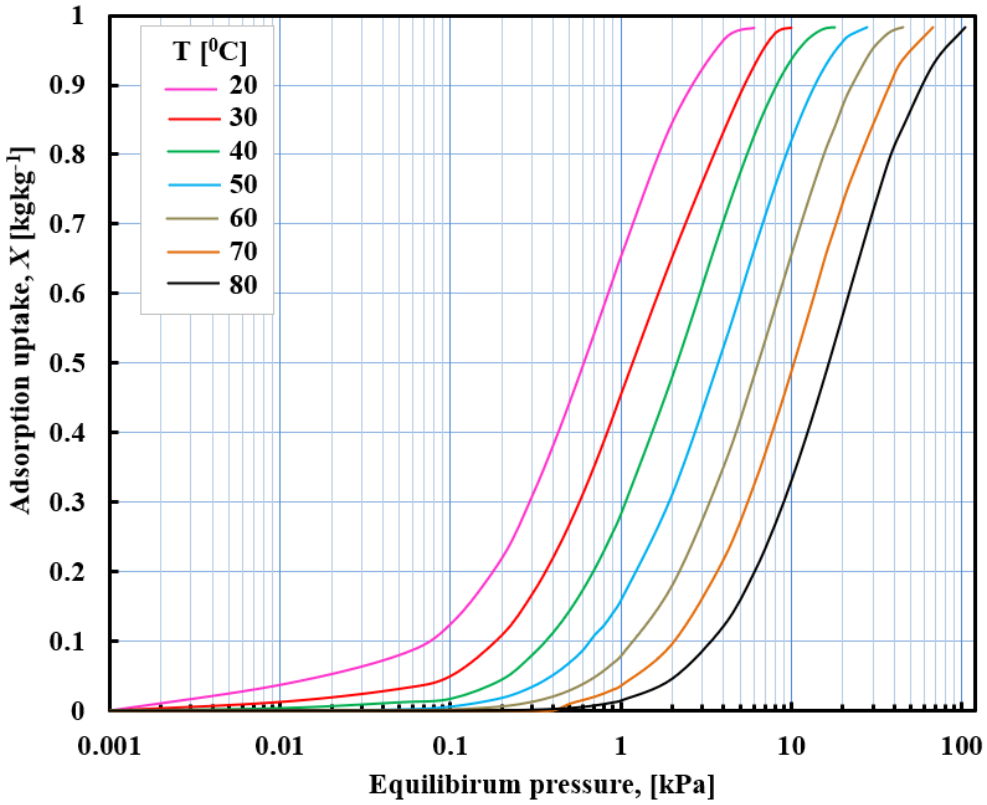

Fig. 7.16: Adsorption isotherm of the Composite B-ethanol pair with varying equilibrium pressure over the adsorption temperature range of 20^{0}C to 80^{0}C

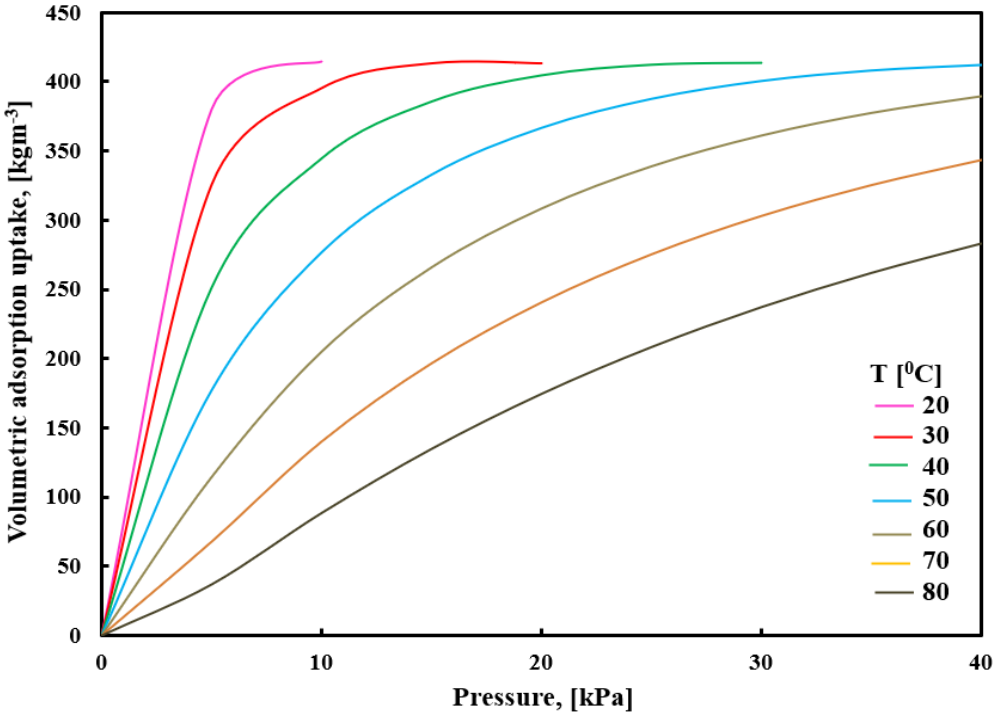

Fig. 7.17: Volumetric adsorption isotherm of Composite B, with the packing density of 421 kgm^{-3} ranging from 20^{0}C to 80^{0}C

The volumetric adsorption isotherm of the Composite B-ethanol pair with varying equilibrium pressure over the adsorption temperature range of 20^0C to 80^0C is depicted in Fig. 7.17. The D-R equation is used to predict the isotherm, and the equilibrium pressure is determined for different values of equilibrium adsorption uptake at constant adsorbent temperature. Adsorption generates heat, which raises the adsorption temperature and reduces adsorption capacity. As a result, cooling the system is designed to aid the adsorbent's adsorption capacity, and water is utilised as a cooling medium to remove the heat generated in the system. Hence it is important to enhance the heat transfer properties of adsorbent so that it can attain thermal equilibrium with the cooling fluid temperature. During this uptake the packing density is approximately taken as 421 kgm^{-3}. Figure 7.18 shows the volumetric uptake differences of adsorption cooling cycles employing a Composite B-ethanol (solid line PQRS) and activated carbon-ethanol (dotted line P'Q'R'S') pair at 5^0C, 30^0C, and 80^0C, respectively, for the evaporator, adsorption, and desorption temperatures. According to Fig 7.18, the volumetric uptake differential between composite B-ethanol and the parent adsorbent-ethanol combination is approximately 24.38% higher. Hence composite B, made up of MOF-MIF-53Al, expanded graphite powder, and PVP in

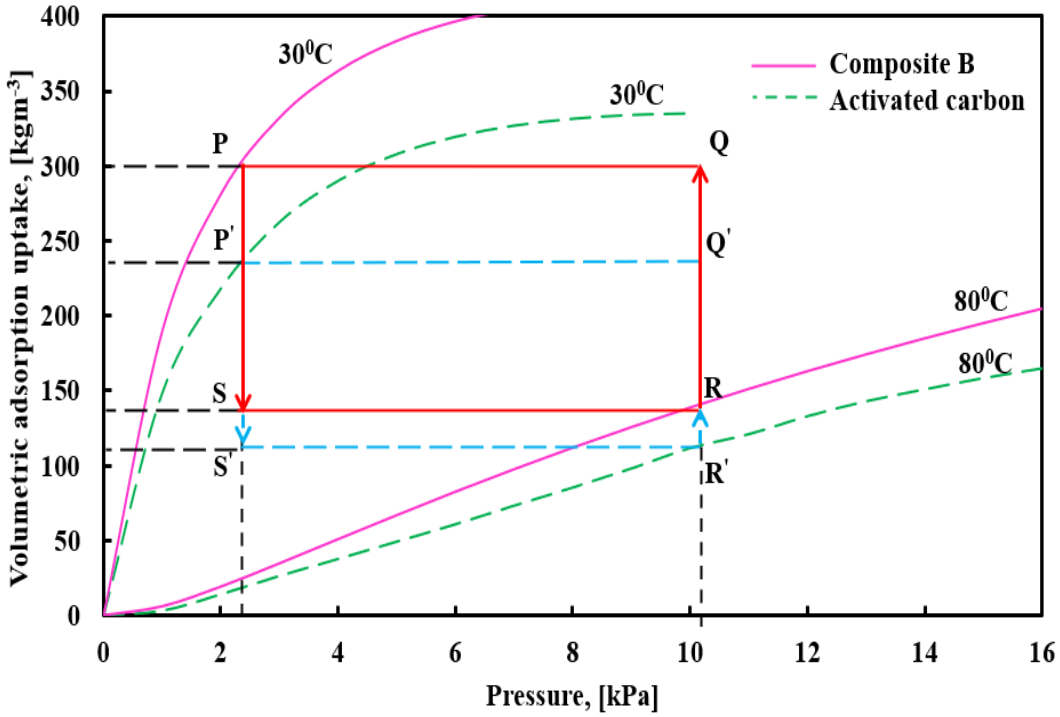

Fig. 7.18: Volumetric adsorption isotherm of Composite B-ethanol and activated carbon-ethanol pairs at adsorption, desorption and evaporator temperatures of 30^0C, 80^0C and 5^0C

activated carbon, has been selected as a good candidate for adsorption cooling applications. Composite B has a higher volumetric adsorption uptake due to its enhanced pore capacity and high affinity towards the refrigerant vapour.

Summary

This chapter gives an overview of composite adsorbent consisting of activated carbon, MOF MIL-53Al, expanded natural graphite and binder that has been developed. The adsorption uptake of activated carbon and composites with N_2 is performed to determine the BET surface area and pore volume. The sample made up of 70 % activated carbon, 10 % expanded graphite powder, 10 % metal organic framework MIL-53AL and 10 % binder PVP has been selected as the composite adsorbent for the present work which is having a thermal conductivity of 0.29 $Wm^{-1}K^{-1}$, that is 55.17 % greater than the base material activated carbon. This investigation also contributes to the determination of the structural constant of the D-R equation for the proposed composite B. Composite B has a volumetric uptake of 24.38% larger than that of the parent adsorbent activated carbon. The next chapter details the theoretical and experimental evaluation of the SAC system operating with composite adsorbent and ethanol as the working pair.

Chapter 8

Performance Investigation of the Solar Adsorption Cooling System with Composite Adsorbent-Ethanol as Working Pair

This chapter envisages the performance investigation of the SAC system with composite adsorbent/ethanol as the working pair. The thermodynamic modelling and experimental investigations to assess the performance of the system are detailed in this section. The comparative studies of the performance of the SAC system are also detailed in this chapter.

8.1 Methodology

The proposed two bed SAC system has been designed and developed, and the details are given in the chapter 6. The preliminary investigations are conducted by using activated carbon-ethanol as the adsorbent-adsorbate pair. Section 6.10 of Chapter 6 describes the entire experimental method, as well as the results and discussion. The experimental study are extended for the proposed working pair, composite B- ethanol. This chapter focuses the thermodynamic modelling and experimental investigation of the SAC system, when it is operated with composite adsorbent B-ethanol as working pair. The

experimental investigations are also conducted with and without energy storage material. Finally a comparative study is also done .

8.2Thermodynamic Analysis of the SAC System with Composite B-Ethanol as Working Pair

The section details the results of the two bed SAC system obtained by the thermodynamic analysis, which is operated with composite B-ethanol as working pair. The performance of the system is assessed with activate carbon-ethanol and composite adsorbent B-ethanol as working pairs.

8.2.1 Two bed adsorption cooling system operated with composite adsorbent-ethanol as working pair

The total heat energy added (Q_{add}) to the SAC system has been determined to be 8793.7 kJ, while 8702.35 kJ of heat is rejected during the cycle. The relative error is estimated as 1.04%, which is very low and confirms the accuracy of the analysis. Figure 8.1 depicts the heat input distribution within the adsorbent bed elements. The total heat

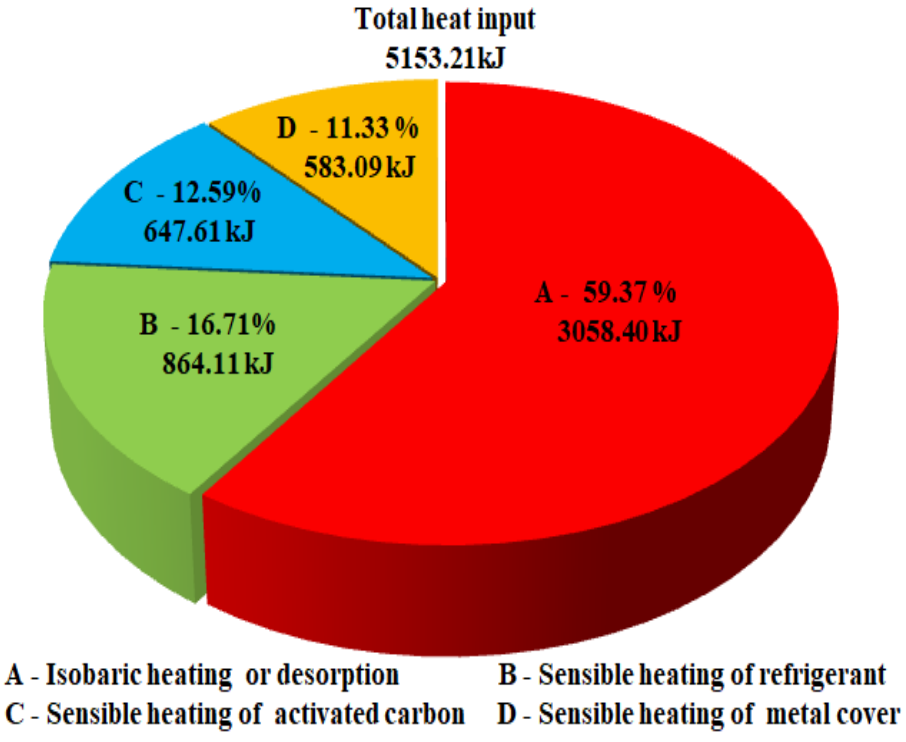

Fig. 8.1: Input heat distribution within the adsorbent bed elements with composite adsorbent-ethanol as working pair

input to the SAC system ($Q_{in}^{1\to2\to3}$) is 5153.21kJ, and the heat distribution within the adsorbent bed elements during the heating processes are $Q_{\text{des}}^{2\to3}$ = 3058.40 kJ, $Q_{ref}^{1\to2\to3}$= 864.11kJ, $Q_{\text{ac}}^{1\to2\to3}$ = 647.61kJ and $Q_{\text{mc}}^{1\to2\to3}$ = 583.09kJ, respectively. The composite B - ethanol working pair reduces the overall heat input to the system by 25.13 % when compared to the activated carbon-ethanol working pair. This reduction in heat input also reduces the energy required for desorption and heating of the refrigerant, activated carbon, and metal cover. Thus, the composite-ethanol working pair for the SAC system is found to be superior as compared to the basic working pair. In addition, the good thermal conductivity of the composite materials contributes to the improvement of the thermal conductivities, thus improving the desorption process of the adsorbate from the adsorbent, which strengthens the performance of the system.

8.2.2 Effect of adsorption bed temperature on the adsorbate concentration ratio and volume fraction

The effect of the adsorbate concentration ratio with cycle temperature at equilibrium (Fig 8.2) is determined based on Eq. (5.53. The adsorbate concentration ratio varies from

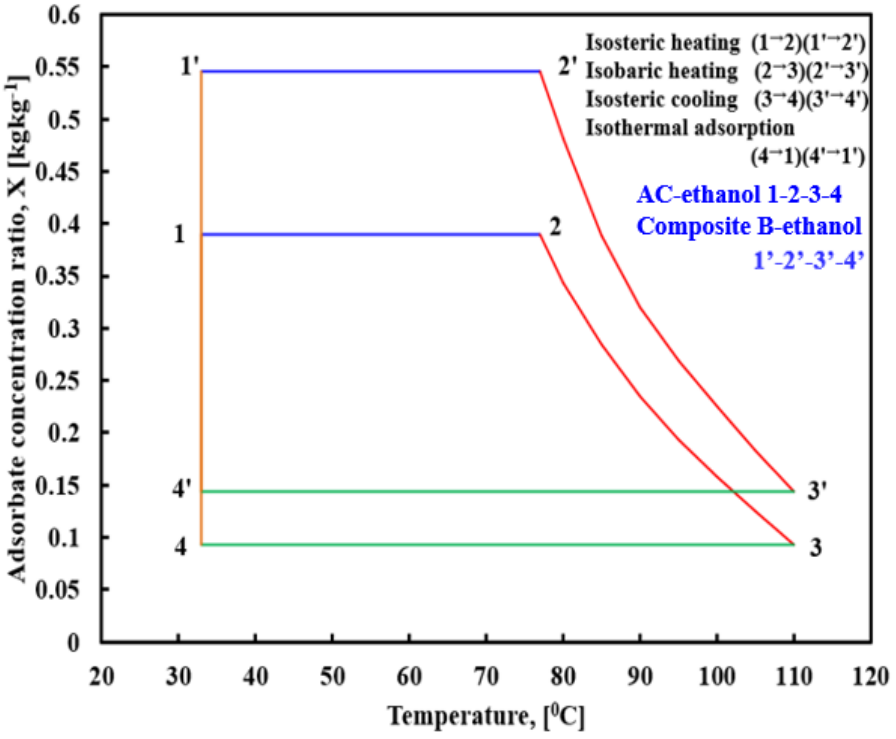

Fig. 8.2: Adsorbate concentration ratio with cycle temperature

the 0.56 to 0.13 kgkg^{-1}. When the system operates with the composite adsorbent-ethanol as working pair, the adsorbate concentration ratio increases by 31.63% in comparison to activated carbon-ethanol. Figure 8.3 depicts the volume fraction of the adsorbate phase as a function of cycle temperature. The fraction of adsorbed volume varies continuously during the adsorption process, as shown in Fig. 8.3. The fraction of adsorbate refrigerant volume changes slightly in both isosteric heating and isosteric cooling. In the isosteric heating or cooling process, the refrigerant volume fraction varies. In the adsorbent bed, the density of adsorbed refrigerant decreases with increasing temperature. Likewise, during the isosteric cooling process, the density of the adsorbate increases, resulting in a decrease in the phase volume fraction. Thus, according to Eq. (5.19), the maximum and minimum volume fractions obtained in the operations are 0.43 and 0.09, respectively.

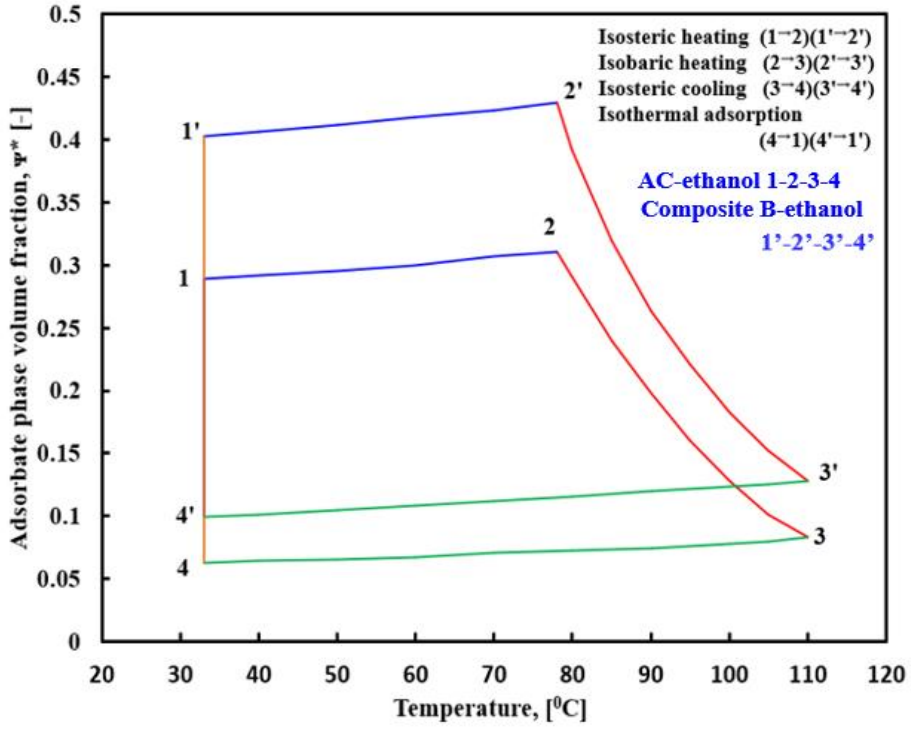

Fig. 8.3: Adsorbate phase volume fraction with cycle temperature

8.2.3Effective mass of refrigerant desorbed or adsorbed during the isobaric heating or isothermal adsorption process

The effect of desorption temperature on effective mass of refrigerant desorbed during isobaric desorption process for composite adsorbent-ethanol as (2′→3’) and (2→3) for the

basic working pair which is depicted in Fig. 8.4. The rate of refrigerant desorbed from the adsorbent bed reaches its peak valve during isobaric heating process. The desorption rate increases continuously as bed temperature rises, and at the end of the process, it reaches a minimum value maintained at minimum concentration and maximum cycle temperature. When compared with AC-ethanol as working pair, the effective desorption rate of composite adsorbent B-ethanol is more, because of its higher thermal conductivity property and as depicted in Fig. 8.4.

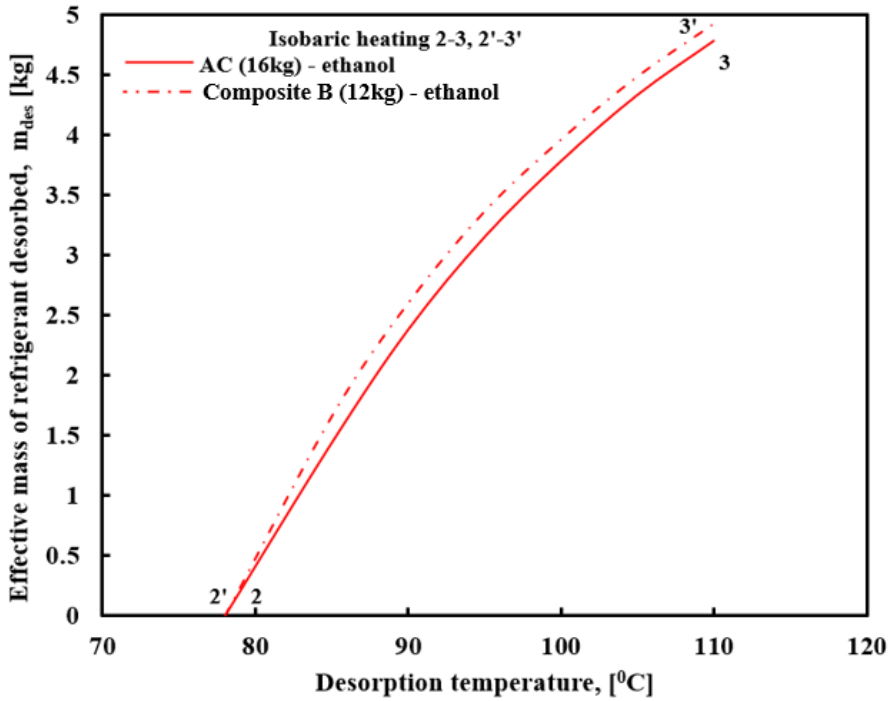

Fig. 8.4: Effect of desorption temperature on total mass of refrigerant desorbed during isobaric desorption process (2'→3')

Figure 8.5 shows the effect of adsorbent bed pressure on the effective mass of refrigerant adsorbed during the isothermal adsorption process (4'→1'). There is an upward trend in the rate of adsorption in isothermal adsorption, which is explained using the Langmuir adsorption isotherm Eq. (5.55) in section 5.9.4. In the low pressure range, the fraction of refrigerant adsorbed by the adsorbent varies linearly with pressure and is known as the first order region of the adsorption process. As depicted in Fig 8.5, the adsorption capacity of the composite adsorbent is found to be better than that of the system operated with parent working pair. This is because, the improved pore volume of the newly developed adsorbent helps to leads the adsorption rate of the adsorbate when compared with parent adsorbent, activated carbon-ethanol.

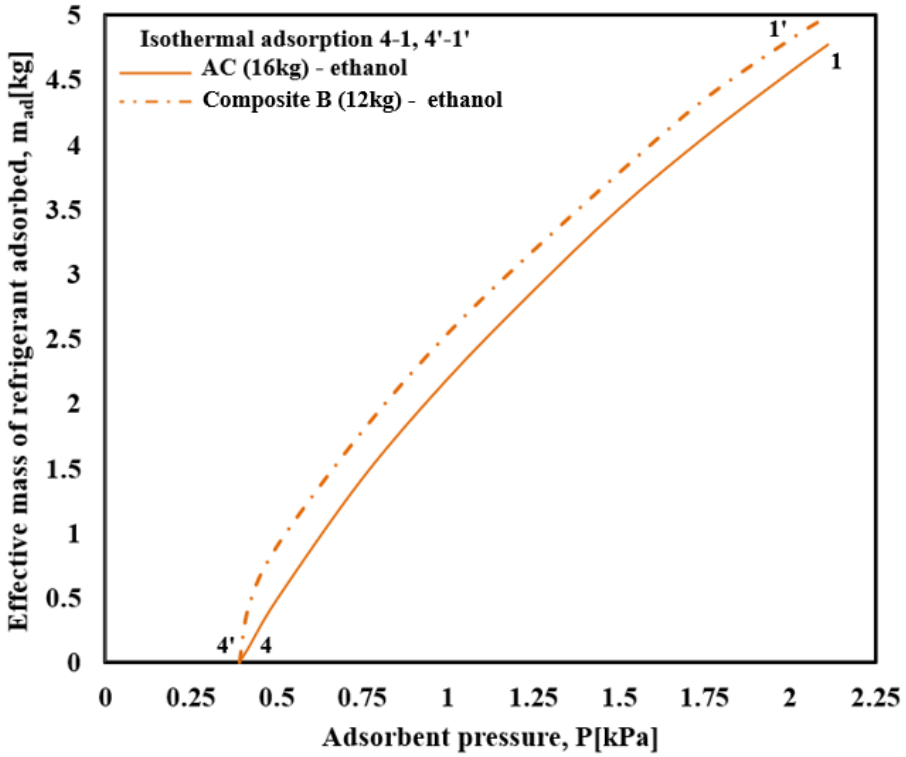

Fig. 8.5: Effect of adsorbent bed pressure on effective mass of refrigerant adsorbed during isothermal adsorption process (4'→1')

8.2.4 Specific energy added or removed during heating or cooling process of adsorbent bed

Figure 8.6 depicts the specific energy added to the adsorbent bed during the heating process of the SAC system. Total specific energy of 420.18 kJkg^{-1} is used to trigger the adsorbent bed. A portion of total heat, i.e., 35.34%, is used to raise the bed temperature from ambient to desorption during the preheating process and the remaining 64.66% has been used for the isobaric desorption process. Figure 8.6 shows the specific energy added to the system during isosteric heating (1'→2'), which is faster than isobaric heating (2'→3'). In the isosteric heating process, the entire input energy has been used for sensible heating of the bed and during the isobaric heating process, a major portion of the total heat input has been used for desorption of the refrigerant from the adsorbent bed. Figure 8.7 shows the specific energy removed from the adsorbent bed during the cooling process, with a total heat energy rejection of 401.74 kJkg^{-1}. Only a portion of this energy, about 36.84%, is lost to the atmosphere during isosteric cooling (3'→4'), and it is used by the bed to maintain its original ambient temperature. The remaining portion of the total energy has been discharged from the adsorbent bed to the atmosphere during isothermal adsorption (4'→ 1').

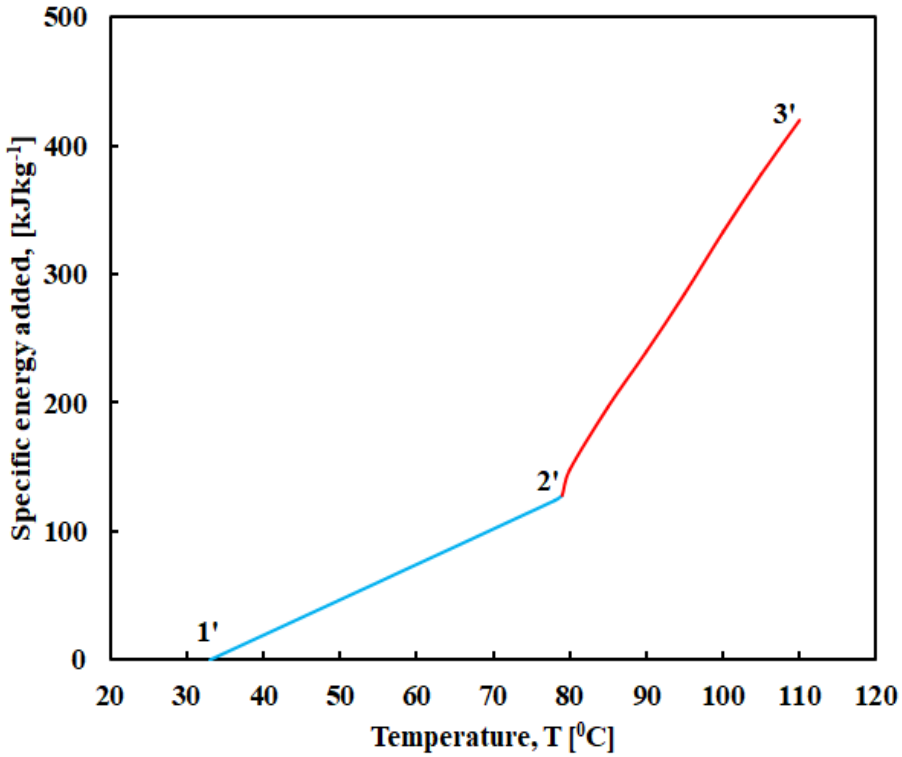

Fig. 8.6: Specific energy added to the adsorbent bed during the heating processes (1′→2′→3’)

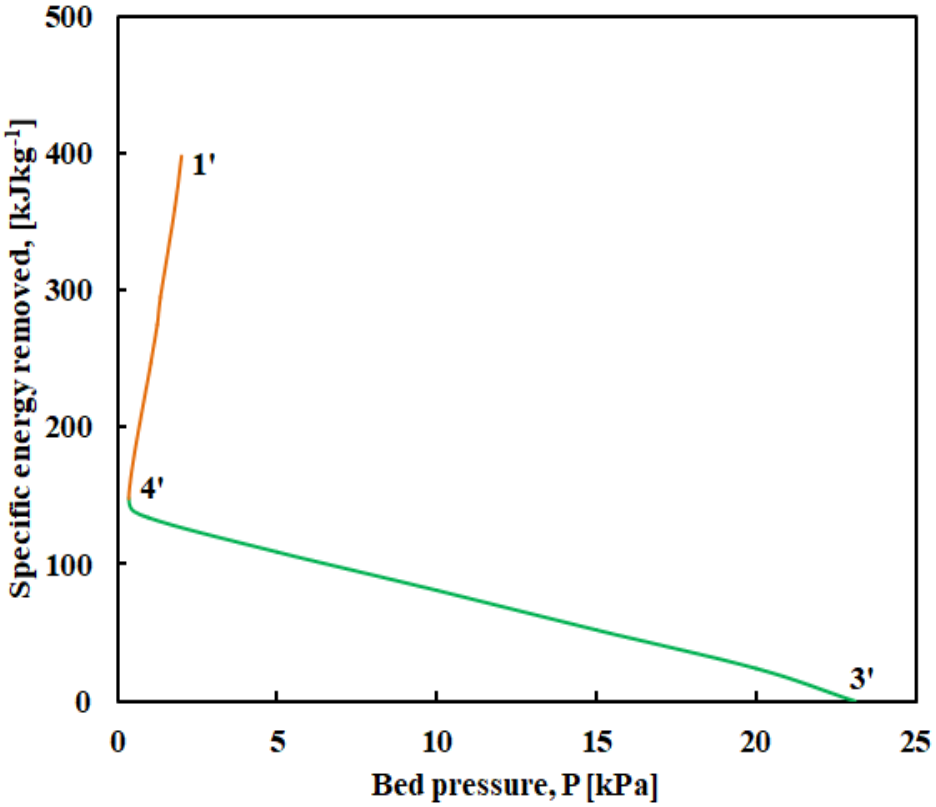

Fig. 8.7: Specific energy removed from the adsorbent bed during cooling processes (3′→4′→1’)

8.2.5 Influence of maximum desorption temperature on the performance of the system

The influence of desorption temperature on the COP and refrigerating effect operating with composite adsorbent-ethanol is presented in Fig. 8.8. The COP of the system increases with increase in desorption temperature, reaches a maximum value, and then gradually decreases when the system is operated at constant atmospheric temperature. The result obtained in this case is also similar to those obtained with AC-ethanol as the working pair. As the desorption temperature rises, the internal desorption of the refrigerant mass increases, resulting in an increase in the refrigerating effect as shown in Fig. 8.8. The COP increases until it reaches an optimal value, after which it decreases. This is because, once the optimal COP is reached, a significant portion of the heat input is used to improve the sensible heat of the adsorbent bed components. As shown in Fig. 8.8, the average COP obtained from the simulation is 0.82 for the maximum desorption temperature of 95^0C and there is 17.07% improvement in the COP is obtained when compared with the system

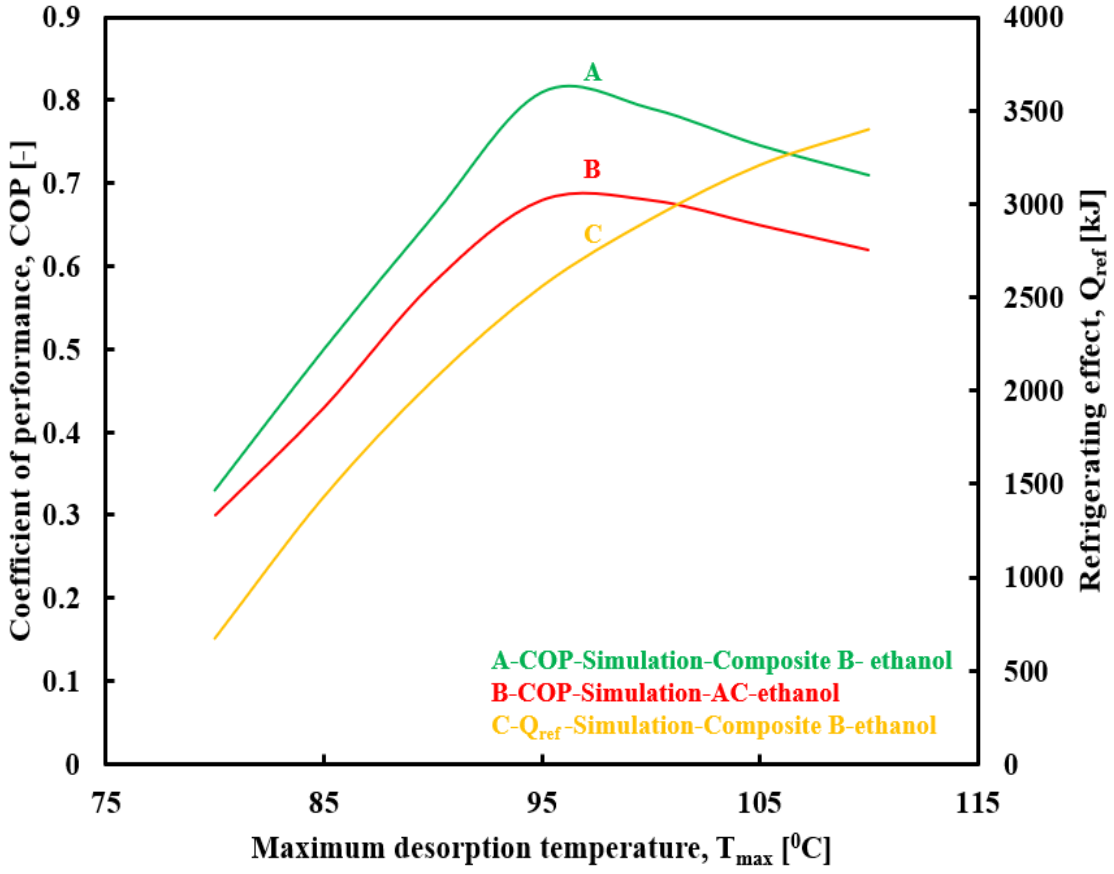

Fig. 8.8: Influence of maximum desorption temperature on COP and refrigerating effect

operated with AC-ethanol as working pair. The influence of maximum desorption temperature on the specific cooling power of the cycle is depicted in Fig. 8.9. One of the deciding factors on the SCP is the maximum desorption cycle temperature. As desorption temperature rises, specific cooling power (SCP) increases, resulting in good desorption and thus improved adsorption refrigeration performance.

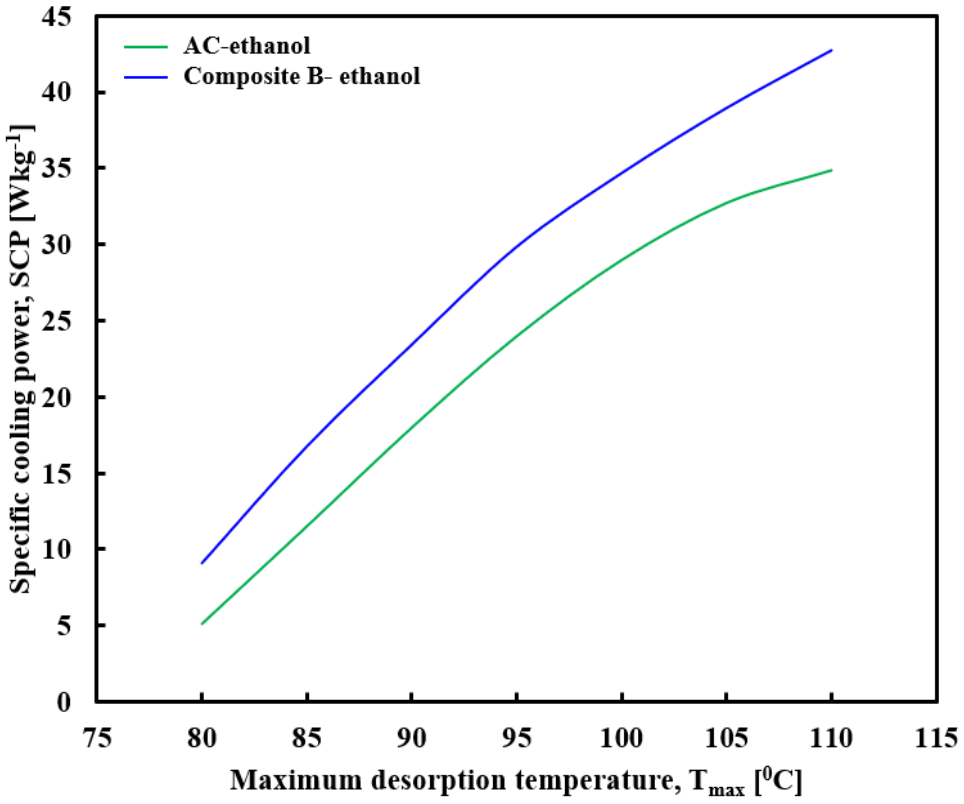

Fig. 8.9: Influence of maximum desorption temperature on the specific cooling power of the cycle

8.3 Experimental Analysis of the SAC System with Composite B-Ethanol as Working Pair with and without Energy Storage Material

The comparative study between the performance of SAC system with composite adsorbent-ethanol and AC-ethanol as the working pair is presented here. Adsorbate vapour from the bed of the adsorbent is generated by the hot water temperature provided by the receiver of the parabolic solar collector. The experimental set up is located at TKM College of Engineering, Kollam, Kerala (India). The detailed study is carried out from January 2021 to December 2021.

8.3.1 Experimental procedure

In order to evaluate the heat transfer performance of the consolidated adsorbate-ethanol, the performance evaluation of the SAC system is conducted using the consolidated pair as the working medium. The procedure for carrying out the experiment has been described in section 6.10 of chapter 6. The adsorption rate of consolidated adsorbent is significantly higher than that of activated carbon-ethanol. Hence, in the present investigation, the adsorbent has been replaced by a composite adsorbent weighing 12 kg instead of 16 kg. In this case, the generating source for desorption is obtained from an energy storage material by circulating cold water through it instead of hot water from the solar collector. Furthermore, when excess energy is generated from the solar collector, it is stored in the storage tank. In order to desorb the refrigerant from the bed, this energy is utilised when the amount of solar energy is insufficient. The experimental procedure is identical to the previous one as described in Chapter 6.

8.3.2 Influence of hot water temperature on the COP of the system

The hot water received from the solar collector is used as the generating or heat source of the SAC system. Consequently, the hot water utilised in the experiment has a maximum temperature range of about 88^0C to 90^0C. Figure 8.10 illustrates the influence of hot water temperature on COP under simulation and experiment conditions using composite adsorbent B- ethanol as the working pair. The experimental profile displays a similar pattern, demonstrating a good agreement with the simulation data. Figure 8.10 indicates that both in simulation and experimental studies, the COP of the system is found to be increases with rise in hot water temperature. The reason for this is because, as the temperature of the hot water rises, more refrigerant mass is being ejected from the adsorbent bed, improving the refrigerating effect than the heat input to the system. This will increase the COP of the SAC system. Moreover, the simulation results mostly reflect the fluctuation in system performance under various operating conditions. However, the experimental results are still somewhat inferior to the simulation results in terms of specific values, mostly for the following causes: (i) in the experimental scenario, there has been a heat loss to the surroundings. (ii) several system processes have not been carried out during the experiment under perfect circumstances. (iii) the specific heat capacity used for the simulation is stable, but it fluctuates significantly with temperature in the experiment. The

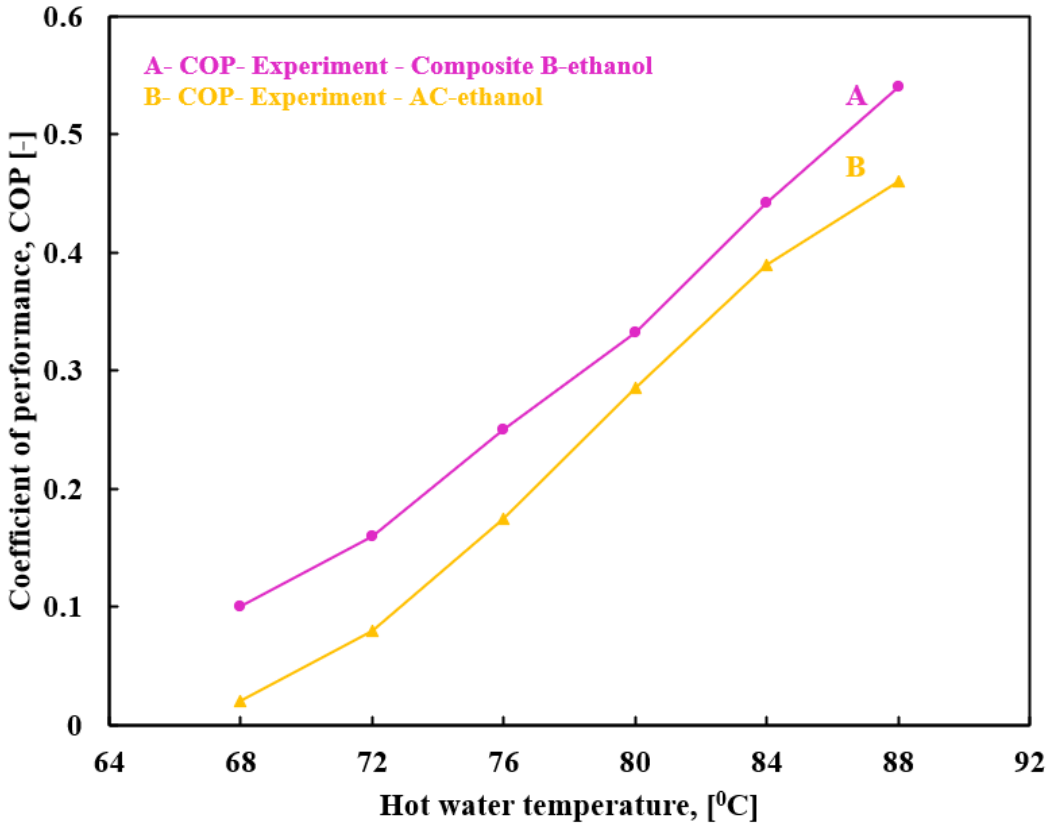

Fig. 8.10: Influence of hot water temperature on COP under experiment and simulation with composite B-ethanol as working pair

maximum COPs obtained from modelling and experimental studies are 0.60, 0.54 and 0.46, respectively. This is due to the fact that the system is simulated in ideal conditions with no heat loss to the environment. In comparison to the parent working pair, the COP of the SAC system operating with consolidated adsorbent shows gives a better result since it is having superior surface properties, high thermal conductivity, and high adsorption/desorption capacity towards the adsorbate.

8.3.3 Influence of hot water temperature on the refrigerating effect and SCP of the system

Figure 8.11 depicts the influence of the hot water temperature or desorption temperature of the adsorption refrigeration system, which is crucial to the refrigerating effect. The refrigerating effect acquired through simulation has significantly rise, while the refrigerating effect obtained through experiment for composite adsorbent-ethanol as working pair is increased from 341 kJ to 1618 kJ. The findings in both situations illustrate the same pattern: as the hot water temperature or the desorption temperature of the SAC

system rises, the refrigerating effect also rises sharply. This is due to the fact that greater driving temperatures result in a rise in the amount of desorbed refrigerant, which in turn causes the increase in refrigerating effect of the system. Due to an increase in heat transfer losses during operation, the discrepancy between the simulation and experiment grows as the hot water temperature rises. The influence of hot water temperature on specific cooling power of the cycle is depicted in Fig. 8.12. The SCP is significantly influenced by the temperature of the hot water. As the hot water temperature rises, the SCP of the system also increases. This is because a higher hot water temperature results in more refrigerant desorption, which enhances the refrigerating effect. Additionally, this action leads to an improvement in the efficiency of refrigerating effect of the system. When compare to the SAC system operated with AC-ethanol, the composite B-ethanol working pair in the SAC system shows better performance.

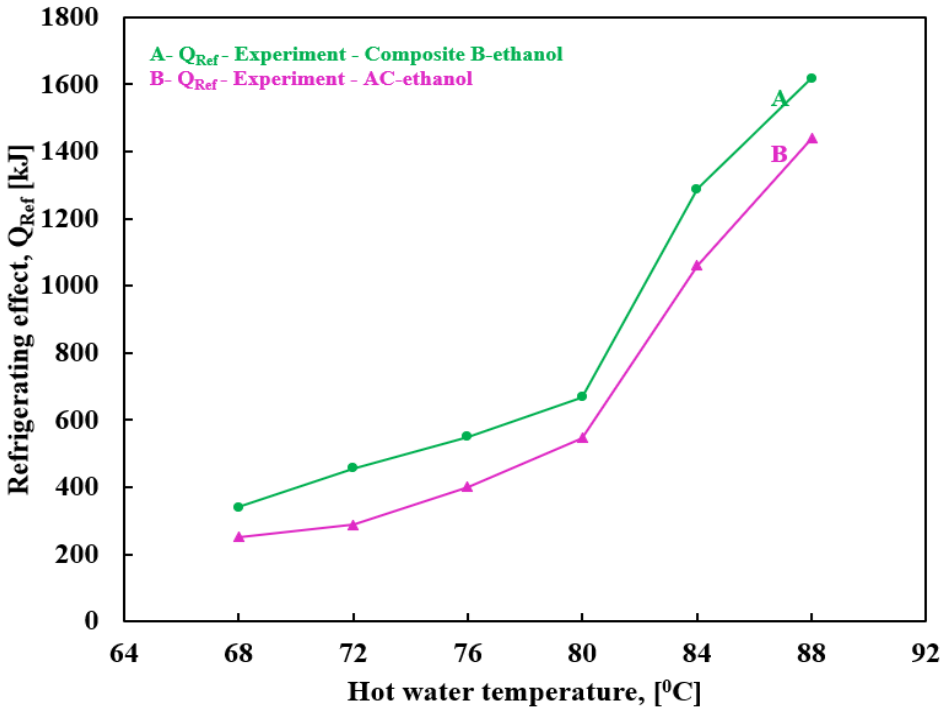

Fig. 8.11: Influence of hot water temperature on refrigerating effect under experiment and simulation with composite B-ethanol as working pair

8.3.4 Influence of evaporator water temperature (inlet) on the performance of the system

The influence of inlet evaporator water temperature on the COP, refrigerating effect and specific cooling power is shown in Figs. 8.13 and 8.14. The increase in temperature

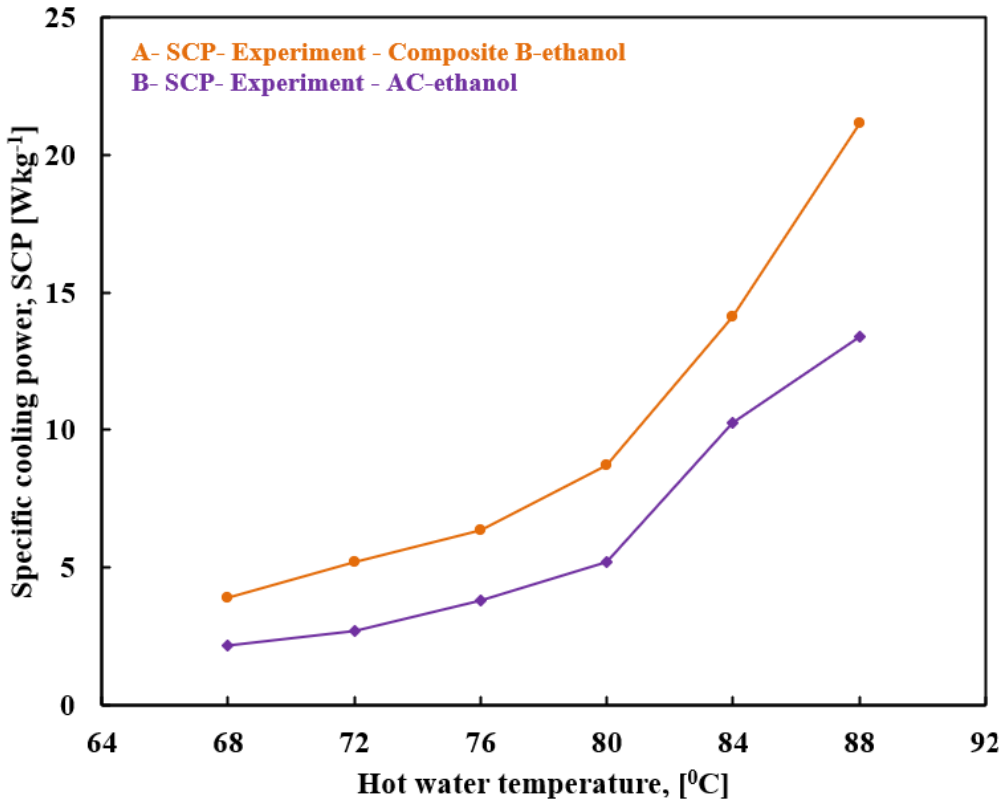

Fig. 8.12: Influence of hot water temperature on specific cooling power under experiment and simulation with composite B-ethanol as working pair

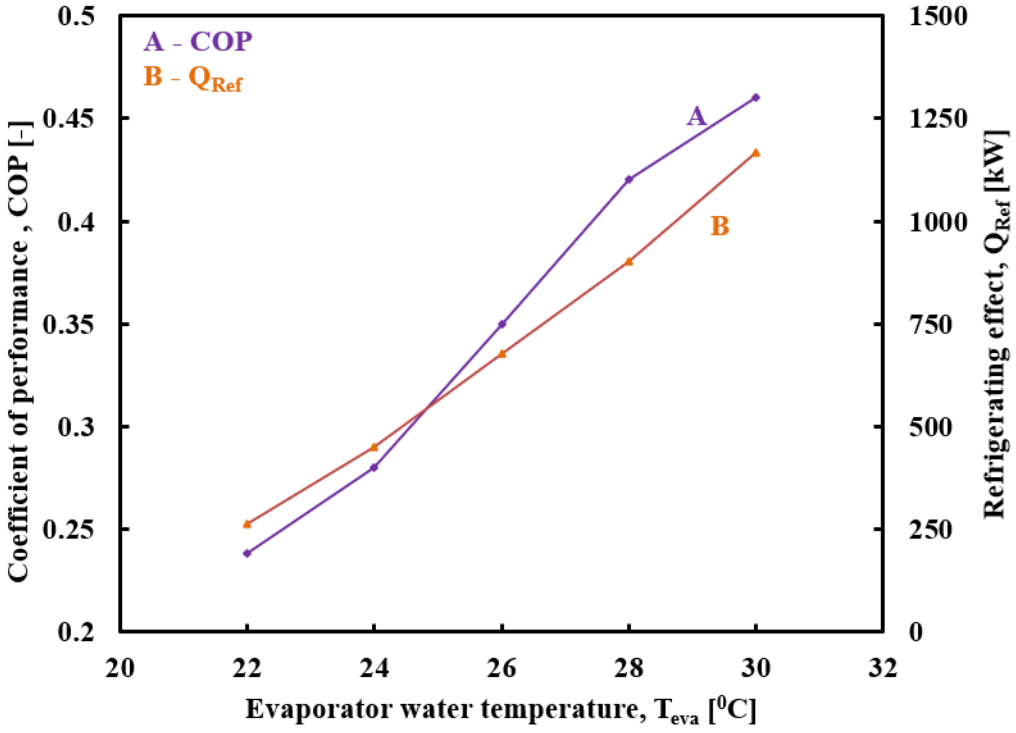

Fig. 8.13: Influence of inlet water temperature of evaporator on COP and refrigerating effect with composite B-ethanol as working pair

of the inlet evaporator water from 22^0C to 30^0C leads to the increases in COP and refrigerating effect. This is due to the inlet evaporator water temperature increase which causes more refrigerant to evaporate from the evaporator causes for increasing the refrigerating effect, which leads to increase in the COP of the system. In addition to that, the lower evaporator temperature more energy input is needed for the evaporation of refrigerant from the evaporator and causes a large cycle time to complete the process of the system, which also leads to a decrease in the performance of the system. The SCP also depends upon the refrigerating effect, so the same effect can be observed as depicted in Fig.8.14.

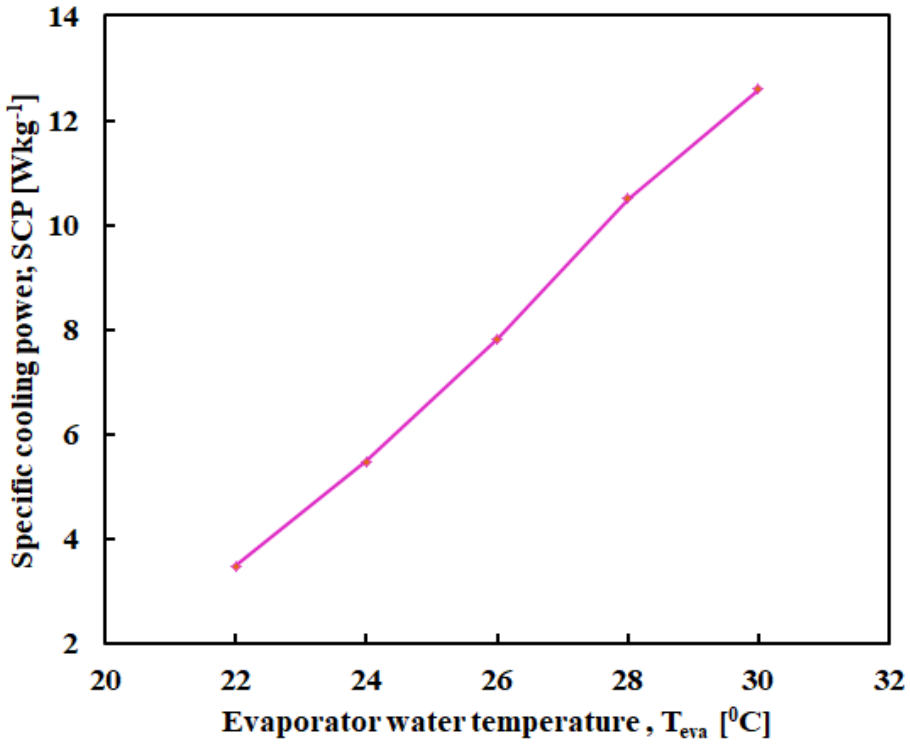

Fig. 8.14: Influence of inlet water temperature of evaporator on specific cooling power with composite B-ethanol as working pair

8.3.5 Influence of mass flow rate of hot water on the performance of the system

The influence of mass flow rate of the hot water on the performance of the system is shown in Figs. 8.15 and 8.16, when the system operated with composite adsorbent-ethanol as working pair. The increase in the inlet hot water mass flow rate, causes more refrigerant to be desorbed from the adsorbent matrix. This aids in improving the COP and refrigerating effect of the system. Furthermore, the same effect for the specific cooling

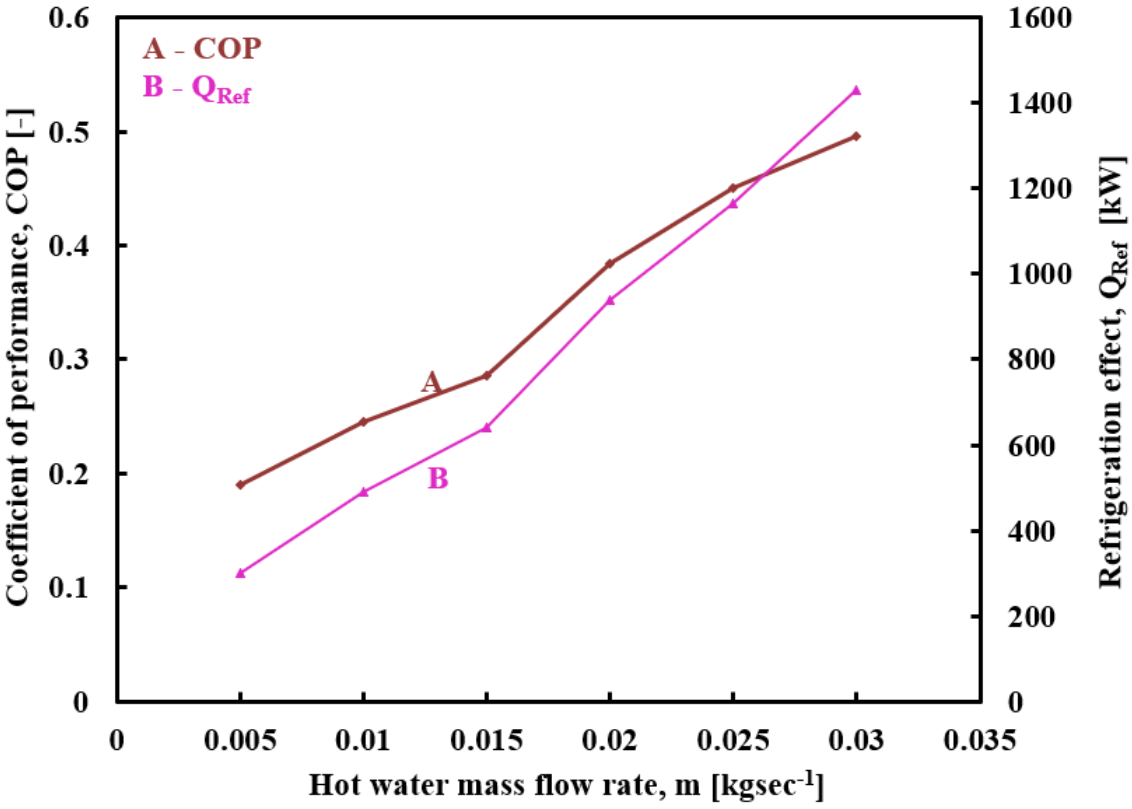

Fig. 8.15: Influence of hot water mass flow rate on COP and refrigerating effect with composite B-ethanol as working pair

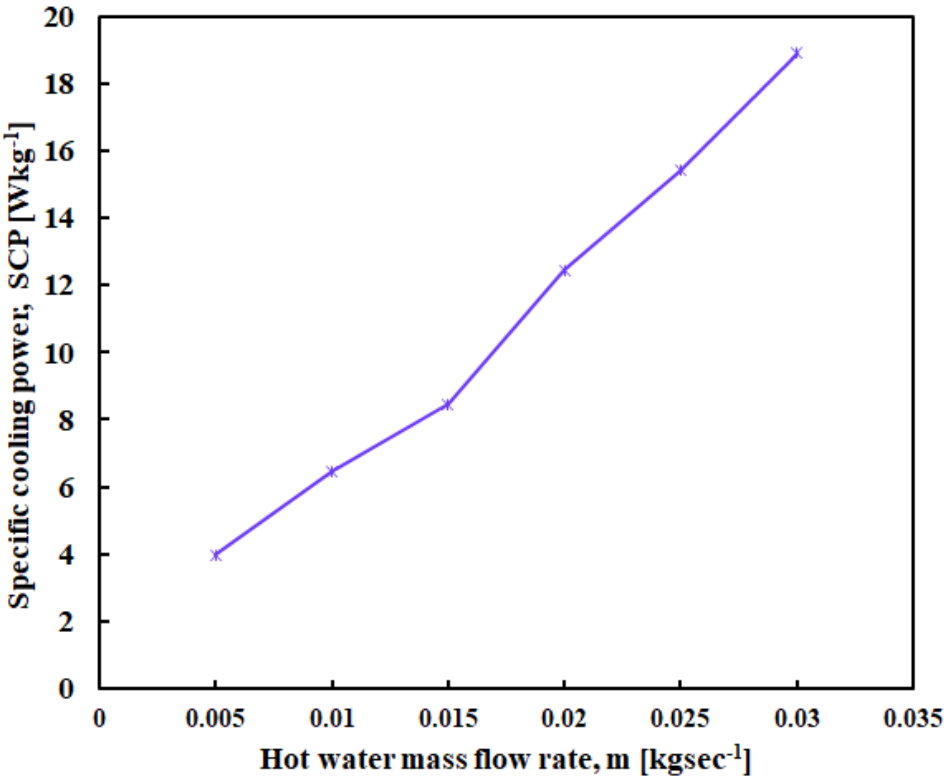

Fig. 8.16: Influence of hot water mass flow rate on SCP with composite B-ethanol as working pair

effect which can be depicted in Fig. 8.16. Due to the low heat input to the system, the lower mass flow rate decreases the rate of the desorption process. However, a suitable hot water mass flow rate of 0.028 kgs^{-1} is preferred for the present investigation. This is because the decrease in the COP of the system is marginal after the specified mass flow rate. This is due to the higher flow rate of inlet hot water results in large energy lost to the atmosphere, and the higher mass flow requires extra pump work which lowers the system performance.

8.3.6 Influence of hot water temperature on the COP of the SAC system operated with energy storage material

The performance of the SAC system with a working pair of composite B-ethanol and energy storage materials of 66% $AlCl_3$ and 34% NaCl has been evaluated and compared to that of systems operating without the energy storage medium. The energy storage material used is intended to store the solar heat energy during the day, especially during the peak of solar irradiation and can be used when heat energy is insufficient to power the SAC system. The heat energy absorbed by the water from the energy storage material kept in the storage tank is used to power the system. It is observed that, water can be obtained at a maximum temperature of 88^0C from the energy storage material. It is observed that, the total operating time for the system with composite working pair and energy storage material is 84 min, which is less than the systems operating without the energy storage material .

The COP of the system mostly depends on the desorbed refrigerant. It is observed that, for the system that directly uses solar energy, the desorption time varies dramatically with the variation in solar irradiation. This results in low refrigerant desorption from the adsorbate from the adsorbent bed during solar downtime, reducing the refrigerating effect. The inconsistent desorption has been overcome by using energy storage material, which provides uniform energy output and has two advantages. The first is that the system can provide refrigerating effect even when the sun is not shining. The second advantage is that it can reduce the entire cycle time by desorbing more refringent from the adsorbent bed, which improves the refrigerating effect as well as the COP of system.

The COP of the SAC system integrated with the energy storage material is found to be greater than that of the SAC system without using the energy storage medium at 88°C hot

water temperature. The COP attained by the modified system during this operating condition is 0.58, while it is 0.54, and 0.46 for the system operating without the energy storage medium. The COP of a SAC system with the composite B-ethanol working pair integrated with an energy storage medium is 6.89% higher than that of a SAC system without an energy storage medium operating with the same working pair. On the other hand, the COP of a SAC system with a composite B-ethanol working pair integrated with an energy storage medium exhibits a significant enhancement of around 20.69% compared to that without the energy storage medium with activated carbon-ethanol working pair. The results show that using a composite working pair in conjunction with energy storage media can significantly improve the performance of SAC systems.

8.4 Comparative Study

This section details a comparative study of the performance of the SAC system like COP, refrigerating effect and SCP, when it is operating with activated carbon-ethanol, composite adsorbent-ethanol with and without energy storage material. It includes the performance results of the SAC system obtained by simulation as well as experiment. Table 8.1 gives the comparison of performance of the SAC system with the percentage improvement of COP. From the table, it is found that the system operated with composite adsorbent-ethanol gives a better performance compare with parent working pair when operating with and without energy storage material. The percentage improvement of the

Table 8.1 Entire results of the SAC system and its percentage improvement

Working pair	**Type of work**	**COP**	**SCP**	**Improvement of COP**
		[-]	**[Wkg^{-1}]**	**[%]**
AC-ethanol	Simulation	0.68	25.45	--
Composite adsorbent-ethanol	Simulation	0.82	29.87	17.07
AC-ethanol	Experiment	0.46	13.72	--
Composite adsorbent-ethanol	Experiment	0.54	21.13	14.81
Composite adsorbent-ethanol with energy storage material	Experiment	0.58	23.47	20.69

COP in the thermodynamic modelling with composite adsorbent-ethanol is 17.07 % when compare with AC-ethanol. Similarly, a 14.81 % and 20.69 % improvement has been observed for the COP of the SAC system when it operated with composite adsorbent-ethanol with and without energy storage material as compared with parent working pair in the case of experimental work.

Summary

The chapter provides thermodynamic modelling and experimental study for the investigation of the performance of the SAC system with composite adsorbent B-ethanol as the working pair. The adsorbate concentration ratio of the system operating with the proposed working pair is 31.63 % higher than the system operating with activated carbon-ethanol. The highest COP achieved from the experimental study is 0.54 at a desorption temperature of 88^0C. The system achieves SCP of 21.13 Wkg^{-1} at the maximum desorption temperature, which is 35.02 % higher than the SCP of the system operating with activated carbon-ethanol as the working pair. This chapter also concludes that the integration of PCM with the proposed system outperformed than the system without using energy storage. The maximum COP and SCP achieved under these working conditions are 0.58 and 23.27 Wkg^{-1}, respectively, indicating an improvement in performance of the system when the system is integrated with the energy storage material. The next chapter provides the conclusion of the present research work.

Chapter 9

Conclusions and Scope for Future Work

This chapter presents, conclusions and scope for future work for the present research work. Also, the chapter includes limitations and recommendations of the work for future study.

Several locations in India and around the world are still cut off from the electrical grid, and there is a need for solar-powered cooling systems for various applications in villages and coastal areas. Adsorption cooling system powered by solar energy is a better choice than conventional refrigeration due to its eco-friendliness, low operating cost, less moving parts, and simplicity. However, an efficient solar powered adsorption cooling system with no power interruption caused by the intermittent nature of solar energy needs to be explored in detail for further improvements. The present study is primarily focused on three areas: literature review for adsorption cooling system, modelling and experimental investigation of adsorption cooling system and developing a suitable composite adsorbent-adsorbate for the adsorption cooling system. The different types of adsorption cooling applications, and its development around the world have been reviewed and analysed in detail. Different types of adsorption cooling system with different working pairs have been summarised, including the research work in India and worldwide are included in the literature review section and it helps to develop the problem formulation in this work. The

thermodynamic modelling of the adsorption cooling system and its development has also been introduced. The section also covered an in-depth review of composite adsorbent and the energy storage materials used now a day for cooling and heating application. The present work introduces composite B-ethanol as a new working pair for the two-bed solar adsorption cooling system. The composite B comprises of MOF MIL-53Al, EGP, PVP and activated carbon as parent material in the appropriate proportion by weight. Thus, the relevant conclusions drawn from the research work has been summarised as follows:

i. The transient modelling of two-bed solar vapour adsorption cooling system is done in SIMULINK. The highest performance of the system, COP is for the optimum range of the desorption or adsorption time i.e., 500 to 900 s and for the switching time of 10 and 30 s

ii. The results reveals that the cooling water and hot water inlet temperatures have a substantial effect on the COP, refrigerating effect and SCP

iii. Thermodynamic modelling in MATLAB R2019b environment showed that the isothermal adsorption process is more effective than the conventional isobaric process

iv. The COP of the SAC system depends on the maximum desorption temperature. The maximum COP of the system obtained is 0.68 at a maximum desorption temperature of 95^0C

v. The major part of heat input to the system is used for the desorption of adsorbate from the adsorbent bed. In the present study, it is estimated as 66.01%. The adsorbate concentration ratio of the system varies from 0.39 $kg.kg^{-1}$ (maximum) to 0.09 $kg.kg^{-1}$ (minimum), corresponding to adsorbed refrigerant phase mass 6.20 kg and 1.56 kg, respectively. Thus, the refrigerant mass consumption efficiency of the system is estimated as 74.85%

vi. The exergy efficiency (η_{Ex}) decreases with decrease in maximum cycle temperature (T_{max}). When the maximum cycle temperature increases from 85^0C to 110^0C, η_{Ex} decreases from 35.8% to 28.3%. The energy-exergy of the entire system has been investigated, and it has been determined that the maximum exergy loss of the adsorbent bed is computed as 0.20 kW

vii. Different parts of the two-bed adsorption cooling system, namely, evaporator, condenser, adsorbent bed, energy storage tank and solar concentrator have been designed and developed for experimental study

viii. The performance of the system increases with increases in the hot water inlet temperature and at 88^0C, simulations and experiments have shown COP values of 0.49 and 0.467, respectively, with an acceptable deviation of 4.69%

ix. New consolidated composite adsorbent A, B C and D are developed for the adsorption cooling system by consisting of activated carbon as the parent material with MOF MIL-53Al, EGP, SG and PVP as the additives

x. In terms of BET surface area, pore volume, and thermal conductivity, the adsorbent (composite B), which consists of 70% activated carbon, 10% expanded graphite powder, 10% metal organic framework MIL-53AL, and 10% binder PVP, outperforms the other considered pairs

xi. The thermal conductivity of the developed composite is 0.29 $Wm^{-1}K^{-1}$, which is 55.17% greater than the base material having a moderate packing density of 421 kgm^{-3}

xii. The Dubinin-Radushkevich (D-R) equation has been used to fit the adsorption uptake measurement, and it has been observed that the maximum adsorption of the composite B has been 0.983, which is approximately 19.63% higher than the adsorption uptake of the activated carbon/ethanol pair

xiii. The volumetric adsorption uptake of the developed composite has been 24.38% greater than the volumetric adsorption uptake of activated carbon-ethanol and in the simulation the average COP attained by the SAC system is 0.82 for the maximum desorption temperature of 95^0C, which is 17.07% more than the system operated with activated carbon-ethanol as working pair

xiv. It is observed that, the COP of the system obtained through the experiment study using consolidated adsorbent - refrigerant combination is 0.54 at a desorption temperature of 88^0C which is 14.81% greater when compared to activated carbon-ethanol as the working pair

xv. The maximum COP of the system obtained with energy storage material is about 0.58, which 20.69% greater than the system operated with activated carbon-ethanol as the working pair

The most significant contribution of the present study is the development of a two-bed adsorption cooling system employing activated carbon-ethanol and consolidated adsorbent-ethanol as working pairs. In addition, transient and thermodynamic simulations of the two-bed continuously functioning adsorption cooling system utilising the

SIMULINK-based MATLAB platform is also proposed. To explore the transient effect, the adsorption cooling system, Simulink model has not yet been studied. This work presented a mathematical simulation of an isothermal adsorption instead of isobaric to improve the overall performance of the SAC system. The proposed model is used to evaluate the energy distribution in various system processes (including the isothermal adsorption process), the effect of cycle temperature on adsorbate phase volume fraction, the maximum desorption temperature on the effective mass of refrigerant desorbed, and the chilled water outlet temperature. Additionally, the COP, refrigerating effect, and SCP are evaluated. Based on simulation results, a two-bed solar-assisted adsorption cooling system has been devised to address the intermittent nature of the single-bed system.

In order to increase the performance of the two-bed solar adsorption cooling system, the current research also designed a new composite adsorbent – adsorbate pair. The newly developed composite adsorbent is composed of 70% activated carbon, 10% expanded graphite powder, 10% metal organic framework MIL-53AL, and 10% binder PVP. $AlCl_3$+NaCl also been presented as the energy storage material for the SAC system. The introduction of a composite adsorbent-adsorbate working pair and energy storage material has the potential to improve the performance of adsorption cooling systems. In remote locations where solar energy is available, the proposed system provides cooling water that can be used to preserve food and medicine.

9.1 Limitations

The benefits of SAC over conventional refrigeration are significant, but it does have a few disadvantages that researchers are trying to resolve. The currently developed SAC system exhibited enhanced performance in terms of performance. However, future research in this area should consider the following recommendations.

i. Gravity flow has been thought to be responsible for current solar water circulation and fluid transfer. Nonetheless, the flow rate of desired cooling water can be maintained with little pump work
ii. The system is run in a vacuum, and keeping the vacuum in the system for a longer duration is a disadvantage of this experimental setup

iii. For getting a better result in the experimental setup, the generating temperature can be more than 95^0C. As a result, combining water with nanoparticles or oils improves the performance of the system by improving heat transfer

iv. The performance of adsorption cooling system will slow down after times because of the degradation in the adsorption properties of adsorbate; hence adsorbate needs to be replaced from adsorbent bed in the period of time

9.2 Recommendations

The following are some additional suggestions for improving the performance of the system:

i. The data logger and electronic controller to the system can improve systematic operation of experimental set up thereby improving the performance of the system

ii. Improved generator temperature and mass flow rate of hot water can reduce overall cycle time for the SAC system

iii. Adding metal additives to the adsorbent helps to improve the performance of the system by improving the thermal conductivity

iv. Using a higher heat source temperature as the generating temperature may also improve the performance the system

9.3 Scope for Further Work

The presented work discussed the potential of developing the two bed adsorption cooling system working with activated carbon-ethanol and composite adsorbate-ethanol for low temperature application. The following ideas for future work can be considered:

i. Synthesising a variety of composites helped to improve performance even more

ii. Designing the SAC system with heat available from biomass, waste heat and exhaust gas are another option

iii. Thermal conductivity of the adsorbent can be improved by adding steel additives, aluminum additives and nano powder
iv. The efficiency of thermal conductivity of the heat exchanger can be improved by using fin type heat exchanges in the system

Combining a solar water heater/desalination system with an adsorption cooling system can meet water heating/pure water production from salt water, and food and medicine preservation requirements. The working environment in terms of hot water temperature, evaporator temperature, and hot water flow rate can be easily managed with available resources for the production of cooling effect via the developed system. Furthermore, proper electronic instruments and software with the system can enable off-site observation and control. Solar adsorption cooling systems have many advantages which make them more competitive compared to the traditional cooling system like vapour compression system. The environmental regulations and safety considerations, the costly and limited conventional energy sources, leads to solar thermal cooling system, particularly solar adsorption cooling system. Since the adsorption cooling technology is more costly than conventional cooling, it has not yet been applied to mass production. Moreover, the COP is very low compared to the conventional system, but research has indicated that there is ample scope for further development to improve the heat output of adsorption cooling systems including new adsorbent materials, new refrigerants, heat exchanger design and bed enhancement techniques.

LIST OF OUTCOMES OF THE RESEARCH

I. RESEARCH PUBLICATION

(i)INTERNATIONAL JOURNAL

1. **A. Asif Sha, V. Baiju,** "Performance investigations of carbon based consolidated composite adsorbents effective for adsorption cooling systems", ***- Applied Thermal Engineering –vol. 217, 119199, 2022. [Elsevier Publication– SCIE indexed, Impact Factor: 6.465]***

2. **V. Baiju, A. Asif Sha,** "Energy and Exergy Based Assessment of a Two Bed Solar Adsorption Cooling System" - ***International Journal of Refrigeration, vol. 141, pp. 90-101, 2022. [Elsevier Publication– SCIE indexed, Impact Factor– 4.14]***

3. **A. Asif Sha, V. Baiju,** "Thermodynamic Analysis and Performance Evaluation of Activated Carbon-Ethanol Two-Bed Solar Adsorption Cooling System" – ***International Journal of Refrigeration, vol.123, pp. 81-90, 2021. [Elsevier Publication– SCIE indexed, Impact Factor – 4.14]***

4. **V. Baiju, A. Asif Sha,** "Simulation and Performance Study of a Two-Bed Activated Carbon-Ethanol Adsorption Cooling System" – ***Proc. IMecE, Part C: J Mechanical Engineering Science, vol. 236, pp. 3804-3817, 2022. [SAGE Publication– SCI indexed, Impact Factor -1.758]***

5 **V. Baiju, A. Asif Sha, "**Theoretical and Experimental Analysis of a Two-bed Vapour Adsorption Cooling System with Composite Adsorbent", ***Applied Energy. Elsevier Publication – (Communicated)***

II. CONFERENCE

(i) INTERNATIONAL CONFERENCE

1. **A. Asif Sha, V. Baiju.** "SIMULATION OF SINGLE BED ADSORPTION REFRIGERATION SYSTEM DRIVEN BY SOLAR ENERGY" - ***publication in Begell Digital Portal through the proceedings of the 25th National and 3rd International ISHMT-ASTFE Heat and Mass Transfer Conference (IHMTC-2019), December 28-31, 2019, IIT Roorkee, Roorkee, Uttarakhand, India.***

2. **A. Asif Sha, V. Baiju.** "ANN FOR SOLAR-ASSISTED ADSORPTION COOLING DEVICE PERFORMANCE PREDICTION WITH PCM AS THERMAL ENERGY STORAGE" ***- publication in Elsevier SSRN series through the proceedings of the International Conference on Business Management, Innovation, and Sustainability (ICBMIS-2020), Amity University Dubai, UAE on 15th - 16th of June 2020.***

3. **A. Asif Sha, V. Baiju,** "THERMODYNAMIC ANALYSIS OF TWO BED ADSORPTION REFRIGERATION SYSTEM DRIVEN BY SOLAR ENERGY" - ***publication in Elsevier SSRN series through the proceedings of the International Conference on Aerospace and Mechanical Engineering ICAME'21, 16-18 December, 2021, Thangal Kunju Musaliar College of Engineering, Kollam, Kerala, India.***

(ii) NATIONAL CONFERENCE

1. **A. Asif Sha, V. Baiju,** "PERFORMANCE ASSESSMENT OF SOLAR ADSORPTION REFRIGERATION SYSTEM WITH PCM AS ENERGY STORAGE " ***– 6th NCRAC Conference – 20-22 Feb. 2020 organized by IIT Chennai and ISHRAE.***

III. BOOK CHAPTER

1. **A. Asif Sha, V. Baiju,** "SOLAR ADSORPTION COOLING SYSTEM", ***has been published in edited book*** *titled* ***Advances in Renewable Energy Engineering (Volume - 3), (Ref. No: AREE:03-06), Akinik Publications, New Delhi – 110085.***

Bibliography

[1] J. M. Calm, “Emissions and environmental impacts from air-conditioning and refrigeration systems”, International Journal of Refrigeration, vol. 25(3), pp. 293-305, 2002.

[2] J. T. McMullan, “Refrigeration and the environment-issues and strategies for the future”, International Journal of Refrigeration, vol. 25(1), pp. 89-99, 2002.

[3] M. Protocol, “Montreal protocol on substances that deplete the ozone layer” Washington, DC: US Government Printing Office, pp. 26- 29, 1987.

[4] M. Grubb, C. Vrolijk, D. Brack, “The Kyoto Protocol: a guide and assessment. Royal” Institute of International Affairs Energy and Environmental Programmed, 1997.

[5] Retrieved 21, "National Action Plan on Climate Change", Climateaction.org, September 2020.

[6] Kai Wang, A. Edward, P. E Vineyard, “A new Approach for solar adsorption refrigeration” ASHRAE Journal, vol. 53(9). pp. 14-24, 2011.

[7] G. E. Hulse, “Freight car refrigeration by an adsorption system employing silica gel”, Refrigeration Engineering, vol.17(2), pp. 41-54, 1929.

[8] B. B. Saha, S. Koyama, J. B. Lee, K. Kuwahara, K. C. A. Alam, Y. Hamamoto, A. Akisawa, T. Kashiwagi, “Performance evaluation of a low-temperature waste heat driven multi-bed adsorption chiller”, International Journal of Multiphase Flow, vol. 28(8), pp. 1249-1263, 2003.

[9] F. Meunier, “Sorption Contribution to Climate Change mitigation”, Proceedings of the International Sorption Heat Pump, Conference, Shanghai. pp.24-27, September 2002.

[10] S. D. Sharma, Kazunobu Sagara, “Latent heat storage materials and systems: A review”, International Journal of Green Energy, vol. 02(1), pp. 1-56, 2005

[11] R. Delgado, A. Choisier, P. H. Grenier , F. IsmailI, Meunier , Pons M. Etude “du cycle Intermittent charbon actif-méthanol en vue de la realisation d’une machine à fabriquer de la glace fonctionnant àl 'énergie solaire”, International Proceedings of the Meeting of Commissions E1–E2, International Institute of Refrigeration; Jerusalem, Israel; French. Publication, pp.185–191, 1982.

[12] R. H. Exell, “Solar cooling activities in the Asian Institute of Technology”, Renewable Energy Technology and The Environment. Oxford: Pergamon Press, pp.700–7007, 1992.

[13] F. Buchte, P. Dind, M. Pons, “An experimental solar-powered adsorptive Refrigerator tested in Burkina-Faso”, International Journal of Refrigeration, vol. 26, pp:79–86, 2003.

[14 N. M. Khattab, “A novel solar-powered adsorption refrigeration module”, Applied Thermal Engineering, vol. 24, pp.2747–2760, 2004.

[15]Himssar Ambaritai, Hideki Kawai, “Experimental study on solar-powered adsorption refrigeration cycle with activated alumina and activated carbon as adsorbent”, Case Studies in Thermal Engineering, vol. 7, pp. 36-46, 2016.

[16] K. Anupam, A.V. Palodkar, G.N. Halder, “Experimental study on activated carbon-nitrogen pair in a prototype pressure swing adsorption refrigeration system”, Heat and Mass Transfer, vol. 52(4), pp. 753-761, 2015.

[17] Yunfeng Wang, Ming Li, Wenping Du, Xu Ji, Lin Xu , “Experimental Investigation of a solar –powered adsorption refrigeration system with the enhancing desorption”, Energy Conversion and Management , vol. 155, pp.253-261, 2018.

[18] D. Y. Li, “Adsorption refrigeration system with multiple generators”, WO0235161 (2002)

[19] W. S. Chang, C. C. Wang, C. C. Shieh, “Design and performance of a solar- powered heating and cooling system using silica gel/water adsorption chiller”, Applied Thermal Engineering, vol. 29, pp. 2100-2105, 2009.

[20] S. Li, J. Y. Wu, “Theoretical research of a silica gel–water adsorption chiller in a micro combined cooling, heating and power (CCHP) system”, Applied Energy, vol. 86, pp. 958–967, 2009.

[21] Sadeghlu Alireza, Mortaza Yari, Mahmoudi, S. M. S. Hossein Beidaghy Dizaji, “Performance evaluation of Zeolite 13X – Calcium Chloride Two-bed adsorption refrigeration system”, International Journal of Thermal Sciences, vol. 80(1), pp. 76-82, 2014.

[22] Ramesh P Sah, Biplab Choudhury, Ranadip K Das, “Study of a two-bed silica gel – water adsorption chiller: performance analysis”, International Journal of Sustainable engineering, vol. 37(1), pp. 30-46,2016.

[23] Mahmoud B. Elsheniti, A. T. Abd El-Hamid, O. A. El- Samni, S. M. Elsherbiny, E. Elsayed, “Experimental evaluation of a solar two-bed lab-scale adsorption cooling system”, Alexandria Engineering Journal, vol. 60, pp. 2747-2757, 2021.

[24]Rifa Ara Rouf, M. A. Hakim Khan, K. M. Ariful Kabir , Bidyut Baran Saha, " Energy management and heat storage for solar adsorption cooling", Joint Journal Of Novel Carbon Resource Sciences and Green Asia Strategy , vol. 03, pp. 01-10, 2016.

[25] S. C. Kaushik, A. Mahesh, "Solar adsorption cooling systems: some materials and collectors aspects", Centre for Energy Studies, IIT Delhi, 2010.

[26] Banker, N.D., Srinivasan, K., Prasad, M., Performance analysis of activated carbon + HFC-134a adsorption coolers, Carbon. 42, 117–127. 2004.

[27] K. Anupam, S. C. Sarkar, A. Chatterjee, G. N. Halder, "Experimental investigation of a single-bed pressure swing adsorption refrigeration system replacement of halogenated refrigerants", Chemical Engineering Journal, vol. 171, pp.541–548, 2011.

[28] E. C. Boelman, B. B Saha, Takao Kashiwagi, "Computer simulation of a silica gel water adsorption refrigeration cycle - the influence of operating conditions on cooling output and COP", ASHRAE Transactions, vol. 101(2), pp. 348-357, 1995.

[29] B. B Saha, I. I. El-Sharkawy , A. Chakraborty, S. Koyama, "Study on an activated carbon fibre-ethanol adsorption chiller: Part II- system description and modelling", International Journal of Refrigeration, vol. 30, pp. 86-95, 2007.

[30] M. Umair, Atsushi Akisawa, Yuki Ueda, "Simulation Study of Continuous Solar Adsorption Refrigeration System Driven by Compound Parabolic Concentrator.", The Open Renewable Energy Journal, vol. 7, pp. 1-12, 2007.

[31] K. F. Fong , C. K. Lee, C. K. Chow, S. Y. Yuen, "Simulation–optimization of solar–thermal refrigeration systems for office use in subtropical Hong Kong", Energy, vol. 36(11), pp. 6298-6307, 2011.

[32] H. Z. Hassan, A. A. Mohamad, R. Bennacer, "Simulation of an adsorption cooling system", Energy, vol. 36(1), pp. 530-537, 2011.

[33] E. E. Anyanwu, "Thermodynamic design procedure for solid adsorption solar refrigeration", Renewable Energy, vol. 30, pp.81-96, 2005.

[34] H. Z Hassan, "Energy analysis and performance evaluation of the adsorption refrigeration system", Research Article – Hindawi Publishing Corporation, ISRN Mechanical Engineering, pp:01- 16, 2013.

[35] Najeh Ghilen, Slimane Gabsi, Riad Benelmir, Mohammed El Ganaoui, "Performance simulation of two-bed adsorption refrigeration chiller with mass recovery", Journal of Fundamentals of Renewable Energy and Applications, vol. 07, pp. 01-07, 2017.

[36] Ali Alahmer, Xiaolin Wang, R. Al-Rbaihat, K. C. A. Alam, B. B. Saha, "Performance evaluation of a solar adsorption chiller under different climatic conditions", Applied Energy, vol. 175, pp. 293-304, 2016.

[37] R. A. Rouf, N. Jahan, K. C. A Alam, A. A. Sulthan, B. B Saha, S. C. Saha, "Improved cooling capacity of a solar heat driven adsorption chiller", Case Studies in Thermal Engineering, vol. 17, pp. 1-7, 2020.

[38] Nasoul Nikbakhti , Xiaolin Wang, "Andrew Chan, Performance analysis of an integrated adsorption and absorption refrigeration system", International Journal of Refrigeration, vol. 117, pp. 269-283, 2020.

[39] Ali Alahmer, Xiaolin Wang, K. C. Amanul Alam, "Dynamic and economic investigation of a solar thermal-driven two-bed adsorption chiller under Perth climatic conditions", Energies, vol. 1005 (13), pp. 1-19, 2020.

[40] L. W. Wang, J. Y. Wu, R. Z. Wang, Y. X. Xu, S. G. Wang, X. R. Li, "Study of the performance of activated carbon–methanol adsorption systems concerning heat and mass transfer", Applied Thermal Engineering, vol. 23, pp. 1605-16017, 2003

[41] J. J. Guilleminot, M. Pons, "Design of an experimental solar powered solid adsorption ice maker", Journal of Solar Energy, vol. 108(4), pp. 332-337, 1986.

[42] K. Sumathy, L. Zhongfu, "Experiments with solar powered adsorption ice maker", Renewable Energy, vol. 16, pp. 704-707, 1999.

[43] Mortaza Yari, S. M. S. Mahmoudi, Hossein Beidaghy Dizaji, "Performance evaluation of Zeolite 13X – Calcium Chloride Two-bed adsorption refrigeration system -Part II", International Journal of Thermal Sciences, vol. 81(1), pp. 86-91, 2015.

[44] A. V. Palodkar, K., Anupam, Z. Roy, B. B. Saha, G. N. Halder, "High pressure adsorption isotherms of nitrogen onto granular activated carbon for a single bed pressure swing adsorption refrigeration system", Heat and Mass Transfer, vol. 53(10), pp. 3155-3166, 2017.

[45] Thomas Robbins, Srinivas Garimella, "A centrally heated, air-coupled adsorption cooling system driven by waste heat", International Journal of Refrigeration, vol. 120, pp. 58-65, 2020.

[46] Vikas H. Chaudhari, Avinash D. Desai, "Experimental study of single bed prototype adsorption refrigeration unit using waste heat energy", Materials Today Proceedings, vol. 49(5), pp. 1799-1803, 2021.

[47] A. Dzigbor, A. Chimphango, “Evaluating the potential of using ethanol/water mixture as a refrigerant in adsorption cooling system by using activated carbon - sodium chloride composite adsorbent”, International Journal of Refrigeration, vol. 97, pp. 132-142, 2019.

[48]G. Cacciola, G. Restuccia, L.Mercadante, “Composites of activated carbon for refrigeration adsorption machines”, Carbon, vol. 33(9), pp. 1205-1210, 1995.

[49] Animesh Pal, Ibrahim I. El-Sharkawy, B. B. Saha, Skander Jribi, Takahiko Miyazaki, Shigeru Koyama, “Experimental investigation of CO_2 adsorption onto a carbon based consolidated composite adsorbent for adsorption cooling application”, Applied Thermal Engineering, vol. 109, pp. 304-311, 2016.

[50] C. Y. Tso, Christopher Y. H. Chao, “Activated carbon, silica-gel and calcium chloride composite adsorbents for energy efficient solar adsorption cooling and dehumidification systems”, International Journal of Refrigeration, vol. 35, pp. 1626-1638, 2012.

[51] K. C. Chan, Christopher Y. H. Chao, C. L. Wu, “Measurement of properties and performance prediction of the new MWCNT-embedded zeolite 13X/$CaCl_2$ composite adsorbents”, International Journal of Heat and Mass Transfer, vol. 89, pp. 308-319, 2015.

[52] L. W. Wang, Z. Tamainot-Telto, R. Thorpe, R. E. Critoph, S. J Metcalf, R. Z. Wang, “Study on thermal conductivity, permeability, and adsorption performance of consolidated composite activated carbon adsorbent for refrigeration”, Renewable Energy, vo. 36, pp. 2062-2066, 2011.

[53] B. B Saha, Ibrahim I. El-Sharkawy, I. Miyazaki, S. Koyama, S. K. Henninger, A. Herbst, “Ethanol adsorption onto metal organic framework: theory and experiments”, Energy, vol. 7, pp. 363–70, 2015.

[54] A. A. Askalany, S. K. Henninger, M.Ghazy, B. B. Saha, “Effect of improving thermal conductivity of the adsorbent on performance of adsorption cooling system”, Applied Thermal Engineering, vol. 110, pp. 695-702, 2017.

[55]Ibrahim I. El. Sharkawy, A. Pal, T. Miyazaki, B. B. Saha, S. Koyama, “ Study on consolidated composite adsorbents for cooling application”, Applied Thermal Engineering, vo. 98, pp. 1214-1220, 2016.

[56] Ibrahim I. EL-Sharkawy, K. Uddin, T. Miyazaki, B. B Saha, S. Kyamma, J. Miyawaki, Seong-Ho Yoon, “Adsorption of ethanol onto parent and surface treated activated

carbon powders", International Journal of Heat Mass Transfer, vol. 73, pp. 445–455, 2014.

[57] Eduard Oro, Antoni Gil, Laia Miro, Gerard Peiro, Servando Alvarez, Lusia F Cabeza, "Thermal energy storage implementation using phase change mateials for solar cooling and refrigeration applications", Energy Procedia, vol. 30, pp. 947-956, 2012.

[58] Nattaporn Chaiyat and Tanongkiat Kiatsiriroat, "Energy reduction of building air-conditioner with phase change material in Thailand", Case Studies in Thermal Engineering, vol. 04, pp. 175-186, 2014.

[59] Amin Haighighi Poshtiri, Azadeh Jafari, "24-hour cooling of a building by a PCM-integrated adsorption system", International Journal of Refrigeration, vol. 79, pp. 57-75, 2017.

[60] L. W, Wang, R. Z. Wang, J. Y. Wu, K. Wang, "Compound adsorbent for adsorption ice maker on fishing Boat", International Journal of Refrigeration, vol. 01, pp. 401-408, 2004.

[61] M. A. Alghoul, M. Y. Sulaiman, B. Z. Azmi, M. A. Wahab, "Advances on multi-purpose solar adsorption systems for domestic refrigeration and water heating", Applied Thermal Engineering, vol. 27, pp. 05-06, 2007.

[62] D. M. Ruthven, "Principles of adsorption and adsorption processes", York: John Wiley & Sons, 1984.

[63] C. S. H. Wilkins, "New uses of activated carbon", CODEN:CMERA, pp. 15-23, 1983.

[64] Ralph T. Yang, "Gas separation by adsorption Processes", Series of Chemical Engineering, University of Michigan, 1997.

[65] L. Z. Zhang, "Design and testing of an automobile waste heat adsorption cooling system", Applied Thermal Engineering, vol. 20(1), pp. 103-114, 2000.

[66] N. C. Srivastava, I. W. Eames, "A review of adsorbents and adsorbates in solid-vapour adsorption heat pump systems", Applied Thermal Engineering, vol. 18, pp. 707-714, 1998.

[67] Faizan Shabir, Muhammed Sultan, Talahiko Miyazaki, "Recent updates on the adsorption capacities of adsorbent-adsorbate pairs for heat transformation applications", Renewable and Sustainable Energy Reviews, vol. 119, pp. 01-37, 2020.

[68] V. Valkov, R. Cote, G. Perron, G. B. B La, "Experimentation of a new thermochemical material based on carbon fiber", In Proceedings of the International Sorption Heat Pump Conference, Munich, Germany, vol. 239245, 1999.

[69] R. Z. Wang, R. G. Oliveria, “Adsorption refrigeration-An efficient way to make good use of waste heat and solar energy”, Progress in Energy and Combustion Science, vol. 32, pp. 424-458, 2006.

[70] I. F. Odesola, J. Adebayo, “Solar adsorption technologies for ice-making and recent developments in solar technologies: A review”, International Journal of Advanced Engineering Technology, vol. 1, pp. 284–303, 2010.

[71] A. Sur, R. K. Das, “Review on solar adsorption refrigeration cycle”, International Journal of Mechanical Engineering Technology, vol. 1, pp. 190–226, 2010.

[72] Hearther E. Kennady, “ASHRE hand book fundamentals”,180 Technology Parkway NW , Peachtree Corners, GA 20092, 2021.

[73] Christopher W. Ashling, Duncan N. Johnstone, Remo N. Widmer, Jingwei Hou, Sean M. Collins, Adam F. Sapnik, Alice M. Bumstead, Paul A. Midgley, Philip A. Chater, David A. Keen, Thomas D. Bennett, “Synthesis and Properties of a Compositional Series of MIL-53(Al) Metal−Organic Framework Crystal-Glass Composites”, Journal of The American Chemical Society, vol. 141, pp. 15641−15648, 2019.

[74] Peifu Cheng, Yung Hang Hu, “Dubinin-Astakhov model for acetylene adsorption on metal-organic frameworks”, Applied Surface Science, vo. 377, pp. 349-354, 2016.

[75]Z. Li, W. G. Sun, G. Wang, Z. G. Wu, “Experimental and numerical study on the effective thermal conductivity of paraffin/expanded graphite composite”, Solar Energy Materials and Solar Cells, vol. 128, pp. 447-455, 2014.

[76] L. Sun B. Liao, D. Sheberla, D. Kraemer, J. Zhou, E. A. Stach, M. A Dinca, “A Microporous and Naturally Nanostructured Thermoelectric Metal-Organic Framework with Ultralow Thermal Conductivity”, Joule, vol. 1(1), 168–177, 2017.

[77] Y. Jin, C. P. Huynh , S. C. Hawkins, S. Su , “ Expanded graphite/phenolic resin-based carbon composite adsorbents for post-combustion CO_2 capture”, RSC Advances, vol. 5(77), pp. 62604–62610, 2015.

[78] Chi Yan Tso, Sau Chung Fu, Christopher Y. H. Chao, “Modeling a solar-powered double bed novel composite adsorbent (Silica activated carbon/$CaCl_2$)-water adsorption chiller”, Building Simulation, vol. 7, pp. 185-196, 2014.

[79] A. Mahesh, S. C. Kaushik, “Solar adsorption cooling system: An overview”, Journal of Renewable and Sustainable Energy, vol. 04, 22701-22720, 2012.

[80] M. M Younes, I. I. El-Sharkawy, A. E. Kabeel, K. Uddin, B. B Saha, Animesh Pal, Sourac Mitra, Kyaw Thu, B. B Saha, “Synthesis and characterization of silica gel

composite with polymer binders for adsorption cooling applications", International Journal of Refrigeration, vol.98, pp. 161-170, 2019.

[81] A. Joseph, M. Kabbara, D. Groulx, P. Allred, M. A. White, "Characterization and real time testing of phase-change materials for solar thermal energy storage", International Journal of Energy Resources, vol. 40, pp. 61–70, 2016.

[82] V. V. Tyagi, K. Chopra, S. K. Tyagi, Richa Kothari, "A comprehensive review on phase change materials for heat storage applications: Development, characterization, thermal and chemical stability", Solar Energy Materials and Solar Cells, vol. 234, 111392, 2022.

[83] M. M. Dubinin, V. A. Astakhov, "Description of adsorption of vapors on zeolites over wide ranges of temperature and pressure", Advances in Chemistry Series, vol. 44, pp. 69-85, 1971.

[84] M. M. Dubinin, V. A. Astakhov, "Development of the concepts of volume filling of micropores in the adsorption of gases and vapors by micropores adsorbents" Russ. Chem. Bull, vol. 20, pp. 3-7, 1971.

[85] M. M. Dubinin, "Physical adsorption of gases and vapours in micropores", Progress in Surfaces and Membrane Science, vol. 9, pp. 1-70, 1975.

[86] S. G. Johnson, "NIST Reference Fluid Thermodynamic and Transport Properties Database", Version 10, 2013.

[87] Ibrahim I. El-Sharkawy, B. B Saha, Shigeru Koyama, Kim Choon Ng, "A study on the kinetics of ethanol-activated carbon fiber: Theory and experiments", International Journal of Heat and Mass Transfer, vol. 49, pp. 3104–3110, 2006.

[88] E. Glueckauf, "Formula for diffusion into spheres and their application to chromatography", Transactions of Faraday Society, vol. 51, pp.1540-1551, 1955.

[89] B. B. Saha, I. I. El-Sharkawy, A. Chakraborty, S. Koyama, "Study on an activated carbon fibre-ethanol adsorption chiller: Part II - system description and modelling", International Journal of Refrigeration, vol. 30(1), pp. 96-102, 2007.

[90] F. Shabir, Muhamed Sultan, T. Miyazaki, B. B. Saha, Ahmed Askalany, Imral Ali, Yuguang Zhou, Riaz Ahmed, Redmond R. Shamshiri, "Recent updates on the adsorption capacities of adsorbent-adsorbate pairs for heat transformation applications", Renewable and Sustainable Energy Reviews, vol. 119, pp. 01-37 2020.

[91] Marlinda, Aep Saepul Uyun Takahiko Miyazaki, Yuki Ueda, Atushi Akisawa, "Performance analysis of a double-effect adsorption refrigeration cycle with a silica gel/water working pair", Energies, vol. 3, pp. 1704-1720, 2020.

[92] Faizan Shabir, Muhammed Sultan, Talahiko Miyazaki, “Recent updates on the adsorption capacities of adsorbent-adsorbate pairs for heat transformation applications”, Renewable and Sustainable Energy Reviews, vol. 119, pp. 01-37, 2020.

[93] C. Y. Tso, Christopher Y. H. Chao, S. C. Fu, “Performance analysis of a waste heat driven activated carbon based composite adsorbent-water adsorption chiller using simulation model”, International Journal of Heat and Mass Transfer, vol. 55, pp. 7596-7610, 2012.

[94] K. C. A Alam, B. B. Saha, A. Akisawa, Kashiwagi, “Mass recovery adsorption refrigeration cycle-improving cooling capacity”, International Journal of Refrigeration, vol. 27, pp. 225-234, 2004.

[95] E. K. Andrey, “Modeling of an Isothermal Pressure Swing Adsorption Process”, Technical report, AEK-NZ-01, Stockholm University, 2015.

[96] Ramesh P.Sah, Biplab Choudhury, Ranadip K. Das, “ Study of a two-bed silica gel-water adsorption chiller: performance analysis”, International Journal of Sustainable Energy, vol. 27, pp.30-46, 2018.

[97]Ghilen Najeh, Riad Benelmir, Gabsi Salimane, Mohammed El Gananui, “Performance simulation of two-bed adsorption refrigeration chiller with mass recovery”, Journal of Fundamental Renewable Energy Applications, vol. 7(3), pp. 1–7, 2017.

[98] M. H. Mahfuz, A. Kamyar, O. Afshar, M. Sarraf, M. R. Anisur, M. A. Kibria, R. Saidur, I. H. S. C. Metselaar, “Exergetic analysis of a solar thermal power system with PCM storage”, Energy Conversion and Management, vol. 78, pp. 486–492, 2014.

[99] Noueddine Cherrad, Adel Benchabane, Lakhdar Sedira, Amar Rouag, “Transient numerical model for predicting operating temperature of solar adsorption refrigeration cycle”, Applied Thermal Engineering, vo. 130, pp. 1163–1174, 2017.

[100] J. A. Duffie, W. A. Beckman, “Solar Engineering of Thermal Processes”, Wiley, New York, 1980.

[101] M. Yaghoubi, K. K. Azizian, Kenery, “Simulation of Shiraz power plant for optimal assessment”, Renewable Energy, vol. 28, pp. 1985–1998, 2003.

[102] Baiju V., Muraleedharan C., “Exergy and Energy analysis of solar hybrid adsorption refrigeration system”, International Journal of Sustainable Engineering, vol. 6(4), pp.289-300, 2013.

[103]Sardeshpande, R. Vishal, Ajay G. Chandak, Indhu R. Pillai, “Procedure for thermal performance evaluation of steam generating point-focus solar concentrators”, Solar Energy, vol. 85, pp. 1390-1398, 2011.

[104] Naef A. A. Qasem, Maged A. I. El-Shaarawi, “Thermal analysis and modelling study of an activated carbon solar adsorption icemaker: Dhahran case study”, Energy Conversion Management, vol.100, pp. 310–323, 2015.

[105]C. P. Kothanadaraman, “ HMT Data book”, New Age International Publishers, 9th Edition, 2018.

[106] Eltahir Ahmed Mohamed, “Design and testing of a solar parabolic concentrating collector”, International Conference on the Energies and Power Quality, Bilbo, Spain, vol. 01(11), pp.72-76, 2013.

[107] E. Y. Mertsoy, Emine Sert, Suheyda Aralay, Ferhan Sami Atalay, “Fabrication of chromium based metal organic framework (MIL-101)/ activated carbon composites for acetylation of glycerol”, Journal of the Taiwan Institute of Chemical Engineers, vol. 120, pp. 93-105, 2021.

[108] Animesh Pala, Kutub Uddin, Kyaw Thua, B. B. Saha, “Activated carbon and graphene nanoplatelets based novel composite for performance enhancement of adsorption cooling cycle”, Energy Conversion and Management, vol. 180, pp. 134-148, 2019.

[109] Z. Yu, J. Deschamps, Loming Hamon, Prasanth Karikkethu Prabhakaran, Pascaline Pre, Hydrogen adsorption and kinetics in MIL-101(Cr) and hybrid activated carbon-MIL-101(Cr) materials”, International Journal of Hydrogen Energy, vol. 42, pp. 8021-8031, 2017.

[110] Prasanth Karikkethu Prabhakaran, Johnny Deschamps, “Doping activated carbon incorporated composite MIL-101 using lithium: impact on hydrogen uptake”, Journal of Materials Chemistry A, vol. 3(13), pp. 7014-7021, 2015.

[111]C. Y. Tso, Christopher Y. H. Chao, “Activated carbon, silica-gel and calcium chloride composite adsorbents for energy efficient solar adsorption cooling and dehumidification systems”, International Journal of Refrigeration, 35 (2012) 1626-1638.

[112] E. Y. Mertsoy, Emine Sert, Suheyda Aralay, Ferhan Sami Atalay, “Fabrication of chromium based metal organic framework (MIL-101)/ activated carbon composites for acetylation of glycerol”, Journal of the Taiwan Institute of Chemical Engineers, 120 (2021) 93-105.

[113]Vinod Kumar Singh, E. AnilKumar, “Experimental investigation and thermodynamic analysis of CO_2 adsorption on activated carbons for cooling system”, Journal of CO_2 utilization, 17 (2017) 220-304.

[114]Decagon Devices, KD2 Pro Thermal Properties Analyzer Operator's Manual. Decagon Devices, Inc. 2016.

[115]Zhequan Jin, Bo Tian, Liwei Wang, Ruzhu Wang, "Comparison on thermal conductivity and permeability of granular and consolidated activated carbon for refrigeration". Chinese Journal of Chemical Engineering, 21(6) (2013) 676-682.

[116]Niyaz Mohammad Mahmoodi, Mohsen Taghizadeh, Ali Taghizadeh, "Activated carbon/metal-organic framework composite as a bio-based novel green adsorbent: Preparation and mathematical pollutant removal modelling", Journal of Molecular Liquids, 277 (2019), 310-322.

Appendices

Appendix I

Activated Carbon and Ethanol Data Sheet

1. AC Sample supplier: Indo German Carbon Limited, Cochin , Kerala		
Properties of AC:		
1	Carbon content	84.77%
2	Moisture content	1.72-2.53%
3	Ash Content	<1.44%
4	Surface area	900 – 1150 m^2g^{-1}
5	pH	3.45 – 3.6
6	Pore size	15.64 A^0
7	Density	0.434 gcm^{-3}
8	Decomposition temperature	5300^0C
9	Mesh size	12
Adsorption properties of activated carbon:		
1	Ni Metal Ions	27-28%
2	Copper ions	14-16%
3	Zinc Ions	15-17%
4	Pb Ions	40-24%
5	Chromium	97-98% with 5000 µgm
6	Sulphur dioxide	84-87%with 30 ppm
7	Hydrogen Sulphide	87 -88 with 30 ppm
8	Acid vapour	50-52%
9	Organic vapours	89 to 96%for Benzene, CTC, Hexane,
2. **Ethanol Supplier:** Siddha Chemicals, Pune, Maharashtra, India (Batch No-E45A/1274/456/2020, 99.5% Ethanol)		
1	Molecular weight	46.07 $gmol^{-1}$
2	Density	0.79 gcm^{-3} at 20^0C
3	Boiling point	78.37^0C
4	Melting point	-114^0C
5	Thermal conductivity	0.17 $Wm^{-1}K^{-1}$

Appendix II

Experiment results for Calculation

The amount of heat absorbed by adsorbent bed,

Q_{in} = mass flow rate of hot water x C_p *x* (T_{in}-T_{out}) x time (AII. 1)

= m_f x C_p x (T_{in}-T_{out}) x t

Date of experiment	Time (t)	Mass flow rate (m_f)	Hot water inlet temperature (T_{in})	Hot water outlet temperature (T_{out})	Heat input, Q_{in}
	(min)	(kgs^{-1})	(^0C)	(^0C)	(kJ)
12/04/2021 (12.45 p.m. to 02.30 p.m.)	15	0.028	87.5	82.5	526.68
	15	0.028	88	84	421.34
	15	0.028	88	84.5	368.68
	15	0.028	88.5	85	368.68
	15	0.028	88	83.5	474.01
	15	0.028	88.5	85	368.68
	15	0.028	88	84.5	368.68
Total heat input during the whole cycle (Q_{in}) =					2896.74kJ

The minimum temperature attained during this operation is 10^0C from 31^0C

Refrigerating effect (Q_{Ref}) = Mass of water in the evaporator x C_p x ($T_{eva,\ final} - T_{eva,\ initial}$) (AII. 2)

= M_{eva} *x* C_p *x* ($T_{eva,\ final} - T_{eva,\ initial}$)

Q_{Ref} = 1580.04kJ

COP $= \frac{Q_{ref}}{Q_{in}}$ (AII. 3)

$$= 0.54$$

$$\text{Cooling power } (Q_{eva}) = \frac{Q_{Ref}}{Operating\ time\ in\ sec} \quad \text{(AII. 4)}$$

$$= 250.81 \text{ W}$$

$$\text{Specific cooling power (SCP)} = \frac{Q_{eva}}{\mathrm{m_{ac}}} \quad \text{(AII. 5)}$$

$$= 20.83 \text{ Wkg}^{-1}$$

Appendix III

Uncertainty Analysis of the ethanol uptake Measurement

The total uncertainty arising due to independent variable is given by Eq. (AIII. 1)

$$W_R = \sqrt{\left(\frac{\partial R}{\partial X_1} W_1\right)^2 + \left(\frac{\partial R}{\partial X_2} W_2\right)^2 + \cdots + \left(\frac{\partial R}{\partial X_n} W_n\right)^2} \quad \text{(AIII. 1)}$$

The result R is a given function in terms of independent variables. Let WR be the uncertainty in the result w_1, w_2, w_3, ……., w_n be the uncertainties in the independent variables.

The uncertainty in measuring ethanol adsorption accumulation ($kgkg^{-1}$) by the newly selected composite adsorbent using the experimental test rig is given by Eq. AIII. 2 and Eqs (AIII. 3) to (AIII. 5) represents the corresponding derivatives

$$\delta X = \sqrt{\left(\frac{\partial X}{\partial Di_{eva}} \delta dDi_{eva}\right)^2 + \left(\frac{\partial X}{\partial M_{com}} \delta dM_{com}\right)^2 + \left(\frac{\partial X}{\partial Hi_{eva}} \delta dHi_{eva}\right)^2} \quad \text{(AIII. 2)}$$

$$X = \rho_{liq}\ Hi_{eva}\ \frac{\pi}{4}\left(\frac{Di_{eva}^2}{M_{com}}\right) \quad \text{(AIII. 3)}$$

The following are the detailed specifications for calculating uncertainty analysis of the ethanol adsorption uptake, where Di_{eva} = 6.5 mm, δdDi_{eva} = 0.1 mm, M_{com} = 1.9 gms, δdM_{com} = 0.01 gms, δdHi_{eva} 0.01 mm and Hi_{eva} = 0.078 m

= 0.98

$$\left(\frac{\partial X}{\partial Di_{eva}} \delta dDi_{eva}\right)^2 = \left[\rho_{liq}\, Hi_{eva}\ \frac{\pi}{4}\left(\frac{2Di_{eva}}{M_{com}}\right)\right]^2 \quad \text{(AIII. 4)}$$

$$= 8.90 \times 10^{-4}$$

$$\left(\frac{\partial X}{\partial M_{com}} \delta dM_{com}\right)^2 = \left[-\rho_{liq}\ Hi_{eva}\ \frac{\pi}{4}\left(\frac{Di_{eva}^2}{M_{com}^2}\right)\right]^2 \quad \text{(AIII. 5)}$$

$$= 2.601 \times 10^{-5}$$

$$\left(\frac{\partial X}{\partial Hi_{eva}}\delta dHi_{eva}\right)^2 = \left[\rho_{liq}\ \frac{\pi}{4}\left(\frac{Di_{eva}^2}{M_{com}}\right)\right]^2 \quad \text{(AIII. 6)}$$

$$= 1.89 \times 10^{-6}$$

$$\delta X = 0.030$$

$$= 3.12\%$$

The ethanol adsorption uptake measurements is found to be having an average value of 3.12% uncertainty.

Appendix IV

Uncertainty Analysis of the performance of the SAC system

The Q_{Ref}, Q_{gen}, and COP of the SAC system are all functions of several variables, each of which is uncertainty

$$\delta Q_{Ref} = \sqrt{\left(\frac{\partial Q_{Ref}}{\partial m}\delta dm\right)^2 + \left(\frac{\partial Q_{Ref}}{\partial C_p}\delta C_p\right)^2 + \left(\frac{\partial Q_{Ref}}{\partial \Delta T}\delta d\Delta T\right)^2} \quad \text{(AIV. 1)}$$

$\left(\frac{\partial Q_{Ref}}{\partial m}\delta dm\right)^2$ = 7.705 x 10^7

$\left(\frac{\partial Q_{Ref}}{\partial \Delta T}\delta d\Delta T\right)^2$ = 5.661 x 10^7

δQ_{Ref} = 11561.3

= 0.73%

$$\delta Q_{gen} = \sqrt{\left(\frac{\partial Q_{gen}}{\partial \dot{m}}\delta d\dot{m}\right)^2 + \left(\frac{\partial Q_{gen}}{\partial C_p}\delta C_p\right)^2 + \left(\frac{\partial Q_{gen}}{\partial \Delta T}\delta d\Delta T\right)^2 + \left(\frac{\partial Q_{gen}}{\partial t}\delta t\right)^2} \quad \text{(AIV. 2)}$$

$\left(\frac{\partial Q_{gen}}{\partial \dot{m}}\delta d\dot{m}\right)^2$ = 1.033 x 10^6

$\left(\frac{\partial Q_{gen}}{\partial \Delta T}\delta d\Delta T\right)^2$ = 5.437 x 10^9

δQ_{gen} = 73743

= 2.54%

$$\delta COP = \sqrt{\left(\frac{\partial COP}{\partial Q_{Ref}}\delta dQ_{Ref}\right)^2 + \left(\frac{\partial COP}{\partial Q_{gen}}\delta dQ_{gen}\right)^2} \quad \text{(AIV. 3)}$$

$\left(\frac{\partial cop}{\partial Q_{Ref}}\delta dQ_{Ref}\right)^2$ = 1.592 x 10^{-5}

$\left(\frac{\partial COP}{\partial Q_{gen}}\delta dQ_{gen}\right)^2$ = 1.928 x 10^{-4}

δCOP = 0.014

= 2.67%